Interpenetrating Polymer Network Adhesives

Gary Robert Weber

A dissertation

submitted in partial fulfillment of the

requirements for the degree of

Doctor of Philosophy

University of Washington

2012

Reading Committee:

Brian D. Flinn, Chair

Christine K. Luscombe

Hong Ma

Program Authorized to Offer Degree:

Materials Science & Engineering

University of Washington

Abstract

Interpenetrating Polymer Network Adhesive

Gary Robert Weber

Chair of the Supervisory Committee:
Research Associate Professor, Brian D. Flinn
Materials Science & Engineering

Recent products in commercial aerospace such as the Boeing 787 and the Airbus A350 have featured an increased use of thermoset adhesive bonded primary structure assemblies. In addition to carbon fiber laminates and fiber metal laminates like GLARE and TiGr, one potential growth area is selective fiber reinforcement of metallic structures. The thermal expansion differential between metals and composite laminates leads to thermal residual stresses and thermal distortions when elevated temperature cure adhesives are used. Room temperature cure paste adhesives offer a potential solution, but they are messy to use, have limited working lives and have unsatisfactory environmental durability. Radiation cured adhesives also offer room temperature curing capability, but they suffer from low toughness since traditional phase separated, elastomeric or thermoplastic toughening mechanisms are not compatible with the rapid cure rates of radiation curing.

The proposed solution explored in this research was the use of interpenetrating polymer networks (IPNs) to toughen electron beam cured acrylate adhesives. The proposed solution involves an initially cured stiff acrylate network to provide the strength of the adhesive system combined with the subsequent cure of a flexible epoxy network to provide the toughness of the adhesive system. Previous IPN research has explored combinations of flexible acrylates with stiff epoxies and stiff acrylates with stiff epoxies, but a literature review did not reveal any combinations of stiff acrylates combined with flexible epoxies.

Electron beam curing was used to explore combinations of different acrylate and epoxy network formulations. To explore the effect of the ratio of the acrylate and epoxy networks, a model IPN material system was explored. IPN material samples were characterized to determine degree of cure, glass transition temperature, density, strength, modulus and fracture toughness. The IPN was also used as the matrix adhesive in a carbon fiber laminate. A parabolic response was found in IPN properties, resulting in deviations from a linear rule of mixtures relationship that can be related to the product of the acrylate and the epoxy phase fractions.

IPN single edge notched beam fracture toughness values in excess of 2.50 MPa $m^{1/2}$ were observed whereas the values for pure acrylate were on the order of 1.00 MPa $m^{1/2}$. Sources of IPN synergy were linked to IPN morphology, to chemical synergy between the acrylate and epoxy monomers and to enhanced shear yielding due to a mismatch between the component networks.

Contents

1. Introduction

1.1 Motivation

Structural parts used for commercial airplanes are generally produced from either metallic or carbon fiber reinforced plastic (CFRP) parts. The structural loads imposed by the part design generally dictate the material selection. Parts with out of plane loads or with significant shear loading are best served by the isotropic properties of metallic materials. Components with loads primarily in one plane are candidates for CFRP where the directional strength of unidirectional fiber tows can be used to tailor laminate properties in the primary load direction.

In addition to these individual material performance domains, there also exist combinations of the two material forms. Fiber metal laminates such as GLARE, ARALL or TiGr are the most common combinations found in the aerospace industry. [1] [2] A lesser known combination is selectively fiber reinforced metal structure. This combination utilizes the isotropic properties of metallic materials supplemented by the unidirectional reinforcement offered by CFRP.

Fiber reinforced metallic structure has been used in other industries. Steel structures have benefitted from reinforcement with CFRP. [3] Both double lap shear coupon tests and non-linear finite element analysis showed that bond failure was the dominant failure mode.

Adhesively bonded assemblies – composite laminates, fiber metal laminates or fiber reinforced metal – rely on adhesion to transfer loads from one substrate to the substrate on the other side of the adhesive bond. Proper surface preparation and process controls are

essential to developing a high quality adhesive bond. If these conditions are successfully controlled, the performance of the adhesive joint is a strong function of the adhesive material properties.

High performance adhesives are generally cured at elevated temperatures. While elevated temperature cure enhances material performance, it also introduces process-related issues. Tooling to hold laminates or parts in the proper orientation during curing represents an additional cost. Autoclaves for introducing pressure during cure represent size limitations as well as capital equipment costs. Finally, the difference in the coefficient of thermal expansion (CTE) between laminate layers or between metallic materials and composite reinforcement introduce thermal residual stresses which decrease bond strength and may manifest themselves as distortion upon cooling to room temperature.

Adhesively bonded joints must be able to absorb substantial amounts of mechanical energy prior to failure. The weakest mode of adhesive bond strength is Mode I, cleavage. Therefore, the selected adhesive must exhibit a combination of strength and toughness. [4]

1.2 Existing Solutions

1.2.1 Room Temperature Cure

Two part epoxy systems that cure at near room temperatures (25 °C) such as Hysol EA9394 have been developed for structural applications. With a post-cure, a service temperature of up to 177 °C with good strength and reasonable toughness can be achieved. [5] However, the limitation of room temperature curing systems is moisture absorption which lowers the glass transition temperature and related properties as measured in “hot/wet tests.” [6] [7] [8]

1.2.2 Novel Cure Techniques

One novel technique to avoid thermal stresses while still achieving elevated temperature cure system performance is a smart cure cycle that incorporates cooling, polymerization and reheating. In this system, a series of heating and cooling cycles is used to initiate polymerization and then quickly cool the adhesive bond down to room temperature to avoid the introduction of thermal stresses in carbon fiber epoxy reinforced steel or aluminum strips. While a reduction in thermal stress of 50% was achieved under laboratory conditions, the complexities of this system limit its abilities to scale up to production part sizes. [9]

A second novel cure technique is the use of segregated adhesive areas incorporating both room temperature and elevated temperature curing epoxy systems. [10] This dual adhesive system was applied to metal/composite joints and was found to offer significant improvement due to the reduction of thermal residual stresses. However, this system requires careful introduction of two separate adhesives to select areas of the adhesive bonding assembly.

1.2.3 Electron Beam Curing

Electron beam curing of adhesives allows the curing to be conducted at room temperature. This eliminates thermal distortion, but it also results in brittle adhesives. [11] Traditional toughening techniques are ineffective for electron beam cured systems due in part to the rapid (non-equilibrium) reaction rates. [12]

1.3 Report Organization

This report will cover theoretical background for polymers, interpenetrating polymer networks and adhesives followed by a review of relevant literature in chapter 2. The research hypothesis will be developed in chapter 3, and the preparation of samples will be addressed in chapter 4. Since the investigation includes the use of results from a variety of thermal, mechanical and microscopic analysis techniques, chapter 5 will detail the specimen preparation, test results and results discussions for each major analysis rather than covering all specimen preparation first, followed by all test result then discussion. Section 6 incorporates a discussion of the results from the different major analysis techniques and conclusions that may be drawn from them. Remaining work is outlined in chapter 7, and research conclusions are stated in chapter 8.

2. Background and Literature Review

2.1 Polymer Fundamentals

Polymers are formed by the conversion of discrete monomer components into extended chain length polymers. The presence of monomer or oligomer units with functionality higher than two will result in the formation of a cross-linked network. [13] Changes in monomer chemical structure such as molecular weight, backbone stiffness and the type of side groups dictate key polymer properties such as modulus, tensile strength and glass transition temperature.

2.1.1 Monomer Polymerization

Thermoset monomers are converted to polymers through chemical reactions. Curing reactions are exothermic, and the heat generated can also lead to an increase in the reaction rate. The polymerization reaction is initiated once the activation energy threshold has been reached. Depending on the formulation, the polymerization energy can be provided by either thermal energy at room temperature, thermal energy at elevated temperatures or by other energy sources such as ultraviolet or electron beam radiation.

Monomers are homopolymerized if the monomer units directly react with each other. An addition polymerization occurs if a reactive curing agent or second monomer unit is required. Both types of reactions result in increased molecular weight and cross linking.

2.1.1.1 Acrylate polymerization

Acrylic structural adhesives are useful due to their rapid cure rates and structural strength. They may be classified into two broad groups – free radical curing adhesives and

cyanoacrylate adhesives. Both are addition reaction systems. The first system initiates polymerization in the presence of free radicals whereas cyanoacrylates react by anionic polymerization.

The final properties of acrylate adhesives depend primarily on the monomer chemical structure, the cross-linking density and the degree of monomer conversion. Low modulus elastomers are produced from aliphatic monomer chains whereas high modulus, glassy polymers are produced from chains containing aromatic structures. Cross-linking density can be tailored by adding diluents with higher or lower functionality. The degree of monomer conversion is dependent on physical curing conditions such as temperature which govern the balance between gelation and vitrification. [14]

Acrylates can homopolymerize if exposed to electron beam (EB) radiation. The mechanism for EB curing of an acrylate functional unit is shown in Figure 1. An incoming electron destabilizes the acrylate carbon double bond. The bond opens, resulting in two reactive sites per acrylate end unit.

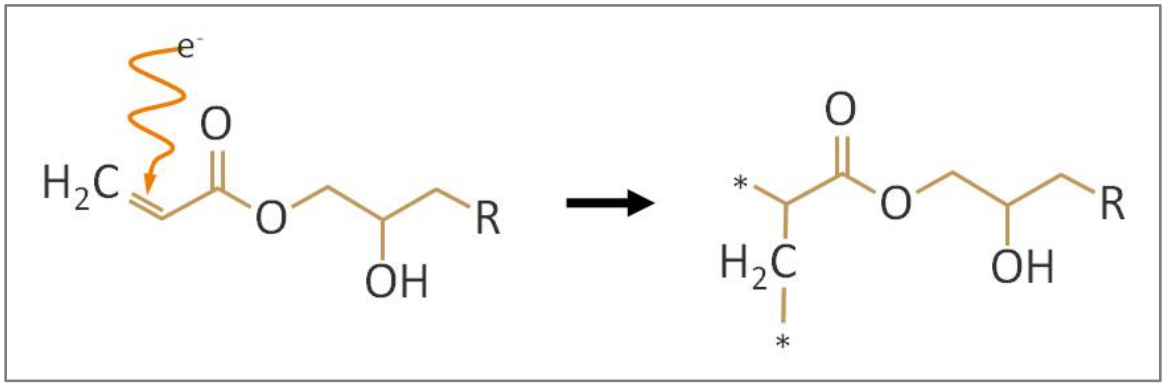

Figure 1: Electron beam destabilization of carbon double bonds in acrylate

With the incorporation of a photo-initiator, acrylates can also be cured with the addition of ultraviolet radiation. The incoming radiation is absorbed by the initiator molecule such as 2-hydroxy-2-methyl-1-phenyl propanone (HMPP) which then cleaves into two separate radical species as shown in Figure 2.

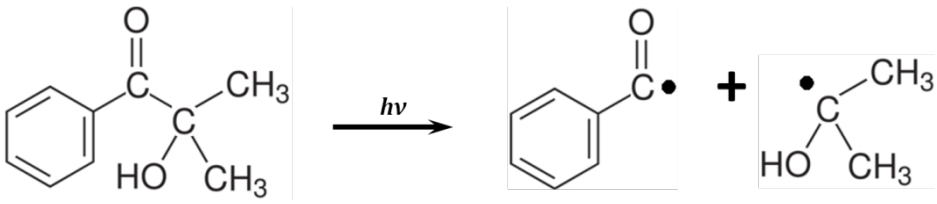

Figure 2: Cleavage of HMPP photo-initiator

The two cleaved radical species then initiate free radical polymerization with the acrylate monomers. The free radical polymerization of HMPP with bisphenol A diacrylate (BPADA) is shown in Figure 3. Although the photo-initiator is incorporated into the final monomer, the amount of photo-initiator can be on the order of 0.1 weight percent or lower. [15] As a result, the photo-initiator properties have a negligible effect on the final network properties.

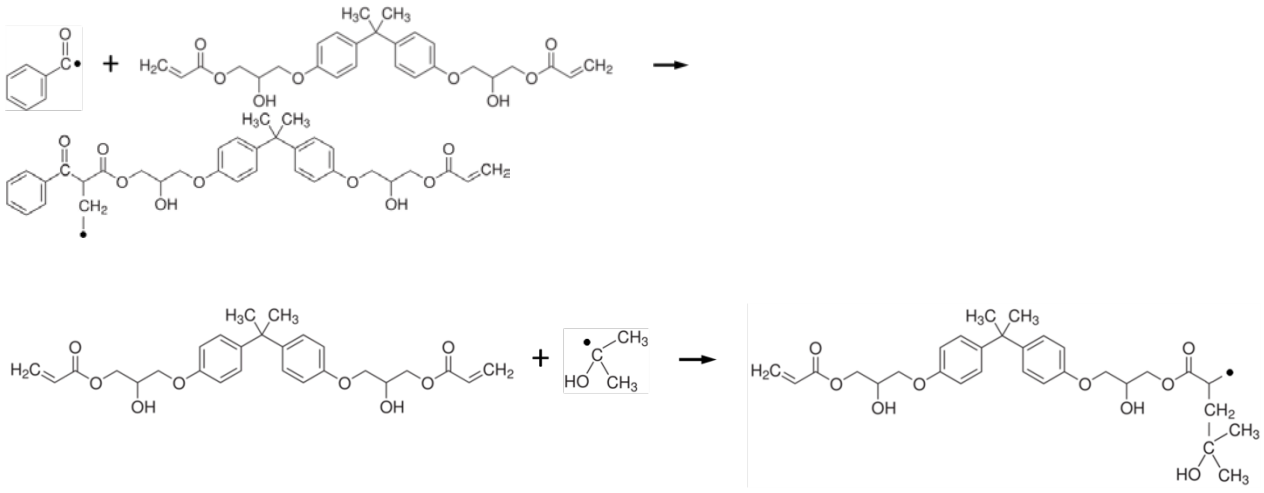

Figure 3: Initiation of free radical polymerization with cleaved photo-initiator radicals

As the molecular weight of the UV-cured polymer increases, its mobility is restricted. As a result, UV-curing is limited by vitrification, and final properties are dependent on the degree of monomer conversion. [16] The degree of conversion for UV-cured BPADA with differing levels of HMPP photo-initiator as a function of the accumulated UV dosage is shown in Figure 4.

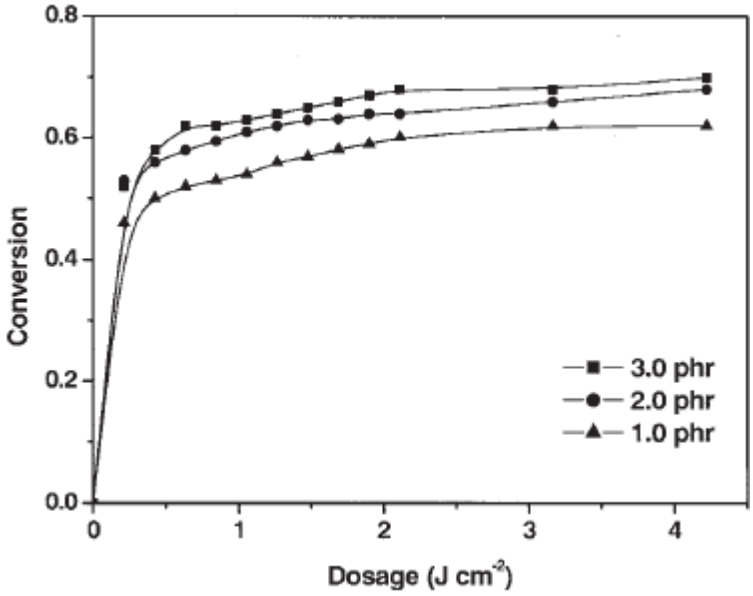

Figure 4: Conversion of BPADA monomer as a function of HDMAP photo-initiator concentration and total UV radiation dosage (from 17)

2.2.1.2 Epoxy polymerization

When epoxy monomers are cured in reactions that involve other types of reactive molecules, the polymerization is classified as an addition reaction. The reactive curing agent molecules are incorporated into the final network, so their properties and the amount used have an influence on the final epoxy polymer properties. They can generally be classified by curing temperature – either curing at low/room temperature or requiring elevated temperatures to polymerize. Crosslink density can be modified by increasing the

functionality of the curing agent or by increasing the reactive agent molecular length. Reactive curing agent molecules include amines, anhydrides and imidazoles. [18] [19]

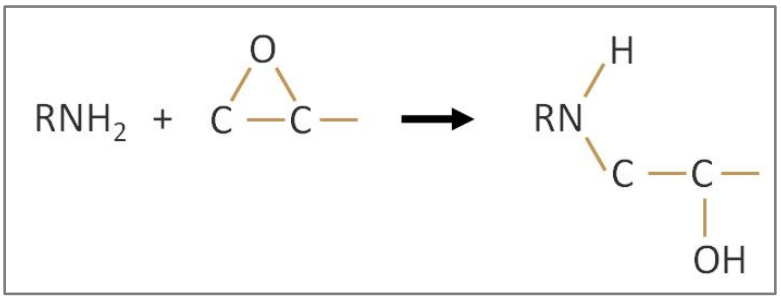

Figure 5: Amine curing agent reaction with epoxy

After amines, acid anhydrides are the second most popular curing agent for epoxy formulations. Whereas amines must be mixed with epoxies in stoichiometric ratios, the anhydride to epoxide ratio can be varied to a degree to tailor the properties of the cured system. Anhydride reactions are generally slow, and the reaction mechanism involves two basic steps. First, the anhydride reacts with a hydroxyl which opens the anhydride ring. Second, the newly generated carboxyl groups then react with the epoxy. The reaction between Hexahydro-4-methylphthalic anhydride (HHMPA) and diglycidyl ether of bisphenol A (DGEBA) is shown in Figure 6.

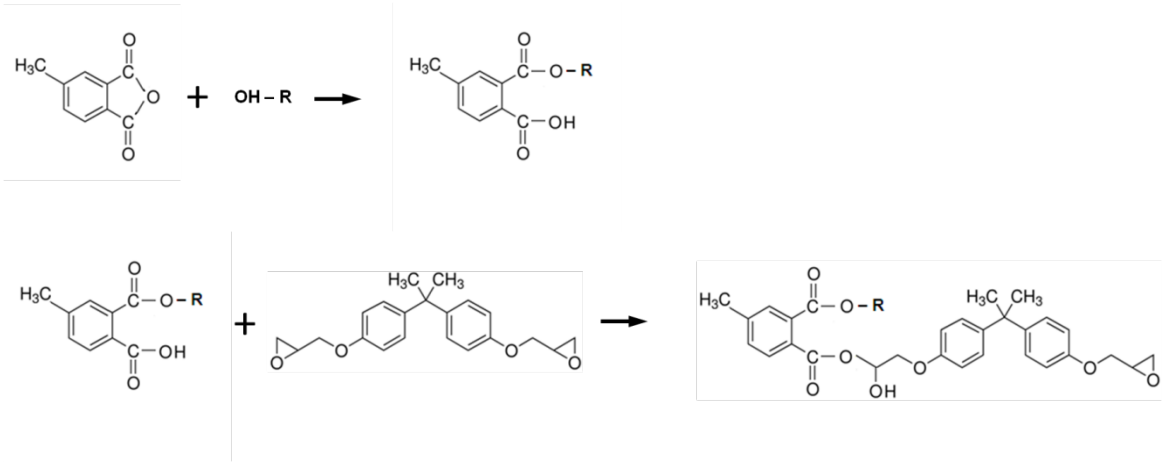

Figure 6: HHMPA anhydride polymerization of DGEBA

A lesser known class of epoxy curing agents is imidazoles. The curing involves two primary mechanisms which occur sequentially. The first mechanism is the formation of an adduct between the imidazole and the epoxy. In this step, the pyridine-type nitrogen reacts with the epoxide functional group, forming a 1:1 adduct. The H* proton is then transferred, producing a pyridine-type nitrogen on the opposite side of the imidazole ring. After reacting with an additional epoxide functional group, a 2:1 adduct is formed (molecule C in Figure 7). As a result of the adduct reaction, the viscosity of the system increases slightly.

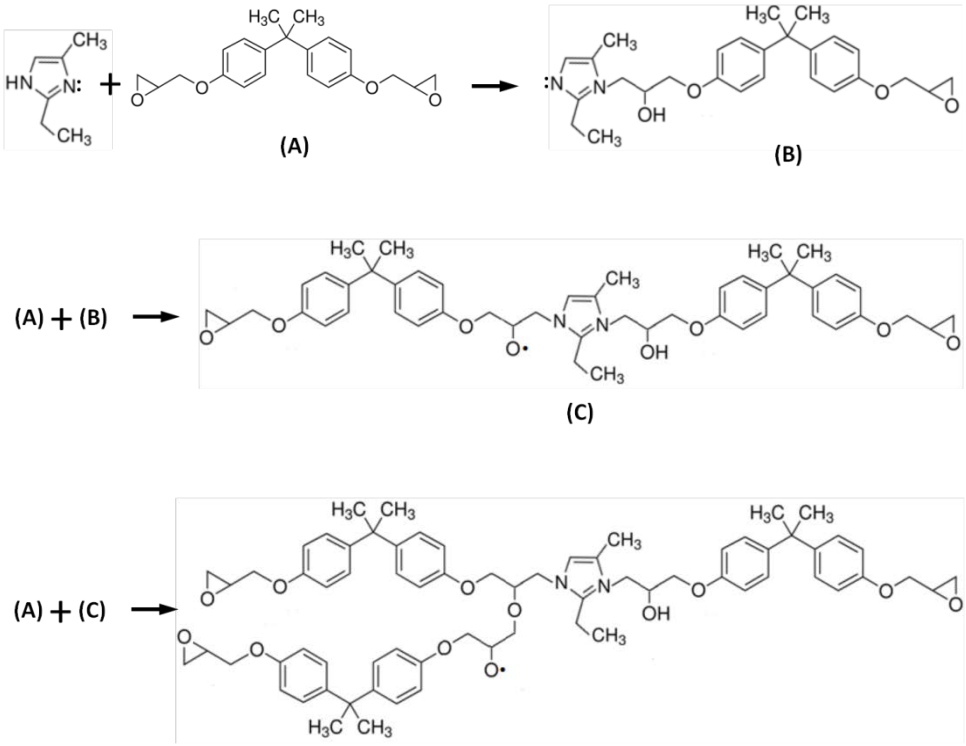

Figure 7: 2-4-EMI curing of DGEBA

If all of the epoxy monomer is not consumed by the adduct reactions, then cross linking can occur through etherification of the O* site created during the adduct reaction. At 25 mol% concentration of imidazole, the adduct reaction consumes approximately half of the epoxy monomer. As shown in Figure 8a, the adduct reaction rate increases as the temperature increases. Epoxide concentration decreases steadily until the 2:1 epoxy:imidazole adduct is achieved. Increasing the temperature allows the etherification reaction to occur, and it is much more rapid than the adduct reaction. Figure 8b shows the heat flow from a differential scanning calorimeter. For the 100 mol% and 50 mol% mixtures, the adduct reaction consumes all of the epoxy monomer. For the 25 mol% mixture, the rapid etherification is represented by a sharp exotherm peak centered near 110 °C. [20, 21]

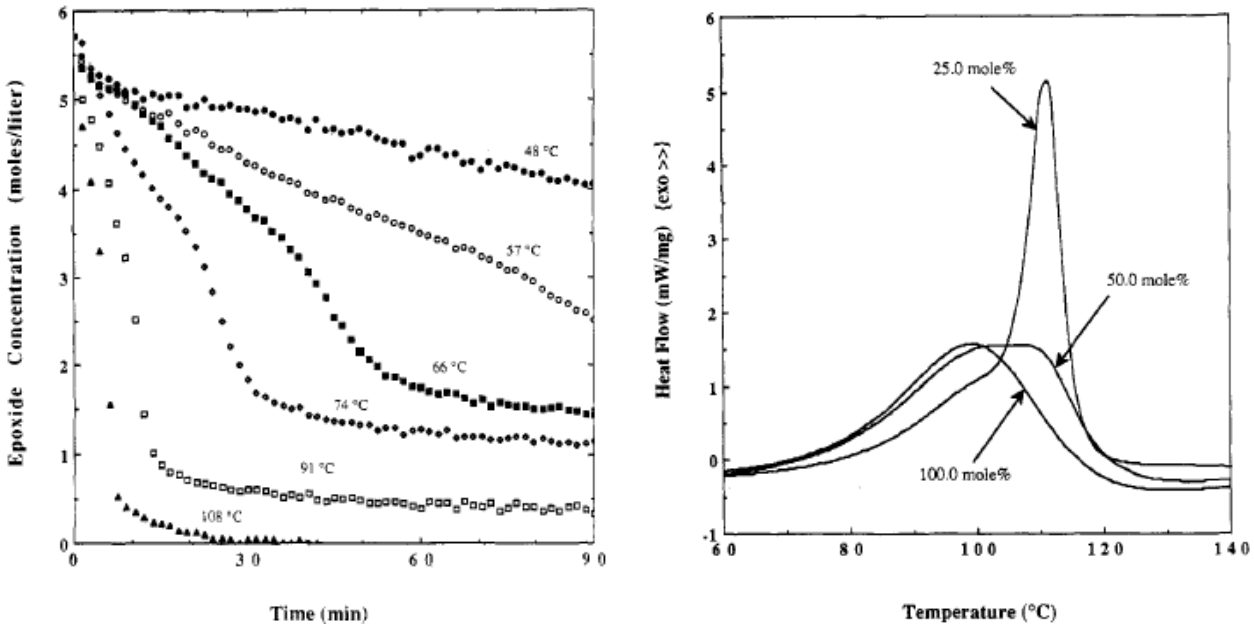

Figure 8: 2-4-EMI curing of DGEBA: a) Epoxide concentration versus time at isothermal temperature for 25 mole% imidazole mixture as determined by FTIR, b) DSC scan of 100, 50 and 25 mole% imidazole mixtures at heating rate of 10 °C/min (from 20)

2.1.1.3 Cure shrinkage

Most polymeric materials shrink during polymerization since the solid, chemically linked mass occupies less volume than the liquid, Van der Waals bonded monomers. Higher shrinkage generally occurs with higher temperature cures. Acrylic resins experience volumetric shrinkage of 5-10 percent whereas epoxy resins shrink approximately 4-5 percent. The result of shrinkage is residual stresses at the adhesive-adherend interface. Additional residual stresses come from differential thermal expansion from the curing temperature to room temperature. More flexible (lower modulus) and more highly filled (reduced coefficient of thermal expansion) adhesives experience lower residual stresses. The net result is that tensile shear strength of bonded joints tested at different temperatures peaks near the adhesive cure temperature. [18]

2.1.2 Cure Models

Thermosetting polymers can be formed by one of two mechanisms – step growth or chain extension. If small molecules evolve as a result of the polymerization reaction, the process is known as a condensation-type. This type of reaction occurs in the formation of polymers such as polyesters, polyimides and polysulfones. If no secondary molecules are formed, the process is known as a non-condensation or poly-addition reaction. This type of reaction occurs in the formation of polymers such as polyurethanes, acrylates and epoxies.

2.1.2.1 Step Polymerization

In step growth polymerization, the initial stage involves individual monomer or oligomer units reacting with each other. Higher molecular weight chains start forming toward the end of the process when most of the initial monomer supply has been consumed.

2.1.2.2 Chain Polymerization

Chain extension polymerizations are initiated by an active center that reacts with a monomer. The active site is regenerated at each step, transferring the active center to the end of the growing chain. The active center can be produced by a free radical, an anion or a cation. High molecular weight chains are formed early in the chain extension process, and the monomer supply is not appreciably diminished until the final stages of polymerization.

Free radical curing of acrylates proceeds by chain polymerization. Amine curing of acrylates or epoxies proceeds according to step polymerization, but curing of epoxies with imidazoles or anhydrides proceeds via chain polymerization.

2.1.3 Evolution of Properties during Polymerization

2.1.3.1 Development of Morphology

During chain polymerization, polymer units continue to grow by extending the ends of the polymer until the polymer coil is too long to remain in solution. The result is nucleation of globules which can then continue to grow or agglomerate into clusters. The evolution of solid areas during cure for electron beam cured ethoxylated bisphenol A diacrylate is shown in Figure 9. At a low degree of conversion, the solid area is primarily due to cluster areas of 75-125 nm^2. As polymerization proceeds, the average cluster area increases as the initially nucleated particles agglomerate into larger clusters. [22] The final morphology is a collection of agglomerated globules as shown in Figure 10.

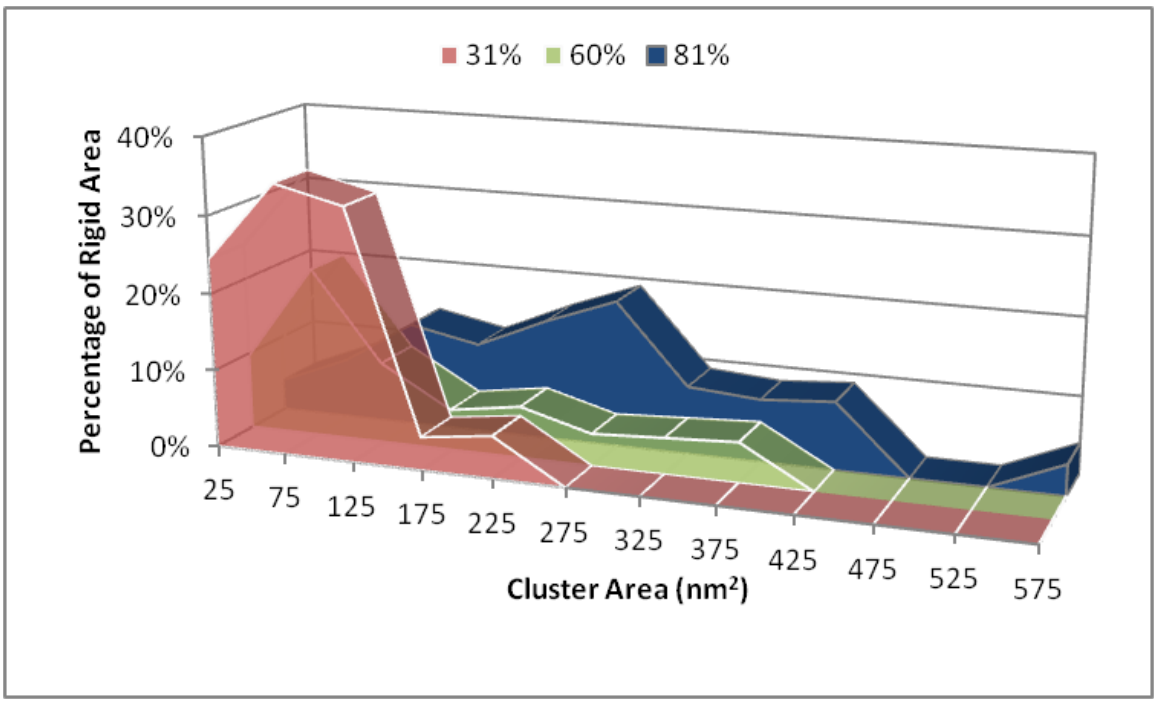

Figure 9: Distribution of the fractional area of clusters relative to the total area of rigid domains for electron beam cured bisphenol A diacrylate at different degrees of monomer conversion (adapted from 22)

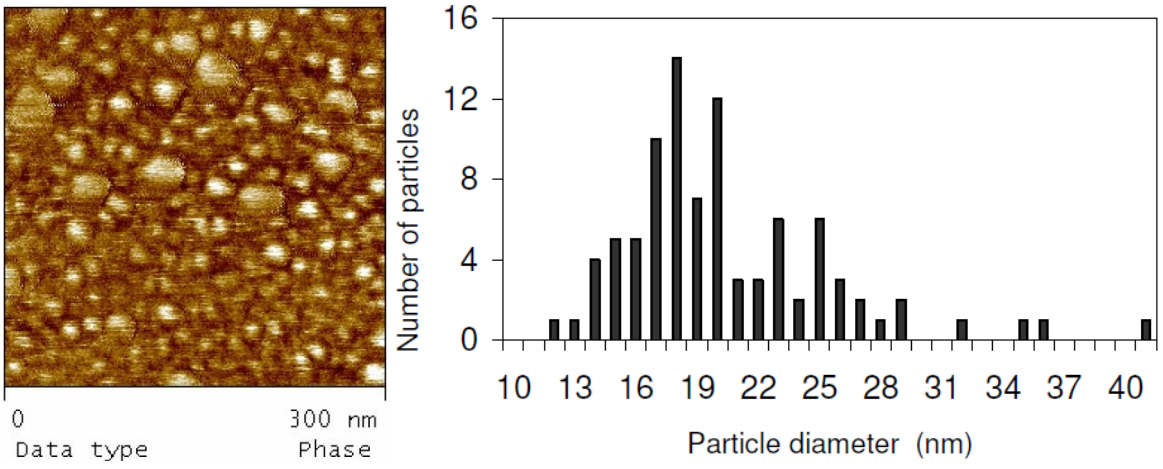

Figure 10: Phase map and particle size distribution for ethoxylated bisphenol A diacrylate cured against a polished silicon wafer (taken from [23])

2.1.3.2 Degree of Monomer Conversion

The degree of monomer conversion has a significant effect on the properties of the resulting polymer. Monomer conversion is primarily set by the limiting behaviors of gelation and vitrification. Gelation is the point at which the growing macromolecular network extends across the reaction medium. It characterizes the transition from a liquid state with suspended polymers to a solid state (infinite viscosity). Vitrification occurs when the system glass transition temperature reaches or exceeds the curing temperature of the polymer system. When the system reaches this glassy state, the reaction kinetics are significantly reduced. The gelation and vitrification conditions are illustrated in a simplified time-temperature-transformation diagram shown in Figure 11.

The diagram shows three glass transition temperatures, one for the monomer resin, one for the gelled system and one corresponding to complete monomer conversion. The dotted gelation line corresponds to the curing time at a specific temperature at which gelation occurs. The difference in crosshatching signifies conditions in which gelation occurs prior to vitrification (upper region) or in which vitrification occurs prior to gelation (lower region). For systems where the curing or post-curing temperature does not exceed $T_{g,\infty}$, the polymer is either gelled or vitrified before the monomer can be completely polymerized.

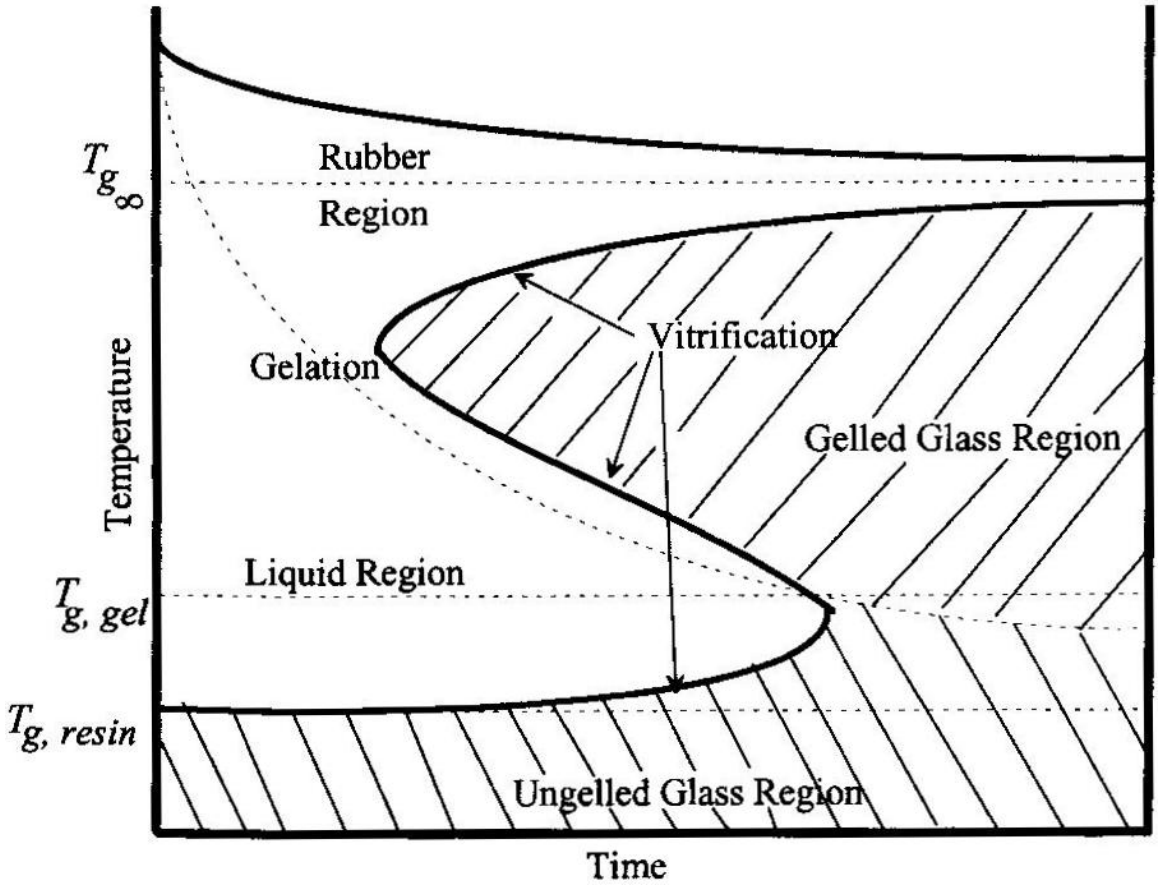

Figure 11: Simplified time-temperature-transformation diagram for thermoset cure (from 4)

Gelation restricts macroscopic flow of the reacting monomer. Phase separation can take place at the micron level due to differences in solubility. If so, it is locked in after gelation. Vitrification locks in the structure at the nanometer scale as the free volume required for chain motion and rotations is lost. [24]

Incomplete monomer conversion decreases the resulting polymer properties. Figure 12 shows the development of tensile strength as a function of monomer conversion for electron bean and ultraviolet light cured bisphenol A diacrylate. The change in glass transition temperature for the same monomer is shown in Figure 13.

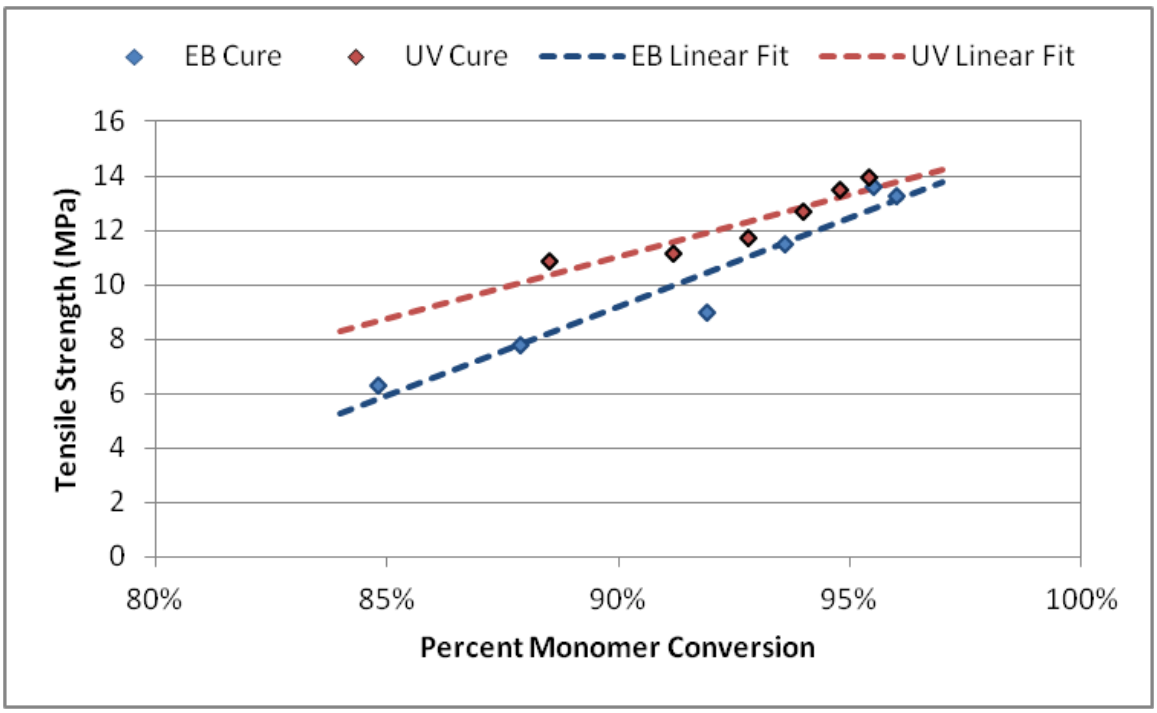

Figure 12: Tensile strength in urethane diacrylate as a function of monomer conversion when cured by electron beam and ultraviolet radiation (adapted from 25)

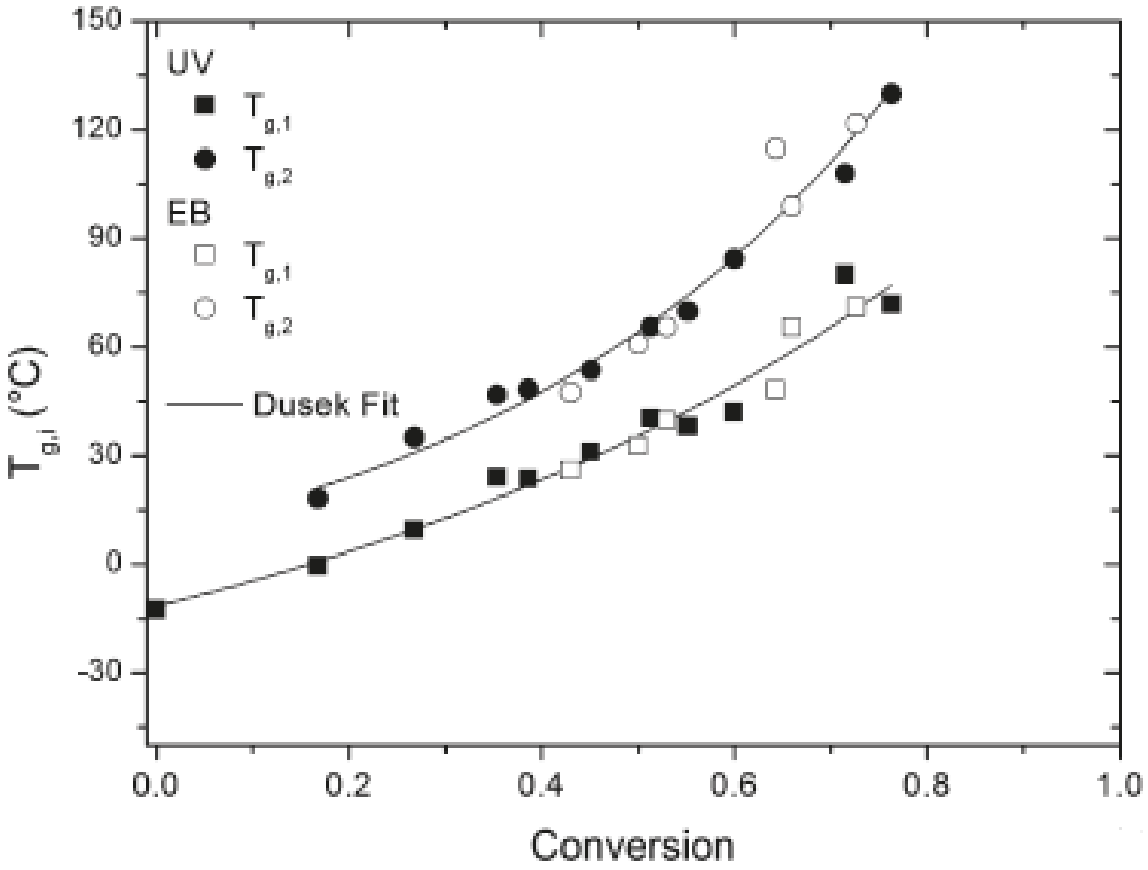

Figure 13: Glass transition temperature versus degree of bisphenol A diacrylate monomer conversion (from 22)

2.2 IPN Fundamentals

Interpenetrating polymer networks consist of two or more polymer systems with at least one of the systems synthesized in the presence of the other. The result is a physically cross linked network formed when polymer chains of the second system are entangled with or penetrate the network formed by the first system. Each individual network retains its individual properties, so synergistic improvements in properties like strength or toughness are possible. IPNs can be created in simultaneous or sequential fashion.

2.2.1 IPNs versus Polymer Blends

Interpenetrating polymer networks consist of two or more polymer systems with at least one of the systems synthesized in the presence of the other. The result is a physically cross linked network formed when polymer chains of the second system are entangled with or penetrate the network formed by the first system. Each individual network retains its individual properties, so synergistic improvements in properties like strength or toughness are possible. IPNs can be created in simultaneous or sequential fashion.

2.2.2 IPN Types

In simultaneous IPNs, monomers and cross linkers for both polymer systems are present at the start of polymerization. To produce an IPN, the two systems must react by different mechanisms. Generally these are via chain (radical) and step (polyaddition) mechanisms. True simultaneous IPNs are not formed since there is generally a difference in reaction rate between the two systems.

To produce sequential IPNs, the first polymer network is fully cured before the second network is polymerized. The traditional approach is to swell the first network with monomer for the second network. However, an in-situ sequential IPN is created if the second network monomer is present while the first network is being cured.

2.2.3 IPN Formation

Simultaneous and in-situ sequential IPNs begin with an initial reacting system that is encompassed in one phase. If the components remain miscible during curing, then a polymer blend is created. However, if the components phase separate, then an IPN is

formed. The instability leading to phase separation may be the result of changes in the interaction between the systems components or an increase in the cross-link density of a component. [26]

Miscibility is determined by a negative free energy of mixing between the initial system components as noted in Equation 1.

Equation 1

Where = *enthalpy of mixing*

T = *absolute temperature*

= *entropy of mixing*

The system will be miscible if $\Delta H_{mix} < 0$ and $T\Delta S_{mix} > 0$ or if $\Delta H_{mix} > 0$ but the magnitude of $T\Delta S_{mix}$ is greater than the magnitude of ΔH_{mix}. For a regular solution,

$$\Delta H_{mix}/N = B\phi_1\phi_2 \qquad \text{Equation 2}$$

Where N = *total number of moles of the two components*

B = *second virial coefficient*

ϕ_1, ϕ_2 = *molar fractions of components 1 and 2*

$$\Delta S_{mix}/N = -R(\phi_1 \ln\phi_1 + \phi_2 \ln\phi_2) \qquad \text{Equation 3}$$

Where R = *ideal gas constant*

So

$$\Delta G_{mix}/N = B\phi_1\phi_2 + RT(\phi_1 \ln\phi_1 + \phi_2 \ln\phi_2)$$ [27] **Equation 4**

Phase separation of an initially miscible mixture can occur by one of two mechanisms: spinodal decomposition or nucleation and growth. Simultaneous IPNs separate via spinodal decomposition whereas sequential IPNs separate by a mechanism of nucleation and growth. [26]

Rewriting the regular solution mixing equation for a solution containing polymers by using the Flory-Huggins mean field theory results in Equation 5, generalized for multiple components.

Equation 5

Where *Flory interaction parameter between components i & j*

For miscible systems, the mixed component interactions (e.g. 1-2) are stronger than the interactions between like components (1-1 and 2-2) and $\chi_{12} < 0$. For large molecules, χ_{12} approaches zero. [28] In the case of ternary systems, two immiscible systems ($\chi_{12} > 0$)may be compatiblized by the selection of a third component which is compatible with components 1 and 2, e.g.$|\chi_{12}\phi_1\phi_2| < |\chi_{13}\phi_1\phi_3 + \chi_{23}\phi_2\phi_3|$.

During polymerization of the first component in an in-situ sequential IPN, the polymer chain grows until it reaches to the point where it is no longer miscible with the surrounding monomer mixture. At this point, the polymer chain collapses from an extended coil and

nucleates a dense globule. [29] These globules assume the form of microspheres to minimize their surface interface area with the surrounding liquid solution. The nucleated globule can continue to grow if monomer units are in position to react with active surface sites. Due to limited mobility, their reaction rate is lower than the rate experienced by a new polymer chain forming in monomer solution. Therefore, it can be expected that new globule nucleation will be favored over growth during the initial stages of polymerization. In the latter stages of polymerization, monomer in the interstitial spaces between globules will begin to link globules into agglomerates as the developing polymer network approaches gelation.

2.2.4 Effect of Cure Order

Since it is still highly deformable, the monomer for the second polymer network decreases the internal stresses in the network which forms first. Due to restrictions imposed by the initial network, the second polymer network cures at a low rate, virtually minimizing internal stresses. The initially cured network determines the strength of the adhesive joint whereas the second network plays the role of plasticizer. [28]

Acrylates experience a higher degree of contraction during polymerization than do epoxies. Moderately cross-linked acrylates have been shown to have approximately 2.5 times the cure shrinkage as experienced by moderately cross-linked epoxies. As a result, the cure-induced residual stress in acrylates can be as high as 8-9 MPa in bulk adhesives and 20 MPa in matrix adhesives.[30] [31] A reduction in the volumetric shrinkage for acrylate-epoxy IPNs with increasing epoxy content has been noted. This is attributed to the fact that instead of

converting all bonds to the spacing exhibited by covalent bonds, some bonds remain at distances characteristic of Van der Waals forces. [32] Curing the acrylate first, therefore, allows some ability to minimize these residual stresses prior to cure of the epoxy monomer.

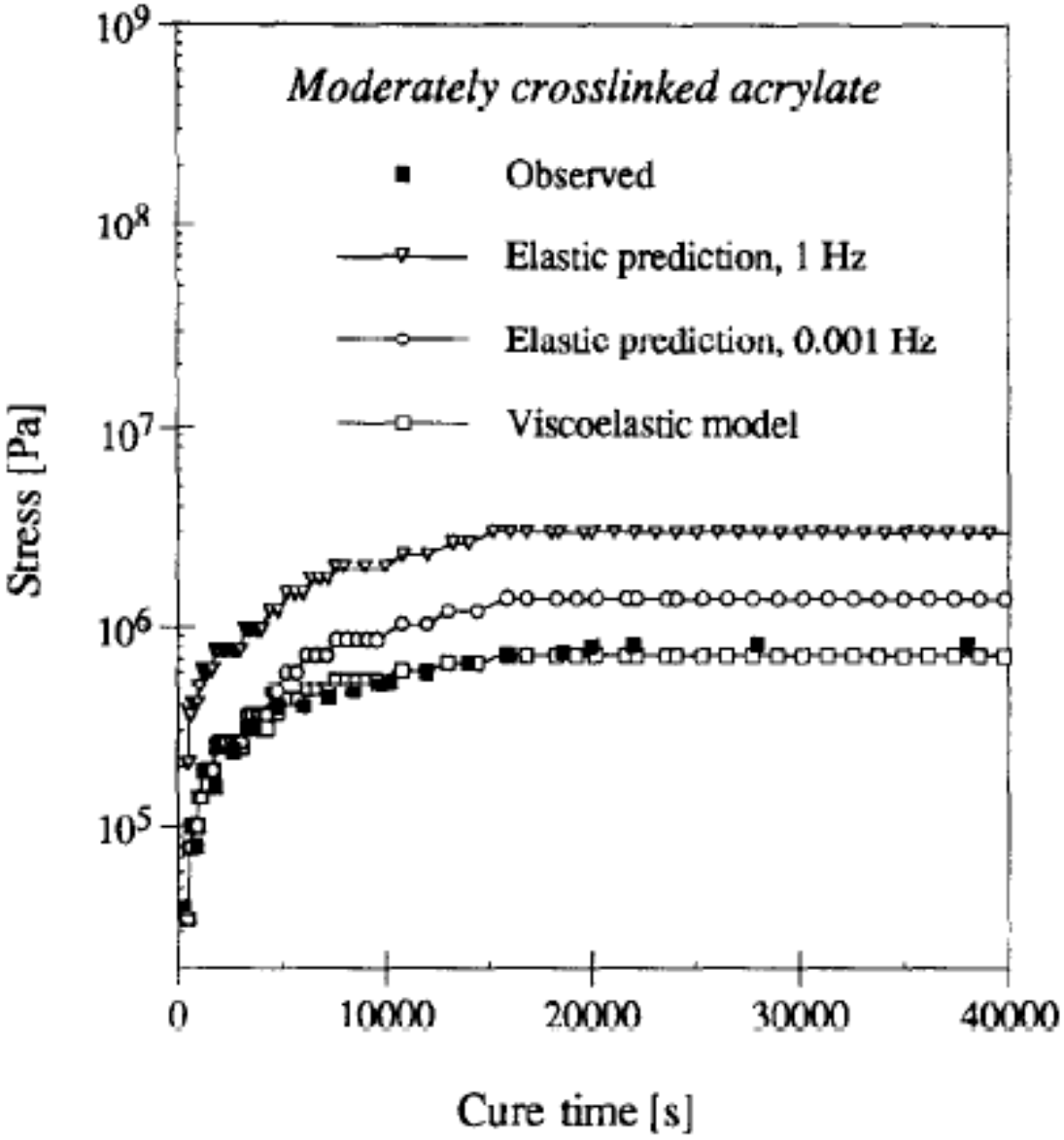

Figure 14: Predicted and observed stress build-up during isothermal cure of moderately crosslinked acrylate (80% BPADA/20% TMPTA) at curing temperature of 115 °C (from 33)

2.2.5 IPN Morphology

Macroporous polymer monoliths are typically formed from spherical beads produced by a suspension polymerization process. However, another option is to cure them directly in molds such as glass tubes via ultraviolet light polymerization. They are produced from agglomerations of microgels that are formed in a mixture of active monomer and unreactive diluents. [34] [35] During the electron beam cure of acrylate-epoxy IPNs, the epoxy monomer is equivalent to unreactive diluents, so the parameters controlling macroporous polymer monolith morphology should be applicable to development of the IPN acrylate network morphology.

Key variables identified for the formation of macroporous structure are temperature, the volume fraction of reactive monomer, the monomer functionality and the composition of the unreactive diluents. [36] Increasing the reaction temperature increases the reaction rate and the rate of microgel nucleation. A higher nucleation rate with a fixed amount of monomer leads to the formation of smaller microgels. The volume fraction of monomer has the simple effect of increasing the amount of the first network to form and a decrease in non-reactive sites. The presence of non-reactive species enhances diffusion of the first network monomer. It can also reduce the polymerization rate, leading to an increase in the final degree of conversion. Higher monomer functionality increases the microgel nucleation rate and also increases the possibility that local polymerization may become limited by monomer diffusion. The unreactive diluents impact the solvating quality of the liquid component. The solvating quality is represented by the square of the difference in the solubility parameters as given by Equation 6.

Equation 6

Where $= solubility\ parameter\ of\ unreacted\ monomer + diluent\ mixture$

$= solubility\ parameter\ of\ polymer$

Solvating quality is related to the Flory interaction parameter as illustrated by Equation 7.

—

Equation 7

The solvating quality of the liquid component changes during the course of polymerization as network 1 monomer is polymerized. Macroporous structures produced in mixtures of poor solvating quality have smaller microgels than those produced in liquids of good solvating quality.

Models for the domain size in sequential IPN networks have been developed. Although the derivations are different, the models point to a few generalizations. Domain sizes range from 100 nm for highly immiscible systems to 10 nm for systems that are heterogeneous on very small scales. Phase separation is limited by cross-links which reduce phase separation and limit domain size. If the phase domains are on the order of 10-20 nm, the IPN performance is dominated by the interphase properties. [32]

The degree of phase separation is related to gelation. If phase separation occurs prior to gelation, then the phase domain sizes will tend to be larger. Most IPNs have co-continuous networks although they may not have dual phase continuity, meaning that some island domains of the second network may be surrounded by a sea of the first network. [37]

2.3 Adhesive Fundamentals

Adhesives based on natural substances have been used for centuries. The rapid growth of synthetic polymers in the past 50 years has provided scientists with a much more diverse property set from which to select adhesive formulations. Optimization of adhesive systems has been made possible through a better understanding of the process, strength and toughness characteristics of polymeric adhesives.

2.3.1 Thermal Properties

Many polymer properties exhibit a dependence on temperature. Many of these properties can be related to the polymer glass transition temperature.

2.3.1.1 Glass transition

The thermally-induced transition of a cross-linked polymer from a brittle, glassy state to a rubbery state is known as the glass transition temperature. This transition generally takes place over a relatively narrow temperature range. Many polymer properties are linked to the glass transition temperature.

In cross-linked amorphous polymers, molecular motions of the polymer chains influence the glass transition temperature. These include vibration of individual atoms around their equilibrium positions, motions of side groups on the main chain, cooperative motion of chain backbone molecular segments and translation of entire molecular chain segments. Factors influencing the glass transition include polymer free volume, attractive forces between polymer segments, internal mobility of chain segments, stiffness of the chain backbones and distance between molecular cross-links.

Glass transition temperatures can be determined by several methods including differential scanning calorimetry (DSC), thermomechanical analysis (TMA) and dynamic mechanical analysis (DMA). All three techniques are used to detect the changes in a polymer that take place near the transition from a glassy to a rubbery state, although the values vary slightly between the different methods as shown in Figure 15. Advances in DMA instrumentation have expanded application of this technique for determination of glass transitions.

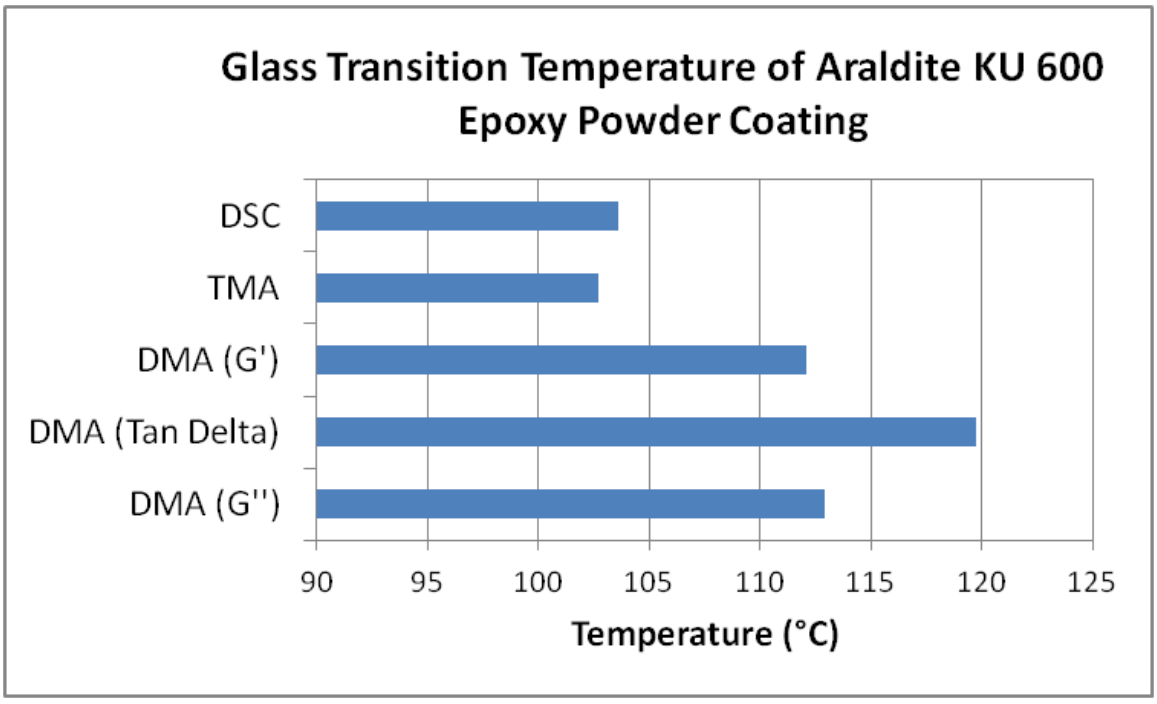

Figure 15: Glass transition temperature variation based on measurement method [38]

DMA results for polymer blends can show three distinct behaviors. For true blends of miscible polymers, a homogeneous mixture is formed, and the glass transition temperature for individual components cannot be determined. For partially miscible polymer systems, there is some affinity between the polymers but not enough to prevent phase separation. Partial miscibility is indicated by a shift in the glass transition temperatures as portions of

each polymer are mixed with their counterparts, driving the individual glass transition temperatures toward an intermediate value. An example is shown in Figure 16. Immiscible blends incorporate polymers which thermodynamically phase separate but have forced compatibility through the action of adhesion promoters such as block copolymers. [39]

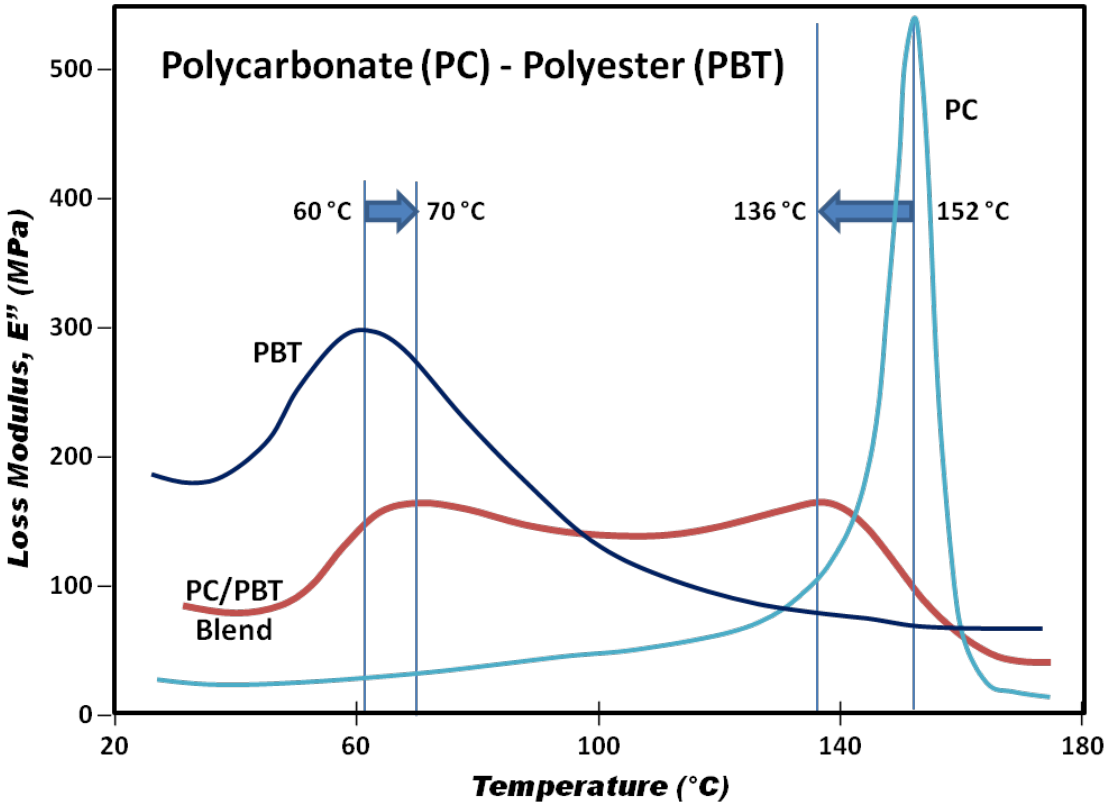

Figure 16: Glass transition temperature shifts in partially miscible polymer blends (adapted from 39)

2.3.1.2 Thermal expansion

Another thermal property of polymers is thermal expansion. Linear thermal expansion can be measured with the use of TMA whereas volumetric thermal expansion can be measured with dilatometry techniques. Changes in the rate of linear thermal expansion as a function

of temperature can be measured with TMA instruments, and the change in the thermal expansion rate provides an additional method for determining glass transition temperature.

The change in thermal expansion at the glass transition temperature provides a measure of the polymer free volume as illustrated in Figure 17. Free volume has been shown to be related to properties such as viscoelasticity, aging, solvent penetration and impact resistance. [40]

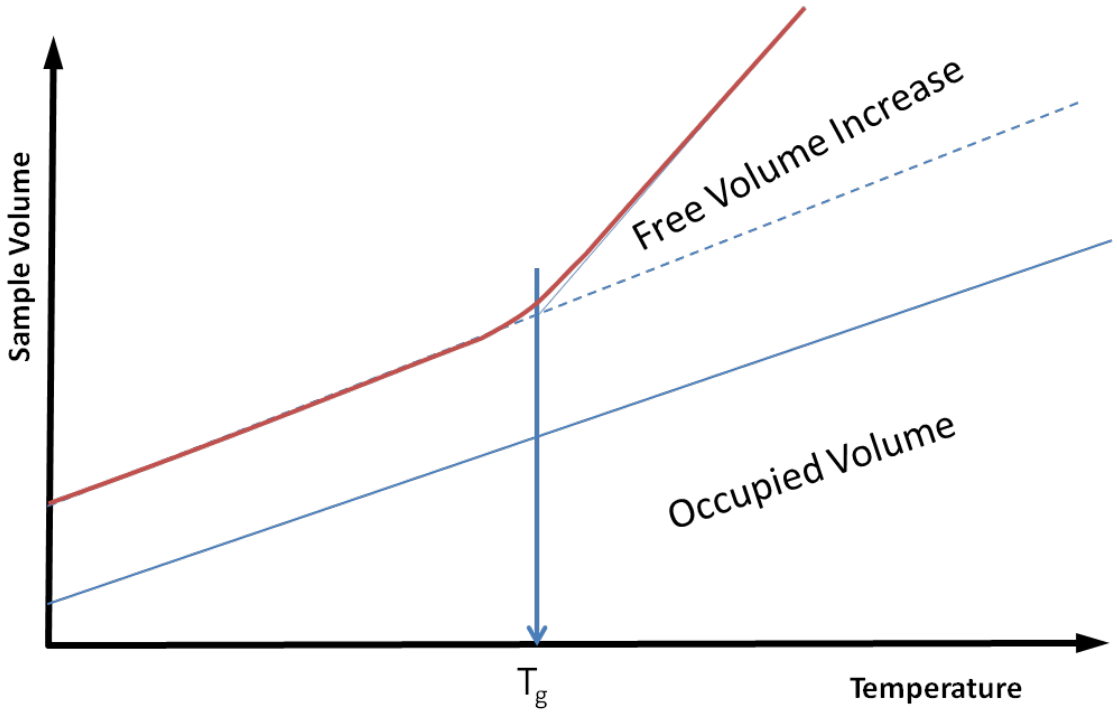

Figure 17: Conceptual representation of occupied volume versus free volume after glass transition

2.3.2 Adhesive Tensile Strength

Unmodified thermoset polymers are brittle materials since the high degree of cross-linking significantly limits the material's ability to undergo viscous flow at a macroscopic level. As a result, the appearance of tensile fracture surfaces can vary significantly with temperature.

While their relative ratios can vary, the fracture surface can be divided into the following regions: initiation, mirror, smooth, rough. [41]

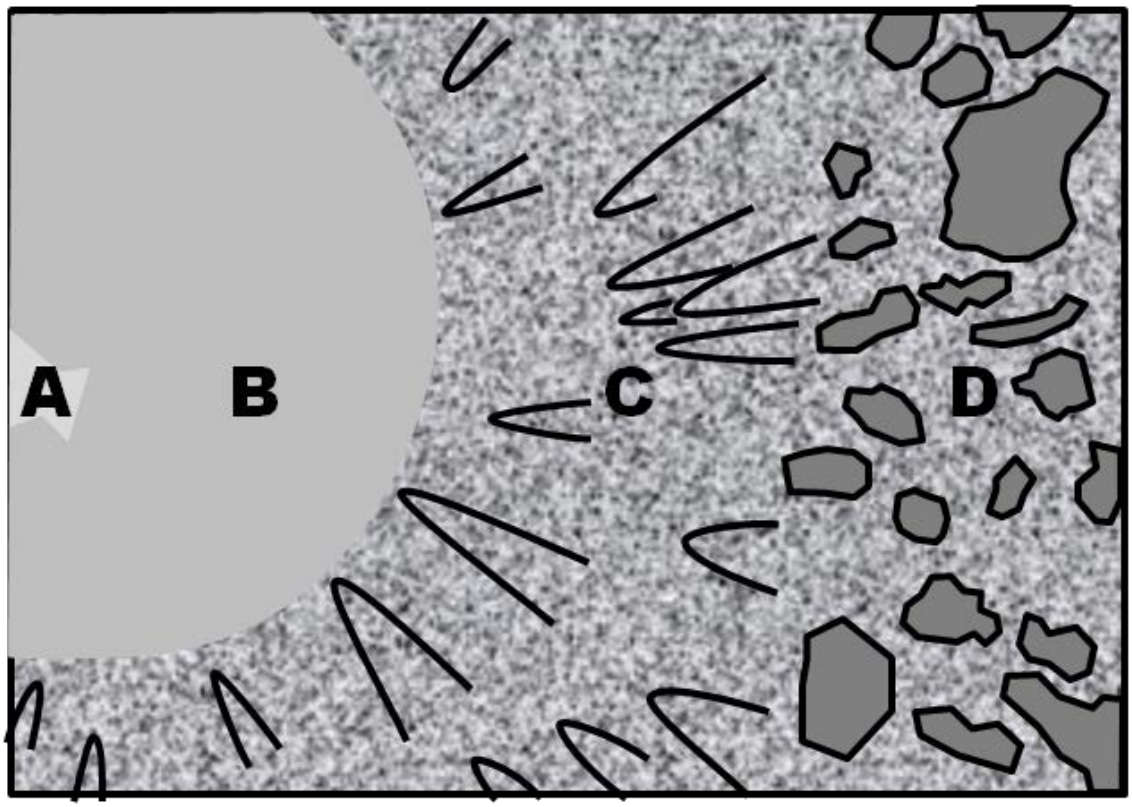

Figure 18: Conceptual Tensile Fracture Surface Showing A) Initiating, B) Mirror, C) Mist and D) Hackle Regions

2.3.2.1 Initiation Region

The fracture toughness of thermoset polymers is so low that once failure initiates, it quickly propagates across the entire cross section. Initiating defects may include microvoids developed during processing, unintentional impurities, localized stress concentrations caused by humidity or solvents or network defects such as un-reacted groups or chain scissions resulting from environmental damage.

2.3.2.2 Mirror Region

The area surrounding the initiation site is known as the mirror region. It is generally smooth with a glossy appearance. It represents a region of relatively slow crack growth rate. The size of the mirror region depends on polymer variables such as flexibility, strain rate, temperature, moisture content and time to failure. In brittle materials like glasses or thermoset adhesives of infinite width, the size of the mirror zone can be correlated to the applied stress through Equation 8.

$$\sigma r_c^{1/2} = \text{constant} \qquad \text{Equation 8}$$

For specimens of finite dimensions the equation is only approximate, but some researchers have found reasonably good correlations. In fact, it has been proposed that fracture toughness can be reasonably estimated based on measurements of fracture region areas and the failure stress. [42]

2.3.2.3 Mist or Smooth Region

The mist region represents an area of higher crack velocity than found in the mirror region. The mist region is substantially rougher and does not have a glossy appearance. In this region, the stable generation of new surface area is no longer sufficient to dissipate fracture energy. Fractures may initiate ahead of the primary crack front. The intersection of cracks growing out of these areas with the primary crack front creates the parabolic or hyperbolic crack features found in this region.

2.3.2.4 Hackle or Rough Region

The hackle region is generally accepted as an area of rapid crack propagation. The fracture surface in this region has a multitude of facets.

2.3.3 Adhesive Toughness

Unmodified, simple thermoset resins have low fracture energies, but this value is two orders of magnitude higher than the energy required for severing covalent bonds. This clearly illustrates that other energy absorbing mechanisms must be active.

Two micro-mechanisms at work in the fracture of unmodified polymers are crazing and shear yielding. Both mechanisms involve localized plastic deformation of the material. Crazing is associated with an increase in volume, followed by the formation of micro-voids which then become stabilized fibrils spanning across directions perpendicular to the developing crack. Shear yielding occurs at constant volume and is manifested in shear bands which develop in the direction of maximum principal shear stress, typically 45 degrees to the direction of crack propagation. Crazing is typically associated with thermoplastic polymers. It has been reported at the crack tips of under-cured epoxies, but not in fully cured ones. It has been shown that a transition from crazing to shear yielding occurs as the polymer cross-link density increases. Therefore, for highly cross-linked polymers like fully cured epoxies, the primary micro-mechanism for fracture energy dissipation and toughness increase is shear yielding. [43]

The flexibility of a resin can be increased by selecting a chemical backbone that is more flexible, increasing the epoxy chain length between cross-links or decreasing the cross-link

density. This increased flexibility can be provided by extending the monomer length or by blending different monomer formulations. Unfortunately, these modifications also result in decreased glass transition temperature and decreased strength.

The toughness of a simple thermoset polymer can be improved through the addition of a second phase. Second phase toughening changes the deformation characteristics of the epoxy, improving its resistance to crack propagation. The second phase can take the form of rubbery particles, thermoplastic particles or hard particles.

2.3.3.1 Rubber toughening

Multi-phase rubber additions are produced through the addition of elastomeric polymers which phase separate during cure. The triaxial stress field produced during plane strain causes shear bands to develop near crack tips as a result of modulus differences. Stress concentrations can also develop at the hemispheres of particles that are located near but not on the fracture path. The net result is that shear yielding in of the epoxy is enhanced by a factor of at least two. [44] Rubbery particles also dissipate fracture energy through interactions with the surrounding matrix. These may include stretching, tearing, cavitation, fracture or disbanding, but these mechanisms are secondary to shear yielding of the primary phase. [45]

However, a portion of the elastomer remains soluble in the cured epoxy matrix, slightly degrading properties such as glass transition temperature, modulus and strength retention in hot-wet conditioning. In order to be effective, the modulus of the rubber particles must remain sufficiently low, limiting the amount of epoxy that can be dissolved in the rubbery

phase. [46] Rubbery particle additions are also ineffective in toughening systems with a high cross-link density such as those produced by tetra-functional epoxy resins. [47]

2.3.3.2 Thermoplastic toughening

The advantage of thermoplastic tougheners is that they do not reduce the matrix glass transition temperature or modulus. Thermoplastic tougheners phase separate during the cure of thermosetting adhesives and can result in either co-continuous or dispersed droplet morphologies based on their volume fraction.

The degree of toughening is dependent on the thermoplastic mechanical properties and on the phase morphology. Most thermoplastic tougheners are selected so that they will not decrease the modulus of the thermoset material that it is modifying. In the case of epoxy toughening with phenoxy, the toughener modulus is 1.9 GPa whereas the modulus of the epoxy based on bisphenol A (Epon 826) is 3.0 GPa. As opposed to thermoplastic additions with moduli comparable to the epoxy modulus, the modulus mismatch can cause stress concentrations that lead to enhanced shear yielding. [48] For thermosets toughened with high modulus thermoplastics such as poly(ether imide) or poly(ether ether ketone) with pendent methyl groups (PEEKM), the primary toughening mechanism is the bridging, drawing and fracture of thermoplastic. [49] [50] [51]

2.3.3.3 Rigid particle toughening

Fillers are frequently incorporated into epoxy resin formulations to modify processing characteristics such as viscosity, density or color as well as modest improvements in fracture toughness. Rigid particle fillers added to adhesive formulations dissipate fracture

energy through transparticle fracture, debonding or crack deflection. Silica particles are impenetrable to advancing cracks and result in crack pinning. The crack front bows out between neighboring particles, the length of the crack front is increased. Recent studies have shown that for low filler volume fractions the increase in toughness is proportional to the derivative of the strain energy increase required to bow out the crack with respect to the interparticle spacing. [44] To decrease interparticle spacing while preserving the same filler volume fraction, recent inorganic filler research has focused on nano-scale silicate particles. [52]

2.3.4 Matrix Adhesive

In addition to bonding substrates together, adhesives are also used as the matrix material in fiber-reinforced plastic composite materials. Their primary role is to transfer loads between fibers and to maintain the fiber structure, particularly when subjected to compression loading. The matrix also provides toughness, damage tolerance, impact resistance, and protection from the environment.

The mechanical properties of fiber-adhesive composite laminates depend on a number of factors including volume fraction, orientation moduli and strength. Fracture toughness depends not only on these constituent material properties but also on their interface. The interface between the matrix resin and the reinforcing fibers is a key aspect of composite material design. Shear loads are transferred from the matrix to the reinforcing fibers through the interface, and composite material optimization involves the modification of several features to improve the matrix/fiber interface performance. [53]

2.4 Relevant Research

Adhesively bonded assemblies must be able to absorb substantial amounts of mechanical energy prior to failure. The weakest mode of adhesive bond strength is Mode I, cleavage. Therefore, the selected adhesive must exhibit a combination of strength and toughness. [4]

A significant amount of research has been conducted in the area of IPNs, and several commercial products have been developed as a result of this research. These applications include automotive parts, sheet molding compounds, insulation, artificial teeth, damping compounds and medical dressings. [54]

Strong, tough adhesives have been produced through the use of IPNs. A German company, Polymerics GmBh, has developed an IPN adhesive that uses elevated temperature cure systems that initiate at different temperatures to produce their PX-100 IPN adhesive. Literature on the company web site indicate that a synergistic interaction between the tensile strength and impact strength of the individual IPN constituents (see Figure 19). [55]

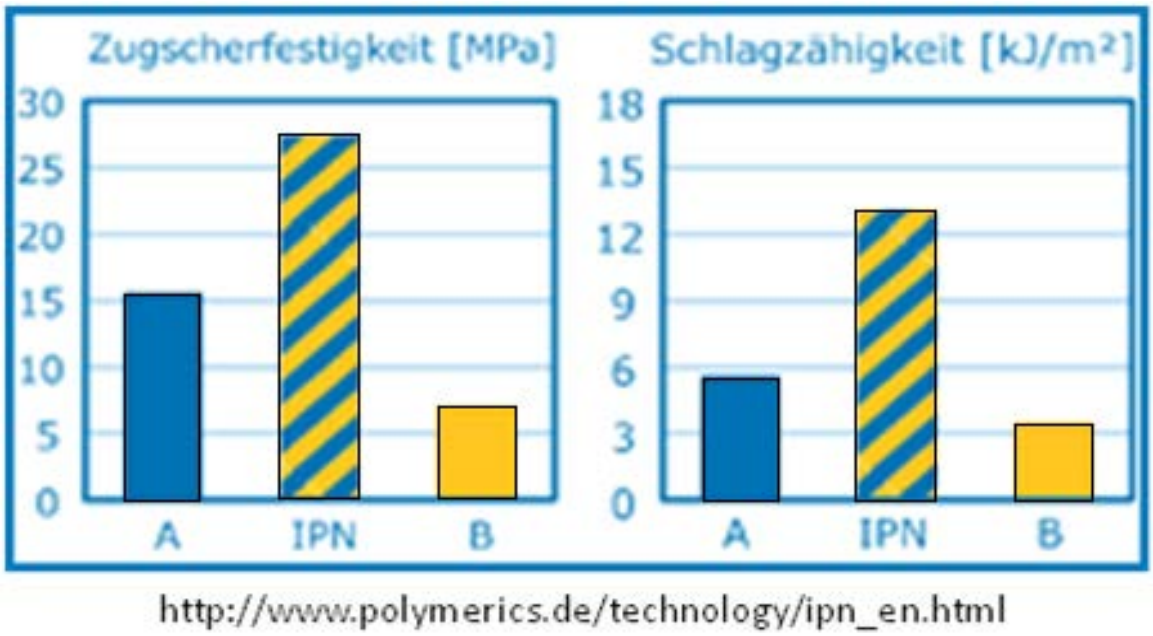

Figure 19: Polymerics GmBh PX-100 IPN adhesive properties

Unlike polymer blends, IPNs offer the capability to maximize the effective properties of constituent networks with the possibility of avoiding unwanted properties. It has been established that when a sequential IPN is created, the network which cures first establishes the strength of the system. Since it is still highly deformable, the monomer for the second polymer network is easily rearranged to decrease the inner stresses in the forming network. Due to restrictions imposed by the initial network, the second polymer network cures at a low rate, minimizing internal stresses. The network which cures second, therefore, plays the role of plasticizer. [56]

A number of researchers have investigated IPNs that are produced from a combination of radiation cured acrylate and thermally cured epoxy components. The key findings from relevant investigations are summarized in Table 1.

Table 1: Radiation/thermal cure acrylate/epoxy IPN investigations

Ref	*Year*	*Title*	*Key Findings*
57	2009	UV and Thermal Curing Behaviors of Dual-Curable Adhesives Based on Epoxy Acrylate Oligomers	The epoxy backbone imparts toughness to the cured films, while the carbon–carbon and ether bonds ameliorate their chemical resistance. The shrinkage of the dual-curable adhesives increased with increase in curing rate, but decreased with increase in thermal-curing agent content.
58	2008	Curing Kinetics and Morphology of IPNs from a Flexible Dimethacrylate and a Rigid Epoxy via Sequential Photo and Thermal Polymerization	When the dimethacrylate component was photocured first, the rate was reduced, but almost complete conversion could be attained. When the epoxy was cured first, photopolymerization was limited by vitrification.
59	2007	Structure-Property Relationships in Acrylate/Epoxy Interpenetrating Polymer Networks: Effects of the Reaction Sequence and Composition	Acrylate/epoxy IPNs formed with a range of compositions and different reaction sequences exhibit a range of conversion, physical properties and morphology. IPNs had higher values than single monomer systems, and reacting the acrylate first generally produced higher properties.
60	2006	Small Angle Neutron Scattering and Dynamic Mechanical Thermal Analysis of Dimethacrylate/Epoxy IPNs	The phase structure of an IPN is strongly dependent on the miscibility of its components. Some systems clearly phase separated, exhibiting two tan delta peaks with a phase separation of 180 angstroms.
61	2006	The Effect of Interpenetrating Polymer Network Formation on Polymerization Kinetics in an Epoxy-Acrylate System	If one polymer is formed before the other, it exerts a significant effect on the subsequent polymerization. This effect is more pronounced for the acrylate system than for the epoxy system.
62	2005	Evaluation of Initiator Systems for Controlled and Sequentially Curable Free-Radical/Cationic Hybrid Photopolymerizations	The onset of cationic epoxy polymerization can be delayed until acrylate polymerization is complete. A potential curing concept might involve transforming resins to a gelled, pressure-sensitive adhesive which can then be further cured to a solid structural adhesive.

63	2004	Azo Initiator Selection to Control the Curing Order in Dimethacrylate-Epoxy Interpenetrating Polymer Networks	For isothermal curing, methacrylate conversion is enhanced and epoxy conversion is retained with a post-cure.
64	2003	Kinetics Studies of Hybrid Structure Formation by Controlled Photopolymerization	UV photopolymerization can be used to explore sequential versus simultaneous polymerization conditions for co monomers that cure by different mechanisms. Amines inhibit the cure of cationic polymerization.
65	2002	Effect of Curing Sequence on the Photopolymerization and Thermal Curing Kinetics of Dimethacrylate/Epoxy Interpenetrating Polymer Networks	When the epoxy component was thermally cured first, dimethacrylate conversion was limited by vitrification or topological restraint.
66	2000	Interpenetrating Polymer Network (IPN) Adhesives for Electron Beam Cure	IPN toughness was nearly double that of the individual monomer adhesives. CTBN toughening can be incorporated into the thermally cured epoxy phase.
67	1980	Homogeneous Epoxy-Acrylic Interpenetrating Polymer Networks: Preparation and Thermal Properties	Single glass transition temperature in IPNs attributed to miscibility of the two networks and to hydrogen bonding

These key findings can be summarized as follows:

Curing epoxy component first

- Acrylate or methacrylate conversion is limited by IPN vitrification
- IPN properties were higher than properties of the individual single component networks

Curing acrylate component first

- Epoxy monomer results in a reduction in the acrylate curing rate

- Acrylate network produced exhibits a higher degree of conversion than produced from a pure acrylate system
- Epoxy network conversion was slightly reduced
- IPN properties were higher than properties of the individual single component networks and generally higher than the epoxy-first networks

Phase structure

- Phase structure is dependent on miscibility of monomers
- For sequential IPNs, the first network to form affects the formation of the second

3. Proposal and General Hypothesis

It is proposed that an improved adhesive for fiber reinforced metal structure can be produced with a sequential Interpenetrating Polymer Network (IPN) where the first network is formed by electron beam cured acrylates and the second network is formed by thermally cured epoxies. Furthermore, it is proposed that the IPN be composed of a strong, stiff acrylate and a tough, flexible epoxy. Based on the literature review, this combination has not been investigated.

> ***Hypothesis: The acrylate network produced by electron beam cure minimizes thermal residual stresses and provides strength while the flexible epoxy network and the IPN morphology provide toughness.***

Several synergistic phenomena originate from this selection, including:

- The presence of epoxy monomer reduces the rate of the normally fast acrylate reaction and enables more diffusion, increasing the degree of acrylate conversion. There is no apparent effect on the degree of epoxy conversion. [61]
- Bisphenol A backbones for both the acrylate and epoxy resins should enhance compatibility and minimize their interaction parameter. [68]
- Bisphenol A backbones for both the acrylate and epoxy resins should enhance compatibility and minimize their interaction parameter.
- Electron beam radiation will not initiate the epoxy cure.

Several researchers have investigated this type of IPN system (see table 1), but their work has primarily been limited to characterization of bulk properties rather than the

investigation of an IPN for adhesive applications. Additionally, nearly all of the IPNs researched involve flexible acrylate systems coupled with strong epoxy systems.

3.1 Research Goal

It is proposed that the IPN adhesive composed of an electron beam cured first component and a thermally cured second component will provide synergistic performance. The goal of this research effort is to investigate and characterize that synergy. In order to optimize performance, bulk adhesive will be tested to determine basic properties. The origin of these properties will be explored by characterizing the bulk adhesive composition and morphology, and these characteristics will be tied back to fundamental scientific principles.

3.2 Research Scope

The scope of this investigation is primarily limited to the use of an acrylate-epoxy IPN adhesive for bonding metallic and carbon fiber reinforced plastic substrates. IPN systems developed through the use of components other than acrylates or epoxies will not be explored, and the IPN system will be further restricted to electron beam cured acrylates and thermally cured epoxies. Interfaces with solids will be explored, but the major focus will be on the interface with solid substrates. Interaction with other solid forms such as filler particles or fibers will also be considered. The use of an IPN as a matrix adhesive will be touched upon briefly, but it will not be explored in depth.

3.3 Research Objectives

To achieve the research goal the properties of IPN adhesives, their component networks and the synergy between the two component systems will be explored. This involves the following specific objectives.

3.3.1 Develop IPN Adhesive Formulations and Measure Key Properties

The performance of an interpenetrating polymer network emanates from both the properties of the individual IPN components and their interactions. The performance of bulk IPNs as well as their constituents will be investigated to identify parameters leading to optimum performance.

3.3.2 Characterize IPN Phase Separation and Governing Parameters

IPN monomer selection and cure conditions are likely to result in IPN structure changes which will then influence performance properties. The effect of IPN composition variations will be used to identify IPN structure-property relationships.

3.3.3 Propose Origins of IPN Toughening

IPNs can exhibit higher toughness than polymer systems comprised of a single network. Potential mechanisms leading to IPN toughness will be identified and explored to confirm the origin of IPN toughness.

4. Sample Preparation

4.1 Materials Selection

Diglycidyl ether of bisphenol A (DGEBA) is an epoxy resin that is widely used for adhesive bonding, so an acrylated resin with the same backbone – bisphenol A diacrylate (BPADA) – was selected as the primary electron beam curing component. A trifunctional acrylate, trimethylolpropane triacrylate (TMPTA), was selected to increase the acrylate cross-link density. Varying the cross-link density was envisioned as a method to modify the strength-toughness characteristics of the acrylate network. TMPTA has functionality of 3, and the individual chain length segments are shorter than many of the other tri-functional acrylates. Cytec Industries provided samples of one of their bisphenol A diacrylate resins, Ebecryl 600. Sigma Aldrich 246808 was procured as the source of TMPTA.

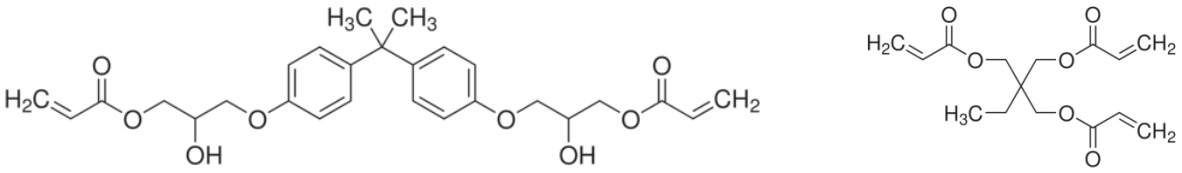

Figure 20: Chemical structures for BPADA (left) and TMPTA (right)

No photo-initiator is necessary for electron beam curing of acrylates. For ultraviolet light curing, 2-Hydroxy-2-methylpropiophenone (HHMP) was selected as the photo-initiator based on a literature survey of photo-initiators used with BPADA that came in a liquid form. It was procured from Sigma Aldrich and was used with BPADA in a weight concentration of 0.3%. [22]

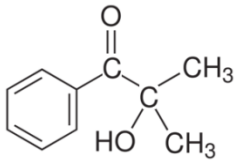

Figure 21: Chemical structure for HHMP photo-initiator

For the flexible epoxy component, two possibilities were considered. The first possibility is bis(3,4-epoxycyclohexylmethyl) adipate (BECA) marketed as Syna Epoxy 28 and previously available as Dow Cyracure UVR6128. BECA is specifically formulated to improve cured resin flexibility and toughness. The second flexible epoxy considered is the combination of diglycidyl ether of bisphenol A (DGEBA) blended with a polypropylene glycol diglycidyl ether (PPGDE) chain extender. Adjusting the relative portions of DGEBA to PPDGE would allow additional flexibility in tailoring the strength-toughness properties of the epoxy network. The DGEBA-PPGDE combination was also selected to minimize the Flory interaction parameter between the Ebecryl 600 diacrylate and the epoxy blends. The DGEBA and PPGDE were supplied as Dow DER 332 and Dow DER 736, respectively, and were procured from Chemical Marketing Concepts. The epoxy chain structures of the candidate epoxies are shown in Figure 22.

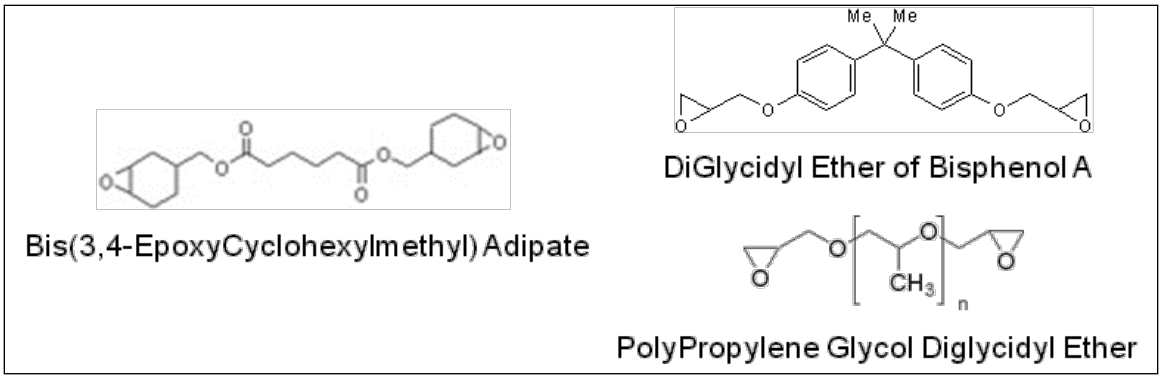

Figure 22: Polymer chain structures for BECA, DGEBA, PPGDE

Amine curing agents are frequently used to polymerize and cross-link epoxy resins. However, amines will also react with diacrylates through a Michael Side Addition reaction, and a thermal curing agent was desired that would react only with the epoxy components. Imidazoles are frequently used in low concentration to accelerate epoxy polymerizations, but they can also be used in higher concentrations as the sole curing agent. The imidazole selected was 2-Ethyl-4-methylimidazole (EMI), procured as Sigma Aldrich E36652. The ratio of EMI to epoxy was selected as 10 wt%. This corresponds to a molar ratio of approximately 25%. Imidazoles cure through an initial adduct reaction followed by an etherification reaction. The temperatures for these reactions were selected as 60 °C and 160 °C, respectively. [19]

EMI was found to be incapable of curing the BECA, presumably due to the structure of the cycloaliphatic epoxides. Therefore, the BECA was cured with methylhexahydrophthalic anhydride (MHPPA). The mix ratio of anhydrides to epoxies is in the range of 50-90 wt% with the precise ratio determined experimentally in order to achieve the desired properties. [18] The ratio of 70 wt% was selected for this study.

Properties of the components of the acrylate and epoxy networks as derived from Manufacturer Safety Data Sheets (MSDS) are shown in Table 2.

Table 2: Properties of IPN Components

Name	Formula	Density (g/ml)	Molecular Weight (g/mol)
BPADA	$C_{27}H_{24}C_8$	1.170	476.15*
TMPTA	$C_{15}H_{20}O_6$	1.100	296.32
HHMP	$C_{10}H_{12}O_2$	1.077	164.20
DGEBA	$C_{21}H_{24}O_4$	1.160	340.41
PPDGE	$C_{12}H_{22}O_5$	1.130	246.30
BECA	$C_{20}H_{12}O_6$	1.149	366.45
EMI	$C_6H_{10}N_2$	0.975	110.16
MHPPA	$C_9H_{12}O_3$	1.162	168.19

* molecular weight not available in MSDS, calculated from chemical formula

4.1.1 Monomer Surface Tension

The surface tension of the IPN components was determined through the use of pendant drop experiments. In the pendant drop method, a fluid drop is suspended from the end of a syringe needle tip. The drop is distorted by the combined effects of gravity and surface tension. If the fluid density is known and the drop shape is determined from a captured video image, then the fluid surface tension can determined by solving the Young-Laplace equation which is listed as Equation 9.

$$\Delta P = \rho g h = \gamma (1/R_1 + 1/R_2) \qquad \text{Equation 9}$$

Where = pressure differential across the liquid-gas interface

= liquid density

g = acceleration due to gravity

h = mean curvature

= liquid surface tension

, = principle radii of curvature of the drops

The pendant drop geometry is shown in Figure 23. Since the fluid is suspended in air, this technique is more accurate than methods like the Wilhelmy plate technique which require a solid surface that is free of contaminants.

Figure 23: Pendant drop geometry

A VCA Optima goniometer from AST Products was used to measure pendant drops. A 100 microliter syringe was used to dispense fluids through a 28 gauge metal needle. Unfortunately, the epoxy and diacrylate monomers have very high viscosity at room temperature, e.g. on the order of 40,000 centipoise for BPADA. [69] For these fluids, a small amount was transferred to the syringe needle with a glass capillary tube. Development of a pendant drop was complicated by the fact that the monomer would flow up the side of the needle until enough volume was accumulated to cause it to flow downware. The viscous fluid then flowed into a drop which took up to an hour to drop from the end of the syringe

tip. This viscous behavior may introduce some error, but the values as determined by the goniometer vision system approached terminal values prior to dropping. An example of the drop movement after flow initiated is shown in Figure 24, and the surface tension values as determined by the goniometer are shown in Figure 25..

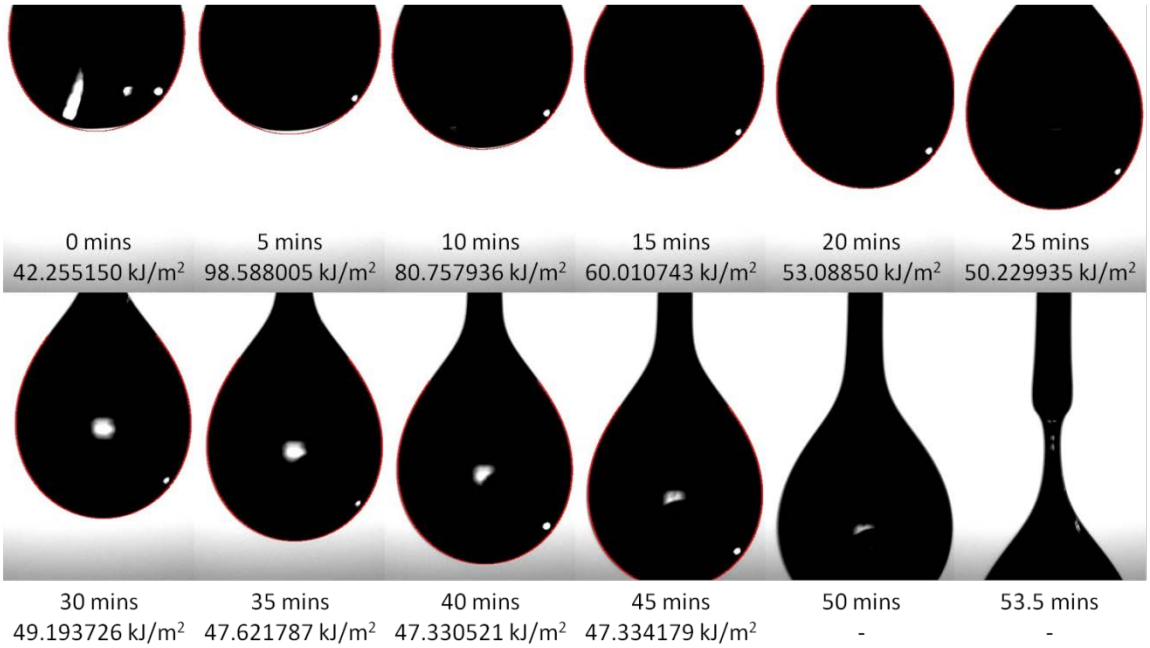

Figure 24: Evolution of BPADA drop shape and calculated surface tension

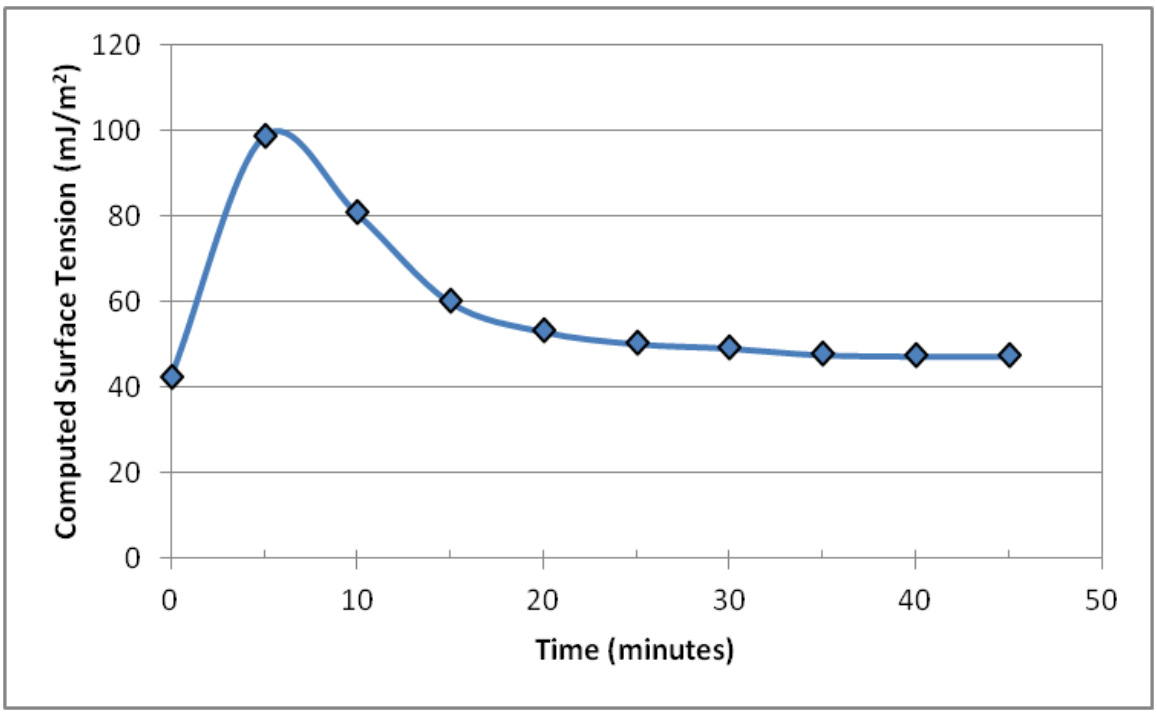

Figure 25: BPADA pendant drop surface tension measurements as determined by AST VCA Optima goniometer

The pendant drop results are shown in Table 3.

Table 3: Surface tension values as determined by pendant drop goniometry

Monomer	Surface Tension (mJ/m^2)	Std Deviation (mJ/m^2)
BPADA	47.534	2 Data Pts, Range = 0.406
TMPTA	34.747	0.128
(80-20)Acrylate	39.522	0.431
DGEBA	48.423	0.376
PPGDE	37.103	0.187
(50-50)Epoxy	40.469	1.129
BECA	45.578	0.504
EMI	36.588	0.291

Literature values are not available for the many of the monomers used, although a few reference points are available. DGEBA procured from Sigma Alrich has been determined to

have a surface tension of 47.2 mJ/m^2, and DGEBA procured as Epon 828 has a surface tension of 44-48 mJ/m2. [7071] TMPTA from Sartomer has a surface tension of 36.1 mJ/m^2. [72] In both cases, the surface tension as measured by the goniometer pendant drop is different than the literature value. Potential sources of error include incorrect calibration of the goniometer or the influence of absorbed air. It may be possible to improve the measurement technique by using PTFE-coated needles and by using needles with a larger internal diameter. However, while the magnitudes may be inaccurate, the relative order between components is expected to be correct.

4.1.2 Monomer Miscibility

Monomer miscibility is approximated by the Flory interaction parameter which was defined in Equation 5 and related to the solubility parameter through Equation 6 and Equation 7. Lower values of the interaction parameter lead to solutions that readily mix due to low free energy of mixing whereas high interaction parameters lead to phase separation. The solubility parameter can be estimated through group-contribution methods as the summation of the values representing the polymer repeating unit. [13]

$$\delta = (\Sigma F_i)/V \qquad \text{Equation 10}$$

Where: δ = solubility parameter

F_i = molecular group molar attraction constant

V = molar volume of the polymer

Using the molar attraction constants developed by Hoy, the solubility parameters were estimated and compiled in Table 4. [13]

Table 4: Solubility parameters for selected monomers estimated by group contribution

Monomer	δ ($MPa^{½}$)
Ebecryl 600	23.8
TMPTA	13.8
DGEBA	21.9
PPGDE	18.4
BECA	14.8
2-4-EMI	23.1
MHPPA	20.8

The difference in solubility parameter between Ebecryl 600, a bisphenol A diacrylate, and diglycidyl ether of bisphenol A (DGEBA) is small, reflecting the similarity of their chemical backbones. To achieve a flexible epoxy, DGEBA is frequently combined with a chain extender, polypropylene glycol diglycidyl ether (PPGDE). A more significant solubility parameter difference will occur if bis(3,4-epoxycyclohexylmethyl) adipate BECA is used in place of the DEGBA/PPGDE combination.

4.2 Electron Beam Bulk Resin Curing

Acrylate and epoxy master mixes were prepared in laboratory specimen jars. The weight of individual components was determined by using the tare function on an electronic scale with readout to the nearest 0.1 gram. The master mixes were heated on a hot plate to reduce their viscosity and then mixed with a wooden stirring stick until visually uniform. They were then placed in a vacuum chamber and subjected to full vacuum to remove air entrapped during the mixing process.

IPN monomer samples involving DGEBA-PPDGE epoxies were created by blending desired weights of acrylate and epoxy master mixes into a 100 ml glass beaker, heating on the hot

plate to reduce viscosity and then subjecting it to vacuum degassing until no visible bubbles remained. EMI was added to the IPN monomer in an amount equivalent to 10 percent of the epoxy weight. The combined mixture was stirred until visually uniform and then subjected to an additional vacuum degassing cycle prior to casting.

IPN monomer samples involving BECA epoxies were created by heating BPADA on a hot plate to reduce the viscosity. BECA epoxy monomer was produced by mixing 100 parts by weight of BECA with 70 parts by weight of MHPPA. The heated BPADA and the appropriate weight of low viscosity BECA/MHPPA mixture was stirred until visually uniform and then subjected to vacuum degassing prior to casting.

4.2.1 Bulk Samples

Approximately 40 grams of the IPN and acrylate compositions were then poured into aluminum weighing tins and degassed one further time in the vacuum chamber. The sample tins were placed inside a box with a 3.2mm aluminum lid which was then placed under a vacuum bag. The sample tins were irradiated under vacuum with electron beams until a dose of 150 kGy was achieved.

The epoxy and epoxy-acrylate compositions were mixed using a similar cycle of weighing, heating, mixing and degassing. The tins of epoxy, epoxy-acrylate and IPN compositions were heated in an autoclave under atmospheric pressure using a cycle of 6 hours at 60 °C followed by 2 hours at 160 °C with a heat-up and cool-down rate of 5 °C/min.

4.2.1.1 Pocket mold samples

The flexural modulus samples were cured in a tool with five rectangular pockets approximately 63.5mm x 114mm x 3.2mm. The tool was produced by waterjet cutting pockets into a 3.2mm thick sheet of aluminum. The lower sides of the pockets were sealed by taping 2.54 mm thick sheets of aluminum sheared to a size slightly larger than the pocket mold opening with Teflon flash-breaker tape. An aluminum lid 1.6mm thick supported by spacers between the pockets was added on top. The flexural modulus samples were cured in a tool with five rectangular pockets approximately 63.5mm x 114mm x 3.2mm. An aluminum lid 1.6mm thick supported by spacers between the pockets was added on top. An image of the pocket mold with cured samples is shown in Figure 26.

Figure 26: Pocket mold with cured samples

4.1.1.2 Bar samples

Fracture toughness single edge notched beam molds were produced from 12.7mm x 25.4mm extruded bars separated by spacers a distance of 4.8mm. The lower mold surface was closed off by using thin (0.5mm) strips of aluminum which were held in place by Teflon flash-breaker tape. The bar mold tool with cast samples is shown in Figure 27.

Figure 27: Bar molds with cast samples

4.2.1.3 Laminate samples

Laminates were produced by wet lay-up of the resin using a balanced [0°/90°] plain weave Fiberlay 1725750 carbon fabric. For each laminate, dry fabric was cut into thirty-two, 203mm x 102mm plies. The target thickness of the finished laminates was 6.35mm. All laboratory surfaces and tools were cleaned with acetone before use. Resin was mixed from master mixes similar to the procedure used for the bulk resin casts except that the vacuum degassing step was not used. Each ply was individually impregnated with resin and then stacked onto a laminate on a caul plate and prepared for bagging according to Figure 28.

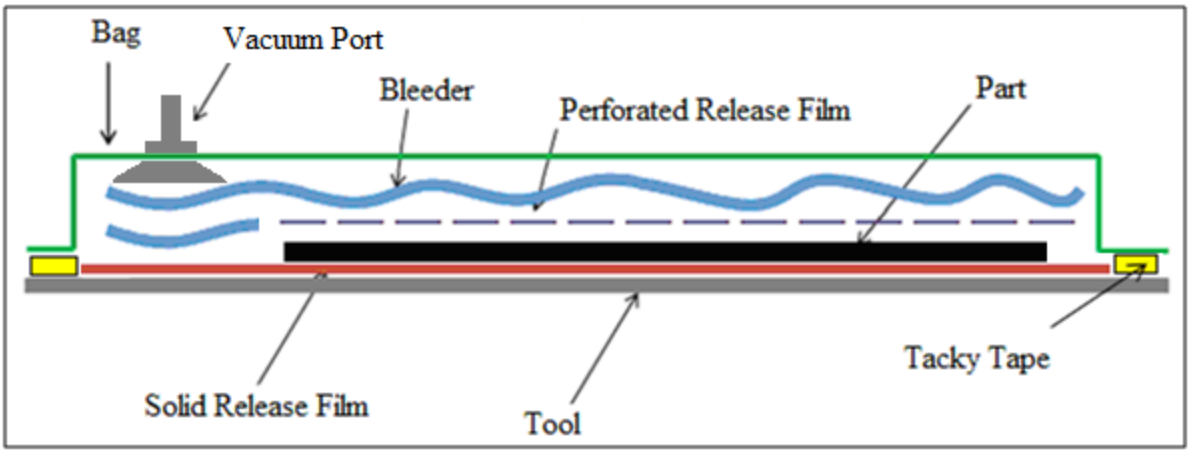

Figure 28: Vacuum bagging procedure for sample laminates

4.2.2 Electron Beam Curing

4.2.2.1 Bulk resin curing

The tool surfaces were coated with mold release compound prior to assembly. After careful filling to avoid air entrapment, the mold assemblies were positioned on an aluminum caul plate and placed under a vacuum bag for electron beam curing. Curing continued until a total dose of 150 kGy was received. Epoxy compositions and the electron beam cured IPN compositions were later heated in an autoclave under atmospheric pressure using a cycle of 6 hours at 60 °C followed by 2 hours at 160 °C with a heat-up and cool-down rate of 2.8 °C/min.

4.2.2.2 Laminate curing

Samples were compacted under vacuum above 600 kPa autoclave pressure at 60 °C for 2 hours. Acrylate and IPN samples were electron beam cured under vacuum until a total dose of 150 kGy was achieved. The IPN laminate was post-cured under vacuum for 2 hours at 160 °C. The epoxy laminate sample was separately cured in one autoclave cycle consisting of 60

°C for 4 hours followed by 160 °C for 2 hours with an autoclave pressure of 0.6 MPa throughout the entire cycle.

4.3 UV Compression Sample Curing

Access to the electron beam curing facility was limited, so ultraviolet (UV) light curing was conducted to explore mechanical properties over a wider range of compositions. BPADA + (50-50)Epoxy was selected as the model system for this investigation.

Ultraviolet radiation was provided by a Magna black light inspection lamp using a Philips E9 bulb. The distance from the bulb to the top of the sample was fixed by use of a face plate bolted onto the lamp assembly.

4.3.1 Compression Sample Tooling

To prepare bulk samples suitable for compression testing, polytetrafluoroethylene (PTFE) tubing with a 12.7 mm inside diameter and a 15.8 mm outside diameter were cut to a length of approximately 32 mm. The tube segments were pushed into an aluminum holding fixture. A sketch of the holding fixture is shown in Figure 29. Grooves were machined into the holding fixture to accept o-rings, but it was discovered that vacuum bag “tacky tape” strips were more effective in sealing the edge of the tube to the holding fixture and to a thin aluminum strip that was used to close the lower end of the tube.

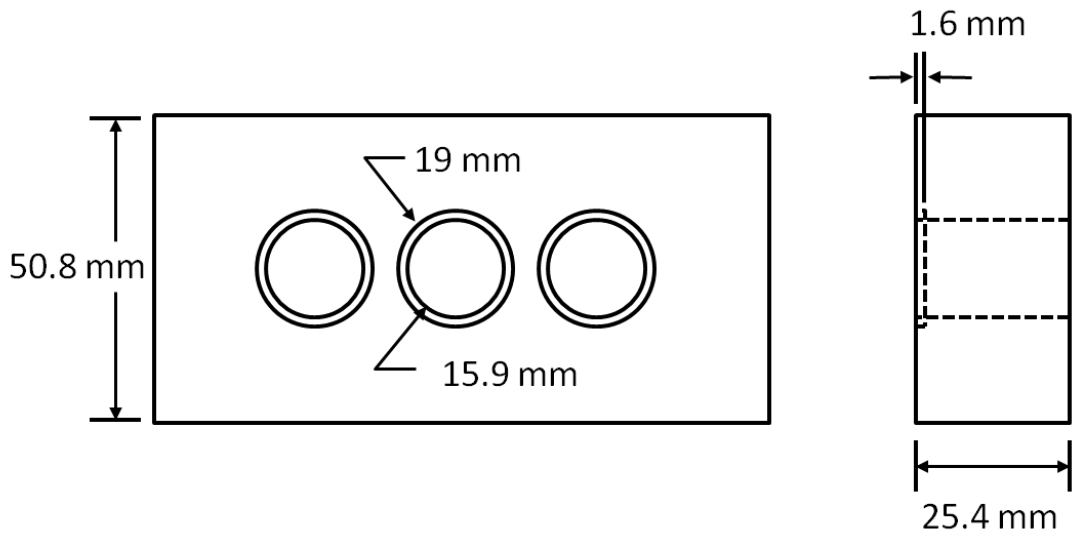

Figure 29: Aluminum holding fixture for PTFE tube segments

4.3.2 UV Bulk Sample Curing

The composition family of BPADA acrylate plus (50-50)epoxy was investigated. BPADA was mixed with approximately 0.3 wt% HMPP photo-initiator. The weight of individual components was determined by using the tare function on an electronic scale with readout to the nearest 0.1 milligram. The acrylate plus photo-initiator master mix was heated on a hot plate to reduce the viscosity and then mixed with a wooden stirring stick until visually uniform. It was then placed in a vacuum chamber and subjected to full vacuum to remove air entrapped during the mixing process. The (50-50) epoxy master mix was produced as previously described.

IPN monomer samples were created by blending desired weights of acrylate and epoxy master mixes into an aluminum weighing tin, heating on the hot plate to reduce viscosity and then subjecting it to vacuum degassing until no visible bubbles remained. EMI was

added to the IPN monomer in an amount equivalent to 10 percent of the epoxy weight. The combined mixture was stirred until visually uniform and then subjected to an additional vacuum degassing cycle prior to casting.

The monomer mixes were carefully poured into the PTFE tube segments to avoid air entrapment. However, a certain amount of air was entrapped during the pouring process. The surface area to volume ratio for these casts was an order of magnitude lower than the surface area to volume ratio for the tensile specimen pocket molds, so degassing after the PTFE molds were filled proved difficult. The mold samples were cured by placing the aluminum holding fixture under a lamp with a Philips black light bulb and subjecting them to UV radiation for 20 minutes. IPN and epoxy samples were then cured using the same 60 °C for 4 hours followed by 160 °C for 2 hours as used with the bulk samples. When the lower cover plate was removed from the first pure acrylate samples following the 20 minute UV cure cycle, the sample surface seemed to be unconverted monomer. Therefore, all of the pure acrylate samples were cured for 20 minutes, the samples were inverted, the lower cover plate was removed, and the samples were subjected to an additional 10 minutes of UV radiation. All cured samples could be extracted from the PTFE tube segments by pushing with light hand pressure.

5. Investigation Results

5.1 IPN Network Formation and Morphology

The physical structure of the bulk IPNs is determined in part by the processes of gelation and vitrification. In pure acrylate compositions cured by electron beam or UV radiation, vitrification seems to begin immediately after gelation. [73] Gelation generally occurs within seconds after the start of radiation whereas properties continue to develop over a more extended period of time. [74]

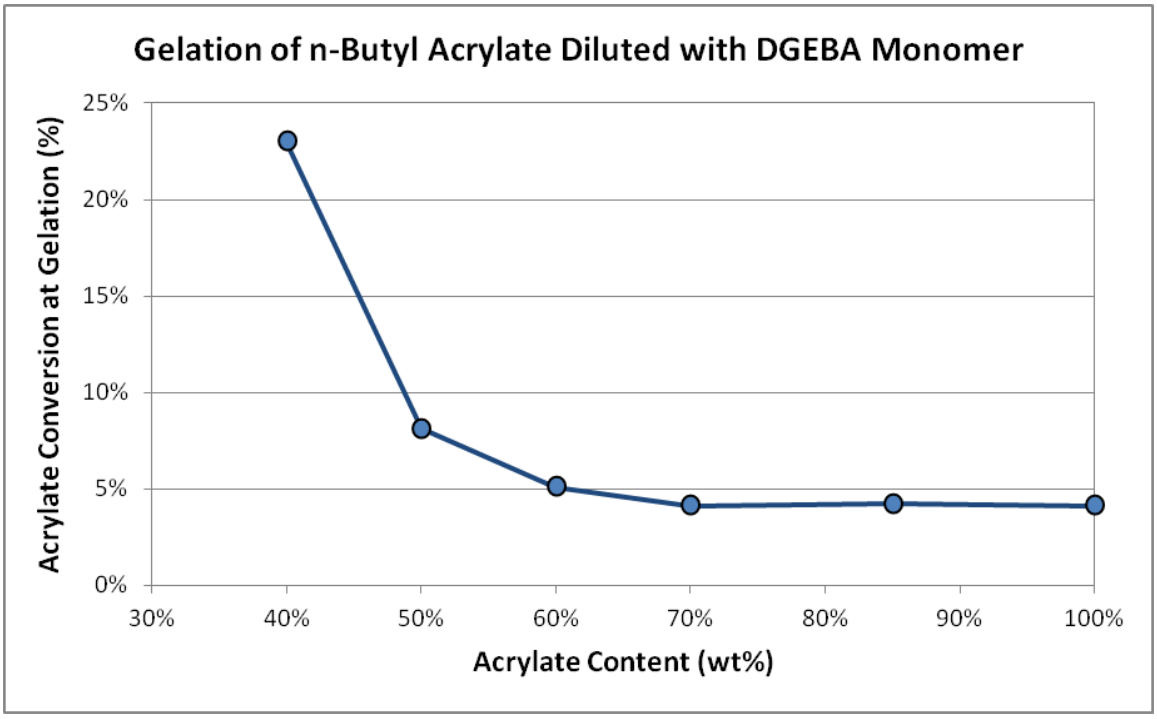

Figure 30: Degree of acrylate conversion at which gelation occurs for thermally cured n-butyl acrylate diluted with varying amounts DGEBA monomer

For in-situ sequential IPNs, the presence of unreacted monomer delays the gelation and vitrification processes. The degree of cure at which gelation occurs for a series of thermally

cured n-butyl acrylate compositions diluted with varying amounts of DGEBA monomer is shown in Figure 30.

As acrylate monomer is converted into an acrylate polymer network, the composition of the monomer mixture changes. The size of the solid polymer globules condensing out of solution is dependent on the solubility mismatch between the growing acrylate polymer and the surrounding monomer solution. A summary of the solubility parameters for monomers used in this research as estimated by the group contribution methodology developed by Hoy is provided in Table 4. Using these values and assuming that triacrylate polymerizes at a rate 1.5 times greater than diacrylate, the solubility parameter mismatch between the instantaneous polymer composition and the surrounding monomer solution is illustrated in Figure 31.

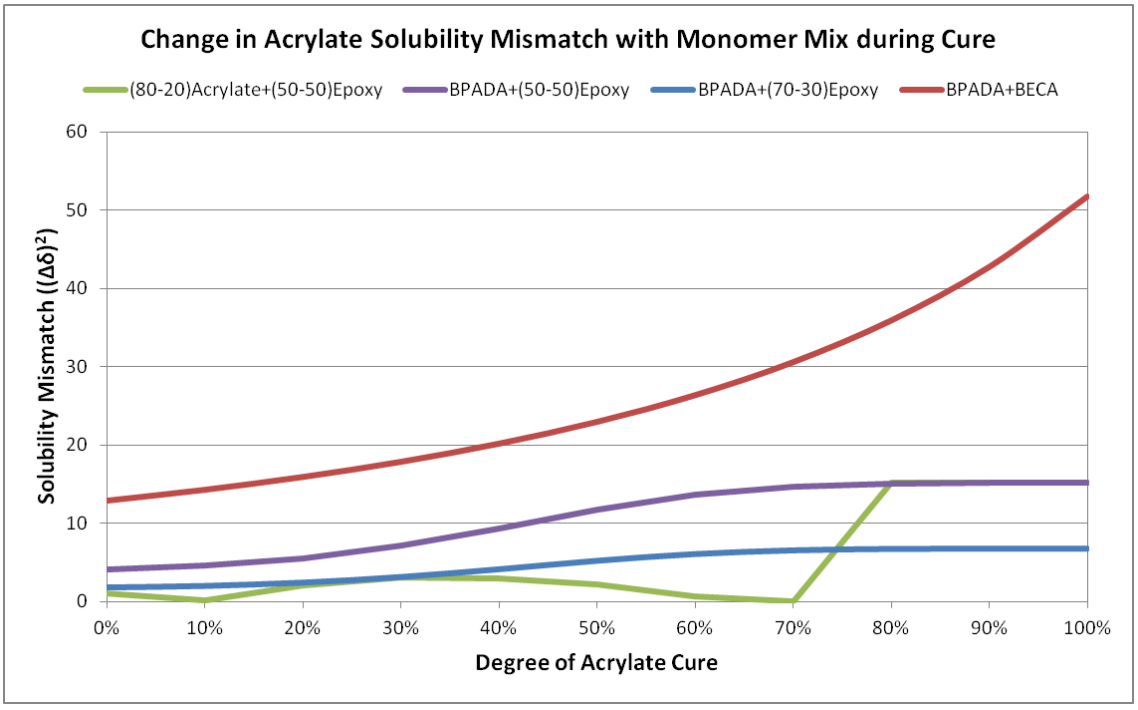

Figure 31: Compatibility of acrylate formation with surrounding monomer mixture as a function of degree of acrylate cure

The presence of TMPTA in the (80-20)Acrylate monomer mixture has a compatibilizing effect until it is exhausted at approximately 70% monomer conversion. The BECA epoxy exhibits the greatest solubility mismatch with the acrylate monomers, and the mismatch continues to grow as acrylate is polymerized. This suggests that the condensed globules or microgels produced during the initial stages of curing should be larger than the microgels produced during the final stages of curing.

5.1.1 SEM

5.1.1.1 SEM Morphology sample preparation

Monomer mix samples were produced by blending the selected acrylate master mix with an equivalent weight of the primary epoxy component (either DGEBA or BECA) with no thermal curing agent. The monomer mix samples were mixed until visually uniform, heated and then vacuum degassed. The monomer mixes were then poured into aluminum weighing tins and placed inside a container under a vacuum bag. The samples were cured to a total dose of 150 KGy.

After the electron beam cure was complete, the cured samples were removed from the tins and cut into sections approximately 6 mm square and then placed into a vial containing acetone. The samples were allowed to soak overnight to remove the un-reacted epoxy. They were then removed from the vial, allowed to dry in air and fractured with a utility knife. The fracture surfaces were mounted on aluminum stubs and sputter coated with platinum prior to viewing with SEM.

5.1.1.2 SEM morphology results

The SEM image for (80-20)Acrylate cured with DGEBA monomer is shown in Figure 32 while the SEM image for BPADA cured with BECA monomer is shown in Figure 33.

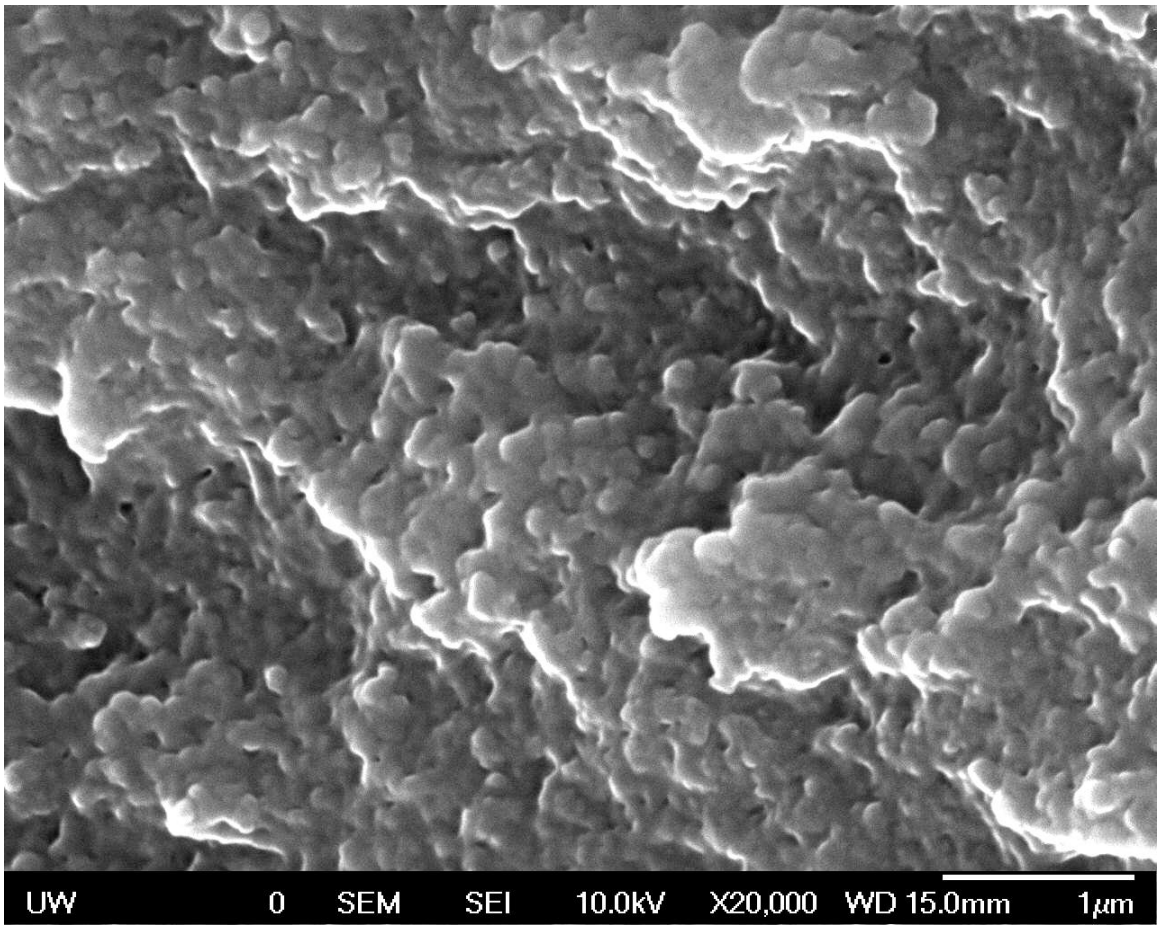

Figure 32: SEM image of (80-20)Acrylate electron beam cured in the presence of DGEBA monomer

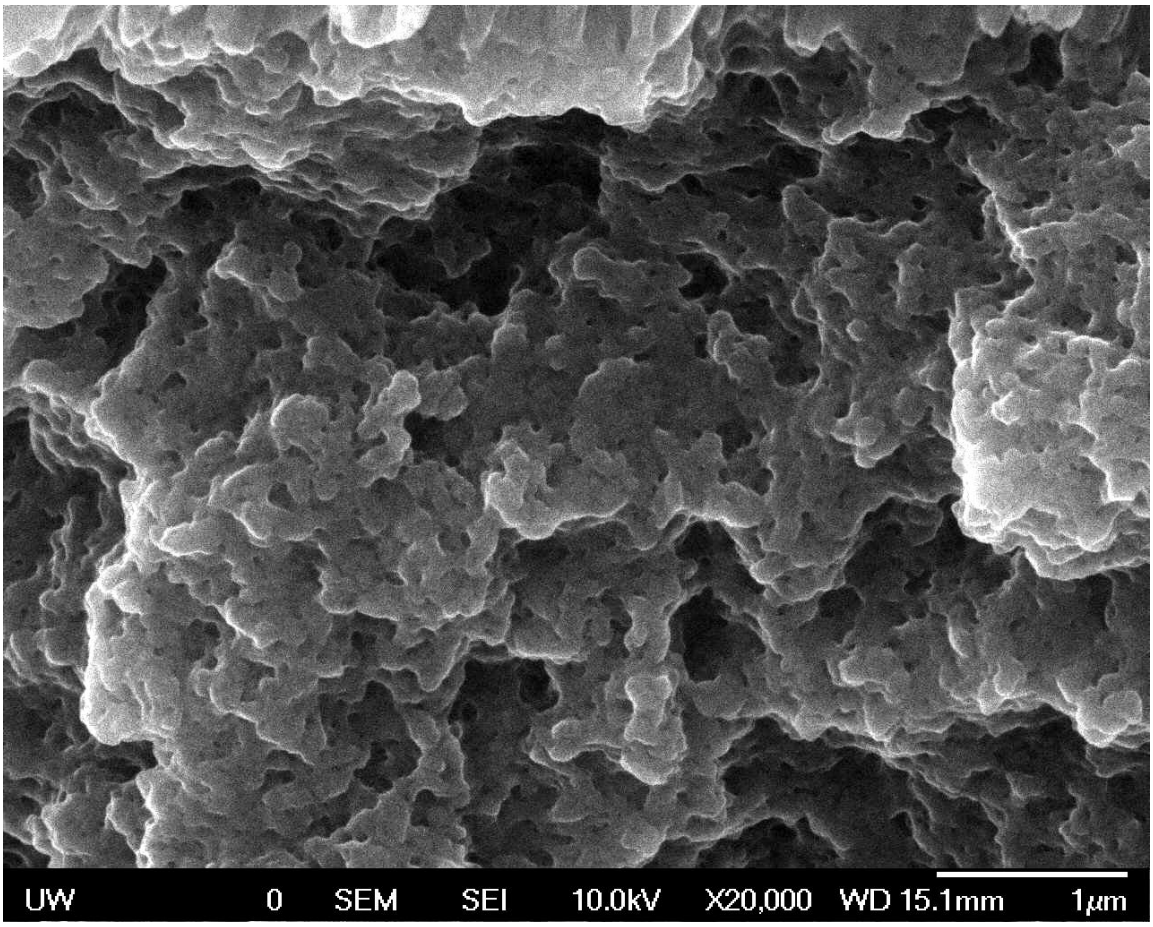

Figure 33: SEM image of BPADA electron beam cured in the presence of BECA monomer

5.1.2 TEM

5.1.2.1 TEM sample preparation

Remnants from three bulk IPN tensile specimens – 58%(80-20)Acrylate + 42%(50-50)Epoxy, 73%BPADA + 27%(70-30)Epoxy and 60%BPADA + 40%BECA – were cut with a slow speed saw to produce 7 mm wide microtome stubs. The microtome slices were shaved from the stubs. They were then mounted to TEM grids and stained with a 4% aqueous solution of osmium tetroxide by suspending the microtome slice top of a drop of solution for 30

minutes. Osmium tetroxide reacts with any remaining acrylate carbon-carbon double bonds which makes acrylate regions darker in transmission microscopy.

5.1.2.2 TEM results

The stained TEM grids were viewed on a Tecnai G2 F20 200 kV scanning transmission electron microscope. The 73%BPADA + 27%(70-30)Epoxy and 60%BPADA + 40%BECA did not show any evidence of staining. The stained area on the 58%(80-20)Acrylate + 42%(50-50)Epoxy as shown in is approximately 20 percent as opposed to the anticipated 60 percent.

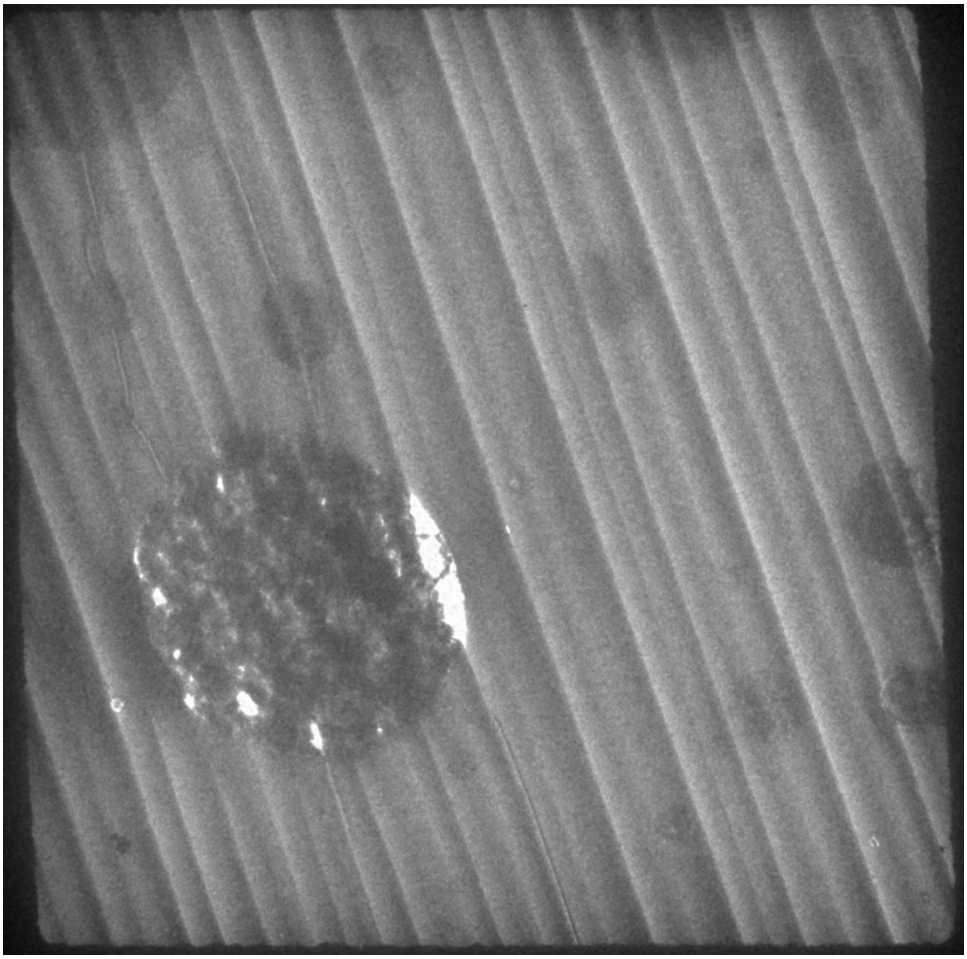

Figure 34: Osmium tetroxide stained sample of 58%(80-20)Acrylate + 42%(50-50)Epoxy

5.1.2.3 TEM discussion

Both acrylate and epoxy are hydrophobic, so the aqueous osmium tetroxide did not have much ability to penetrate the microtome sample. Some references use up to 24 hours for staining polymer samples, and others dilute the aqueous osmium tetroxide with tetrahydrofuran to improve the ability of the osmium tetroxide to be carried to the unreacted acrylate sites. [75] [76] Additional development of a TEM staining technique will be required.

5.1.3 AFM

IPN samples were mounted in epoxy and polished to produce a flat surface. The polished samples were investigated using the tapping mode on a VEECO Dimension 3100 atomic force microscope. Modulus differences between the acrylate and epoxy components as shown in a phase map were used to determine the network structure.

Phase map results for 48%(80-20)Acrylate + 52%(50-50)Epoxy IPN are shown in Figure 35. The acrylate network is represented by the darker brown color, and the epoxy is represented by the golden color. Phase map results for the 50%BPADA + 50%BECA IPN are shown in Figure 36. The acrylate network is represented by the brown color, and the epoxy is represented by the golden color.

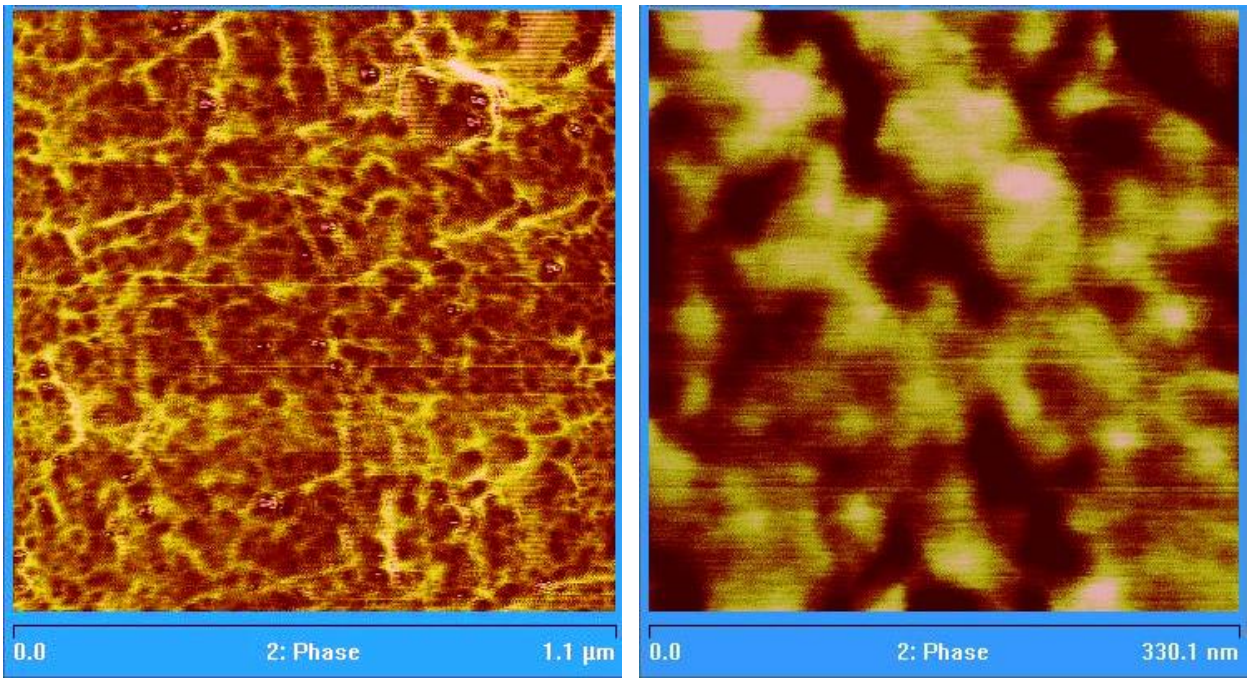

Figure 35: AFM phase maps for 48%(80-20)Epoxy+52%(50-50)Epoxy IPN

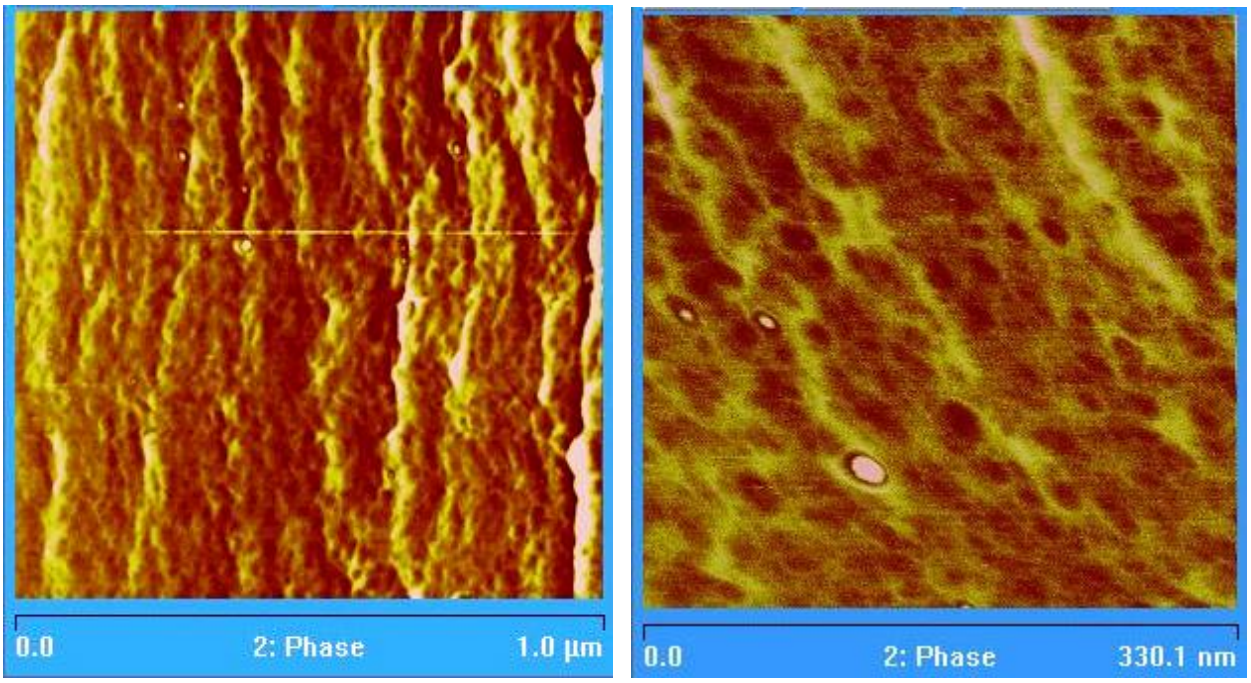

Figure 36: AFM phase maps for 50%BPADA + 50% BECA IPN

Both images show the spherical microgels produced as the electron beam cured acrylate polymer chains condense out of the monomer solution. At the end of the electron beam curing cycle, the acrylate network is fully developed, and the epoxy monomer has been redistributed to spaces between the acrylate microgel agglomerations. As a result, the thermally cured epoxy network fills the spaces around the acrylate network.

While the composition of the IPNs in Figure 35 and Figure 36 are approximately 50 percent acrylate, the size of the acrylate microgels is noticeably larger in the IPNs with the (50-50)Epoxy. This is consistent with the solubility parameter predictions.

5.1.4 Confocal Fluoresence Microscopy

Fluorescence microscopy utilizes the phenomenon that in laser wavelengths around 480 nm, the epoxy network fluoresces whereas the acrylate network does not. Combined with confocal microscopy, this technique may enable three-dimensional imaging of the IPN networks. [77] Spatial resolution on the order of 100 nm is possible. [78] [79] One advantage associated with this technique is the ability to determine the true size of microgel particles rather than relying on the information provided from a two-dimensional cross-section. An image generated using the confocal fluorescence microscope at the University of Washington Nanotech Center is shown in Figure 37. The epoxy network is shown in dark green whereas the acrylate network is shown in light green. Representative dimensions were calculated by scaling the 450nm sample width. The distribution of the acrylate and epoxy networks is consistent with those captured via AFM.

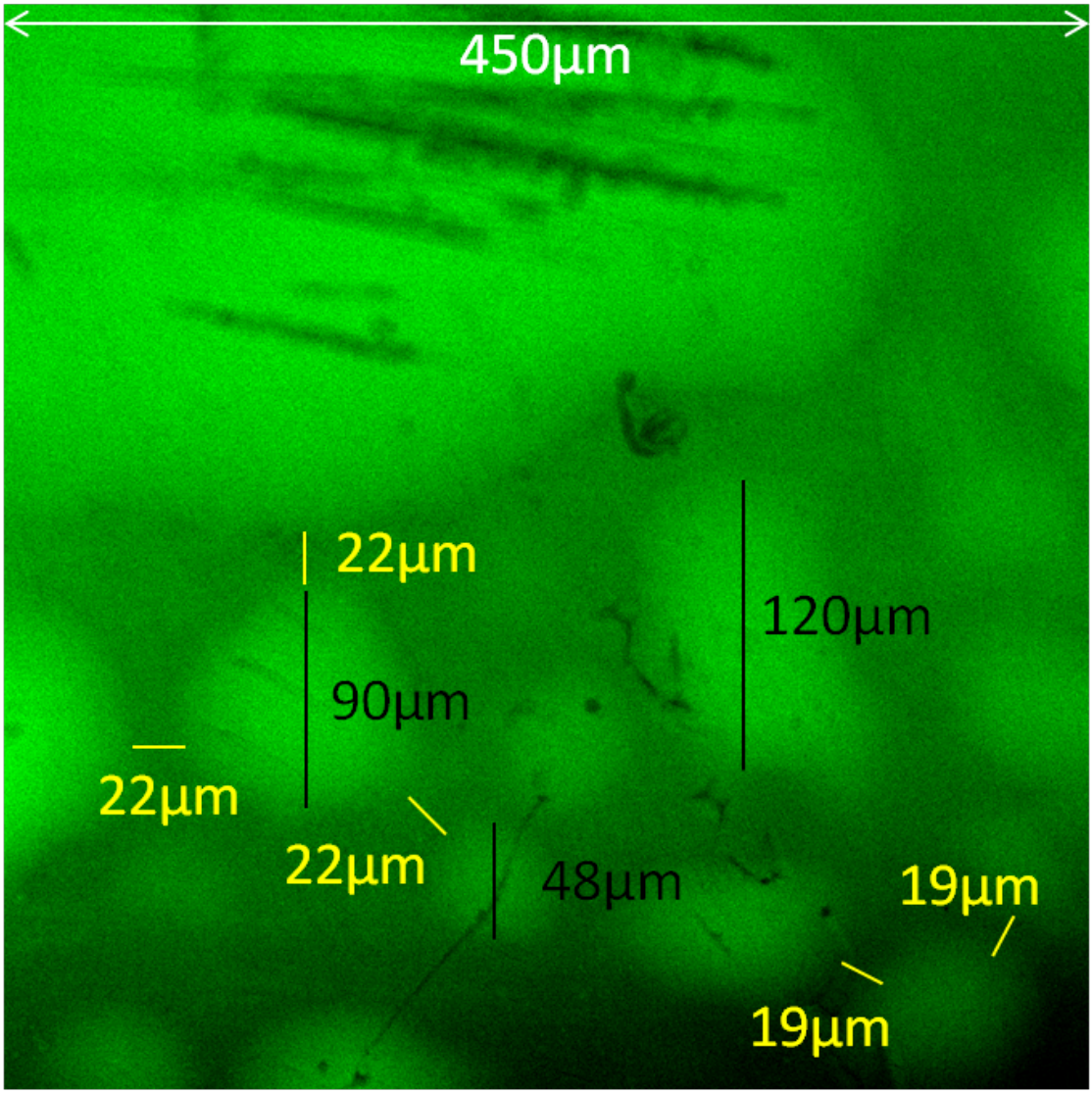

Figure 37: Confocal fluorescence image of electron beam cured 50BPADA + 50(50-50)Epoxy IPN (epoxy = darker green)

5.2 Degree of Cure

5.2.1 Fourier Transform Infrared Spectroscopy

Infrared spectroscopy determines the amount of infrared light absorbed by a sample over a range of wavelengths in order to draw conclusions about the functional groups that are present. Fourier Transform Infrared Spectroscopy (FTIR) uses an interferometer to

determine the amount of infrared light that is absorbed by a sample. Wavenumbers, the inverse of the infrared wavelength, in the 400 cm^{-1} to 1400 cm^{-1} range represent bond bending vibrations whereas wavenumbers in the 1600 cm^{-1} to 3500 cm^{-1} range represent bond stretching vibrations. The simple stretching vibrations are the most characteristic and predictable. [80]

Conventional FTIR studies use a direct path through a sample to collect spectra. With the use of an attenuated total reflectance (ATR) accessory, a crystal interface can be used to gather multiple reflections from a sample that is in direct contact with the crystal. Diamond ATR crystals are popular since diamond has good mechanical properties. The diamond chemical structure absorbs wavenumbers from 1800 cm^{-1} to 2500 cm^{-1}.

Acrylate polymerization proceeds by the opening and subsequent chemical bonding of carbon-carbon double bonds. Therefore, the degree of cure can be determined by tracking the disappearance of the conjugated acrylate carbon-carbon double bonds which have a wavenumber in the range of 1620 cm^{-1} to 1640 cm^{-1}. [59]

5.2.2 FTIR Sample Preparation

Bulk adhesive sample remnants from tensile and fracture toughness tests were measured on a Bruker FTIR with a Pike Instruments GladiATR attenuated total reflectance accessory with a diamond crystal. Prior to measurement, the samples were sanded with 600 grit sandpaper to provide a fresh and flat measurement surface. Background spectra were collected prior to clamping the sample against the ATR crystal. Spectra were then collected

from 4000 cm^{-1} to 600 cm^{-1} using the average of 16 scans. The spectra for BPADA monomer is shown in Figure 38.

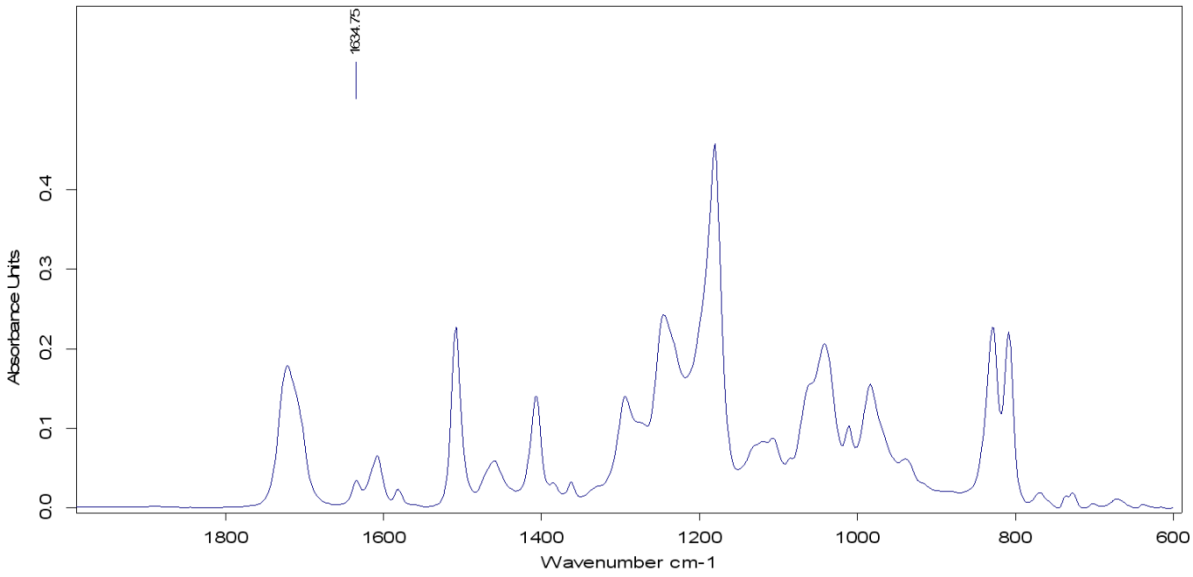

Figure 38: FTIR spectra for BPADA with 1635 cm^{-1} wave number peak identified

5.2.3 FTIR Results

Since the diamond ATR crystal absorbs the wavenumbers from 1800 cm^{-1} to 2500 cm^{-1}, all measurements used the 1800 cm^{-1} wavenumber as a baseline. The highest peak count in the range of 1620 cm^{-1} to 1640 cm^{-1} was used as the measure of the unreacted acrylate carbon-carbon double bonds. The peak was near 1635 cm^{-1} which correlates with techniques used by other researchers. [72] The degree of cure was determined by comparing the sample peak count to the peak count from pure monomer using Equation 11.

$$\alpha = 1 - (\quad) \qquad \text{Equation 11}$$

Where α = degree of monomer conversion

= intensity of 1635 cm^{-1} peak

Two electron beam cured test specimen remnants were selected from different composition ranges for the (80-20)Acrylate+(50-50)Epoxy, BPADA+(70-30)Epoxy and BPADA+BECA material systems. The composition ranges were 35-45 percent acrylate, 45-55 percent acrylate, 60-80 percent acrylate and pure diacrylate. No remnants were available for the BPADA+(70-30)Epoxy material system with a composition below 48%. No relationship was found between degree of cure and acrylate content. Most specimens exhibited a degree of cure in the range of 80-90 percent monomer conversion as shown in Figure 39.

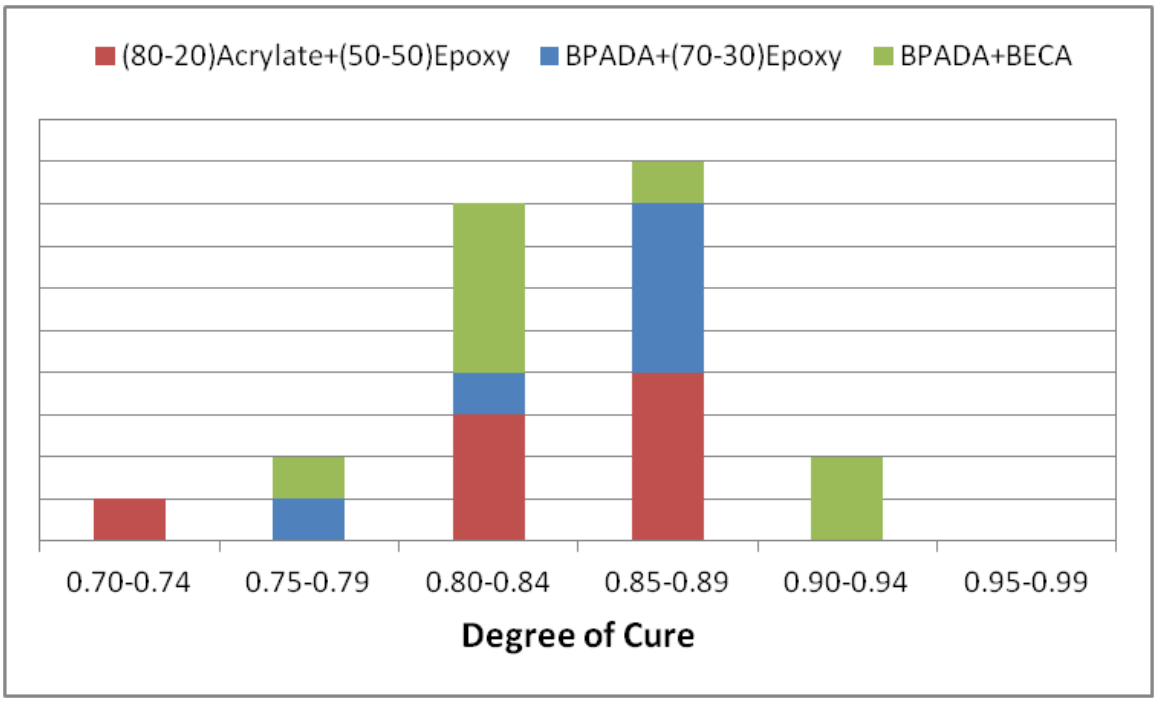

Figure 39: Degree of acrylate monomer conversion for electron beam cured specimens in the (80-20)Acrylate+(50-50)Epoxy, BPADA+(70-30)Epoxy and BPADA+BECA material systems

Trimmed ends from UV cured samples in the BPADA+(50-50)Epoxy material system were also examined by FTIR. One sample was tested from each UV curing batch. The results are shown in Figure 40.

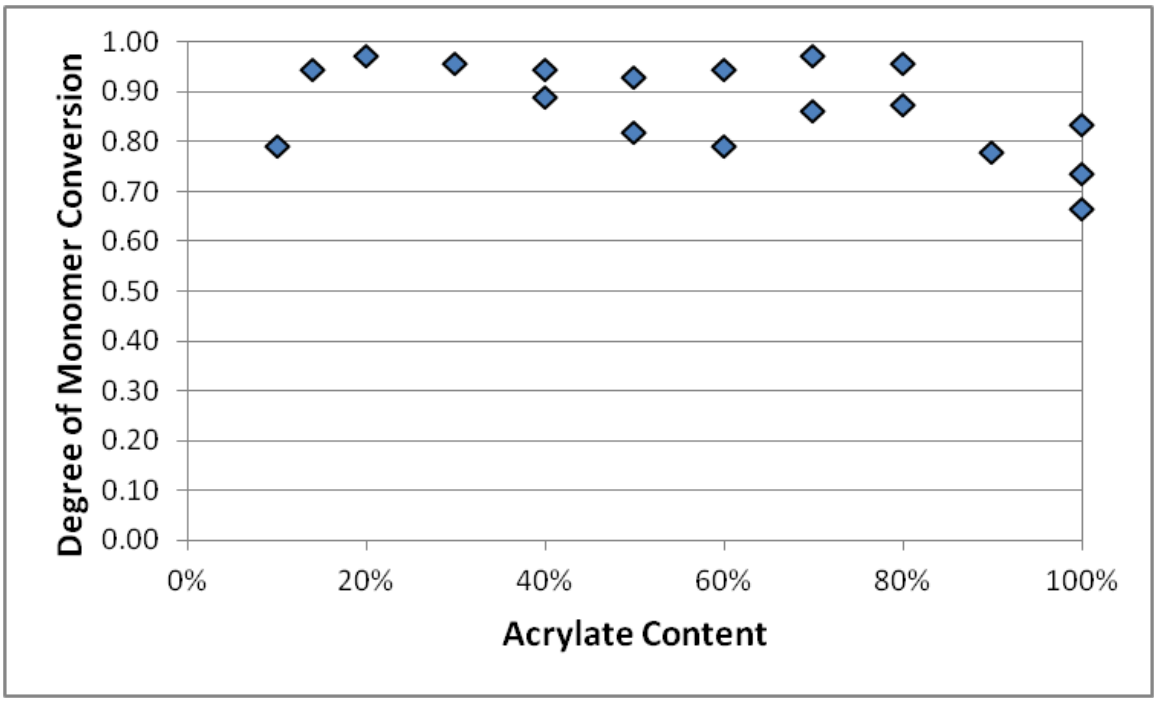

Figure 40: Degree of cure for UV cured BPADA + (50-50)Epoxy material system as determined by FTIR

With a few exceptions, the IPN formulations between 20 percent and 80 percent acrylate averaged at least 90 percent monomer conversion. The formulations at 14 percent and 90 percent acrylate experienced lower conversion, similar to that exhibited by the pure BPADA samples. This may represent the outer range of curing synergy for the BPADA + (50-50)Epoxy. In systems with less than 20 percent acrylate, the acrylate may be too disperse and limited by diffusion distances. In systems with greater than 80% acrylate, the epoxy

concentration may be too low to mitigate the rapid cure and vitrification of the acrylate network.

5.3 Thermal Properties

5.3.1 Glass Transition Temperature

Dynamic mechanical analysis (DMA) measures the response of a specimen to oscillatory forces over a range of temperatures. The material's ability to store energy in the form of elastic deformation versus its ability to lose energy through heat in the form of viscous damping is compared over the temperature range of interest. Free volume changes at the glass transition temperature result in a change in the material's storage modulus and loss modulus. The glass transition temperature can be determined by examining changes in the storage or loss moduli or by examining the ratio between the two (tan delta). Thermomechanical analysis (TMA) uses accurate measurement techniques to determine the dimensional change in a specimen as it is heated. The increase in free volume at the glass transition temperature is marked by an increase in the rate of dimensional change. [81]

Glass transition temperatures were measured primarily through the use of DMA techniques, although some material compositions were also investigated with TMA.

5.3.1.1 DMA Sample Preparation

Remnants from fracture toughness tests were employed to assess the glass transition of the compositions that were tested. A slow speed saw was used to produce rectangular cross section specimens approximately 1.0 mm x 9.5 mm x 17 mm. These specimens were then tested in a Perkin-Elmer Dynamic Mechanical Analyzer (DMA). The specimens were tested

in three point bending using a cyclic load of 125 mN at a frequency of 1 Hz over a temperature range of 30 °C to 170 °C.

Results were analyzed with the DMA Pyris software. Raw data files were also exported to Excel. A minimum of three samples were tested for each composition.

5.3.1.2 DMA Results

The glass transition temperature, T_g, was determined by plotting the logarithm of the storage modulus against the specimen temperature per ASTM D7028-07. [82] A tangent line was drawn from the curve prior to transition, and a second line was drawn tangent to the midpoint of the storage modulus drop. The DMA glass transition temperature was recorded as the intersection of these two tangent lines. This construction is shown in Figure 41.

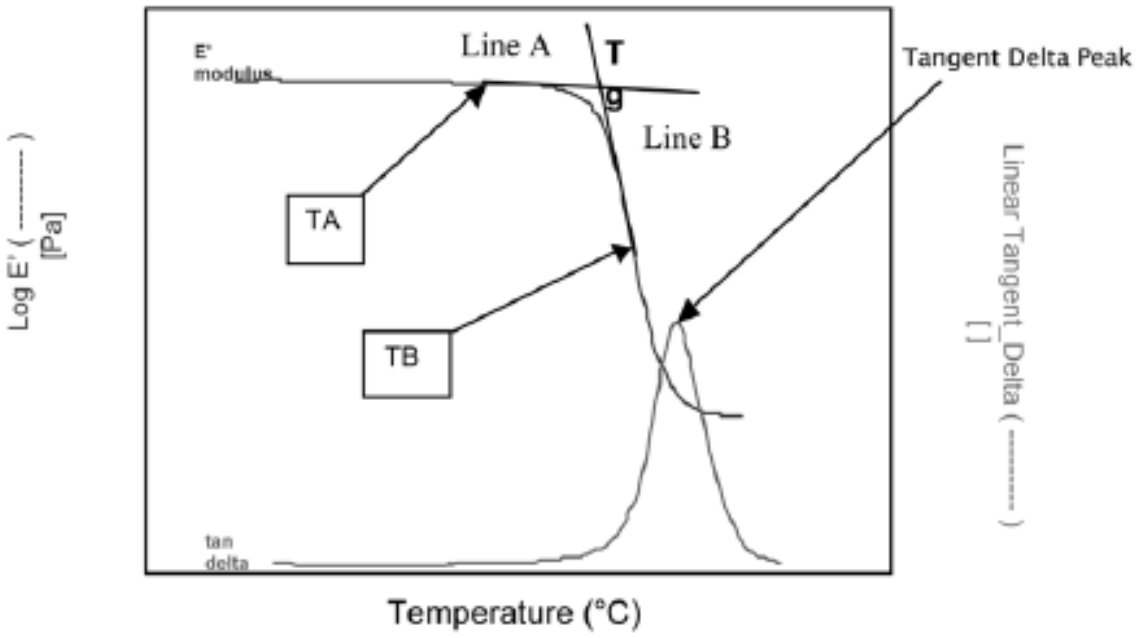

Figure 41: Determination of DMA glass transition and tangent delta peak per ASTM D7028-07

The tangent delta peak, T_t, was determined by recording the temperature corresponding to the peak in the tangent delta curve.

The DMA glass transition and tan delta transition temperatures are listed in Table 5.

Table 5: IPN glass transition and tan delta transition temperatures

Composition	*Glass Transition, T_g, °C*	*Tan Delta Transition, T_t, °C*
(50-50)Epoxy	40.3	63.9
48%(80-20)Acrylate + 52%(50-50)Epoxy	66.4	90.9
(80-20)Acrylate	111.7	137.1
(70-30)Epoxy	101.5	130.1
48%BPADA + 52%(70-30)Epoxy	121.5	142.6
BPADA	79.8	105.6
BECA	76.55	103.6
50%BPADA + 50%BECA	90.95	108.8
BPADA	79.8	105.6

For the (80-20)Acrylate combined with (50-50)Epoxy, the DMA glass transition temperature and the tan delta transition temperature lie between the transition temperatures for the pure (80-20)Acrylate and the pure (50-50)Epoxy transition temperatures. For the BPADA

combined with either (70-30)Epoxy or BECA epoxy, both the glass transition temperature and the tan delta transition temperature are higher than the transition temperatures for the pure acrylate and pure epoxy constituents.

Representative storage modulus (E') and tangent delta DMA curves for three IPN compositions are shown in Figure 42. They indicate single glass transition temperatures.

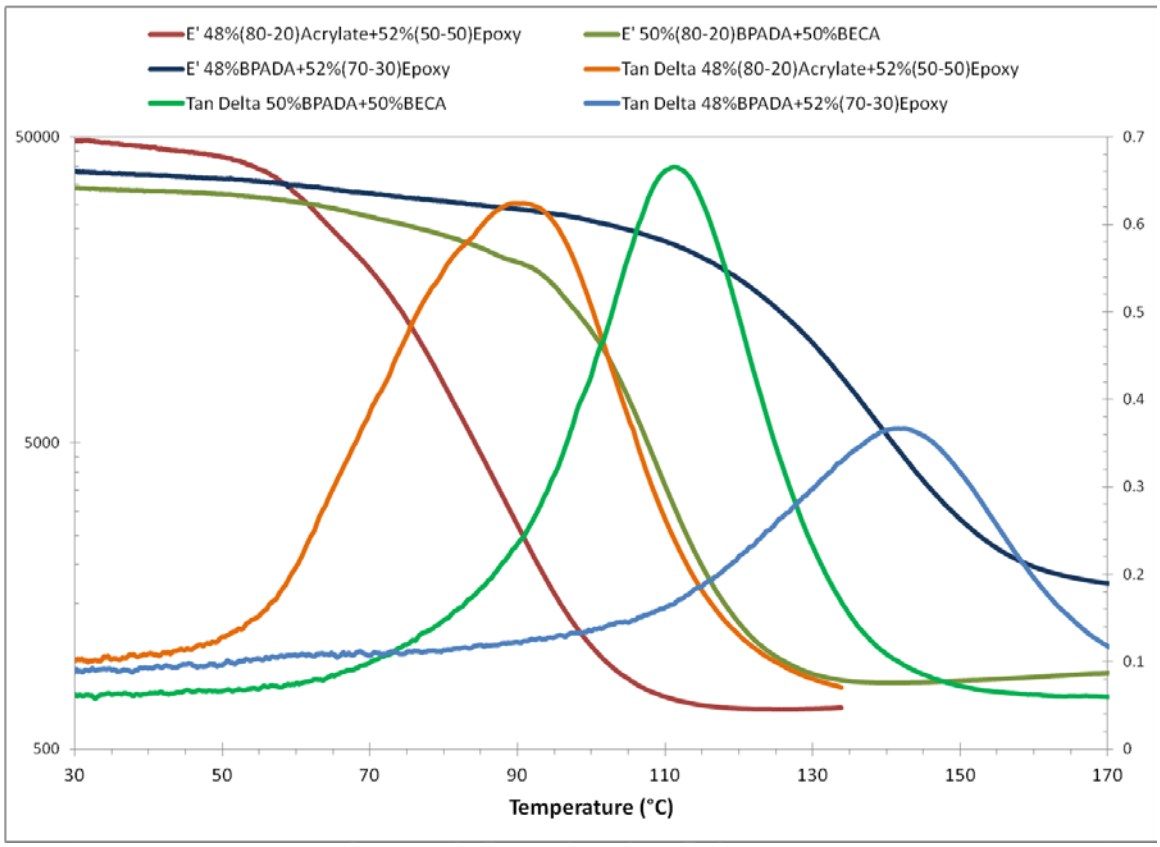

Figure 42: DMA storage modulus and tan delta curves for 50-50 IPNs in (80-20)Acrylate + (50-50)Epoxy, BPADA + (70-30)Epoxy, BPADA + BECA material systems

5.3.1.3 DMA Results Discussion

Comparing the glass transition curves in Figure 42 reveals single glass transition temperature despite the differences in the glass transition temperatures of the individual

networks components. When compared to the partially miscible blend thermal properties shown in Figure 16, this indicates that the acrylate and epoxy network separation occurs at a very small scale.

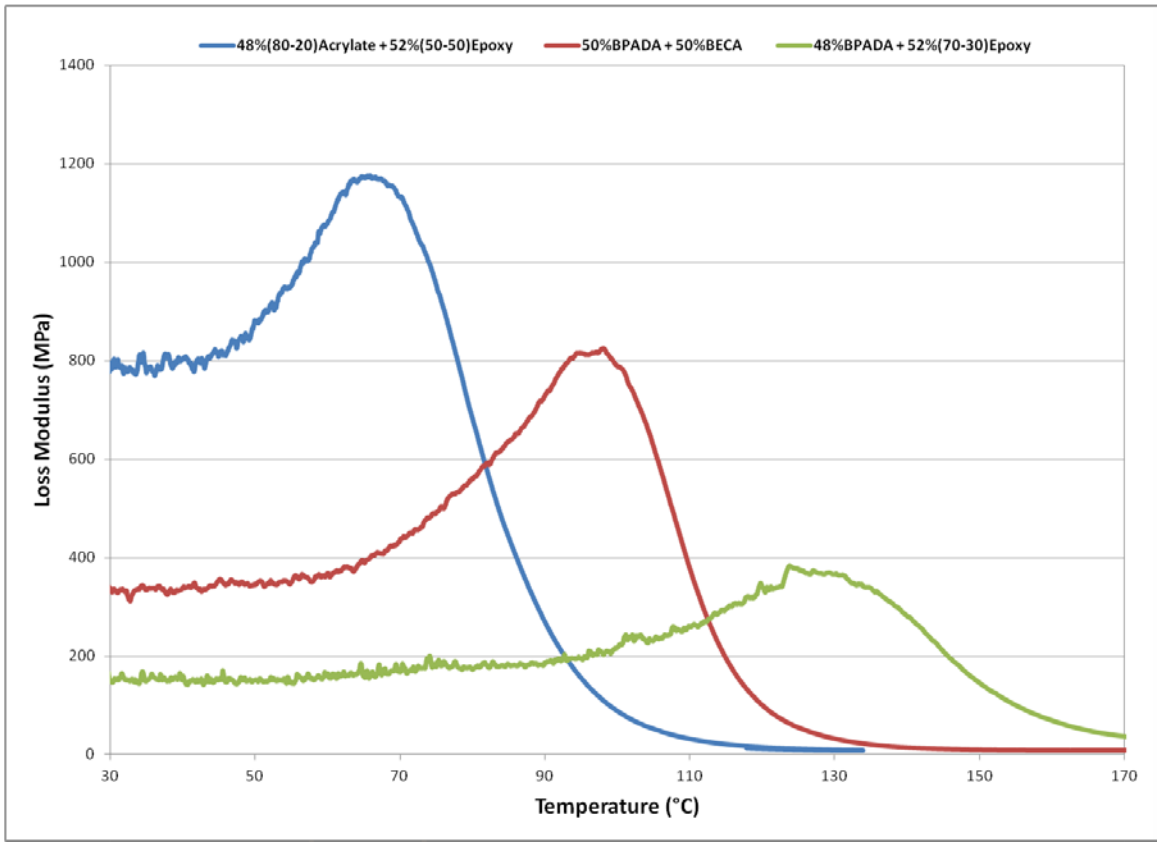

Figure 43: Loss modulus peaks for IPNs representing three different epoxy networks

Values for glass transition temperature versus acrylate weight percentage are shown in Figure 44. It is evident that the glass transition temperature represents a deviation from a linear rule of mixtures.

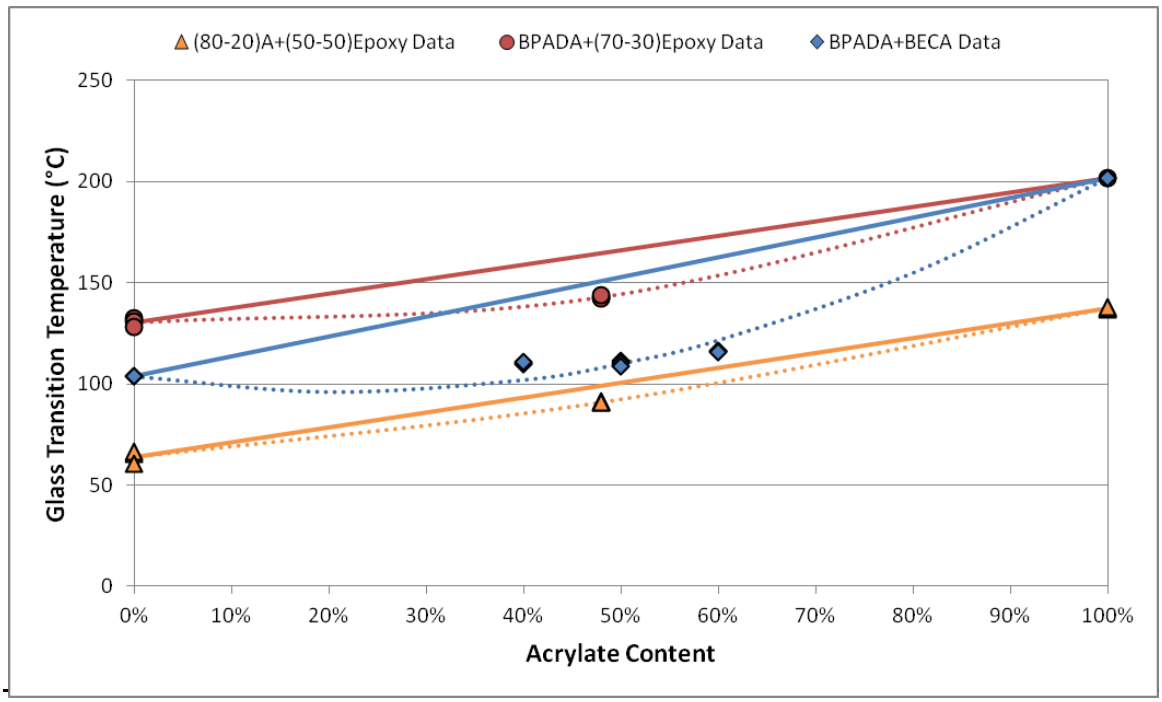

Figure 44: Glass transition temperatures for electron beam cured IPNs

Many binary polymer systems demonstrate this type of compositional dependency. Based on theoretical derivations, several researchers have proposed equations to model the compositional glass transition dependence of binary systems. One model that has been tested against a variety of systems with negative deviation, positive deviation and close approximation of a linear rule of mixtures is shown in Equation 12.[83]

Equation 12

Where:

For miscible polymer blends with compositional glass transition temperatures lower than a linear rule of mixtures, conformational arrangements of the more flexible component weaken the interactions of chain segments from the stiffer component. For this class of polymer blends, the values of the fitting parameters are $a_0 \neq 0$ and $a_1 = a_2 = 0$. An example showing the parabolic deviation from a linear rule of mixtures imposed by the product of the weight fractions ( ) is shown in Figure 45.

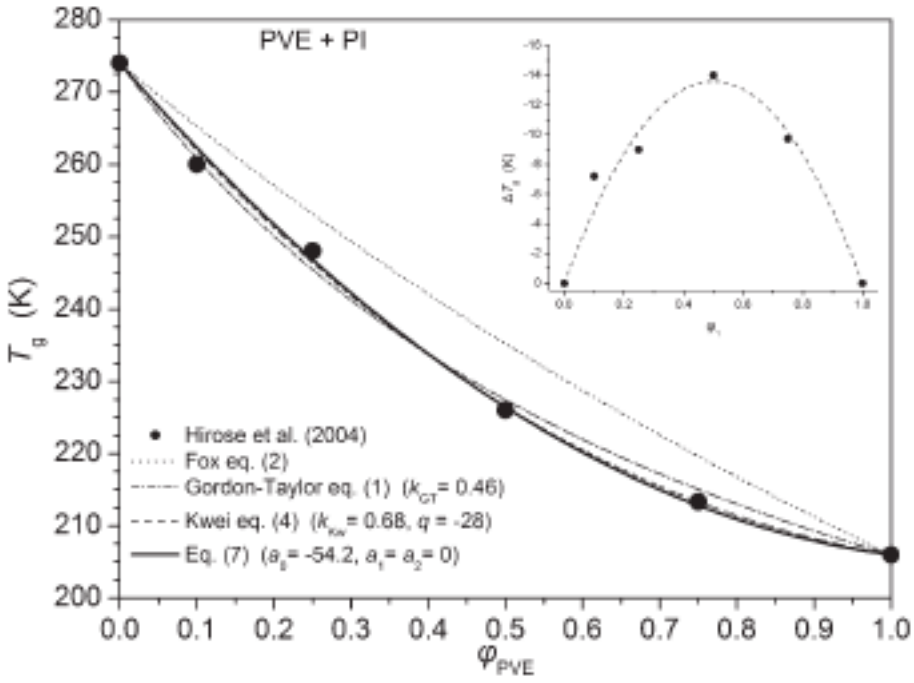

Figure 45: Compositional dependence of the glass transition temperature in a polyvinyl ether + polyimide material system. Inset graph shows the deviation from a linear rule of mixtures. (from [83])

Setting the fitting parameters $a_1 = a_2 = 0$ reduces Equation 12 to the form of equations for compatible polymer blends developed by Couchman from theoretical considerations. [84]

— **Equation 13**

Where:

This equation in turn matches the form of the Jenckel & Heusch equation which was proposed in 1953 based on an empirical fitting of glass transition results:

Equation 14

Where:

5.3.2 Thermal Expansion

Another method for determining the glass transition temperature is to measure the instantaneous thermal expansion coefficient for a sample over a range of temperatures that encompasses the glass transition temperature. The glass transition is determined by a change in the thermal expansion coefficient that corresponds to the increase in free volume at the glass transition. Accurate measurements of thermal expansion can be made with a thermal mechanical analyzer (TMA).

Two different material bonded together will experience a differential thermal expansion from curing temperature to room temperature. This differential expansion produces

thermal residual stresses. The bending of thin bi-material panels can be used as an indicator of the magnitude of the thermal residual stresses.

5.3.2.1 TMA Investigation

TMA Sample Preparation

TMA specimens were prepared from fracture toughness test remnants to confirm the results of the DMA glass transition tests. Individual specimens (one per composition) were cut with a slow speed saw to produce flat, parallel surfaces.

TMA Results

TMA tests were conducted from 25 °C to 150 °C. The results were exported into MS Excel, and plots of probe height versus temperature were produced. Tangent lines were drawn to the linear segments before and after the transition temperature, and the glass transition temperature was calculated as the intersection of the two tangent lines. The TMA glass transition results plus the corresponding DMA glass transition results are shown in Table 6: DMA versus TMA glass transition temperatures.

Table 6: DMA versus TMA glass transition temperatures

Composition	DMA Tg, °C	TMA T_g, °C
(50-50)Epoxy	40.3	55.0
48% (80-20)Acrylate + 52% (50-50)Epoxy	66.4	62.5
(70-30)Epoxy	101.5	104.4

The coefficients of thermal expansion as calculated from TMA thermal expansion curves are shown in Table 7. The thermal expansion information was used to extrapolate the thermal strain that would be induced by the epoxy thermal cure from room temperature to the peak curing temperature of 160 °C.

Table 7: Network component thermal expansion coefficients from TMA data

Composition	T_g (°C)	Sub T_g CTE (µm/m/°C)	Post T_g CTE (µm/m/°C)	ε_T, 25°C–160°C
BPADA	109.5	70.4	152.6	1.43%
(80-20)Acrylate				
(50-50)Epoxy	55.0	143.7	228.5	2.65%
(70-30)Epoxy	104.2	82.4	182.8	1.07%
BECA	76.5	86.6	200.4	2.02%

TMA Result Discussion

Different techniques to determine the glass transition temperature result in slightly different values of the glass transition. For the 48% (80-20) Acrylate + 52% (50-50)Epoxy and (70-30)Epoxy samples, the DMA and TMA glass transition temperatures were reasonably close. For the (50-50)Epoxy sample, however, there was a significant difference although the TMA glass transition temperature was within a few degrees of the tan delta transition temperature. Since the TMA results are based only on a single sample, this difference could also be due to experimental error.

5.3.2.2 Bimaterial Cure

To validate the premise that electron beam curing the acrylate network first would reduce the thermal distortion from reinforcing metallic structure with CFRP, double cantilever

beam (DCB) specimens were prepared with aluminum on one side of the adhesive bond line and a CFRP laminate on the opposite side.

Bimaterial Sample Preparation

A 2.54 mm thick 6061-T4 panel was used for the aluminum adherend side of the joint. It was prepared for bonding with a phosphoric acid anodize (PAA) treatment. The CFRP adherend was prepared by designing a carbon fiber prepreg laminate to match the spring constant of the aluminum adherend. The selected laminate was $[\text{fabric}/0°/90°/0°/0°/90°]_s$. The laminate was cured in an autoclave at 177 °C for 2 hours at a pressure of 0.61 MPa. The laminate tool side surface was then sanded with 60 grit sandpaper and cleaned with acetone prior to bonding.

For the IPN DCB specimen, 0.5 mm aluminum shims were placed in the center and along the edge of the two specimens to provide a consistent bond thickness. An IPN adhesive mix of 48% (80-20)Acrylate + 52% (50-50)Epoxy was degassed and then poured onto the aluminum adherend. The CFRP adherend was closed onto the aluminum adherend in a hinging manner. The DCB assembly was then covered with perforated release, bleeder cloth and a vacuum bag. It was subjected to vacuum pressure for 30 minutes prior to electron beam curing under vacuum until a total dose of 150 kGy was received. Following the electron beam cure, the thermal cure was completed in an autoclave under atmospheric pressure using a cycle of 6 hours at 60 °C followed by 2 hours at 160 °C with a heat-up and cool-down rate of 5 °C/min.

Figure 46: Aluminum adherend with shims prior to bonding with IPN adhesive

For the film adhesive DCB specimen, the aluminum and CFRP adherends were prepared in a similar manner. No shims were used. Hysol EA9696 film adhesive was placed between the two adherends. The DCB assembly was covered with perforated release, bleeder cloth and a vacuum bag. It was subjected to vacuum bag pressure and cured in an autoclave at 120 °C under 0.3 MPa pressure for 2 hours with heat-up and cool-down rates of 5 °C/min.

Bimaterial Distortion Results

The cured DCB panels were removed from the vacuum bag and exhibited significantly different distortion as shown in Figure 47.

Figure 47: Relative distortion of IPN adhesive (front) and file adhesive (rear) specimens

The distortion was quantified by placing a 12 inch (304.8 mm) steel ruler against the exterior edge of the aluminum adherend. The steel ruler was held in contact by rubber bands that were aligned over the contact point between the ruler and the aluminum surface. The chord height displacement at the center of the steel ruler was imaged under an Olympus stereomicroscope, and the markings on the steel ruler were scaled to determine the chord height. The chord height images are shown in Figure 48.

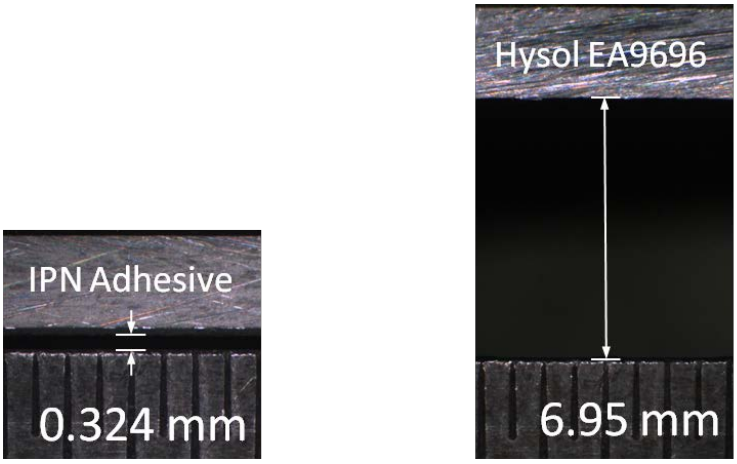

Figure 48: Chord height distortion of IPN adhesive DCB (left) and film adhesive DCB (right)

5.4 Density

Unlike single network systems, the properties of IPNs cannot be solely attributed to the chemical network structure such as the distance between chemical cross-links. With phase

separation on a small scale, a large amount of interface area exists between the individual networks. The nature of this interface will presumably have an impact on the bulk IPN properties.

One aspect of the IPN interface is the packing density or potential interdiffusion of epoxy and acrylate molecules. If the packing density is enhanced at the interface due to chemical similarity or polar attractions, a higher density of bonds should exist in the interface region. In this case, the bulk IPN should exhibit a higher density than would be predicted from a linear rule of mixtures relationship. On the other hand, if the acrylate and epoxy are sterically hindered or exhibit mild repulsion, the bulk IPN should have a lower density. To examine the potential synergy in interface density, the density of samples were measured using the Archimedes method.

5.4.1 Archimedes Sample Preparation

For the electron beam cured IPNs, remnants from SENB fracture toughness tests were salvaged. Samples were trimmed to provide planar edges, and they were visually inspected to verify that they did not contain macroscopic porosity pores. At least two samples were used for each electron beam cured composition tested.

For the ultraviolet cured IPNs, sections without porosity were excised from compression test sample blanks. Only one sample was tested per composition.

5.4.2 Archimedes Measurements

Density is easily calculated once the sample volume and density have been determined, according to Equation 15.

— Equation 15

Where *density*

mass of sample

volume of sample

Samples were held at ambient laboratory conditions prior to measurement. The dry samples were initially placed on a digital scale to record the sample mass. The volume of the sample was determined by submerging the sample in a fluid of known density and determining the weight loss due to the buoyancy effect of the fluid. Volume is calculated using Equation 16.

— Equation 16

Where *weight loss after submergence*

density of fluid

The Archimedes density results for the (80-20)Acrylate + (50-50)Epoxy material system are shown in Figure 49. Near the 50% acrylate IPN composition, the density is greater than the linear rule of mixtures tie line which is shown as a blue dashed line. Deviations of 1 percent from the rule of mixtures are shown as dotted lines.

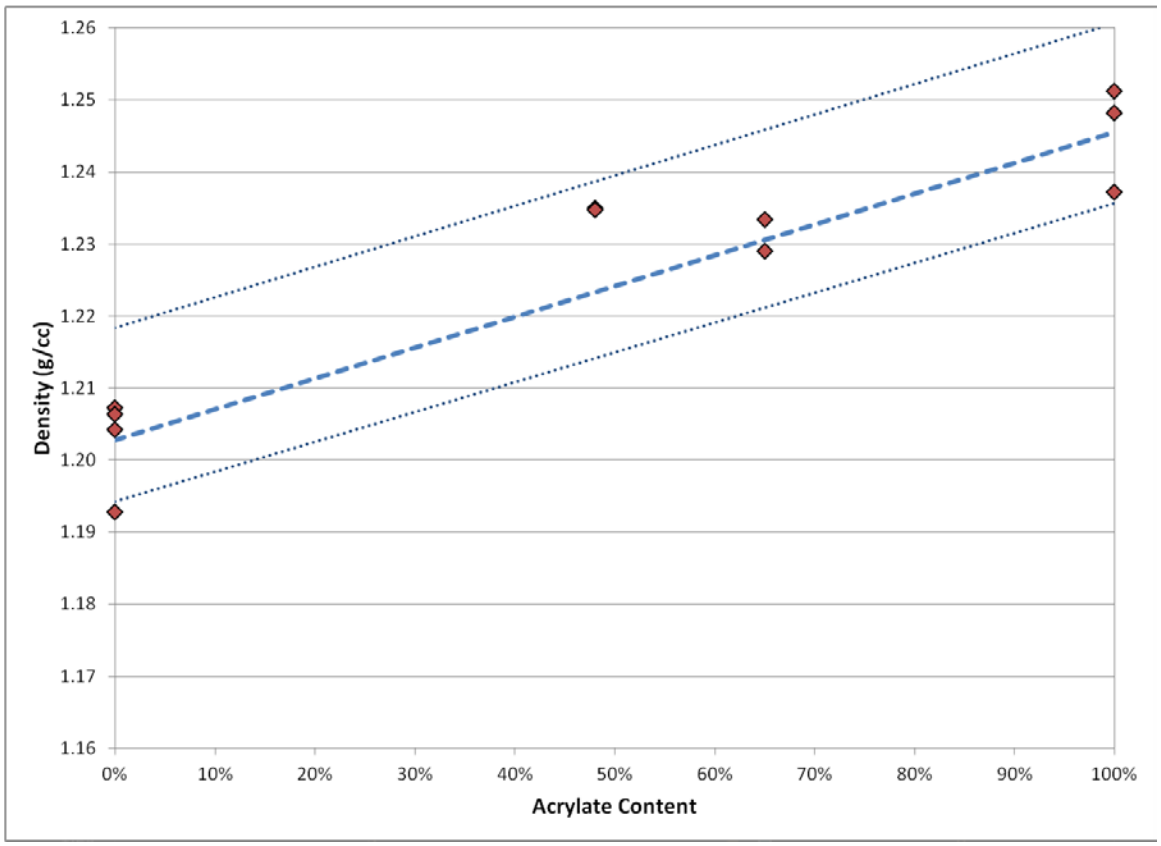

Figure 49: Archimedes density results for EB cured (80-20)Acrylate + (50-50)Epoxy material system

The Archimedes density results for the (80-20)Acrylate + (50-50)Epoxy material system are shown in Figure 50. The rule of mixtures tie line is shown as a blue dashed line, and dotted lines are included to show 1 percent deviations from the rule of mixtures. Although the individual results show a minor deviation from the rule of mixtures, the variation is well within +/- 1 percent and may be due to measurement error.

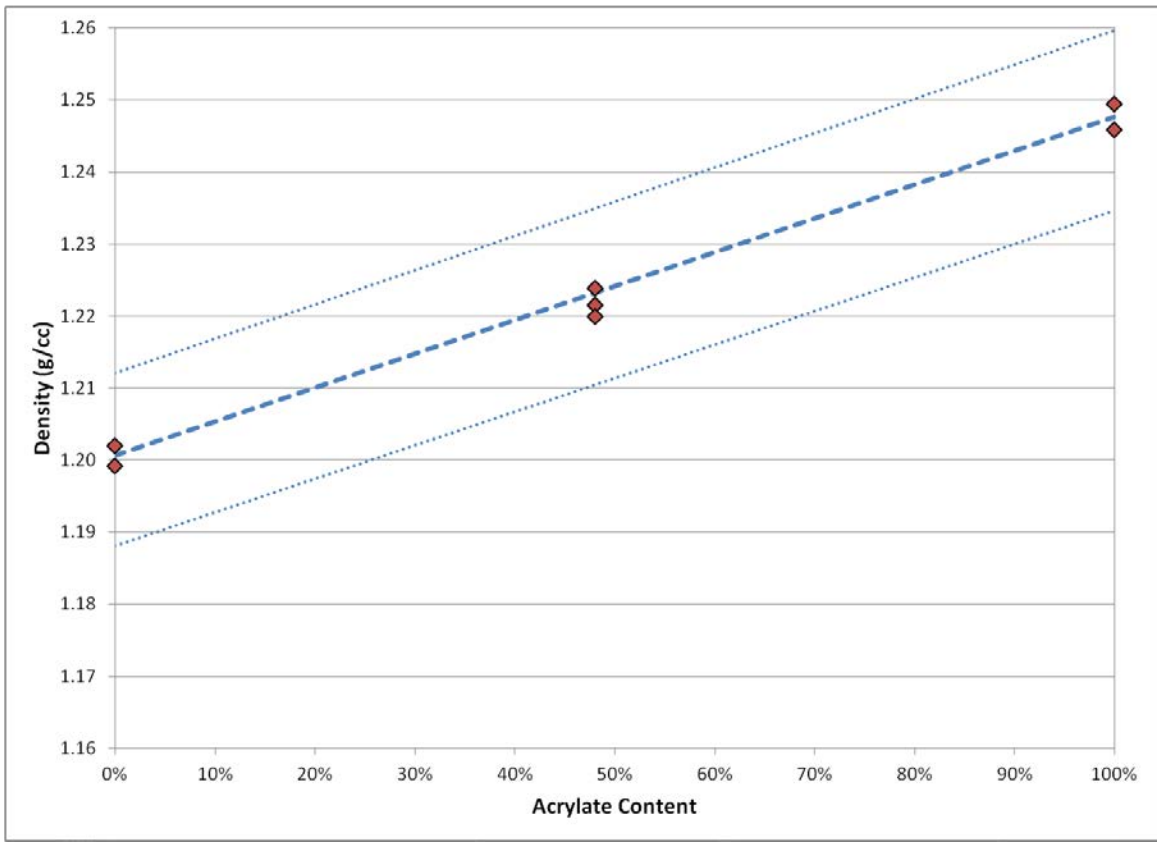

Figure 50: Archimedes density results for EB cured BPADA + (70-30)Epoxy material system

Archimedes density results for the BPADA + BECA epoxy material system are shown in Figure 51. The rule of mixtures tie line is shown as a blue dashed line, and dotted lines are included to show 1 percent deviations from the rule of mixtures. The individual results show a minor deviation from the rule of mixtures at the 50% acrylate composition.

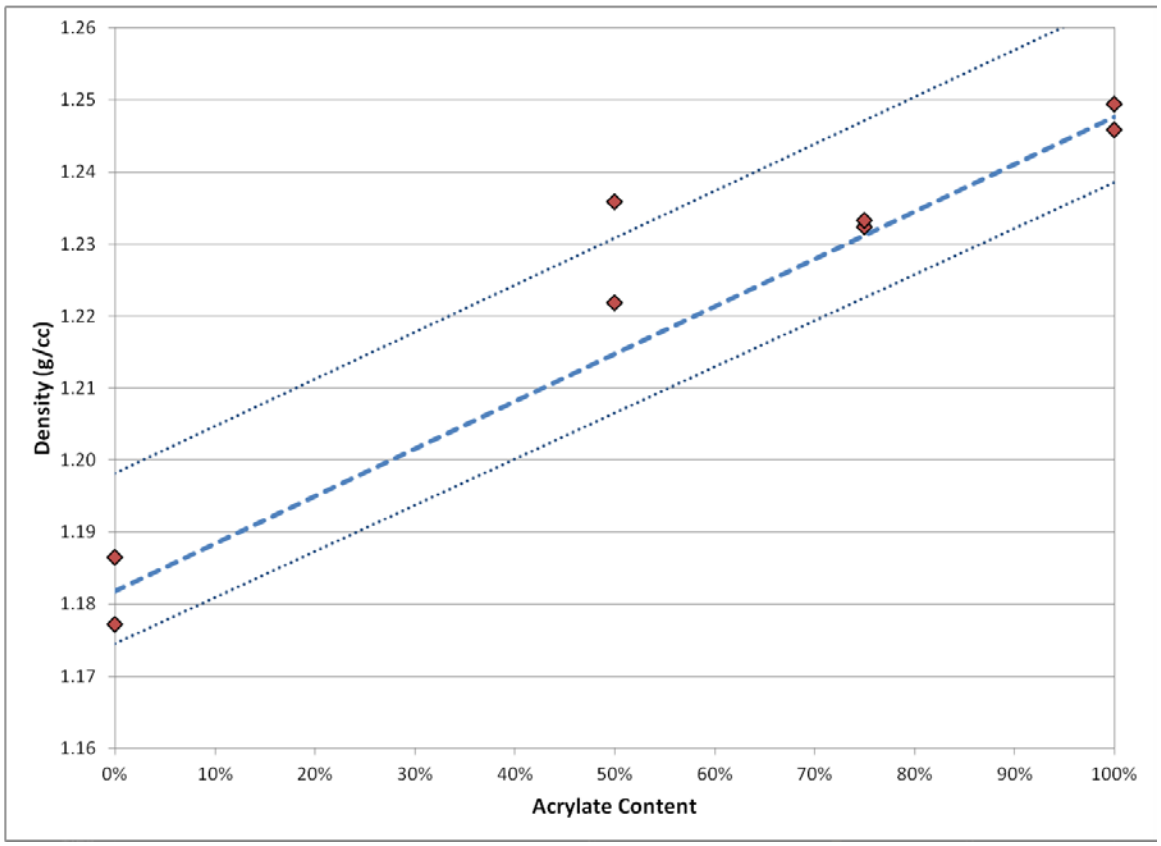

Figure 51: Archimedes density results for EB cured BPADA + BECA material system

Archimedes density results for the UV cured BPADA + (50-50)Epoxy material system are shown in Figure 52. The rule of mixtures tie line is shown as a blue dashed line, and dotted lines are included to show 1 percent deviations from the rule of mixtures. With the exception of the pure acrylate composition, the density measurements show a close correlation to the rule of mixtures. FTIR results show that the pure acrylate sample also had a lower degree of monomer conversion which likely contributes to its reduced density. For comparison, the average density value for electron beam cured BPADA is shown with a round marker.

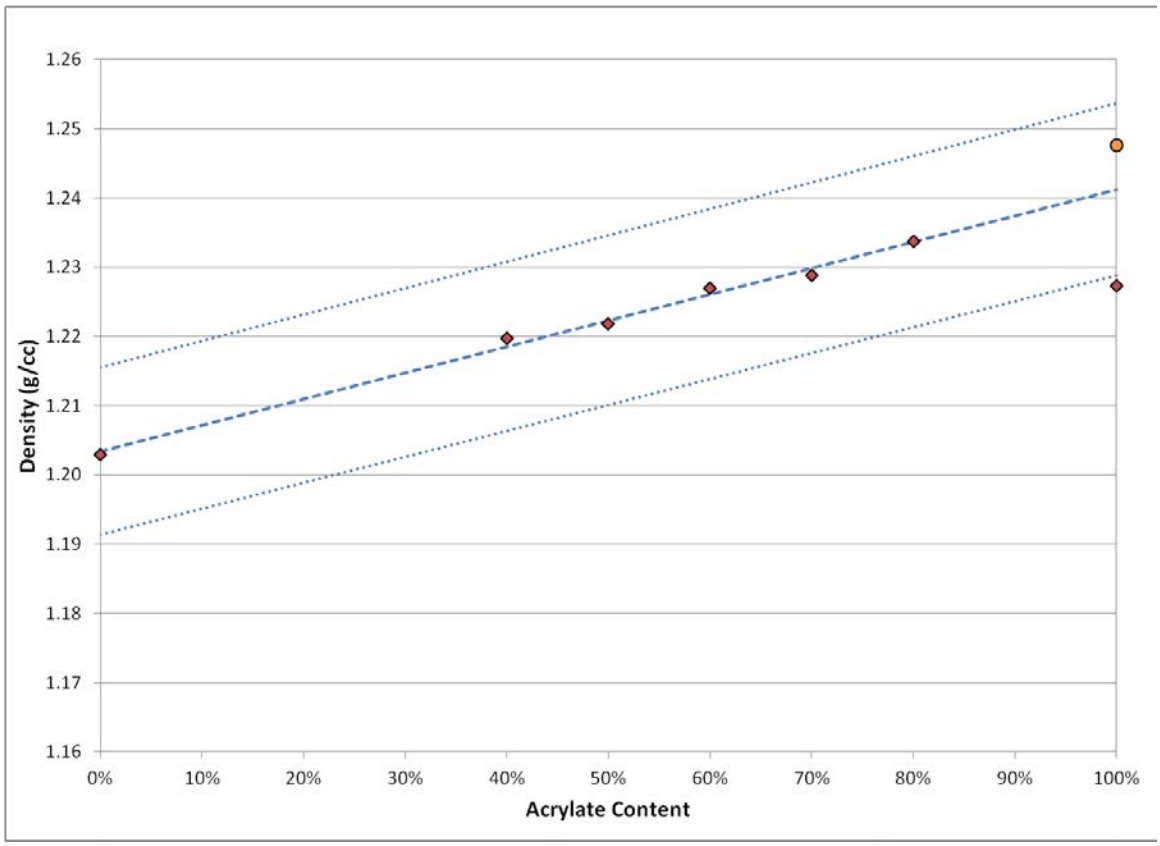

Figure 52: Archimedes density results for UV cured BPADA + (50-50)Epoxy material system

Archimedes density results for the UV cured BPADA + (50-50)Epoxy material system are shown in Figure 52. The rule of mixtures tie line is shown as a blue dashed line, and dotted lines are included to show 1 percent deviations from the rule of mixtures. With the exception of the pure acrylate composition, the density measurements show a close correlation to the rule of mixtures. Secondary bonds are converted to covalent bonds during polymerization, and the volume of the initial sample contracts. FTIR results show that the pure acrylate sample also had a lower degree of monomer conversion which is a plausible explanation for its reduced density. To provide a comparison, the average density value for electron beam cured BPADA is shown in Figure 52 with a round marker.

5.4.3 Archimedes Results Discussion

An example of density variation within an acrylic-polyurethane IPN system is shown in . The original data has been supplemented by lines representing +/- 1 percent variations from the line representing a linear rule of mixtures relationship. Departures of more than 1 percent were exhibited, peaking at a concentration of 80 percent polyurethane. The increased density was attributed to improved molecular mixing which was also reflected by a decrease in polymer free volume and an increase in glass transition temperature. [85] Other research has noted that strong polymer-polymer interactions result in density values greater than linear additivity whereas segregation into distinct phases or blends without interactions between the two components. [86]

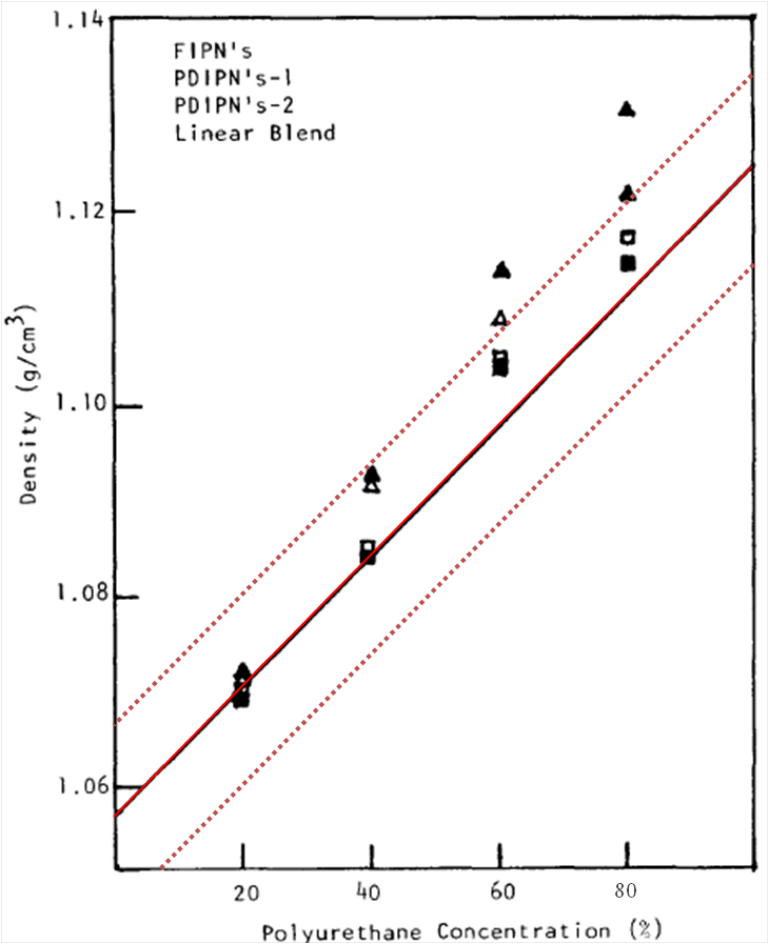

Figure 53: Density variation versus polyurethane content for an acrylic-polyurethane IPN (from 85)

With a few minor exceptions, the compositional density measurements fell within 1 percent of a linear rule of mixtures relationship. For the UV cured BPADA, it is apparent that the departure from linear additivity is due to the lower degree of monomer conversion for the pure acrylate sample. For the 48(80-20)Acrylate+52(50-50)Epoxy and 50BPADA+50BECA compositions, there appears to be some enhanced packing. However, the departure from linear additivity seems to be limited to these approximately 50 percent acrylate + 50 percent epoxy compositions. The source may be connected with IPN morphology near this

50-50 IPN composition, or it may be simply due to experimental error. For the remainder of these material systems plus the electron beam cured BPADA+(70-30)Epoxy and UV cured BPADA+(50-50)Epoxy material systems, the enhanced packing efficiency which was originally postulated by some researchers as a reason for the parabolic material system response can be ruled out.

5.5 Tensile Investigation

Electron beam cured blanks were used to investigate different combinations of acrylate and epoxy formulations. For most IPN material systems, this included a pure acrylate sample and a nominally 50 percent diacrylate + 50 percent IPN. Tensile test data enabled the comparison of both ultimate tensile strength and tensile modulus.

5.5.1 Tensile Specimen Preparation

Tensile specimens were produced from pocket mold samples. The specimens were cut with a waterjet per the geometry defined by ASTM D638 Type IV. Initial specimens were tested as-cut, but later specimens had the cut edges polished with 600 grit sandpaper. The specimens were mounted in an Instron mechanical testing machine with a 10 kN load cell, and strain was measured with a laser extensometer. Testing was conducted at a crosshead rate of 5 mm/min. The setup is shown in Figure 54.

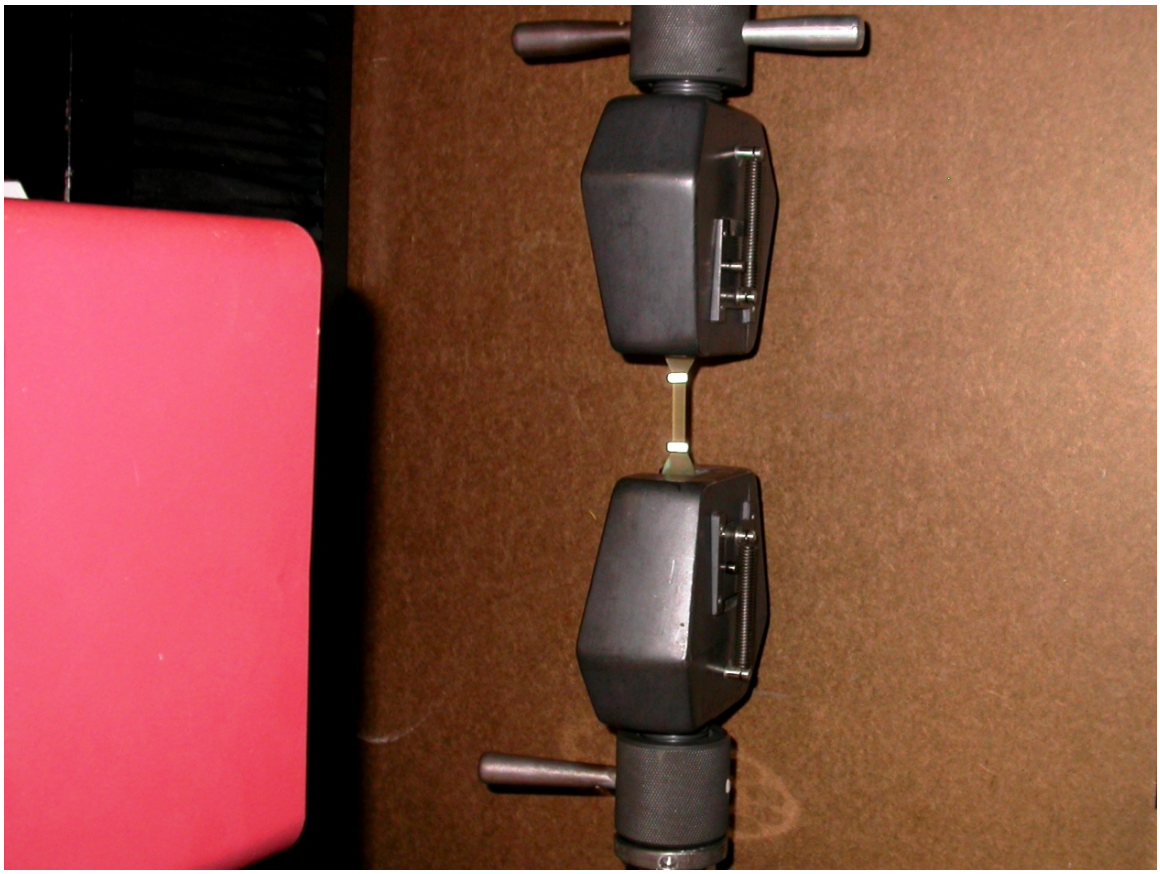

Figure 54: Tension test setup showing laser extensometer targets on IPN tension specimen (laser extensometer on left)

5.5.2 Modulus Results

The tensile modulus was calculated per ASTM D638 guidelines by extending the initial linear portion of the stress-strain curve produce a line that was representative of the initial elastic portion of the curve, ignoring any initial "toe-in" effects. As illustrated in Figure 55, the modulus of elasticity was determined by calculating the slope of this tangent line.

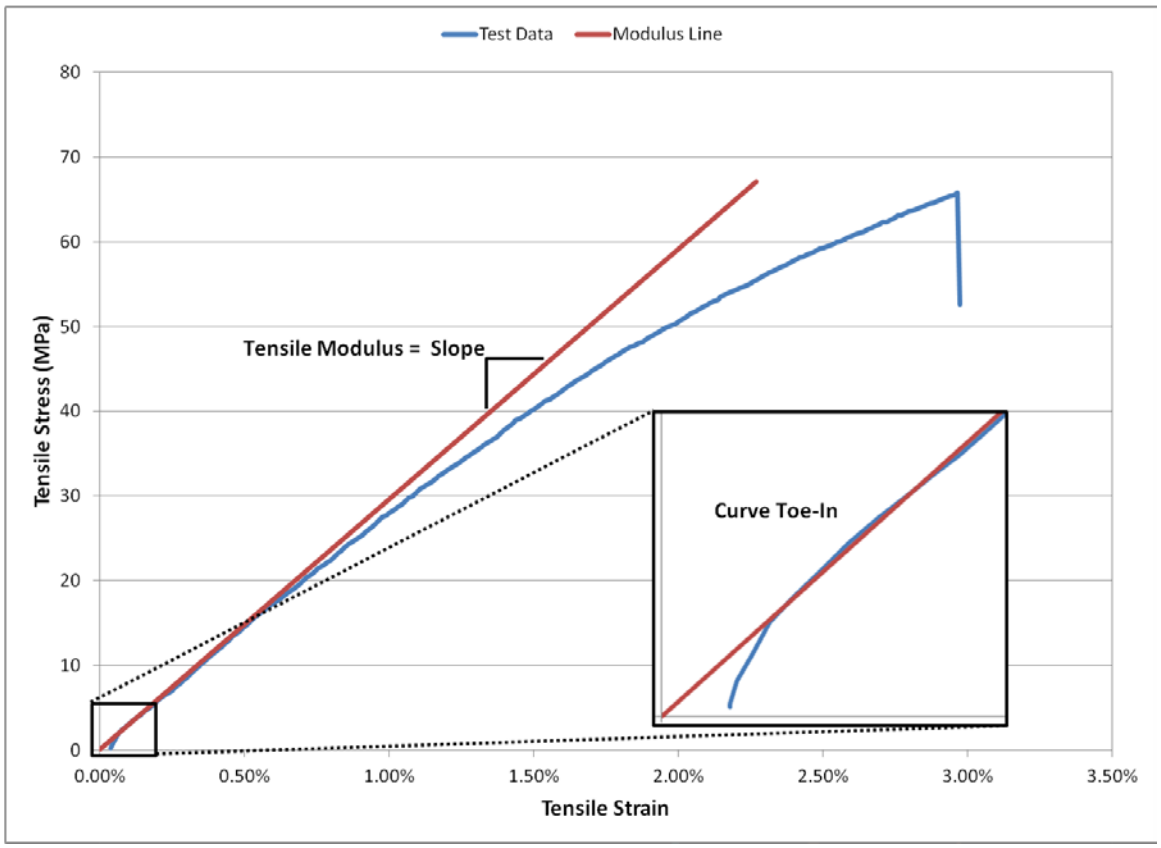

Figure 55 - Tensile modulus determined from initial tangent to the stress-strain curve

The moduli of polymer blends typically exhibit slight deviations from a linear rule of mixtures relationship due to positive or negative synergy between the individual polymers. Kleiner developed a modification to the rule of mixtures that takes into account this synergy. [87] The modified rule of mixtures is calculated with the use of Equation 17.

Equation 17

$$=$$ **Equation 18**

Where $= interaction\ parameter$

$= volume\ fraction\ of\ component$

$= modulus\ of\ component$

$= modulus\ of\ 50\text{-}50\ blend$

The value of the interaction parameter, β, which is calculated by Equation 18 indicates the type of interaction developed within the blended system. Since it is partially based on the product of the two network volume fractions, the interaction parameter equation produces a parabolic material response rather than a linear rule of mixtures response. If $\beta > 0$, positive synergy exists whereas negative synergy exists for values of $\beta < 0$.

The elastic moduli calculated from individual tests are shown in the following figures along with a trend line that represents the Kleiner modified rule of mixtures calculated from an average of the relevant modulus measurements. Volume fractions in the final composition were based on the volume contributions of the uncured monomers. In cases where a 50% acrylate blend was not tested, the value of $E_{50\%}$ was calculated as an interpolation of the modulus values for the compositions bordering the 50-50 composition in accordance with Equation 19.

Equation 19

Where: *modulus of composition a (< 50%)*

modulus of composition b (> 50%)

fraction of acrylate in composition a

fraction of acrylate in composition b

If the properties peak at the composition corresponding to 50% acrylate, the use of interpolation will underestimate the value of $E_{50\%}$. In most cases, however, a composition was tested with an acrylate concentration of 48%.

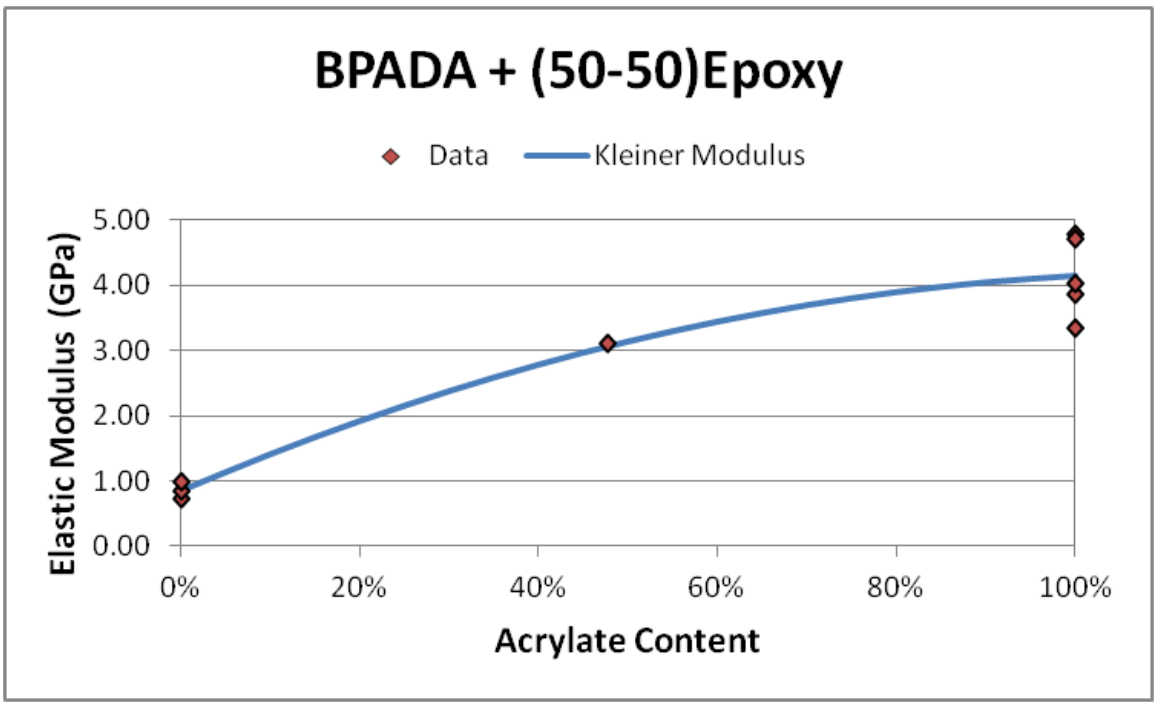

Figure 56: Elastic modulus values plus Kleiner modulus line for BPADA + (50-50)Epoxy system

The modulus values for the bisphenol A diacrylate (BPADA) plus epoxy composed of 50 parts diglycidyl ether of bisphenol A, 50 parts polypropylene glycol diglycidyl ether and 10 parts 2-ethyl-4-methyl imidazole {"(50-50)Epoxy"} are shown in Figure 56. The 48% acrylate IPN formulation exhibited a modulus 21% higher than predicted from a linear rule of mixtures, resulting in a positive Kleiner modulus beta value of 2.57 GPa.

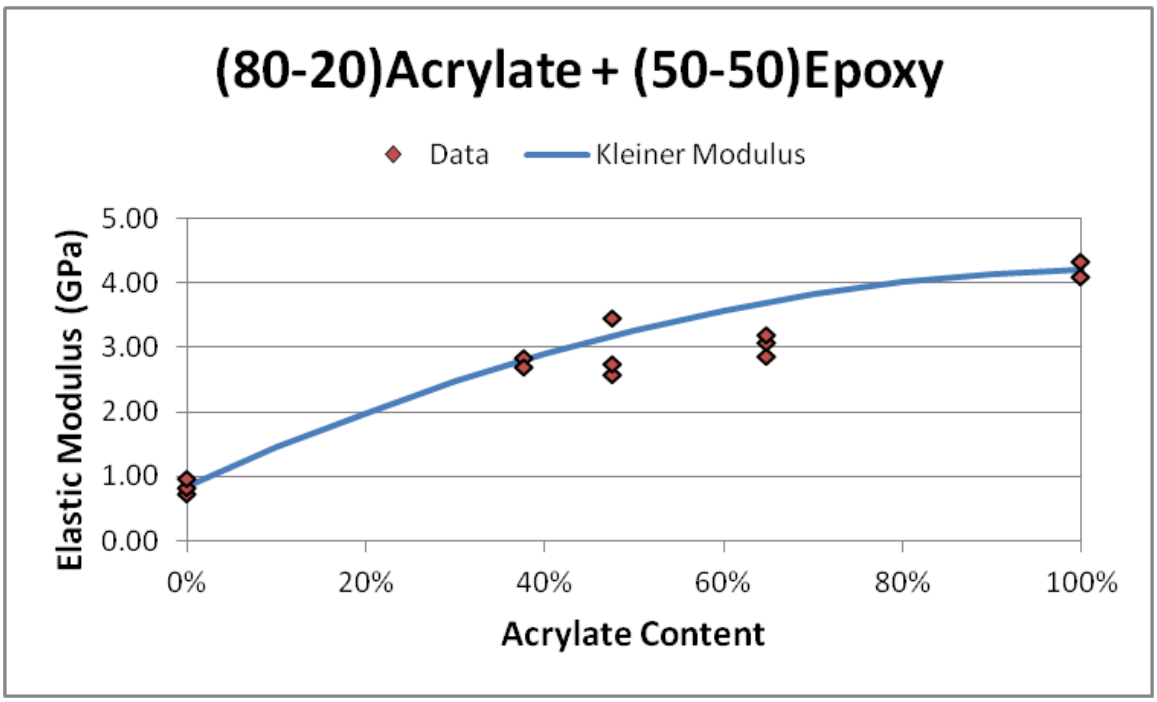

Figure 57: Elastic modulus values plus Kleiner modulus line for (80-20)Acrylate + (50-50)Epoxy system

The modulus values for the acrylate composed of 80 parts bisphenol A diacrylate plus 20 parts trimethylolpropane triacrylate {"(80-20)Acrylate"} plus "(50-50)Epoxy" are shown in Figure 57. The 38% acrylate IPN formulation exhibited an average modulus 30% higher than predicted from a linear rule of mixtures, resulting in a positive Kleiner modulus beta value of 2.94 GPa.

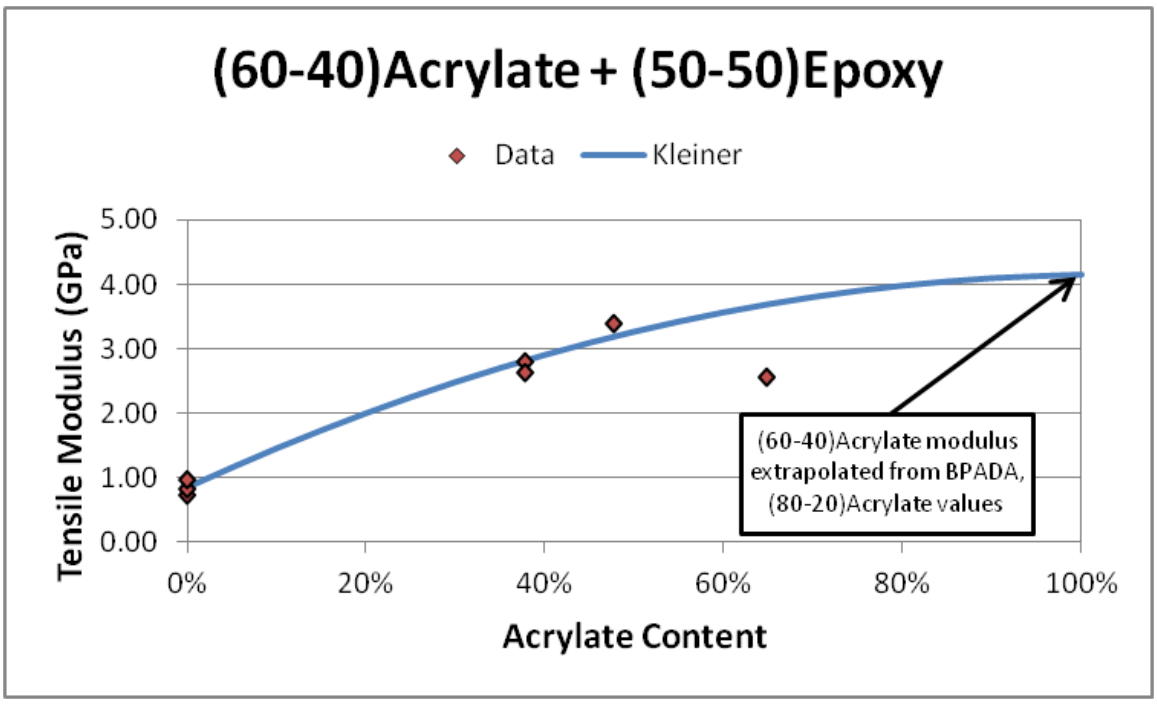

Figure 58: Elastic modulus values plus Kleiner modulus line for (60-40)Acrylate + (50-50)Epoxy system

The modulus values for the acrylate composed of 60 parts bisphenol A diacrylate plus 40 parts trimethylolpropane triacrylate {"(60-40)Acrylate"} plus "(50-50)Epoxy" are shown in Figure 58. Since the pure acrylate tensile blanks for this system all cracked when they were removed from the mold, the modulus was estimated by extrapolating from the compositions with 0% and 20% trimethylolpropane triacrylate. Data sheets from Sartomer for bisphenol A diacrylate diluted with 0%, 20% and 40% trimethylolpropane triacrylate show that the modulus does vary linearly with the trimethylolpropane triacrylate content. [88] [89] [90] The 48% acrylate IPN formulation exhibited an average modulus that was 31% higher than predicted from a linear rule of mixtures, resulting in a positive Kleiner modulus beta value of 2.50 GPa.

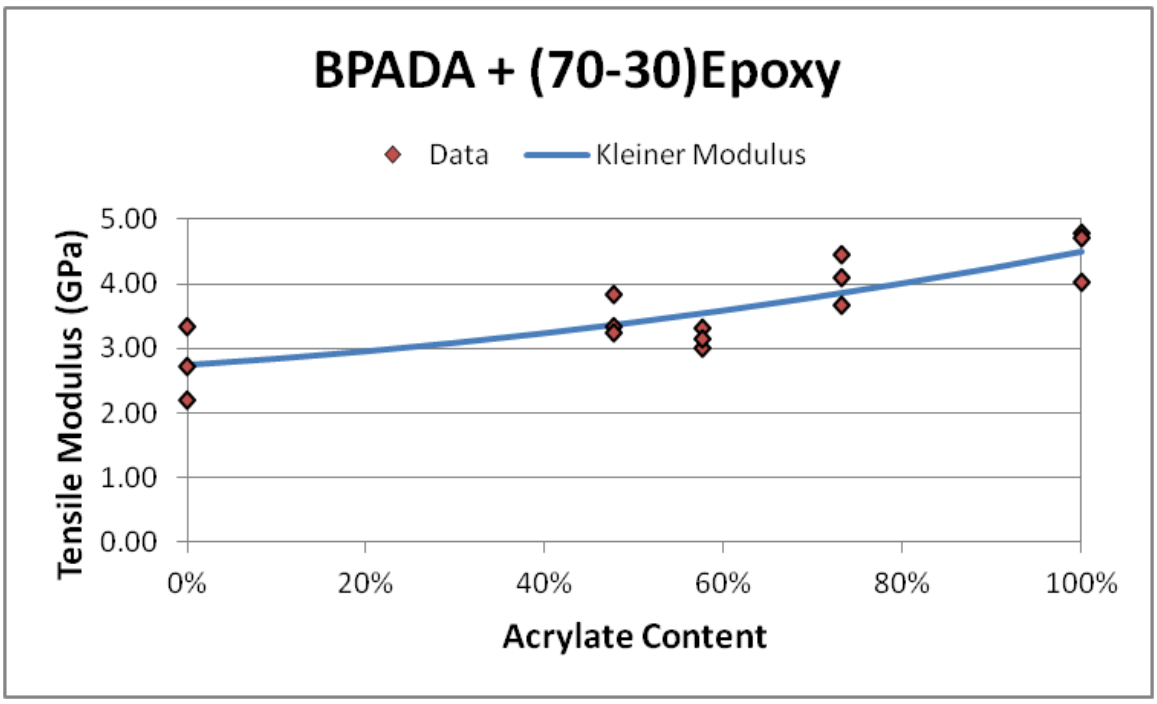

Figure 59: Elastic modulus values plus Kleiner modulus line for BPADA + (70-30)Epoxy system

The modulus values for the bisphenol A diacrylate (BPADA) plus epoxy composed of 70 parts diglycidyl ether of bisphenol A, 30 parts polypropylene glycol diglycidyl ether and 10 parts 2-ethyl-4-methyl imidazole {"(70-30)Epoxy"} are shown in Figure 59. The modulus of the (70-30)Epoxy is significantly higher than the modulus of the (50-50)Epoxy, so the data values seem to fall closer to a straight line. The 48% acrylate IPN formulation exhibited an average modulus that was 16% lower than predicted from a linear rule of mixtures, resulting in a negative Kleiner modulus beta value of -0.87 GPa.

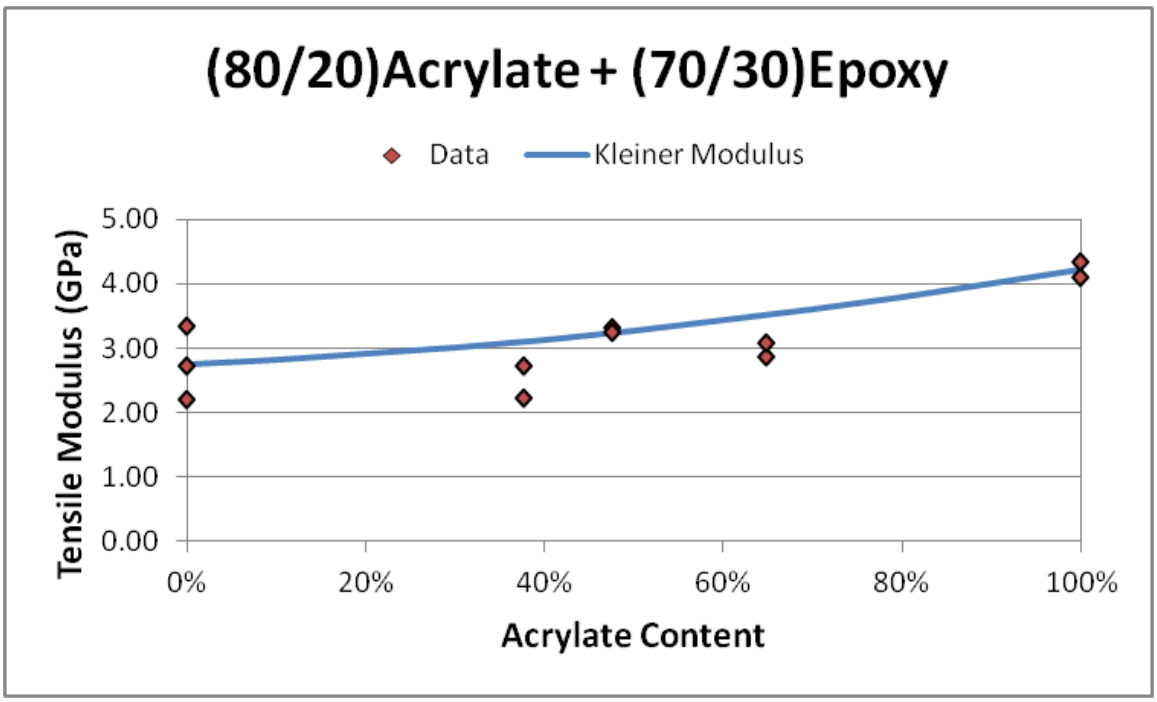

Figure 60: Elastic modulus values plus Kleiner modulus line for (80-20)Acrylate + (70-30)Epoxy system

The modulus values for acrylate composed of 80 weight percent bisphenol A diacrylate plus 20 weight percent trimethylolpropane triacrylate {"(80-20)Acrylate"} combined with epoxy composed of 70 parts by weight diglycidyl ether of bisphenol A, 30 parts polypropylene glycol diglycidyl ether and 10 parts 2-ethyl-4-methyl imidazole {"(70-30)Epoxy"} are shown in Figure 60. Except for a slight reduction in the pure acrylate tensile strength, the performance almost mirrors that of the BPADA + (70-30)Epoxy system. The 38% acrylate IPN formulation exhibited an average modulus that was 25% lower than predicted from a linear rule of mixtures, and the Kleiner modulus exhibited negative synergy with a beta value of -0.84 GPa.

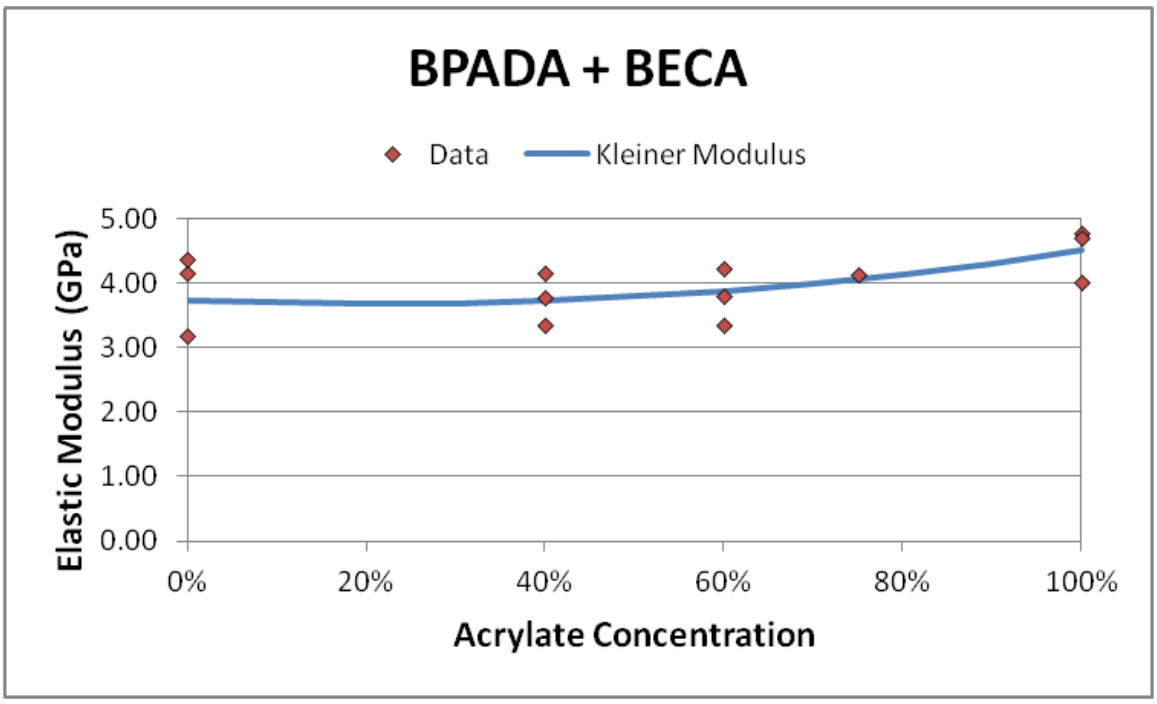

Figure 61: Elastic modulus values plus Kleiner modulus line for BPADA + BECA system

The modulus values for the bisphenol A diacrylate (BPADA) plus epoxy composed of 100 weight percent bis((3,4-epoxycyclohexyl)methyl)adipate (BECA) with 70 weight percent methylhexahydrophthalic anhydride (MHHPA). This system features the closest match between the acrylate and epoxy modulus values for any of the material systems investigated. The 60% acrylate IPN formulation exhibited an average modulus that was 9% lower than the linear rule of mixtures prediction. Although the percentage deviation is small, it resulted in the most negative Kleiner modulus beta value of any material system investigated, -1.32 GPa.

5.5.3 Tensile Results

Unfortunately, the effect of a waterjet cut edge on tensile performance was not realized until after the first major group of specimens had been tested. In the following charts, the

polished samples are denoted with a filled diamond while the waterjet edge samples are denoted with an open circle. The average values for each composition are connected with dashed lines.

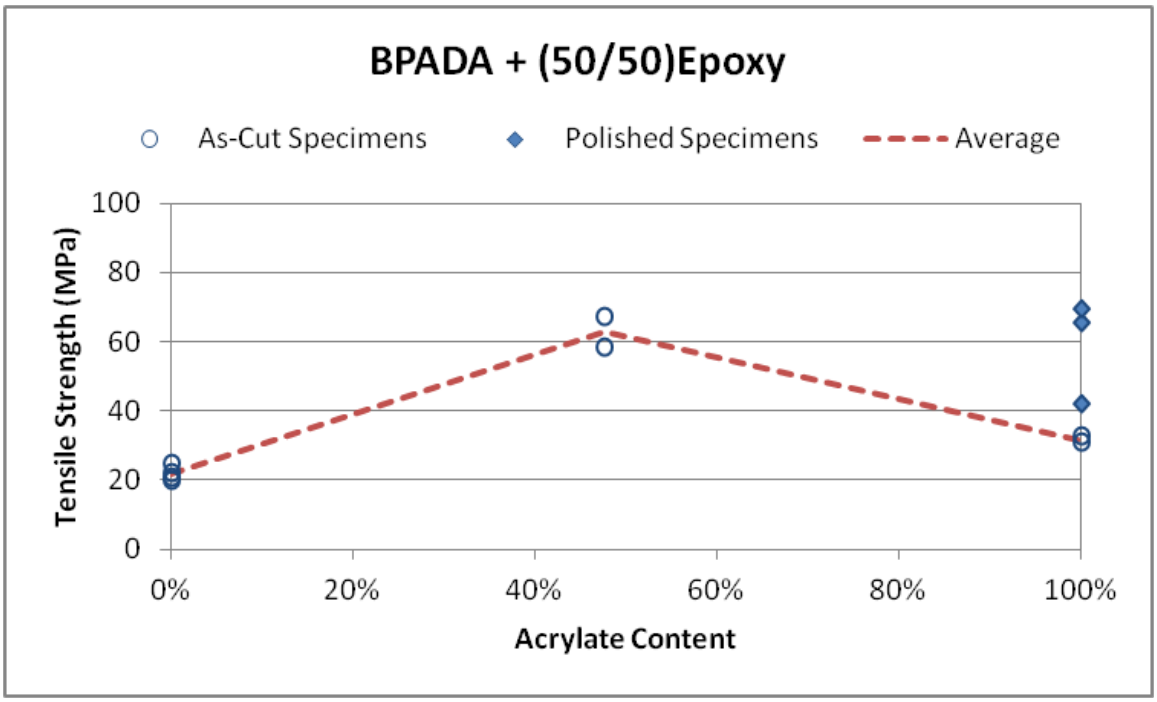

Figure 62: Tensile strength in BPADA + (50-50)Epoxy polymer system

The tensile strength values for the system formulated from bisphenol A diacrylate (BPADA) plus epoxy composed of 50 parts diglycidyl ether of bisphenol A, 50 parts polypropylene glycol diglycidyl ether and 10 parts 2-ethyl-4-methyl imidazole {"(50-50)Epoxy"} are shown in Figure 62. The line connecting the average values is based only on as-cut specimens. Within the as-cut specimen results, the 48% acrylate IPN formulation exhibited a tensile strength 138% higher than predicted from a linear rule of mixtures.

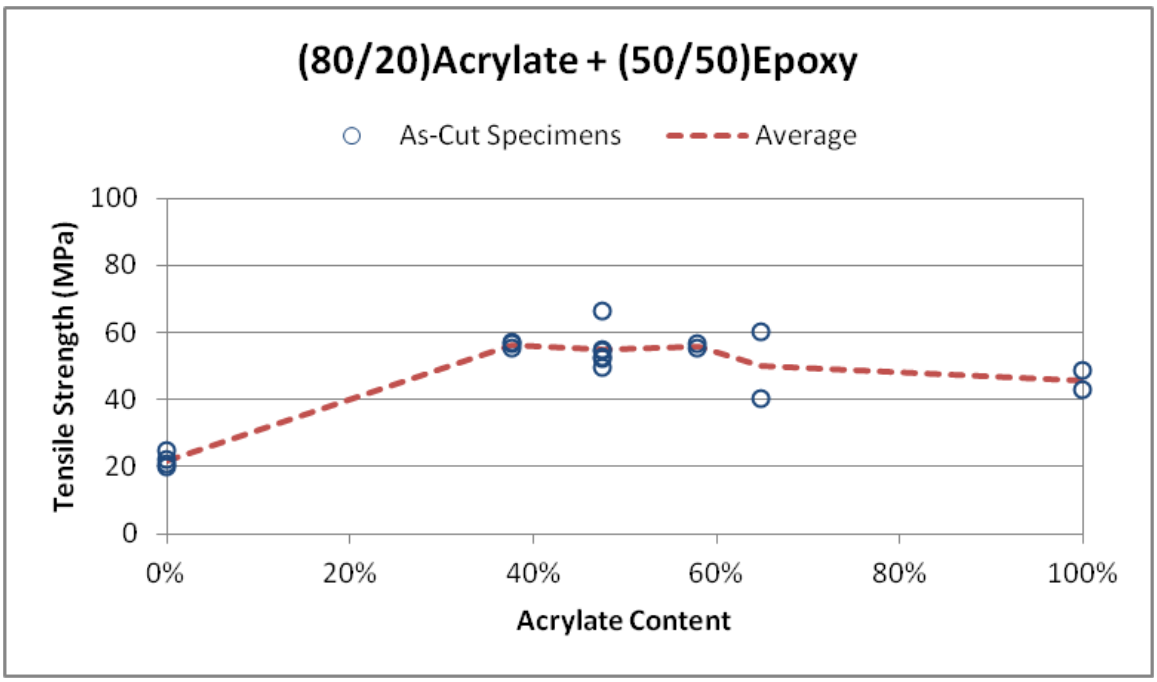

Figure 63: Tensile strength in (80-20)Acrylate + (50-50)Epoxy material system

The tensile strength values for the system formulated from acrylate comprised of 80 parts bisphenol A diacrylate and 20 parts trimethylolpropane triacrylate {"(80-20)Acrylate"} plus (50-50)Epoxy are shown in Figure 63. All of the specimens in this material system were tested in the as-cut condition. The 38% acrylate IPN formulation exhibited the greatest degree of synergy with a tensile strength 83% higher than predicted from a linear rule of mixtures.

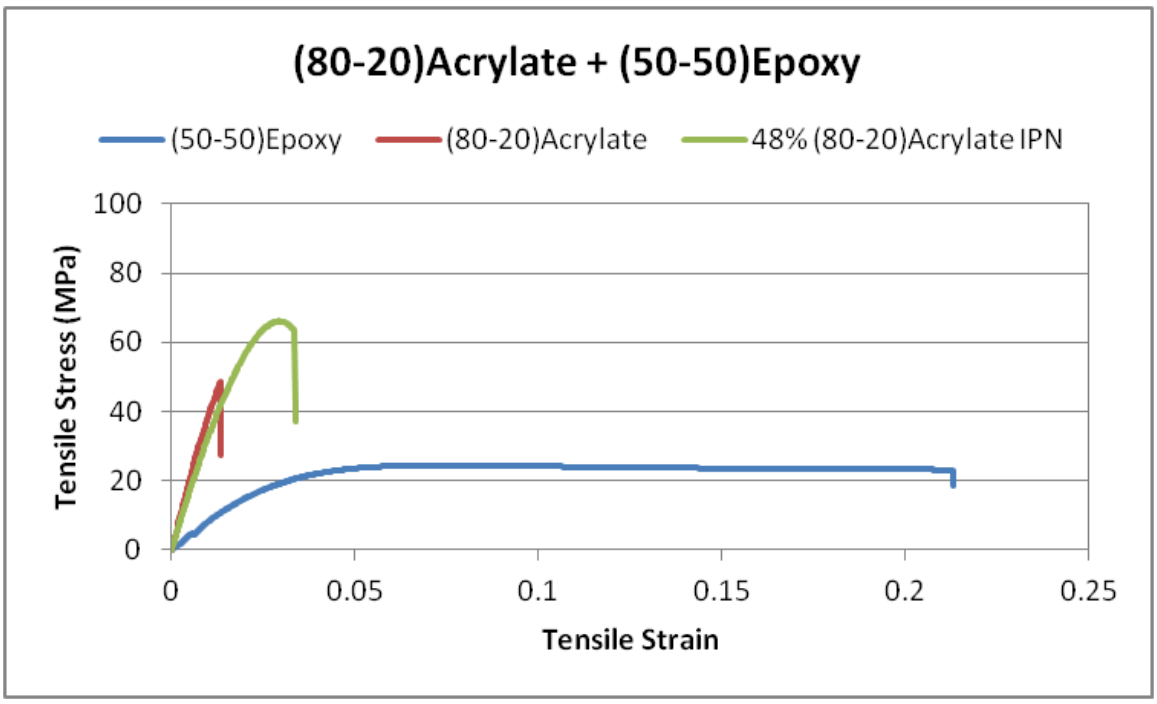

Figure 64: Maximum strength stress-strain curves in (80-20)Acrylate + (50-50)Epoxy material system

The stress-strain curves for the specimens within the (80-20)Acrylate + (50-50)Epoxy material system with the highest tensile strength are shown in Figure 64. Both the (50-50)Epoxy and the 48% acrylate IPN reached a yield stress prior to failure, so the unpolished specimen edges did not artificially reduce their strength. The (80-20)Acrylate has a high modulus but an elongation at failure of only 1.33%. In contrast, the (50-50)Epoxy has low modulus but high elongation to failure for an epoxy. A synergistic combination of these properties is exhibited by the IPN sample composed of 48% (80-20)Acrylate +52% (50-50)Epoxy. It has a modulus that is closer to that of the pure acrylate while it exhibits a yield stress prior to failure. The average modulus of resilience is 0.300 MJ/m^3 for the (80-20)Acrylate specimens, 0.832 MJ/m^3 for the 48% IPNs and 2.167 MJ/m^3 for the (50-50)Epoxy specimens.

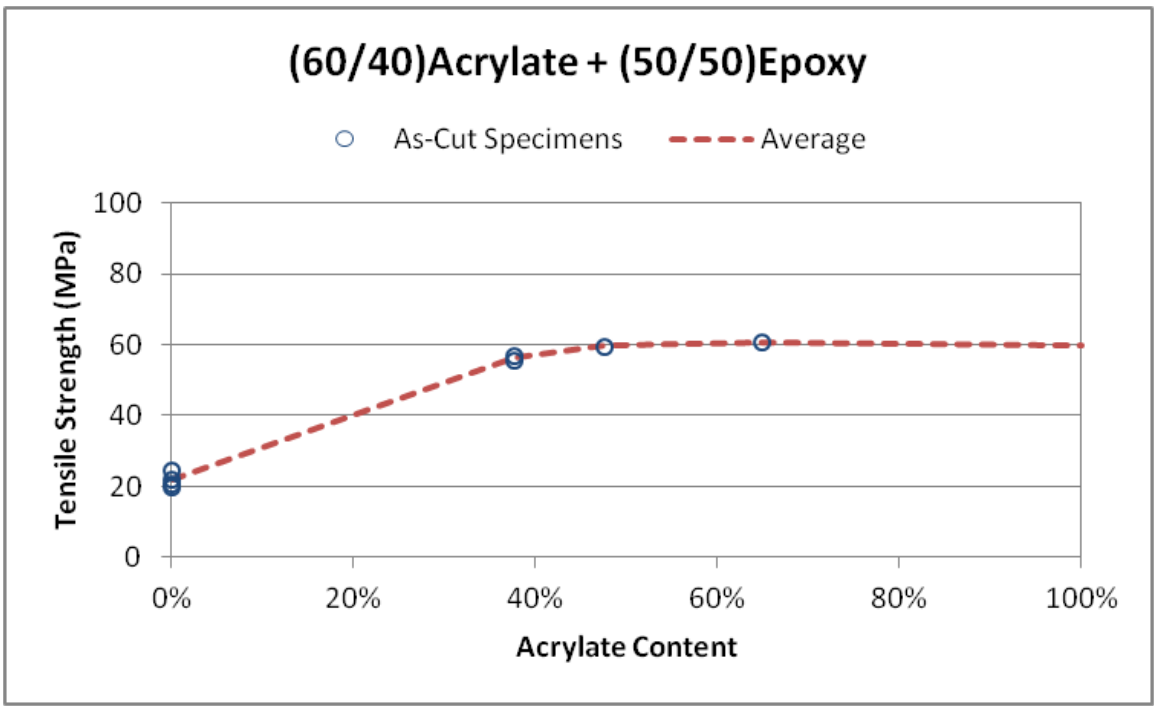

Figure 65: Tensile strength in the (60-40)Acrylate + (50-50)Epoxy material system

The tensile strength values for the system formulated from acrylate comprised of 60 parts bisphenol A diacrylate and 40 parts trimethylolpropane triacrylate {"(60-40)Acrylate"} plus (50-50)Epoxy are shown in Figure 65. All of the specimens in this material system were tested in the as-cut condition. All of the (60-40)Acrylate tensile specimens failed during fabrication, so the tensile strength was estimated by extrapolating from the BPADA and (80-20)Acrylate tensile strengths. The 38% acrylate IPN formulation exhibited the greatest degree of synergy with a tensile strength 56% higher than predicted from a linear rule of mixtures.

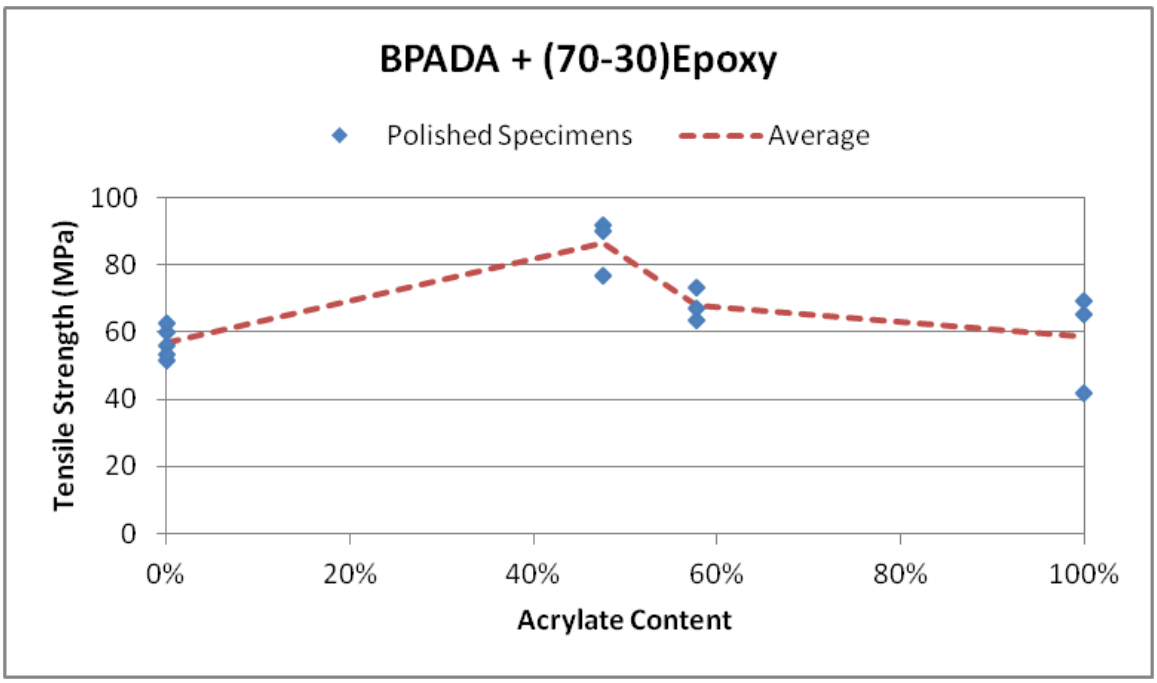

Figure 66: Tensile strength in the BPADA + (70-30)Epoxy material system

The tensile strength values for the system formulated from bisphenol A diacrylate (BPADA) plus epoxy composed of 70 parts diglycidyl ether of bisphenol A, 30 parts polypropylene glycol diglycidyl ether and 10 parts 2-ethyl-4-methyl imidazole {"(70-30)Epoxy"} are shown in Figure 66. All of the specimens had edges that were polished with 600 grit sandpaper prior to testing. The average tensile strengths of the pure BPADA and the pure (70-30)Epoxy were different by only about 2 MPa. The 48% acrylate IPN formulation exhibited the greatest degree of synergy with a tensile strength 28.6% higher than predicted from a linear rule of mixtures.

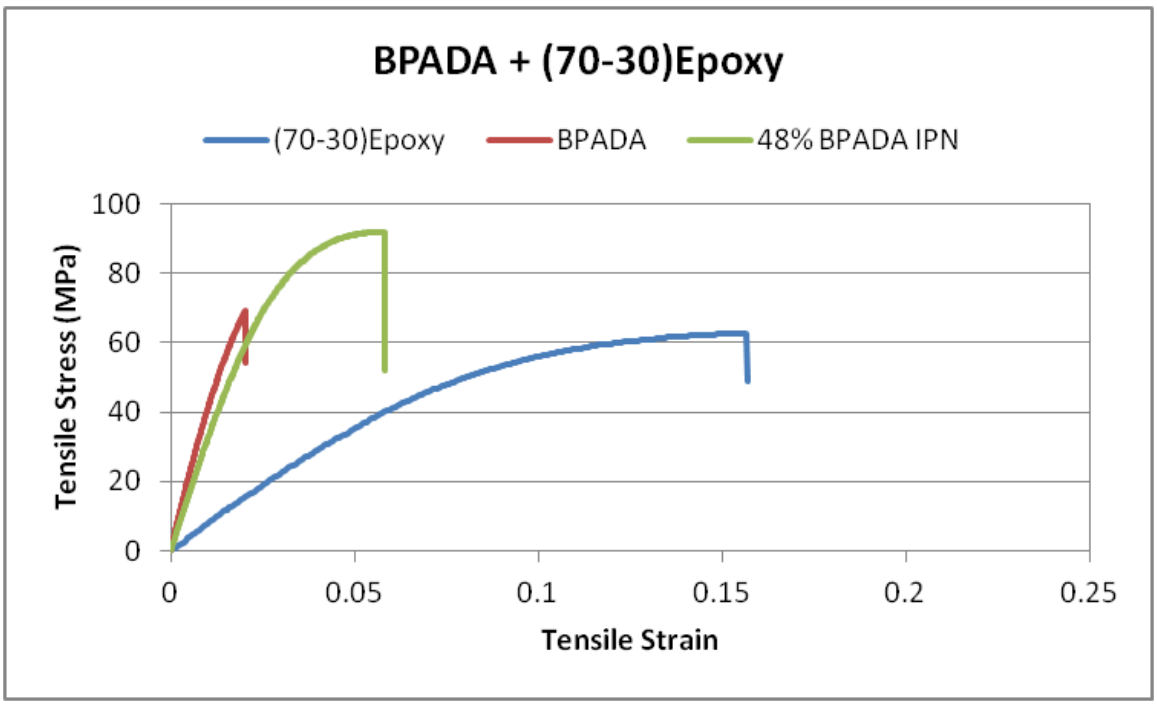

Figure 67: Maximum strength stress-strain curves in BPADA + (70-30)Epoxy material system

The stress-strain curves for the specimens within the BPADA + (70-30)Epoxy material system that exhibited the highest tensile strength are shown in Figure 67. Although both the (70-30)Epoxy and the 48% acrylate IPN showed definite signs of yielding, they did not reach a yield stress prior to failure. As with the (80-20)Acrylate + (50-50)Epoxy material system, the 48% IPN exhibited a synergistic combination of acrylate modulus and epoxy ductility. The average modulus of resilience is 0.577 MJ/m^3 for the BPADA specimens, 1.293 MJ/m^3 for the 48% IPNs and 1.372 MJ/m^3 for the (70-30)Epoxy specimens.

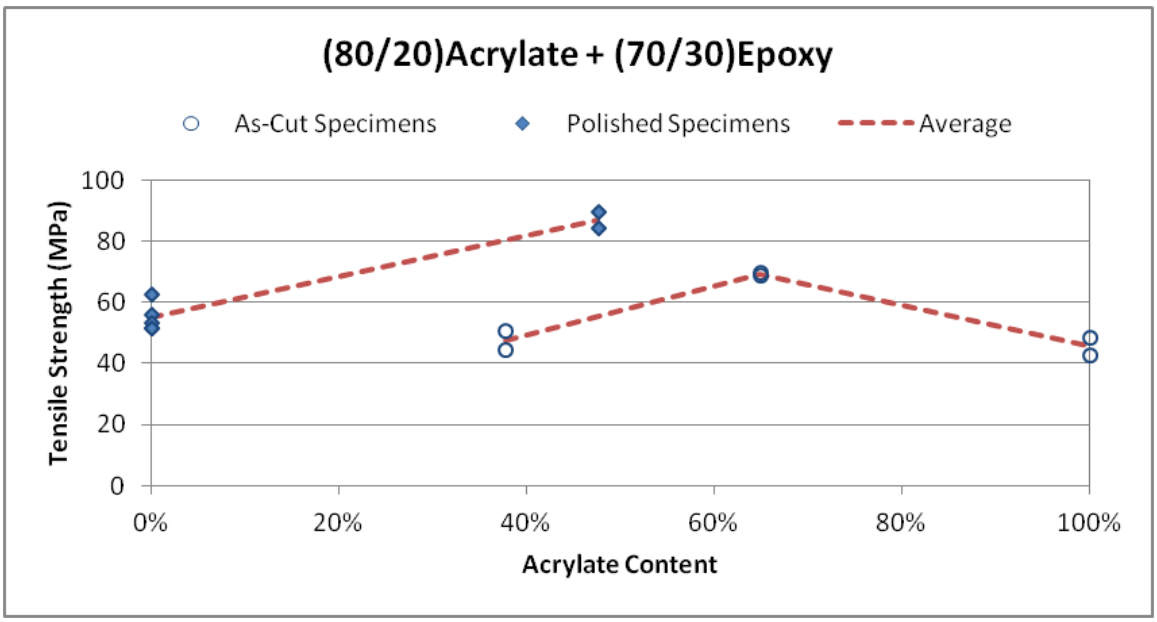

Figure 68: Tensile strength in (80-20)Acrylate + (70-30)Epoxy material system

The tensile strength values for the system formulated from acrylate comprised of 80 parts bisphenol A diacrylate and 20 parts trimethylolpropane triacrylate {"(80-20)Acrylate"} plus (50-50)Epoxy are shown in Figure 68. The specimens in this material system represent a mixture of as-cut and polished conditions, so the average value tie lines are aligned by specimen type. Without compositional end points that represent the same specimen edge condition, it is not possible to calculate numeric values for IPN synergy. However, the average value tie lines do suggest that synergy is present.

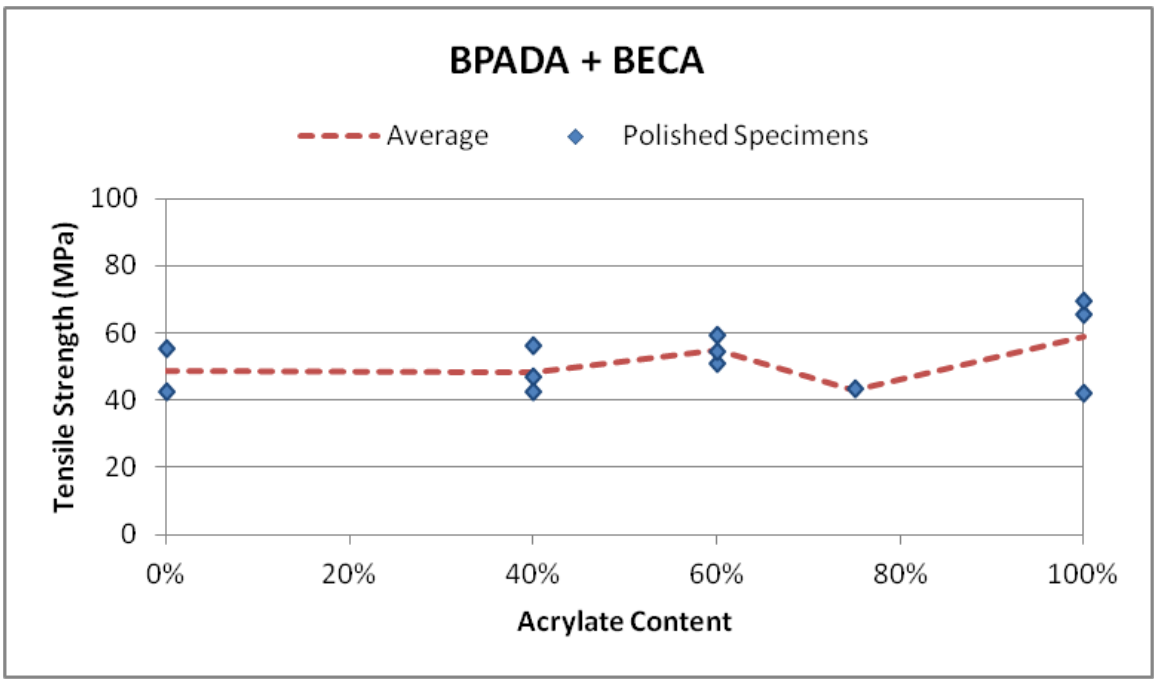

Figure 69: Tensile strength in the BPADA + BECA material system

The tensile strength values for the system formulated from bisphenol A diacrylate ("BPADA") plus epoxy composed of 100 weight percent bis((3,4-epoxycyclohexyl)methyl)adipate with 70 weight percent methylhexahydrophthalic anhydride ("BECA") are shown in Figure 69. All of the specimens had edges that were polished with 600 grit sandpaper prior to testing. The tensile performance of this system closely follows a linear rule of mixtures with the 60% acrylate IPN formulation exhibited a tensile strength equal to the rule of mixtures whereas the single data point for the 75% acrylate IPN formulation had a tensile strength 23% lower than the rule of mixtures value.

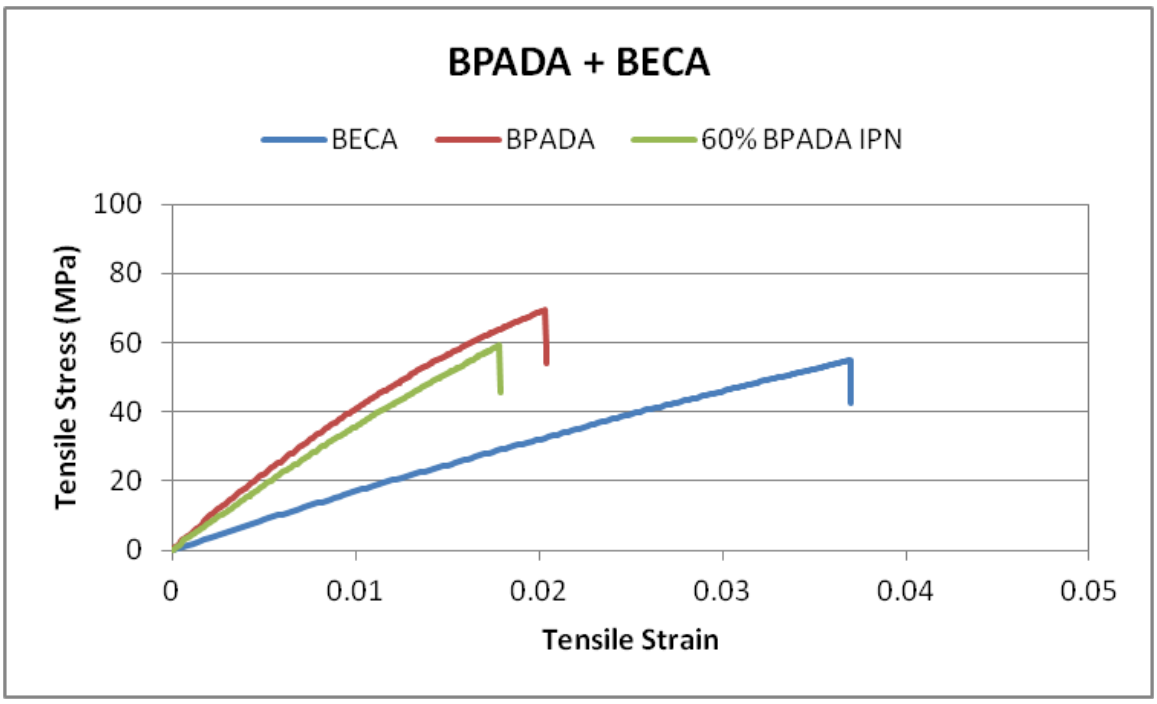

Figure 70: Maximum strength stress-strain curves in BPADA + BECA material system

The stress-strain curves for the specimens within the BPADA + BECA material system with the highest tensile strength are shown in Figure 70. All three representative compositions, the pure acrylate, the pure epoxy and the 60% IPN, exhibited brittle behavior. The IPN modulus was closer to that of the pure acrylate component, but the strain at failure was actually reduced. The average modulus of resilience is 0.577 MJ/m^3 for the BPADA specimens, 1.005 MJ/m^3 for the 60% IPNs and 0.854 MJ/m^3 for the BECA specimens.

The tensile strength, tensile modulus and modulus of resilience for the individual network components are compiled in Table 8.

Table 8: Summary of individual network tensile properties

Network	Tensile Strength (MPa)	Tensile Modulus (GPa)	Modulus of Resilience (MJ/m^3)
BPADA	69.4	4.504	0.577
(80-20)Acrylate	48.7	4.217	0.300
(50-50)Epoxy	22.0	0.844	2.167
(70-30)Epoxy	56.1	2.755	1.372
BECA Epoxy	54.9	3.738	0.854

5.5.4 Tensile Specimen Fractography

Fracture images for the BPADA + (70-30)Epoxy material system are shown in Figure 71. The pure (70-30)Epoxy fracture surface shows a distinct mirror zone followed by an abrupt transition into a mist zone and a more gradual transition into a hackle region. The 48% BPADA + 52% (70-30)Epoxy fracture surface has a very small mirror zone in the center of the fracture surface. The transition from mist to hackle region is gradual. The BPADA fracture surface has a larger mirror zone. The feature that looks like an "O" is a reflection from the circular lighting ring used to illuminate the fracture surface. The mist zone appears to be larger than it was in the other two samples, and the transition into the hackle region is more abrupt.

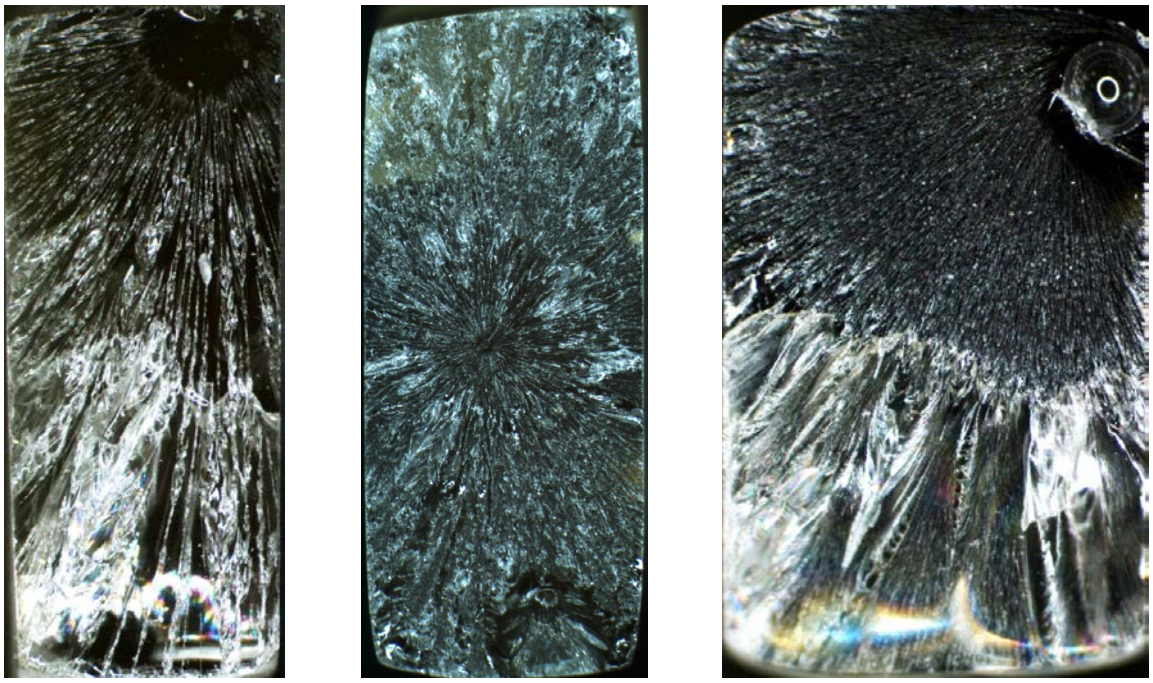

(70/30)Epoxy 48%BPADA + 52%(70/30)Epoxy IPN BPADA

Figure 71: Optical microscopy images of tensile fracture surfaces in BPADA + (70/30)Epoxy material system

The transition from mirror zone to mist zone is determined by the amount of elastic energy stored in the specimen at the time of fracture. The tip of the newly initiated crack accelerates as it propagates across the fracture plane. It transitions from the smooth mirror region to the mist region when the energy dissipated by smooth fracture surface initiation is no longer sufficient to keep up with the fracture energy release rate. Based on equation (7), the smaller mirror zone radius in the IPN specimen suggests that it has the highest strength. This is confirmed from the tensile strength results plotted in Figure 66.

Fracture images for the BPADA + BECA epoxy material system are shown in Figure 72. The mirror zone for the pure BECA epoxy is large, and parabolic markings indicative of fracture initiations ahead of the primary crack face are seen in the mist zone. The mirror zone for

the 40% BPADA + 60% BECA epoxy specimen shows a reduced mirror zone size and a rapid transition into a hackle region. The mist zone for the pure BPADA specimen is again larger than that exhibited by the IPN. The mirror zone radii did not exhibit the dramatic differences seen in the BPADA + (70-30)Epoxy material system, and it can be seen from Figure 69 that the range of tensile strengths in the BPADA + BECA epoxy material system falls much closer to a uniform value.

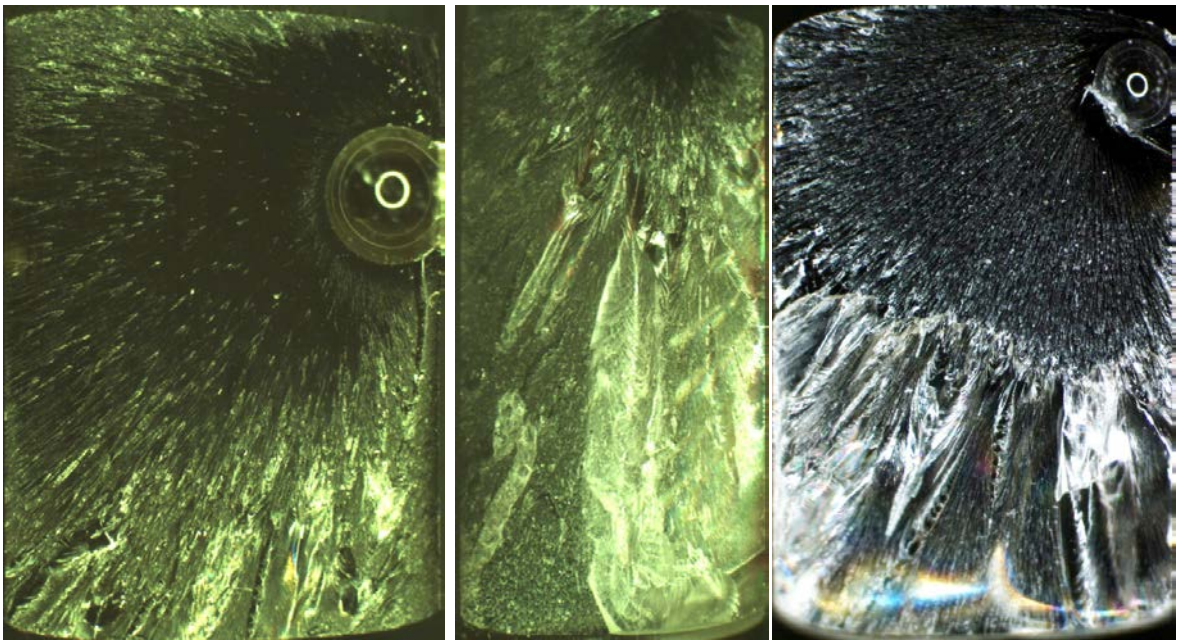

BECA Epoxy 40% BPADA + 60% BECA IPN BPADA

Figure 72: Optical microscopy images of tensile fracture surfaces in the BPADA + BECA epoxy material system

5.5.5 Tensile Results Discussion

The Kleiner modulus equation provides a reasonable fit with the tensile modulus data. A summary of the Kleiner modulus beta values is given in Table 9 along with the ratio of the modulus of the pure epoxy component divided by the modulus of the pure acrylate

component and the difference in the coefficients of thermal expansion for the pure components.

Table 9: Kleiner modulus beta values, modulus rations and strength ratios for IPN systems

IPN Material System	Beta (GPa)	$E_{epoxy}/E_{acrylate}$
BPADA + (50-50)Epoxy	2.57	37%
(80-20)Acrylate + (50-50)Epoxy	1.63	20%
(60-40)Acrylate + (50-50)Epoxy	3.08	27%
BPADA + (70-30)Epoxy	-0.87	60%
(80-20)Acrylate + (70-30)Epoxy	-0.84	63%
BPADA + BECA Epoxy	-1.32	82%

The modulus beta parameter and the modulus mismatch are compared graphically in Figure 73.

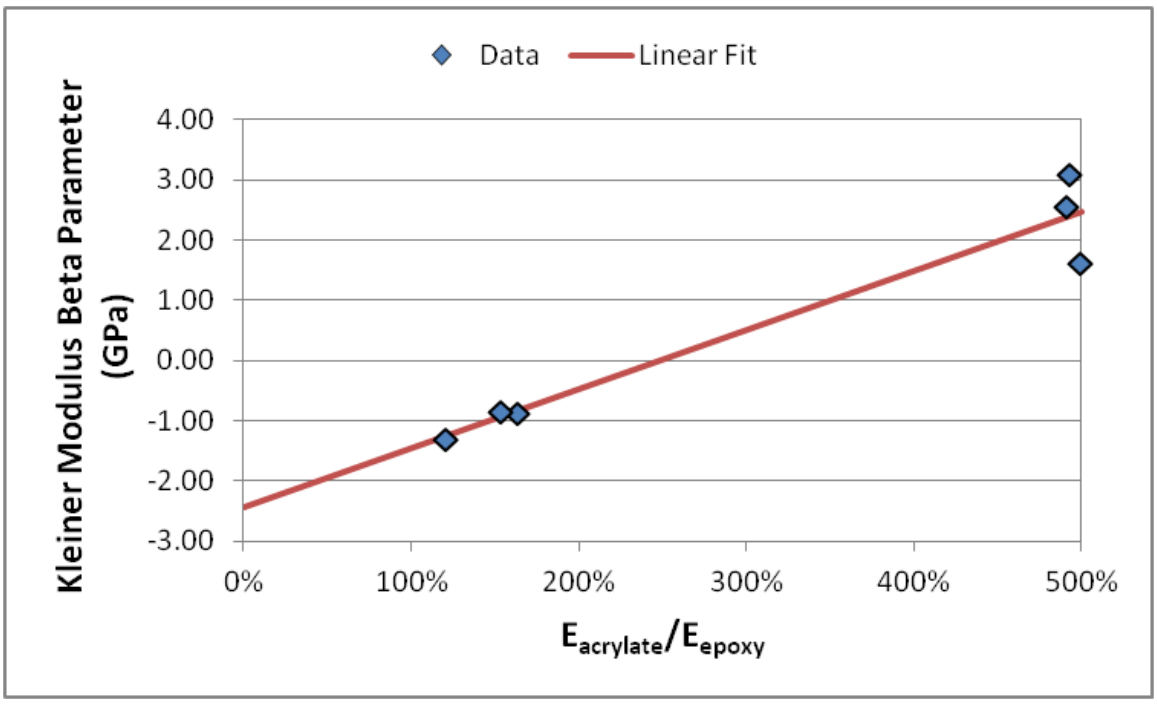

Figure 73: Kleiner modulus beta parameter versus the ratio of epoxy to acrylate tensile moduli

For all IPN material systems with the (50-50)Epoxy, positive values of beta were developed indicating positive synergy in the material blend while all other epoxy systems resulted in negative synergy ($\beta < 0$). The ratio of the IPN material system pure epoxy modulus to pure acrylate modulus ($E_{epoxy}/E_{acrylate}$) appears to correlate with the value of beta indicating that positive values are associated with a higher degree of modulus mismatch. The linear correlation as calculated in MS Excel is -0.9673.

The modulus of a polymer is determined by the stiffness of the polymer backbone bonds and the density of bonds per unit area. This suggests that the origin of the Kleiner modulus synergy could come from two sources: mechanical linkages and bond density. Mechanical linkages should act in a similar manner to chemical cross-linkages, forcing polymer segments to move in concert with each other. The effect of mechanical linkages will be more pronounced on the lower modulus (50-50)Epoxy networks.

Bond density in the network interface regions might be increased by improved compatibility between the two networks. Figure 31 illustrates that change in miscibility between the polymerizing acrylate and the surrounding mixture of acrylate plus epoxy monomer as a function of acrylate conversion as reflected by the square of the difference in solubility parameters (see equation 8). Since their backbone structures are identical, the bisphenol A diacrylate (BPADA) and diglycidyl ether of bisphenol A have less than a 5% difference in solubility parameters. As a result, the BPADA + (70-30)Epoxy system has a low solubility mismatch over the entire course of polymerization. The increase in PPGDE content in the BPADA + (50-50)Epoxy system increases the solubility mismatch, but the addition of TMPTA

in the (80-20)Acrylate + (50-50)Epoxy system decreases the solubility mismatch until the TMPTA is exhausted. The greatest solubility mismatch occurs in the BPADA + BECA material system. The BECA has a significantly different structure from the BPADA, so the solubility mismatch continually increases as BPADA is removed from the monomer mixture during the process of polymerization. Compatibility between the monomer mixture and the composition of the acrylate produced at the end of the polymerization process may affect the density of bonds at the interface between the two networks.

With the exception of the (50-50)Epoxy samples, all of the polymers produced during this investigation exhibited brittle behavior as evidenced by fracture prior to yielding. The strength of a brittle material is related to its fracture toughness by Equation 20. [91]

Equation 20

Where *tensile strength*

plane strain fracture toughness

dimensionless geometry parameter

flaw half length

Assuming a constant flaw size across all samples, the tensile strength will depend on the fracture toughness.

Residual stresses may also play a role in the measured tensile strength. Due to shrinkage and thermal contraction effects during curing, acrylate networks have shown residual

stresses as high as 8 MPa. This residual stress may be eliminated as a result of the IPN cure. Since the acrylate network cures first near room temperature, the epoxy monomer is capable of redistribution to minimize the acrylate network residual stress. The IPN structure is finalized at the elevated temperature cure required to polymerize the epoxy network. However, since the epoxy has a higher coefficient of thermal expansion, during cool-down of the bulk IPN to room temperature the epoxy network will experience tensile residual stresses whereas the acrylate network will experience compressive residual stresses.

5.6 Compression Investigation

Access to the electron beam curing chamber was limited, and it was primarily used to produce samples for screening the effect of individual acrylate or epoxy network compositions incorporated into 50% acrylate + 50% epoxy IPNs. Initial results had shown that these IPNs had performance that deviated from a linear rule of mixtures relationship. To more fully explore the effect of acrylate versus epoxy composition, ultraviolet (UV) curing was employed using the BPADA + (50-50)Epoxy material system. Since most thermoset materials exhibit brittle failure prior to yielding, compression testing was selected because a true yield stress could be determined in addition to compressive modulus.

5.6.1 Compression Specimen Preparation

The samples ends were trimmed on a slow speed saw prior to compression testing to provide flat and parallel edges. ASTM D695, Standard Test Method for Compressive

Properties of Rigid Plastics, assumes that the compression specimens are prepared by machining operations with appropriate finishing steps taken to ensure smooth specimens. As a result, the cross section is assumed to be circular, and the minimum diameter is used to determine the cross sectional area. Since the PTFE tube segments used to cure the specimens exhibited some ovality, the cross section was assumed to be elliptical. Therefore, the effective specimen minimum diameter was calculated from the measurements of the minimum cross section combined with a measurement on the same section taken 90 degrees from the minimum measurement.

Equation 21

Where = *effective diameter used for cross sectional area*

= *minimum diameter measured along length of specimen*

= *diameter at same cross section as rotated* 90°

The specimens were tested in an Instron mechanical testing machine with a 100 kN load cell. The specimens were sandwiched between two ground tungsten carbide platens with PTFE tape placed between the specimen surface and the platen to reduce friction. The specimen/PTFE/platen assembly was placed between the Instron compression anvils. The strain was measured with a laser extensometer with the reflective tape placed on the edge of the compression anvils. Testing was conducted in accordance with ASTM D695 using a crosshead rate of 1.3 mm/min. The setup is shown in Figure 74.

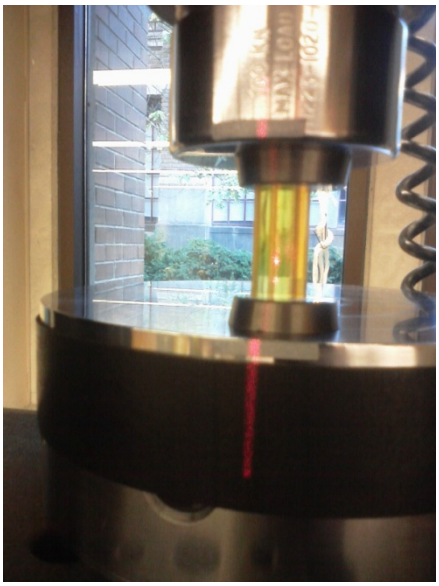

Figure 74: IPN compression testing setup

After yielding, the material undergoes substantial deformation prior to failure. Post-test images of the compression specimens are shown in Figure 75. A representative stress-strain curve is shown in Figure 76.

Figure 75: UV-cured compression test specimens in the BPADA + (50-50)Epoxy material system (after testing)

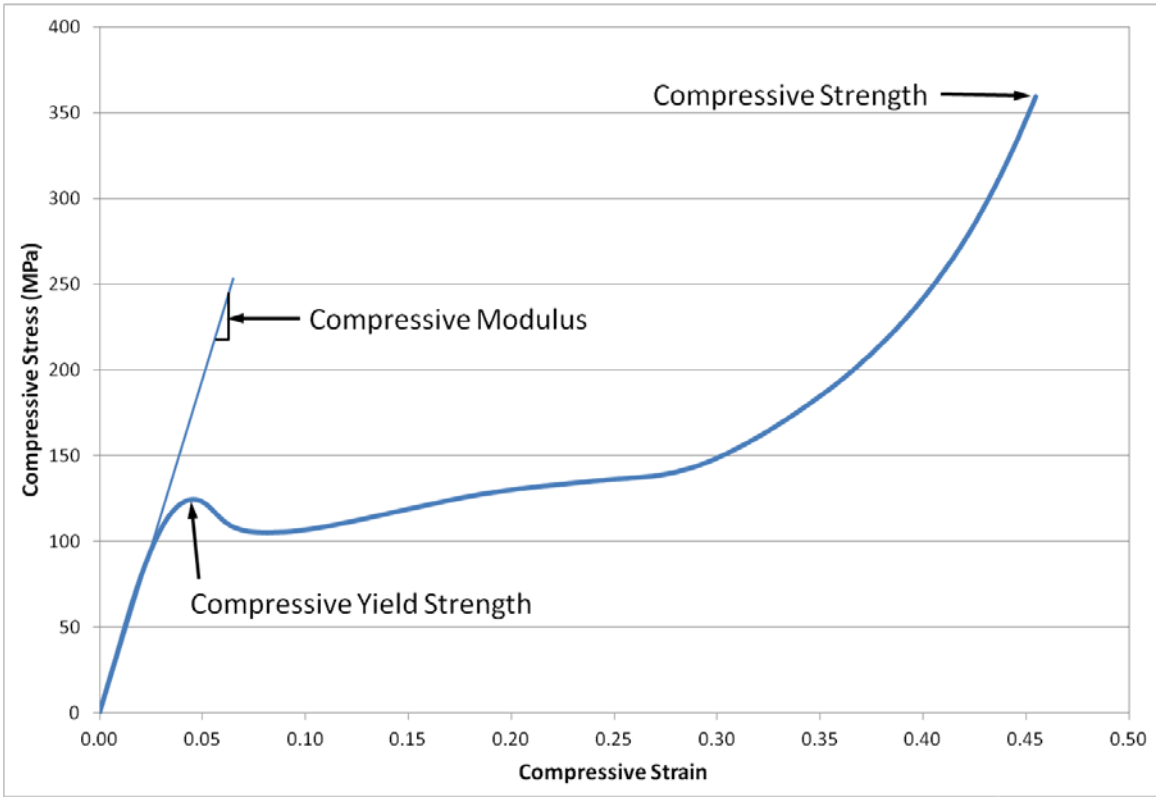

Figure 76: Representative compression stress-strain curve showing yield, modulus and ultimate strength points

5.6.2 Compression Yield Results

Most brittle polymers fail in tension prior to yielding. One advantage of compression testing is the ability to determine the yield stress which is defined as the first point at which an increase in strain does not result in an increase in stress. Using this definition, the compressive yield stress as a function of IPN composition is shown in Figure 77.

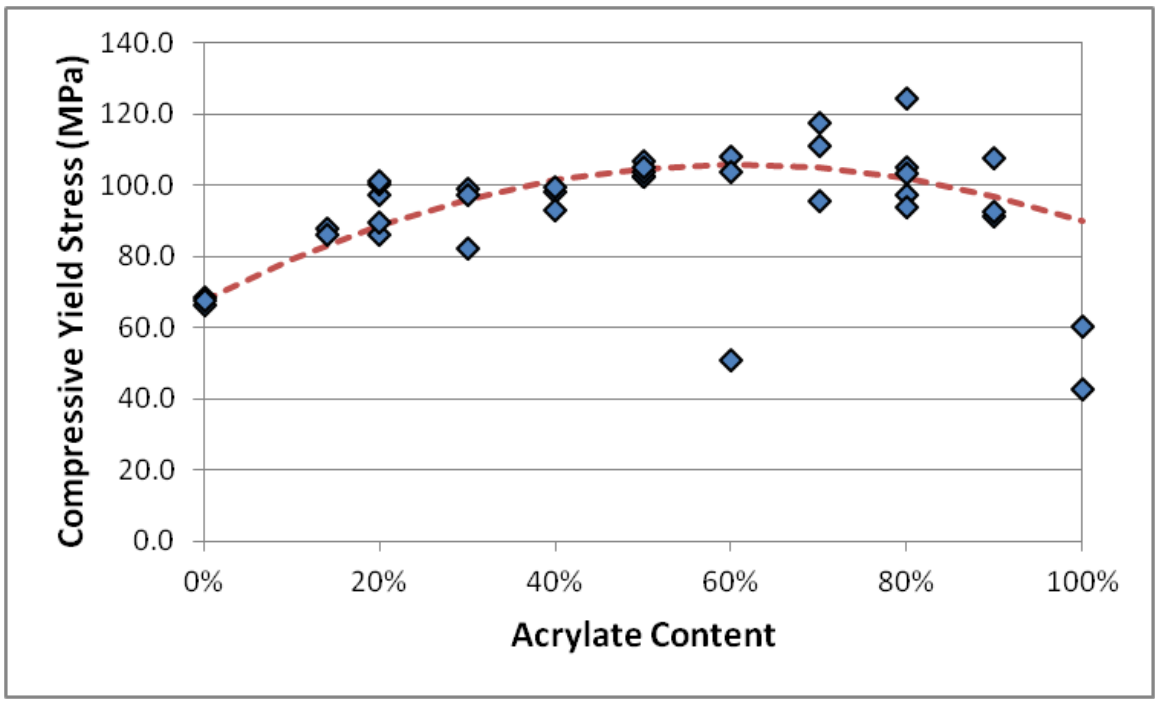

Figure 77: Compressive yield strength as a function of acrylate content in the BPADA + (50-50)Epoxy material system

A parabolic material response as provided by the interaction parameter is shown as a dashed line. The performance of the pure BPADA is deficient due to low degree of monomer conversion. Yield stresses were determined for two of the samples tests, but the third exhibited a substantially low modulus with no discernible yielding point despite a compressive strain of over 40 percent. It was assumed that the pure BPADA samples vitrified during UV cure whereas the IPN compositions did not, so the BPADA compression test values were not included in developing the parabolic response curve. Instead, a value of 90.9 MPa was projected as the compression yield strength of a more fully converted BPADA sample based on a least square error fit. The 60 percent acrylate specimen that exhibited low yield strength was shown by FTIR to have a 79 percent degree of cure

whereas the other 60 percent acrylate samples had a 94 percent degree of monomer conversion.

5.6.3 Compression Modulus Results

The compressive modulus of elasticity was calculated by determining the slope of the initial linear portion of the stress-strain curve. The results are shown in Figure 78.

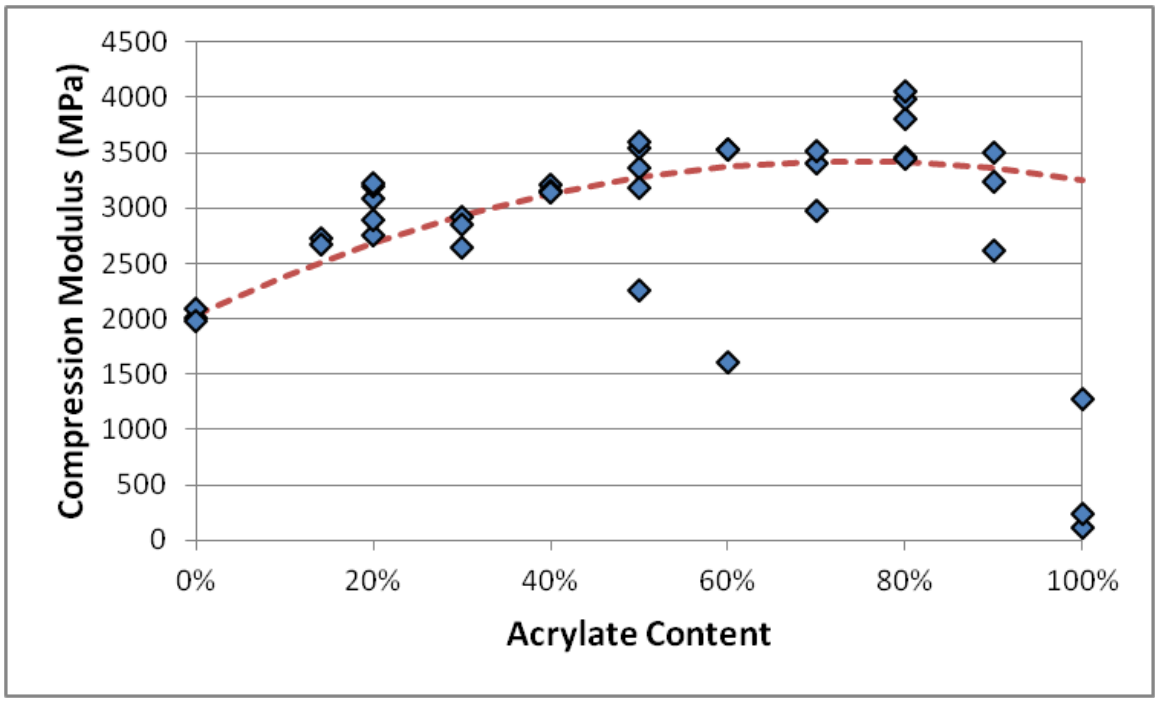

Figure 78: Compressive modulus as a function of acrylate content for the BPADA + (50-50)Epoxy material system

A parabolic material response as provided by the beta parameter is shown as a dashed line. Since the performance of the pure BPADA is deficient due to low degree of monomer conversion, a compression modulus of 2970 MPa for a more fully converted BPADA sample was projected based on a least square error fit. The 60 percent acrylate specimen that exhibited a low modulus was shown to have a 79 percent degree of cure whereas the other

60 percent acrylate samples had a 94 percent degree of monomer conversion. The 50 percent acrylate specimen that exhibited a low modulus was shown to have an 82 percent degree of cure whereas the other 50 percent acrylate samples had a 93 percent degree of monomer conversion.

5.6.4 Compression Test Discussion

Both the yield stress and the modulus showed a linear rule of mixture behavior between the 20 percent acrylate and 80 percent acrylate end points. The UV cured acrylate was not representative of the electron beam cured acrylate. The average modulus was 238 MPa in compression for UV cured BPADA samples compared to 4020 MPa in tension for electron beam cured samples. Due to either the presence of epoxy monomer delaying vitrification or due to BPADA-DGEBA copolymerization during the thermal cure cycle, the acrylate in the IPN compositions cured to a higher degree of conversion.

A comparison between the compressive performance of 80% BPADA + 20% (50-50)Epoxy IPN with tetra-functional epoxy 4,4'-tetraglycidyldiaminodiphenyl methane (TGDDM) cured with 4,4'-Diaminodiphenyl Sulphone (DDS) as tested by other researchers is provided in Figure 79. [92] The moduli of the two systems are comparable. The IPN yields at a lower stress level, but it exhibits higher ultimate strength and elongation prior to failure. It is possible that the IPN yield strength is artificially reduced in the UV compression testing due to surface porosity, incomplete cure or non-uniform specimen dimensions. Optimization of the acrylate or epoxy monomer selections, IPN acrylate/epoxy ratio or refinement of processing conditions such as improved degassing or electron beam curing might lead to an

IPN system that approaches the compression yield strength of this tetra-functional epoxy system which is widely used as the matrix material for carbon fiber composites.

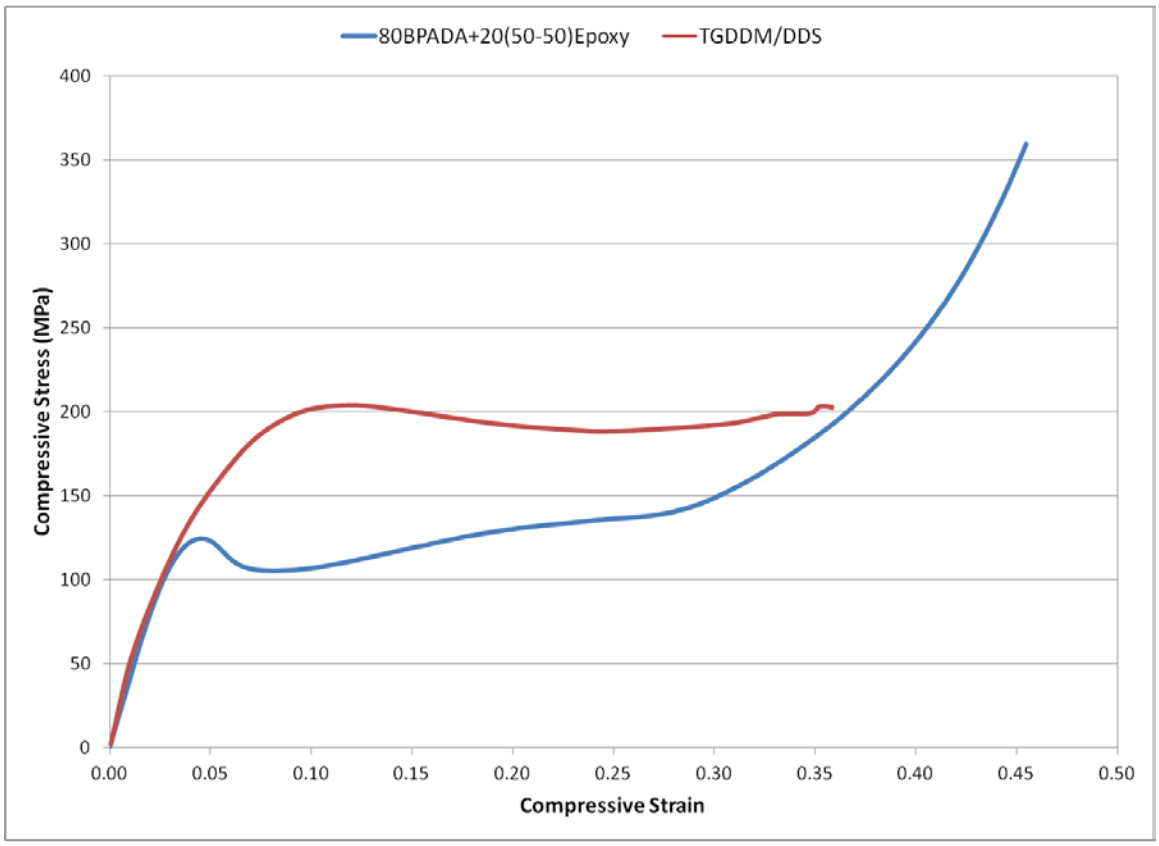

Figure 79: Comparison between compressive performances of 80% BPADA + 20% (50-50)Epoxy IPN and TGDDM/DDS

5.7 Fracture Toughness

The motivation for investigating an IPN adhesive was improved toughness over a single network acrylate system. Fracture toughness is an intrinsic material property, and it represents the material's ability to resist the growth of a sharp crack when subjected to loads that open the crack tip. Fracture toughness of polymeric materials is typically investigated by either single edge notched beams (SENB) or by compact tension (CT)

specimens. Of the two, SENB specimens require less material and are more easily prepared. The SENB geometry and recommended ratios are shown in Figure 80.

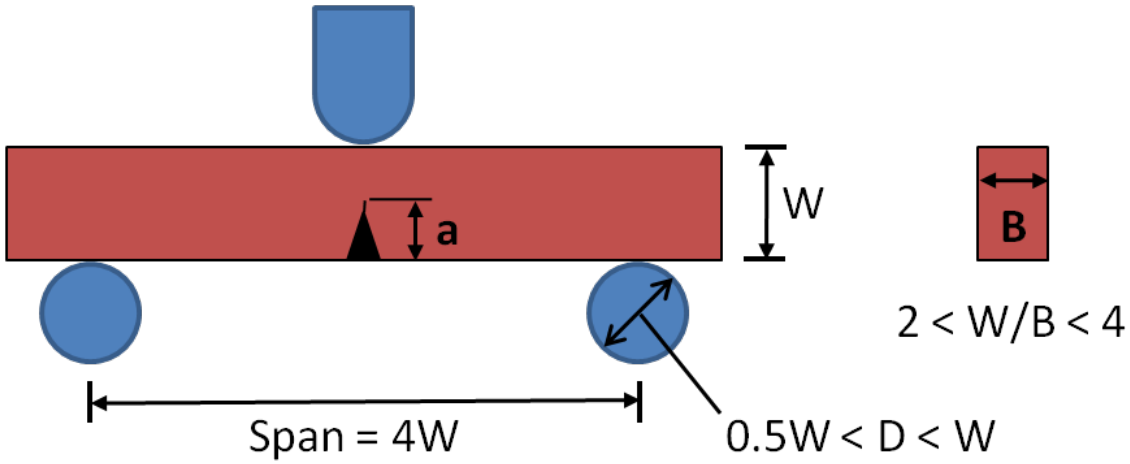

Figure 80: Single edge notched beam specimen geometry

The expectation for investigating toughness of different IPN formulations is to determine the origin of toughness improvements and to determine which parameters can lead to optimized performance. Parameters investigated include composition of the individual acrylate and epoxy networks and their relative volume fractions. Changing the type of epoxy employed also allowed investigation of the influence of miscibility between the acrylate and epoxy components.

5.7.1 SENB Specimen Preparation

Single edge notched beam specimens were prepared from cast resin bars. After removal from the mold, the upper surfaces were machined to produce a uniform sample width corresponding to twice the cast bar base thickness. The specimen blanks were trimmed to length and readied for precracking. Due to their low toughness, it is difficult to generate cracks in thermoset resin fracture toughness specimens.[93] ASTM D5045 recommends

tapping or sliding a fresh razor blade through a pre-cut notch. However, for the thermoset resins investigated in this project, attempts at tapping resulted in complete fracture of the specimen. Sliding the razor blade across pre-cut notches resulted in very minimal "natural crack" depths, and ASTM D5045 states that the depth of the razor notch be at least two times larger than the width of the sawed-in slot or the pre-notch tip radius. Therefore, an alternate procedure was developed.

ASTM D5024 guidelines recommend a total precrack length of 45 to 55 percent of the specimen width to ensure that the precrack satisfies the geometric constraints placed on the crack tip plastic zone. A notch was machined into the specimens using a 30 degree included angle, cone-shaped, 3.2mm diameter carbide cutter to minimize the machined notch radius (see Figure 81). Fracture toughness specimen blanks were clamped into a machinist's vise in a Bridgeport milling machine with several blanks sandwiched between plexiglass edge supports. The carbide cutter was mounted using the 3.2mm collet holder. Considering to the low fracture toughness of the bulk resins, the notch was machined to 37-40 percent of the width.

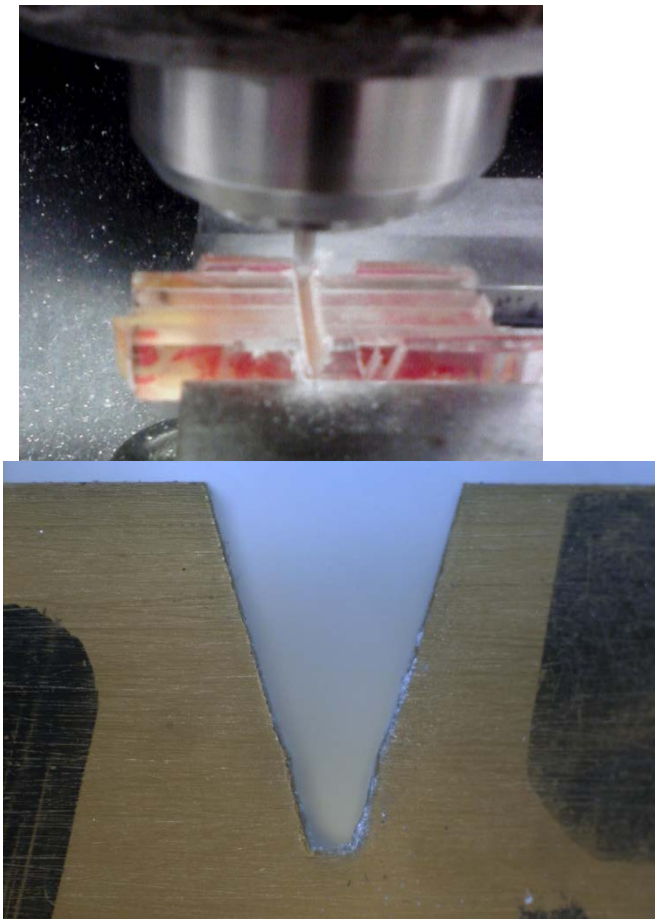

Figure 81: Precrack notch machining and resulting notch

Sharp crack tips were produced by pressing a razor blade into the machined notch using an Instron mechanical testing machine as shown in Figure 82. Pressing of razor blades into ductile resins is not recommended by ASTM D5045 since it can induce residual stresses at the crack tip. However, the samples used in this study were not ductile, so this caution statement is not applicable. Other researchers have used a similar approach by controlling the pressure used to press a sharp razor blade into a specimen. [94] [95] A single edge razor blade was lightly clamped between two strips of metal in the lower mechanical grip so that it extended approximately 6 mm from the end of the metal strips. Prior to tightening the lower grip, the razor blade edge was slowly jogged into contact with the compression test

anvil installed in the upper grip using the crosshead fine adjustment thumb wheel. When the razor blade was normal to the compression anvil, the crosshead was jogged away from the anvil, and the lower mechanical grip was firmly tightened. The Instron load cell was then zeroed, and the gap between the razor blade and the compression anvil was opened sufficiently to allow insertion of a SENB blank. The blade was placed against a full width section of the blank that was immediately adjacent to the machined notch. The crosshead was then jogged using the thumb wheel until a force of 0.5-1.0 N was indicated. The specimen gage length was then zeroed, and the crosshead was lowered so that the SENB blank could be removed. The machined notch was centered over the razor blade, and the crosshead was once again jogged using fine controls until a preload of 0.5-1.0 N was achieved. The Instron precrack routine was then engaged to push a razor blade into the notch at a rate of 1 mm/min to a programmed value of 45 percent of the beam width "W" (45 percent strain). An alternative end-of-test scenario corresponding to a load drop of 5 percent was used to account for development of natural precracks. For more brittle specimens, a peak load constraint of 175 N was also applied in an attempt to prevent fractures. A fresh razor blade edge was used for each specimen blank, and the development of a sharp crack tip was verified by inspecting the edges under an optical microscope. The result of the Instron sharp pre-cracking process was a mix of razor blade notches, sharp natural crack tips and full depth fractures. Prior to testing, the sides of the specimens were colored with a water soluble marker to assist in identification of the precrack features during post-test fractography.

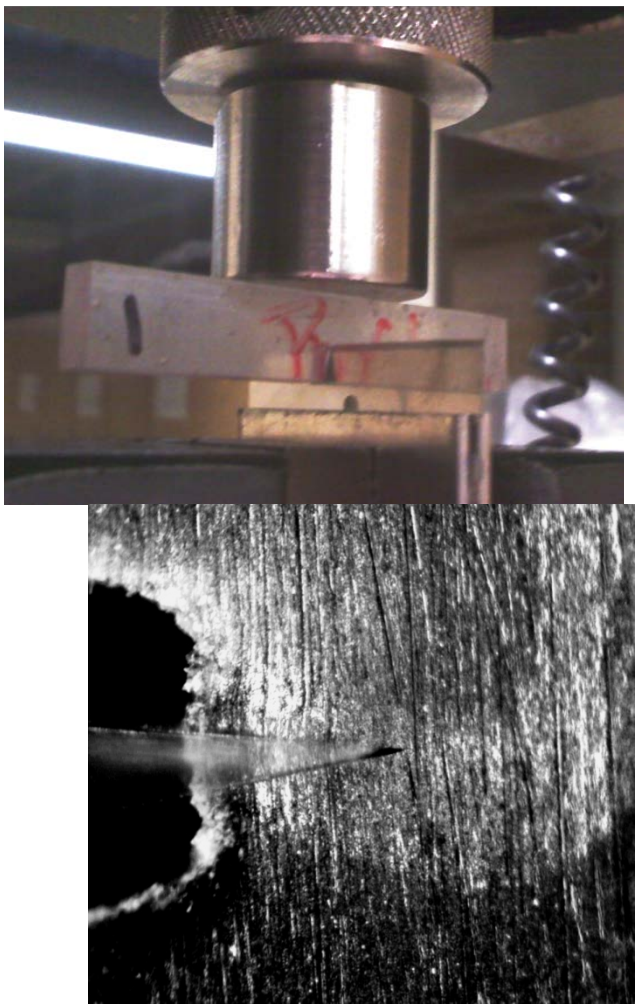

Figure 82: Instron razor blade pressing and sharp crack

Fracture toughness tests per ASTM D5045 were conducted under laboratory conditions using a crosshead rate of 10 mm/min. The precracked specimens were loaded in a three point bending mode with the single center point located on the upper surface opposite to the precrack and the two lower supports placed on a compression anvil that was placed on the crosshead. 6.35 mm diameter load pins were used for the upper and lower contact points. The lower support span was set to approximately four times the specimen width, and its length was measured and recorded. The lower support was centered beneath the upper load pin with the aid of a notched bar. After centering, the load cell was zeroed. The

specimen width, W, and base, B, were measured and recorded for each specimen. Specimens were centered on the lower span so that they were directly beneath the axis of the load cell. The crosshead was then jogged until a specimen preload of approximately 0.5-1.0 N was achieved. The specimen displacement was then zeroed, and the test sequence was initiated. Load-displacement curves were recorded until a drop in load of 20 percent or greater was detected.

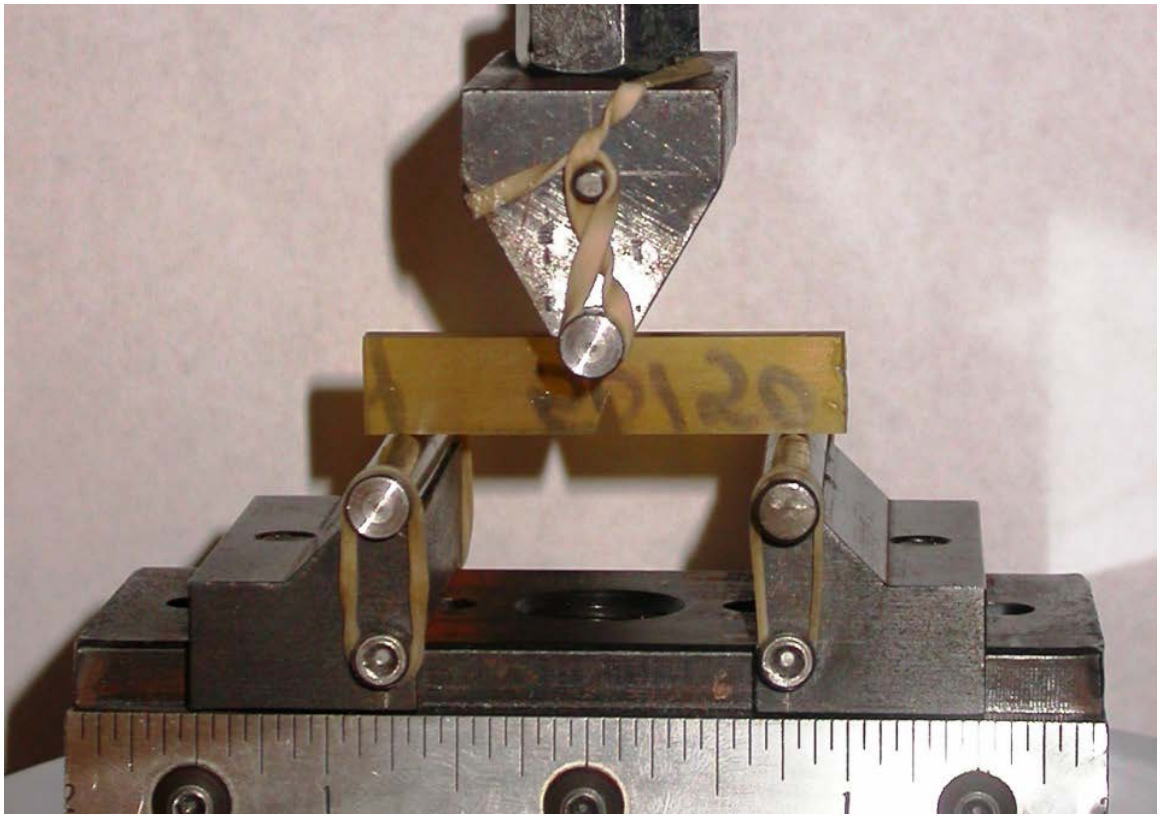

Figure 83: Fracture toughness test

5.7.2 SENB Test Analysis

The first step in determining the fracture toughness is to examine each specimen load-displacement curve to determine the compliance and the conditional fracture load. The load-displacement curve is analyzed by constructing two auxiliary lines, AB and AB'. Line AB

represents the best fit to the initial portion of the load-displacement curve, ignoring any non-linear, "toe-in" results from the initial specimen loading. The inverse of the slope of this line is the specimen compliance. A secondary line, AB', is constructed using the same displacement axis intercept point with a compliance that is 5 percent greater than the compliance of line AB. The conditional critical fracture load, P_Q, is then determined as the maximum specimen load that occurs between line AB and line AB'. A typical SENB load-displacement curve with construction lines AB and AB' is shown in Figure 84.

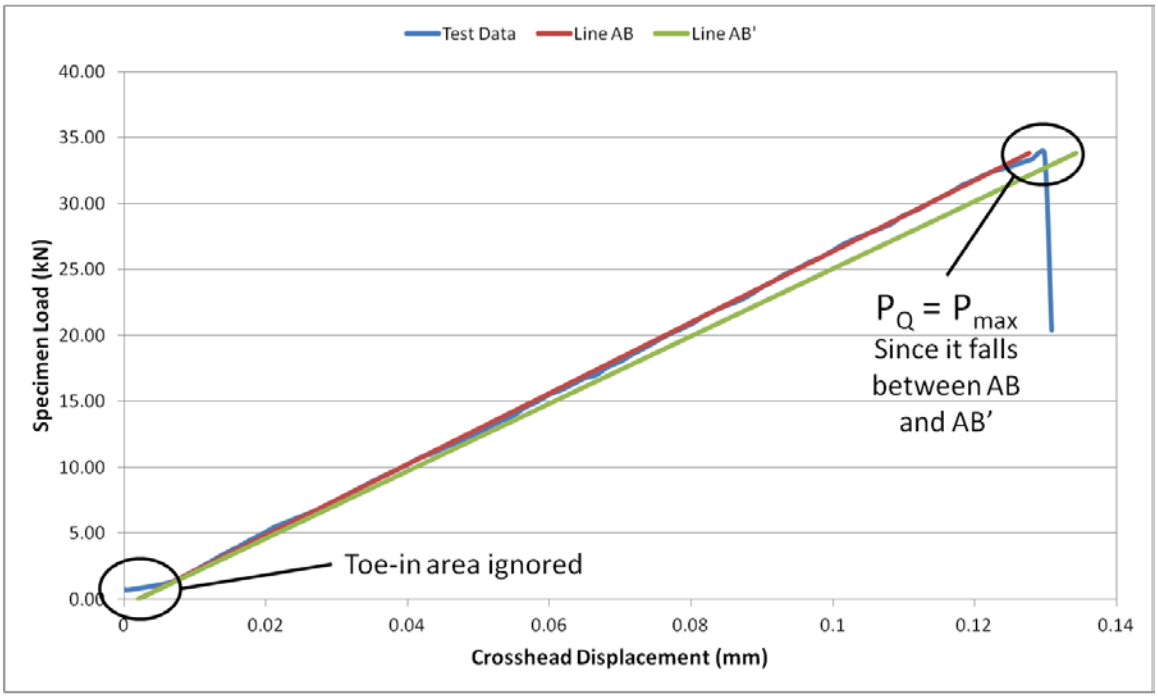

Figure 84: Typical SENB load-displacement curve

The first validity check on the SENB test is to determine the ratio of P_{max}/P_Q. If this ratio is greater than 1.1, the test is considered invalid. The load-displacement curves were nearly linear with P_Q equal to P_{max} for the acrylate, IPN, 70/30 epoxy and BECA epoxy samples. The

50/50 epoxy samples were more flexible, and a few failed the P_{max}/P_Q validity check. An example of an invalid load-displacement curve is shown in Figure 85.

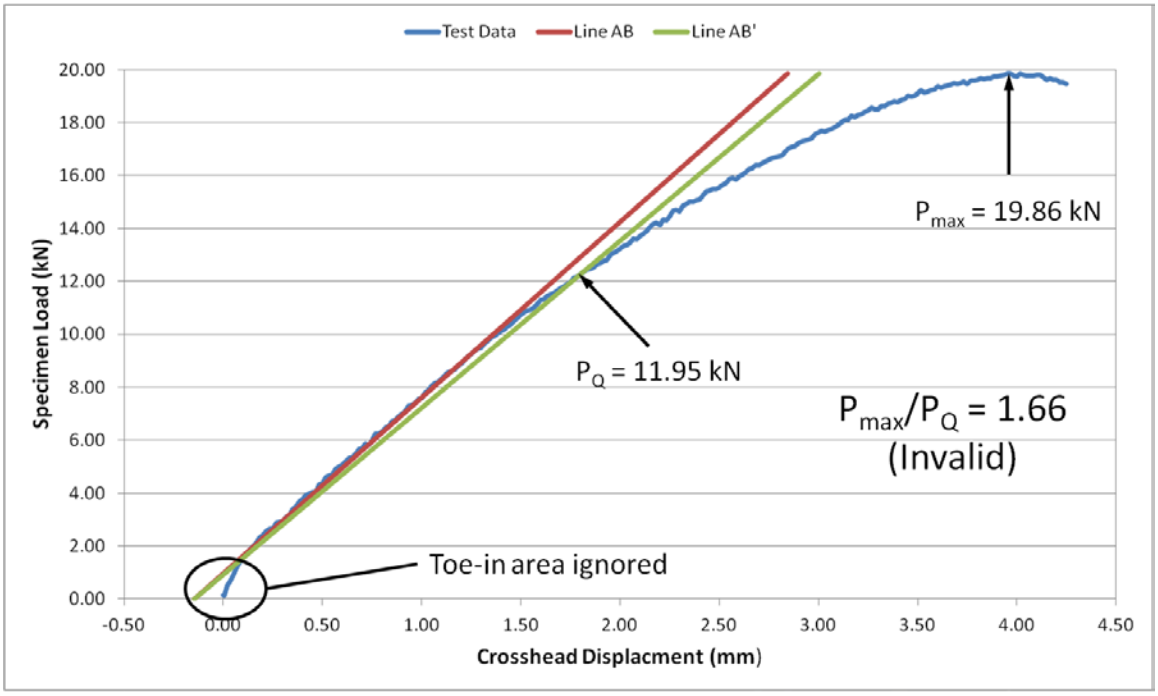

Figure 85: Invalid 50-50 epoxy SENB test load-displacement curve

Once the conditional critical fracture load, P_Q, has been determined, calculation of a provisional fracture toughness, K_Q, can be made using the test specimen geometry. The relevant geometry measurements include the specimen width, W, the specimen base, B, and the initial precrack length, a. The specimen width and base measurements were recorded during the fracture toughness test, but the precrack lengths could not be determined until after the specimens were fractured.

Specimen fracture surfaces were examined using an Olympus optical microscope with a reticle in one of the eyepieces. The microscope was fixed at a magnification of 8.75, and the reticle scale was determined by reading the length on a caliper that corresponded to

100 percent. Using this procedure, the full scale measurement was determined to be 10.4 mm. The precrack lengths were determined by recording the reticle percentage values corresponding to the center and the two edges of each fractured specimen cross section. The precrack length was determined as the average of threes three values multiplied by the reticle scale of 10.4 mm. A typical fracture surface and the three measurement locations used to determine the precrack length are show in Figure 86.

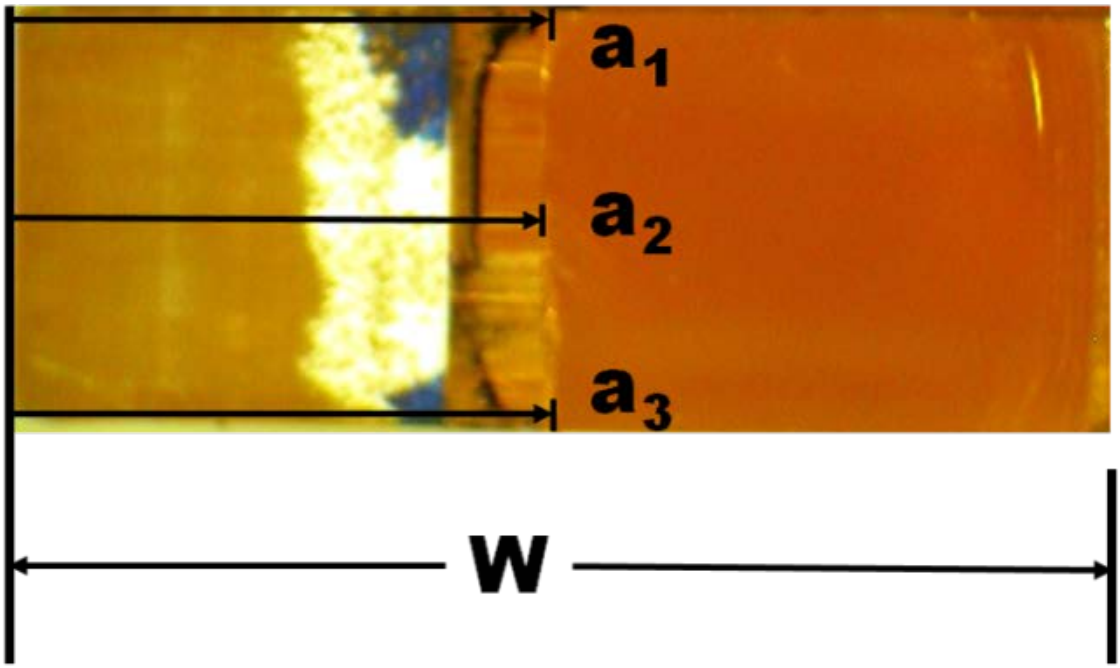

Figure 86: Precrack length measurements

Once the precrack lengths at the three locations were calculated, they were compared to determine the ratio of the longest length to the shortest length. Any specimens with crack fronts that had a longest to shortest length in excess of 1.10 were considered invalid.

With the conditional critical fracture load and the specimen geometry values, the provisional fracture toughness values can be determined through the use of Equation 22

$$K_Q = [P_Q / (BW^{1/2})] * f(x)$$ **Equation 22**

Where x = a/W

= *conditional critical fracture load*

B = *specimen thickness*

W = *specimen width*

a = *precrack length*

f(x) = *calibration factor*

The calibration factor, f(x), can be determined from a reference table or with the use of Equation 23.

$$\frac{\qquad\qquad\qquad\qquad}{\qquad\qquad\qquad\qquad}$$ **Equation 23**

The value of f(x) as a function of x = a/W is shown in Figure 87.

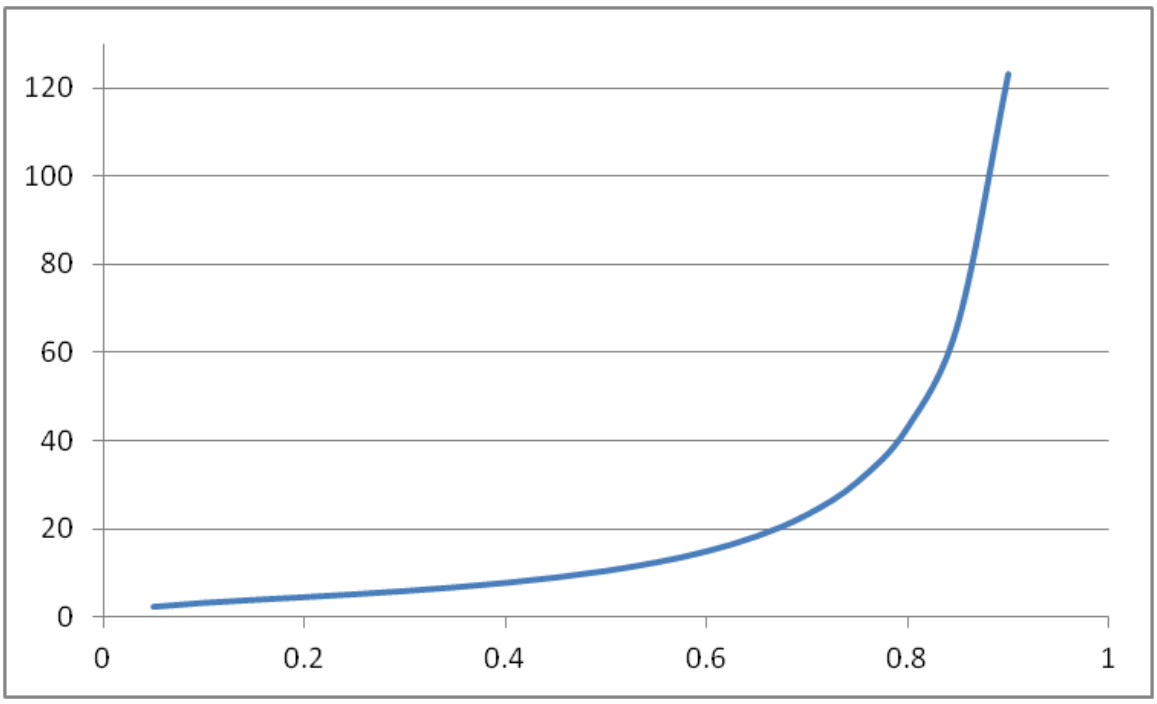

Figure 87: Precrack length function f(x) curve

Once the conditional K_Q has been determined, it is subject to a series of geometric checks to determine its validity. Due to stress concentrations around the crack tip, material within a certain radius has exceeded its yield point and has undergone plastic deformation. This irreversible deformation consumes energy and contributes to the toughness of a material. The size of the crack tip plastic zone is inversely proportional to the tensile yield stress, and it can be estimated by Equation 24.

$$r_P = 2.5 (K_Q / \sigma_y)^2 \qquad \text{Equation 24}$$

Where r_P = *radius of plastic zone*

K_Q = *conditional fracture toughness*

σ_y = *material yield stress*

The definition of yield stress used in ASTM D5045 is based on the maximum load sustained in a uniaxial tensile test divided by the cross sectional area. The terminology normally used to describe this value is "tensile strength". The use of tensile strength is recognized as contributing to a conservative plastic zone size value. The fracture toughness test is valid, and $K_{Ic} = K_Q$, if the value of r_P is less than the values of B, (W-a) and a. Failure to meet these criteria is indicative of the following situations:

$B \leq r_P$: the specimen is too narrow and plane strain conditions are not met

$(W-a) \leq r_P$: excess plasticity is present in the uncracked fracture toughness specimen ligament

$a \leq r_P$: the sharp crack tip is not far enough away from the free edge, resulting in stress field distortion near the crack tip

As discussed in the tensile strength section, some tensile tests were conducted on specimens with water jet cut edges that were not polished. Therefore, the tensile strength results for the unpolished tensile specimens represent an artificially low value due to the stress concentration imposed by the water jet ridges. To compensate, the yield stress for compositions tested in this condition was equated to the maximum tensile yield result obtained rather than the average tensile yield which is the value that was used for polished specimens.

The specimens with natural crack lengths within acceptable limits exhibited fracture toughness values that fell within the range of the razor blade precracked specimens, so the Instron precracking procedure does not seem to have significantly influenced the results.

5.7.3 SENB Results

Fracture toughness results were compiled for five different composition families. Since the IPNs are composed of two separately formed network, phase synergy was estimated by adapting the Kleiner modulus formula to the fracture toughness results as illustrated by Equation 25 and Equation 26.

Equation 25

$$=$$ **Equation 26**

Where $= interaction\ synergy\ parameter$

$= volume\ fraction\ of\ component\ X$

$= fracture\ toughness\ of\ pure\ acrylate$

$= fracture\ toughness\ of\ pure\ epoxy$

$= modulus\ of\ 50\%\ acrylate/50\%\ epoxy\ IPN$

Using the average fracture toughness values for the pure acrylate and pure epoxy components, projected trend lines for phase synergy were added to the chart of valid fracture toughness data points.

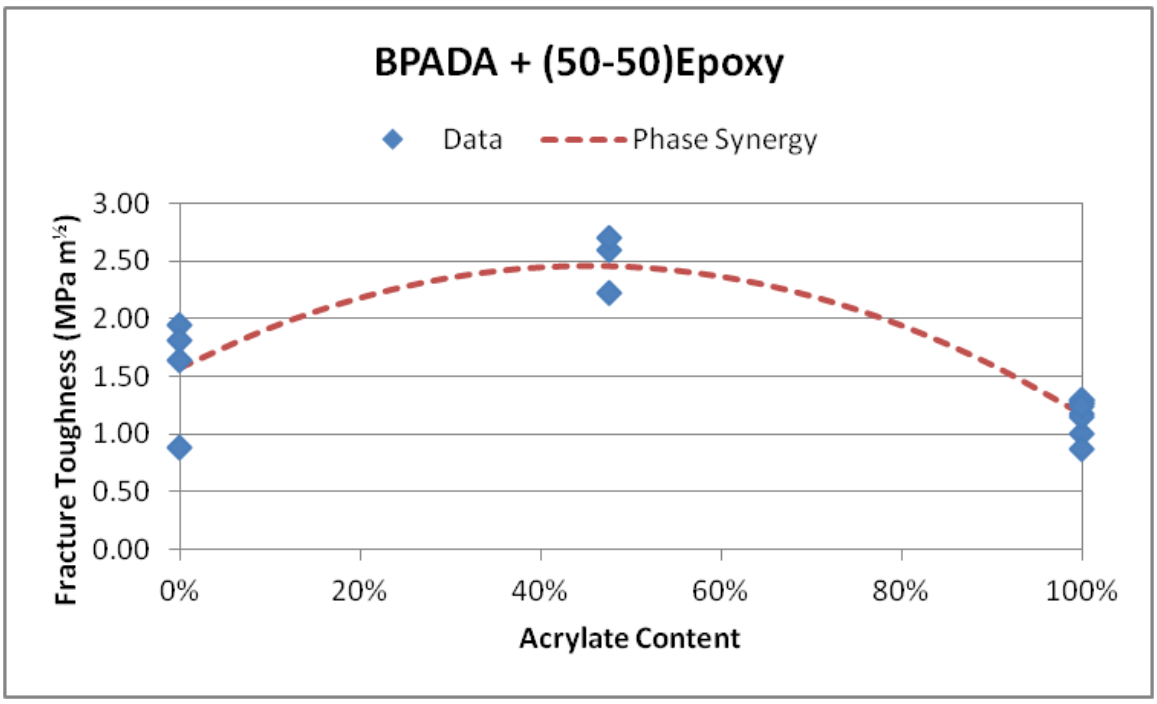

Figure 88: Fracture toughness results and phase synergy trend line for BPADA + (50-50)Epoxy material system

The results for the family composed of bisphenol A diacrylate (BPADA) plus an epoxy formulation of 50 parts by weight DGEBA, 50 parts PPDGE and 10 parts EMI {"(50-50)Epoxy"} are shown in Figure 88. One (50-50)Epoxy specimen failed at a value of 0.89 MPa $m^{½}$ whereas the other three specimens failed at an average value of 1.80 MPa $m^{½}$. The low toughness specimen passed all validity checks, so the resulting average toughness for (50-50)Epoxy was 1.57 MPa $m^{½}$. The BPADA specimens had an average toughness of 1.17 MPa $m^{½}$. The 48% acrylate IPN had an average toughness of 2.60 MPa $m^{½}$, which was 93% greater than the value that would be expected from a linear rule of mixtures relationship. While there is some scatter in the data, this appears to be a real improvement as opposed to the result of experimental error. The interaction synergy parameter, , was calculated to be 4.30 MPa $m^{½}$.

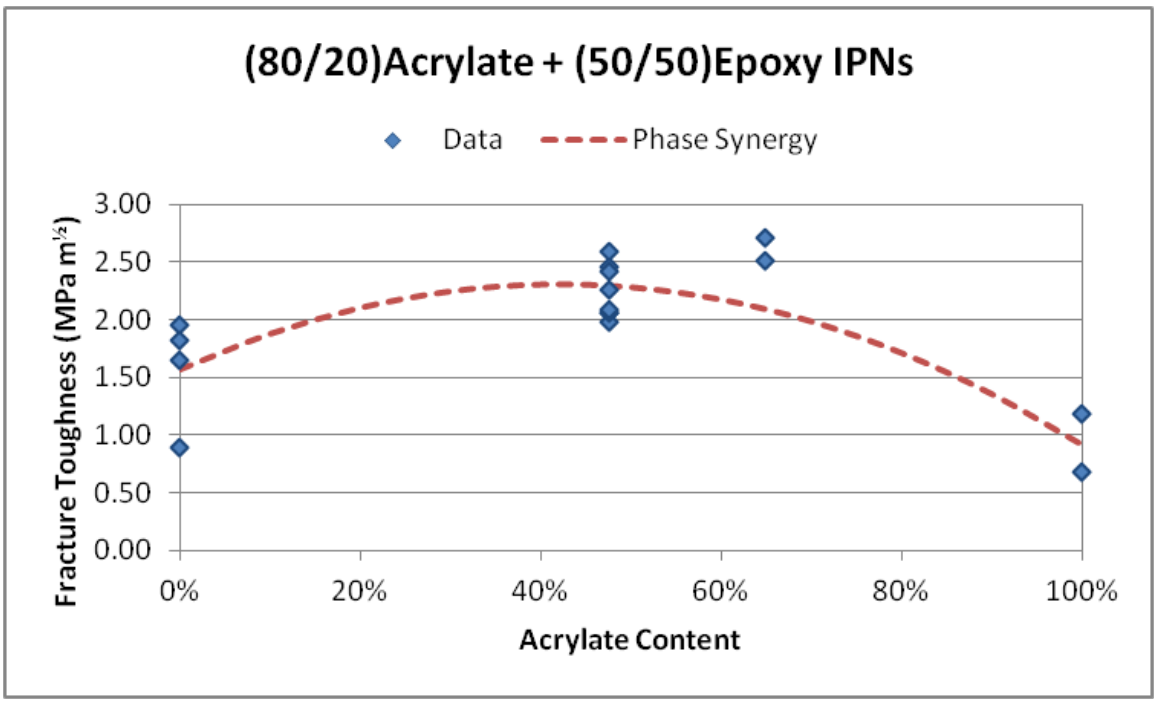

Figure 89: Fracture toughness results and phase synergy trend line for (80-20)Acrylate + (50-50)Epoxy material system

The results for the material system composed of an acrylate mixture of 80 parts bisphenol A diacrylate plus 20 parts trimethylolpropane triacrylate {"(80-20)Acrylate"} combined with (50-50)Epoxy are shown in Figure 89. The (80-20)Acrylate specimens had an average toughness of 0.80 MPa $m^{½}$. The 48% acrylate IPN had an average toughness of 2.23 MPa $m^{½}$, which was 77% greater than the value that would be expected from a linear rule of mixtures relationship. The 65% acrylate IPN toughness was even better with a value of 2.60, resulting in an improvement of 126% over the rule of mixtures. The interaction synergy parameter, , was calculated to be 4.14 MPa $m^{½}$.

Optical microscopy images of the fracture surfaces for the (80-20)Acrylate + (50-50)Epoxy system are shown in Figure 90. The upper portion of all three fracture surfaces show the machined notch area, followed by the razor blade pre-crack with the surface generated by

the SENB test shown in the lower portion of the image. For the (50-50)Epoxy fracture surface in Figure 90 a), there a few striations that disturb the otherwise glassy fracture surface. The (80-20)Acrylate image in Figure 90 c) shows a very short pre-crack region followed by a smooth, glassy fracture surface. The 48% acrylate IPN specimen image reveals a significantly different surface. Although it is not rough, there is a high density of striations in the initial fracture region which gradually transition into a smooth and glassy surface.

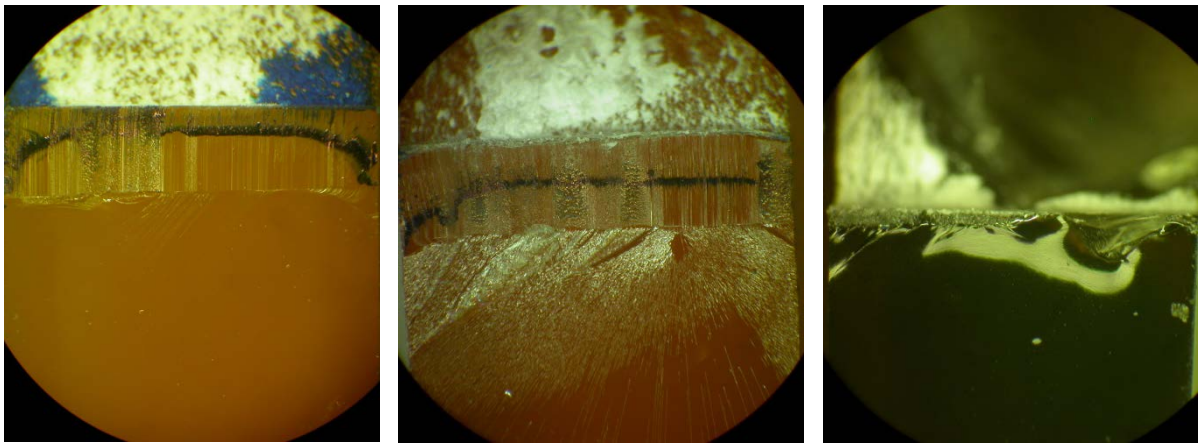

a) b) c)

Figure 90: Fracture surfaces for (80-20)Acrylate + (50-50)Epoxy SENBs - a) (50/50)Epoxy, b) 48%(80-20)Acrylate+52%(50-50)Epoxy IPN, c) (80-20)Acrylate.

An SEM image of the fracture surface for a 65% acrylate specimen is shown in Figure 91. In addition to the striations, the image reveals that some material has been torn away from a surface that is not on the primary fracture plane.

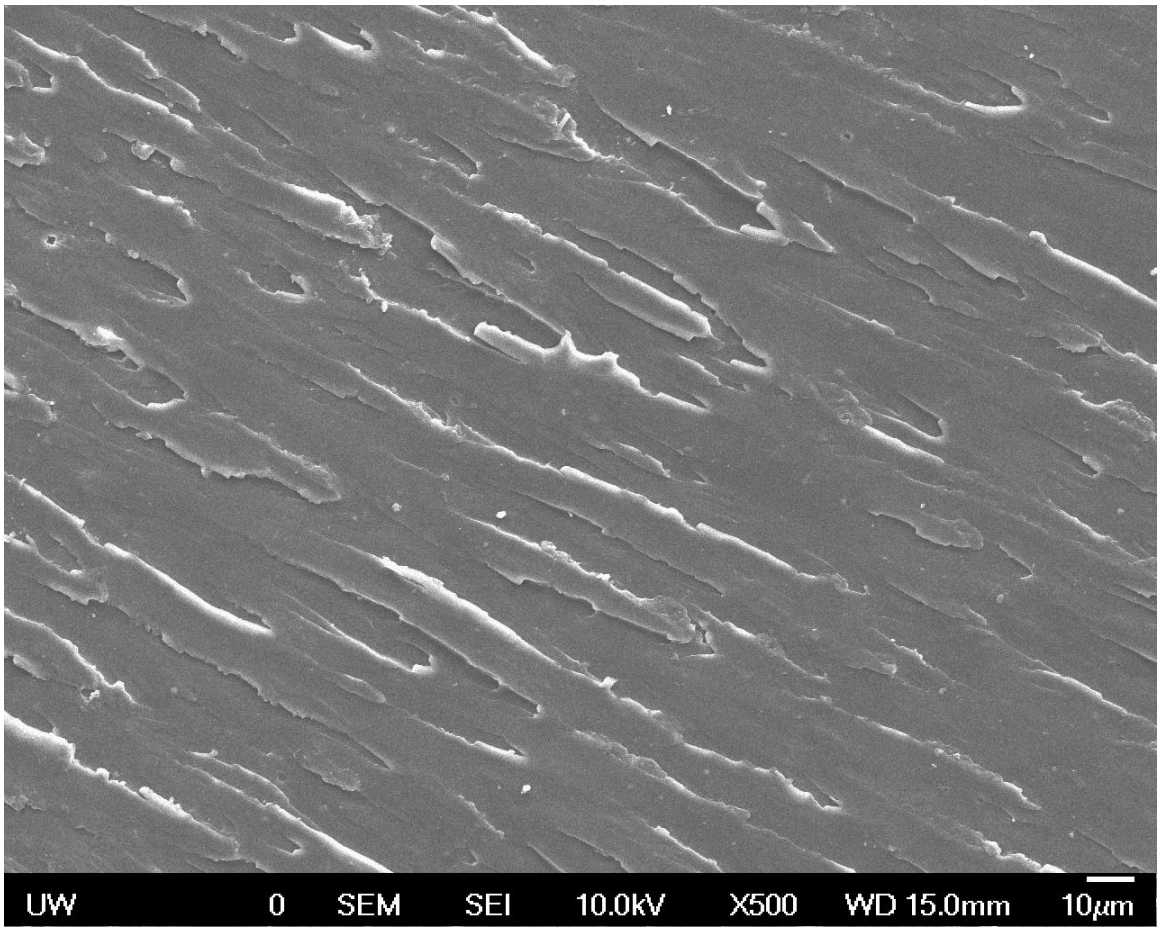

Figure 91: SEM fracture surface image for 65% (80-20)Acrylate + 35% (50-50)Epoxy SENB

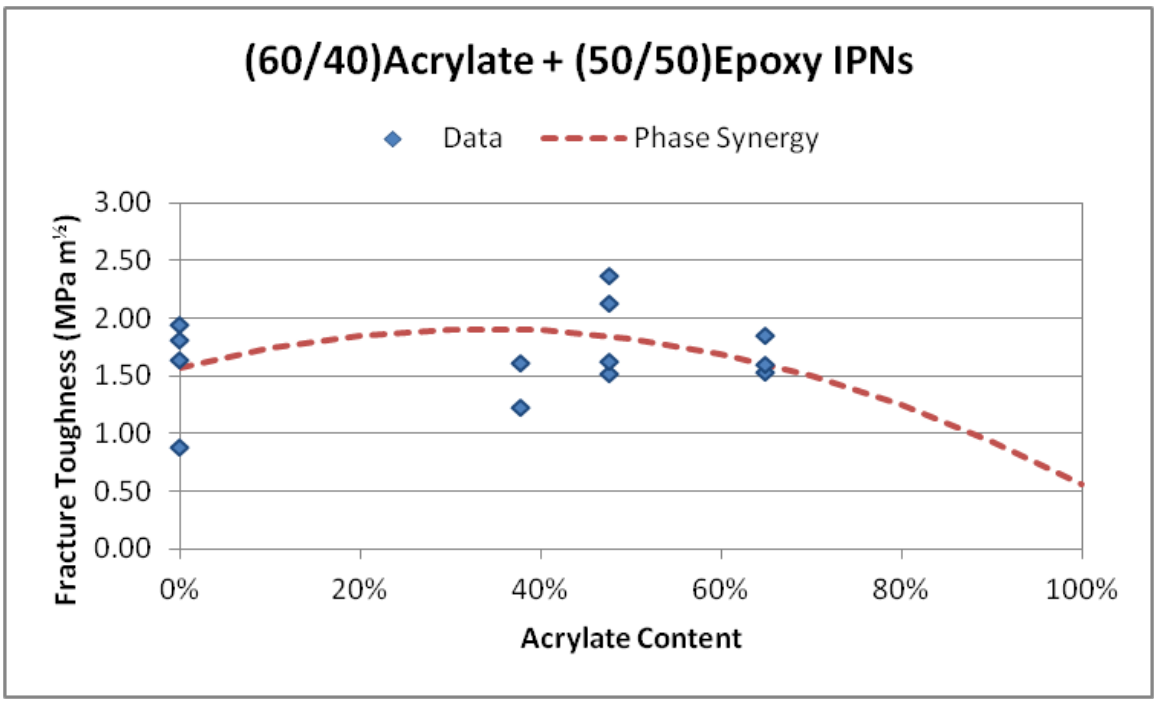

Figure 92: Fracture toughness results and phase synergy trend line for (60-40)Acrylate + (50-50)Epoxy material system

The results for the material system composed of an acrylate mixture of 60 parts bisphenol A diacrylate plus 40 parts trimethylolpropane triacrylate {"(60-40)Acrylate"} combined with (50-50)Epoxy are shown in Figure 92. No valid test results were produced for the pure (60-40)Acrylate composition, so the conditional K_Q value of 0.56 MPa $m^{½}$ for a test specimen that had an invalid precrack geometry due to a "pop-in" crack was used. This value was close to the estimated value of 0.67 MPa $m^{½}$ obtained by extrapolation from the BPADA and (80-20)Acrylate fracture toughness averages. The 48% acrylate IPN had an average toughness of 1.91 MPa $m^{½}$, which was 76% greater than the value that would be expected from a linear rule of mixtures relationship using the conditional (60-40)Acrylate K_Q value. The midrange toughness is less than observed in the (80-20)Acrylate + (50-50)Epoxy system, which is expected since the higher degree of cross linking in the (60-40)Acrylate should

result in a more brittle composition that has reduced capability for local plastic deformation. The interaction synergy parameter, , was calculated to be 3.26 MPa $m^{½}$.

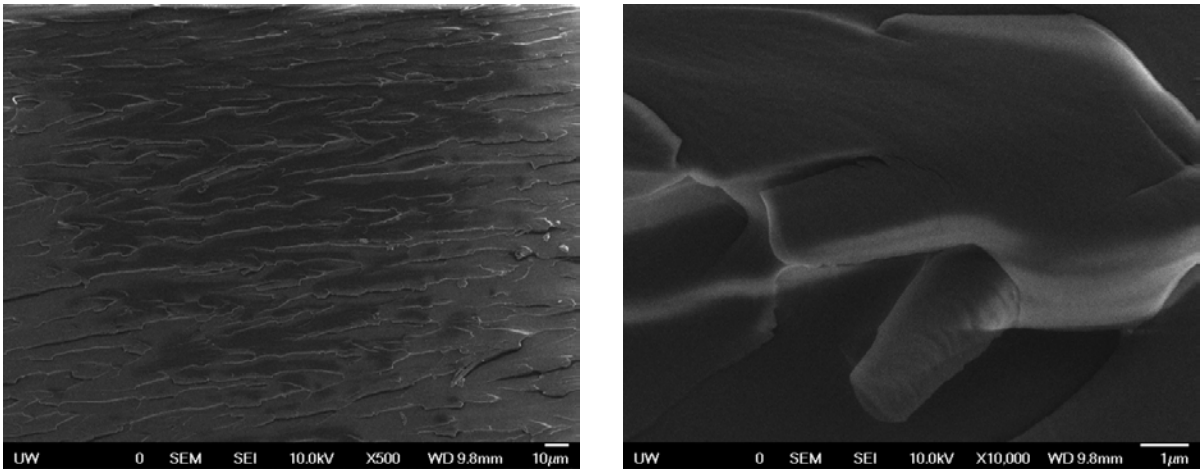

Figure 93: SEM fracture surface images for 65% (60-40)Acrylate + 35% (50-50)Epoxy SENB

SEM images of the fracture surface of a 65% (60/40)Acrylate + 35% (50/50)Epoxy fracture toughness specimen are shown in Figure 93. The image on the left shows material torn away from the primary fracture plane, similar to the surface of the 65% (80-20)Acrylate + 35% (50-50)Epoxy sample in Figure 91. The image on the right shows a close-up image of a partially torn surface feature.

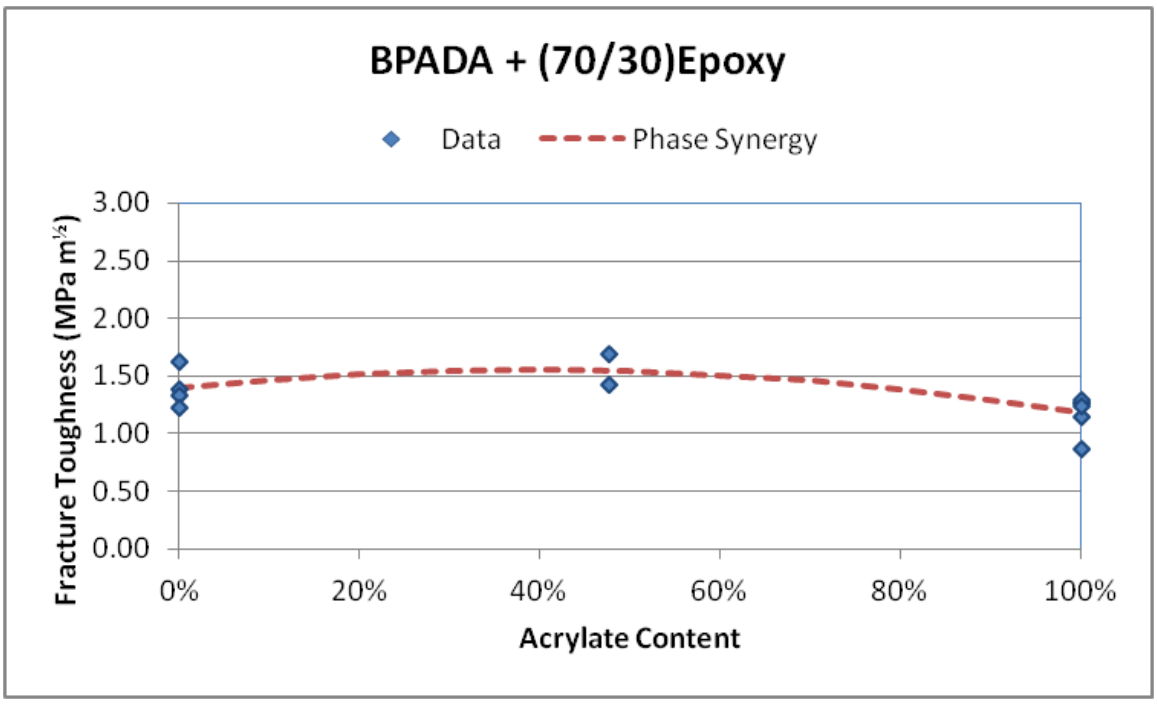

Figure 94: Fracture toughness results and phase synergy trend line for BPADA+ (70-30)Epoxy material system

The results for the family composed of bisphenol A diacrylate (BPADA) plus an epoxy formulation of 70 parts by weight DGEBA, 30 parts PPDGE and 10 parts EMI {"(70-30)Epoxy"} are shown in Figure 94. The (70-30)Epoxy specimens had an average toughness of 1.40 MPa $m^{½}$. The fracture toughness performance of this material system is much closer to a linear rule of mixtures relationship. However, the 48% acrylate IPN had an average toughness of 1.56 MPa $m^{½}$, which was still 21% greater than the value that would be expected from the rule of mixtures relationship. The interaction synergy parameter, , was calculated to be 1.02 MPa $m^{½}$.

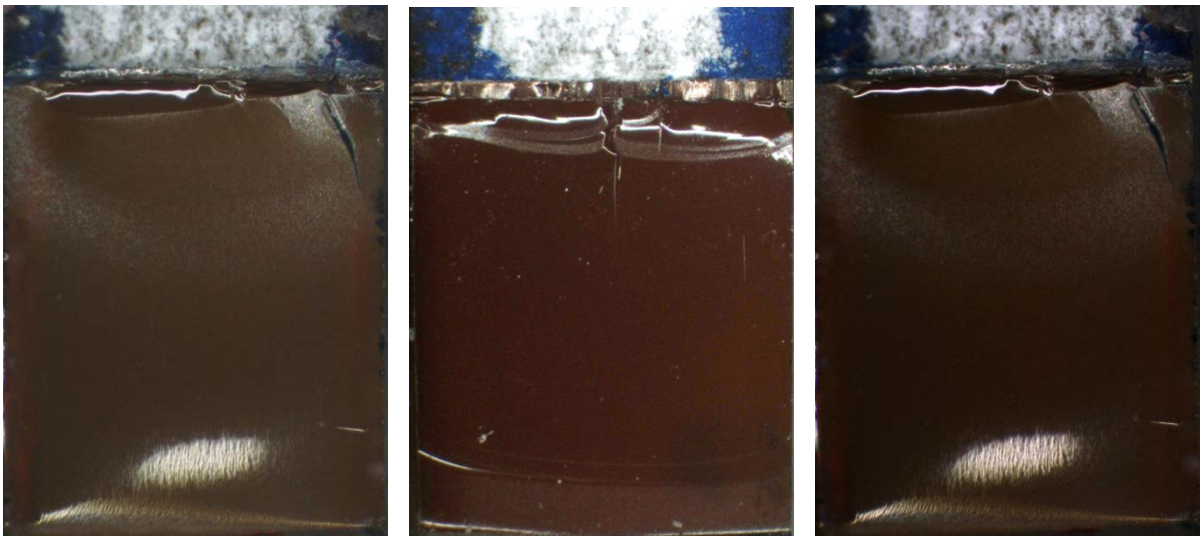

a) b) c)

Figure 95: BPADA + (70/30)Epoxy fracture surfaces -
a) (70-30)Epoxy, b) 48% BPADA + 50% (70-30)Epoxy, c) BPADA

Optical microscopy images of the fracture surfaces for the (80-20)Acrylate + (50-50)Epoxy system are shown in Figure 95. All three images have a shiny area just below the razor blade pre-crack, indicating a short amount of stable crack growth prior to fast fracture. The (70-30)Epoxy fracture surface in Figure 95a) has a fine striation pattern that is barely visible. The BPADA image in Figure 95 c) also shows some fine striations. The 48% acrylate IPN specimen is almost entirely smooth.

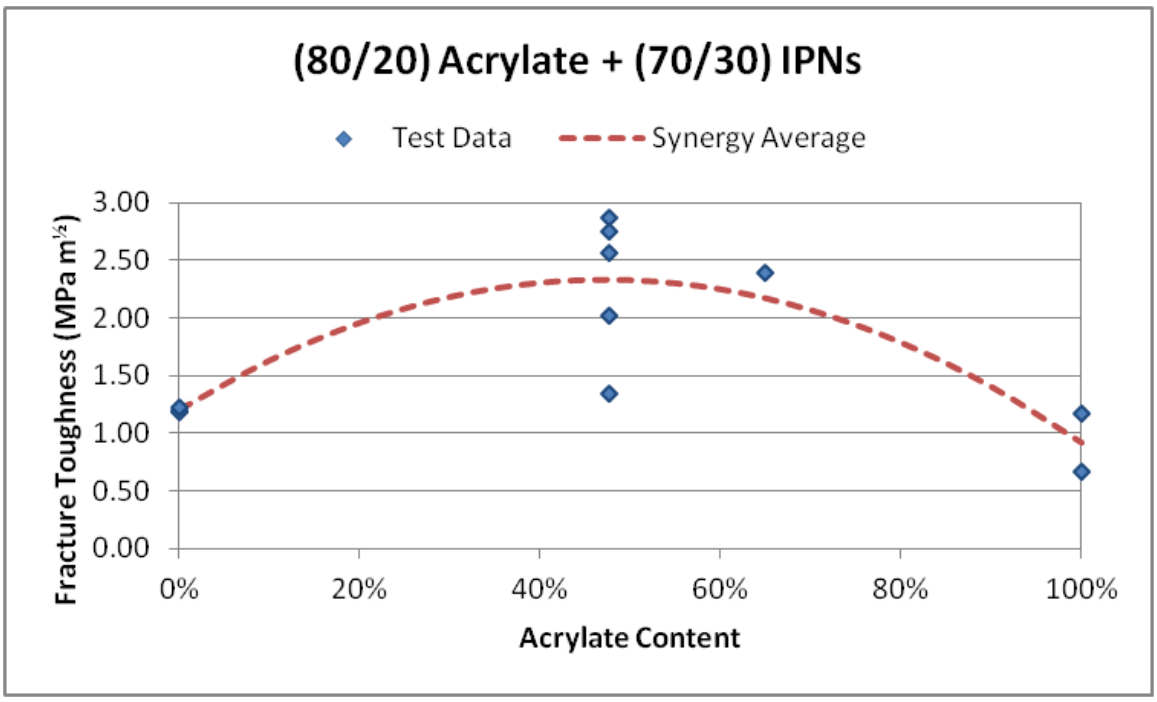

Figure 96: Fracture toughness results and phase synergy trend line for (80-20)Acrylate + (70-30)Epoxy material system

The results for the material system composed of an acrylate mixture of 80 parts bisphenol A diacrylate plus 20 parts trimethylolpropane triacrylate {"(80-20)Acrylate"} combined with (70-30)Epoxy are shown in Figure 96. The 48% acrylate IPN had an average toughness of 2.32 MPa $m^{½}$, which was 116% greater than the value that would be expected from a linear rule of mixtures relationship. The interaction synergy parameter, , was calculated to be 5.04 MPa $m^{½}$.

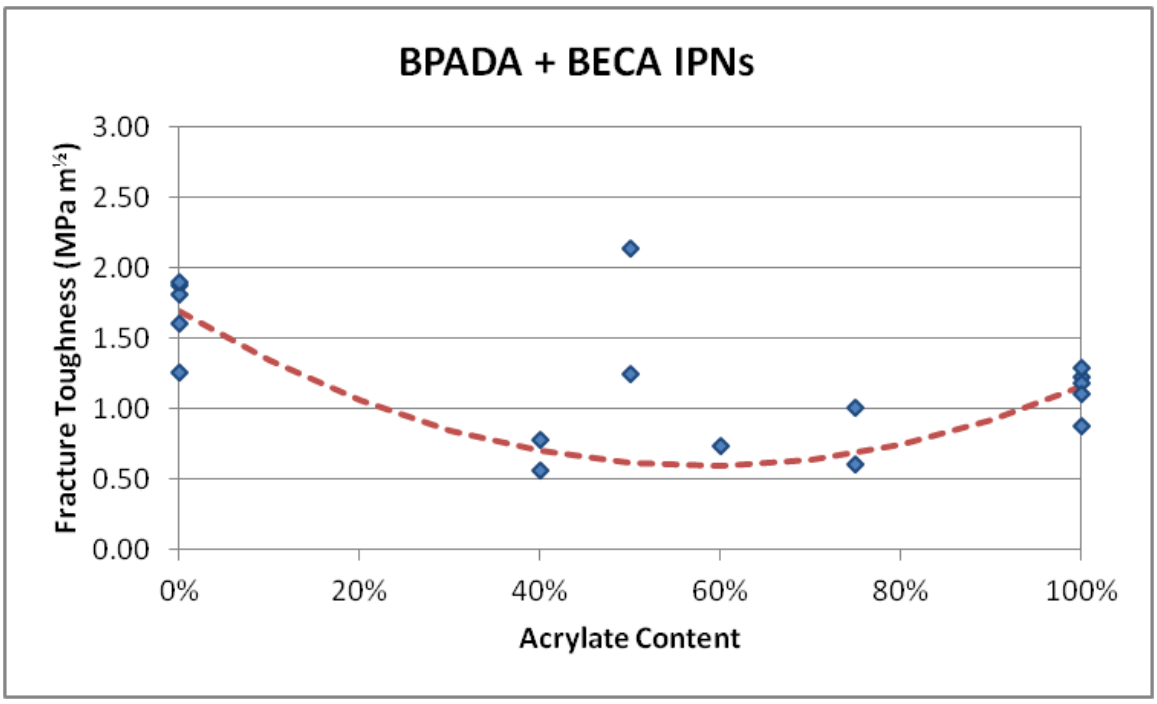

Figure 97: Fracture toughness results and phase synergy trend line for BPADA + BECA material system

The results for the family composed of bisphenol A diacrylate (BPADA) plus an epoxy formulation of 100 weight percent bis((3,4-epoxycyclohexyl)methyl)adipate with 70 weight percent methylhexahydrophthalic anhydride ("BECA") are shown in Figure 97. The BECA epoxy specimens had an average toughness of 1.46 MPa $m^{½}$. The fracture toughness performance of this material system is the only one to demonstrate negative synergy which is observed for the 40% acrylate and 60% acrylate IPNs. However, the 50% acrylate IPN had an average toughness of 1.42 MPa $m^{½}$, which was still 19% greater than the value that would be expected from the rule of mixtures relationship. There was a fairly large difference in the values from the two valid 50% acrylate specimens with the lower of the two values falling below the rule of mixtures prediction. Since the fracture toughness of the 50% acrylate composition varied so significantly from the 40% and 60% acrylate

compositions, the interaction synergy parameter was estimated as an interpolation between these two compositions. The resulting was calculated as -3.24 MPa $m^{½}$.

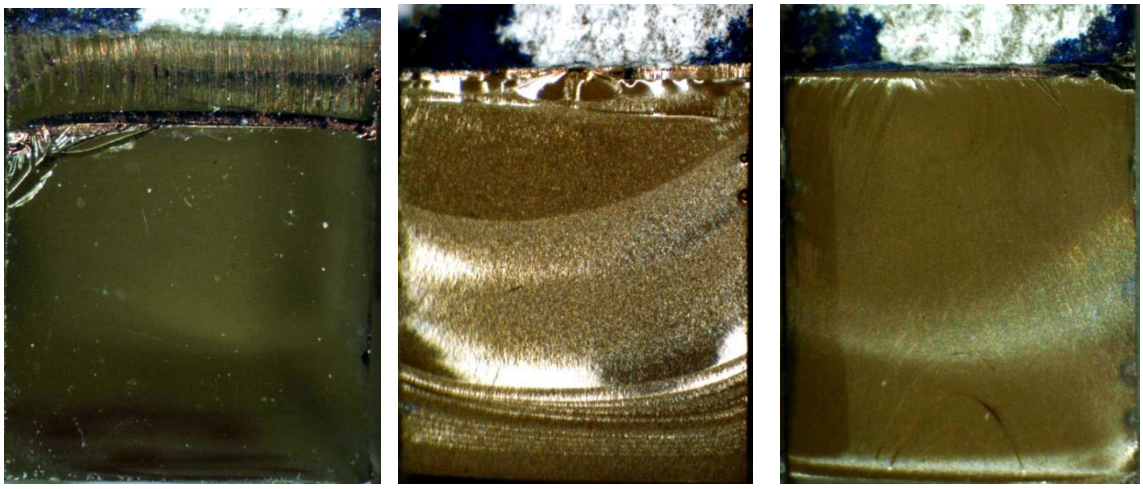

a) b) c)

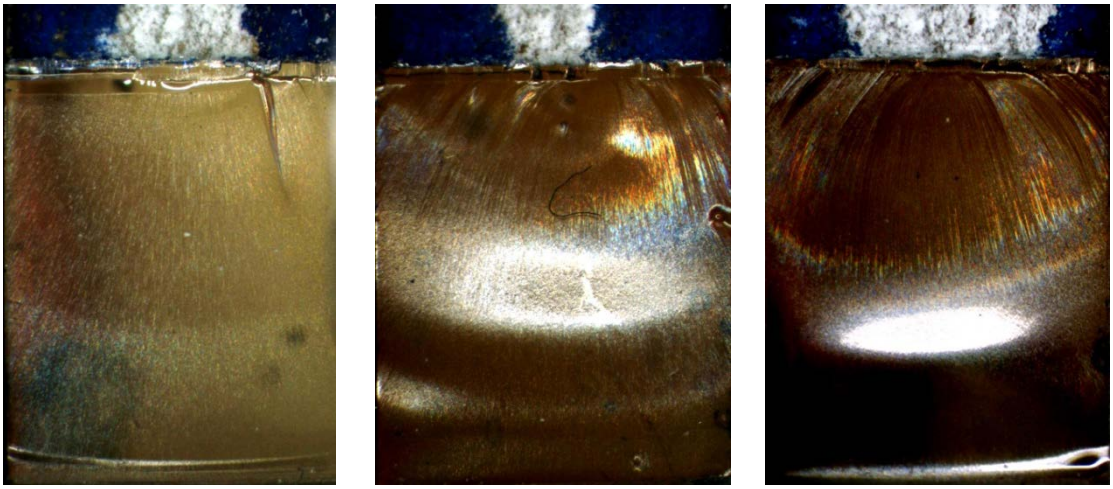

d) e) f)

Figure 98: SENB fracture surfaces for BPADA + BECA system - a) BECA epoxy, b) 40%BPADA+60%BECA, c) 50%BPADA+50%BECA, d) 60%BPADA+40%BECA, e) 75%BPADA+25%BECA, f) BPADA

Optical microscopy images of the fracture surfaces for the BPADA + BECA system are shown in Figure 98. The pure BECA epoxy fracture surface shown in part a) is smooth and

featureless. The IPN images in parts b), c), d) and e) along with the pure acrylate sample in part f) have fine texture that is accentuated by the lighting.

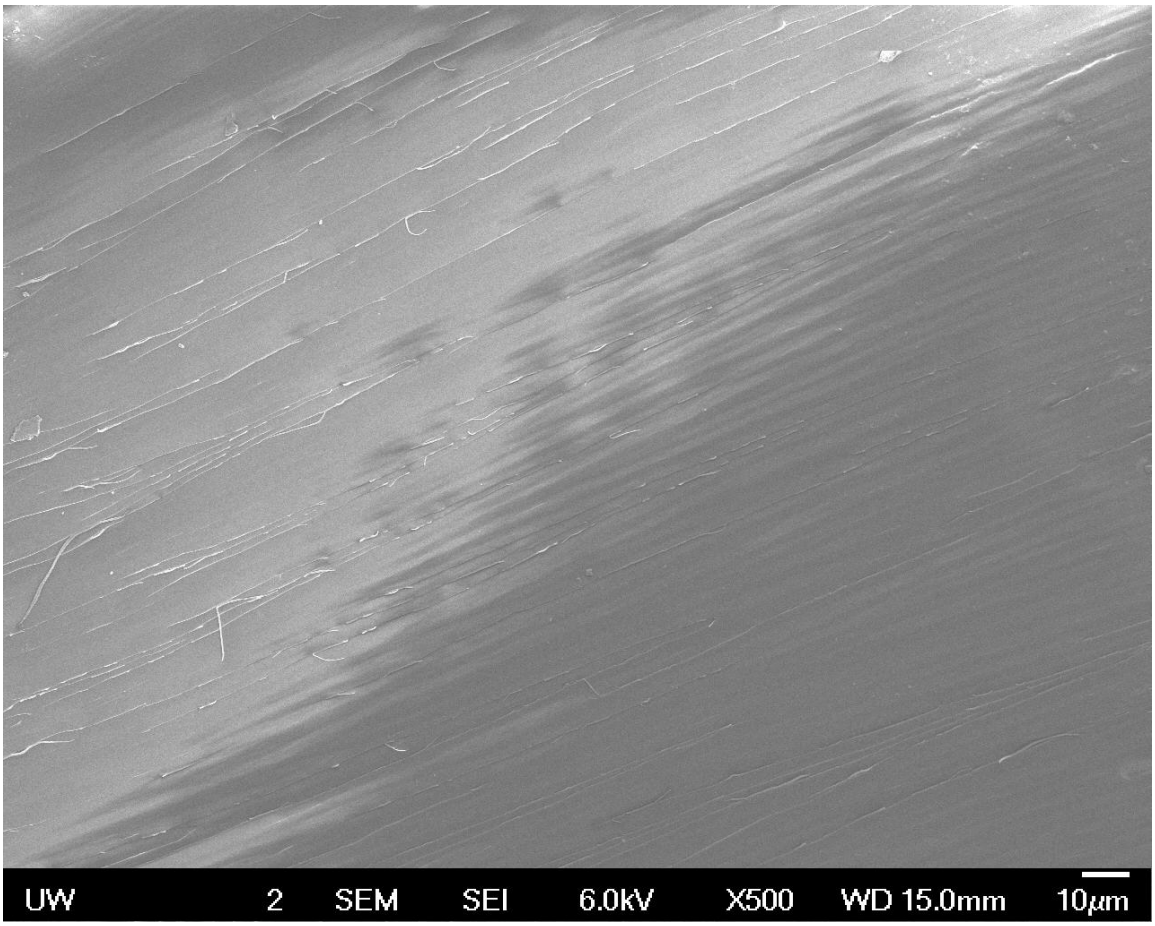

Figure 99: SEM fracture surface image of 60% BPADA + 40% BECA SENB

An SEM image of the 60% BPADA + 40% BECA IPN fracture surface is shown in Figure 99. The fine striation texture is visible, but the surface is otherwise smooth.

5.7.4 Fracture Toughness Discussion

Many of the optical and SEM images of the SENB fracture surfaces had a fine texture that appears to be caused by striations emanating from the crack tip generated during the pre-cracking step. In many cases, these striations disappear some distance away from the initial

crack tip. Similar crack initiation features in other research have been associated with generating a blunt crack tip during the precrack phase. [96] [97] Blunt precracks require higher fracture energy in order to propagate.

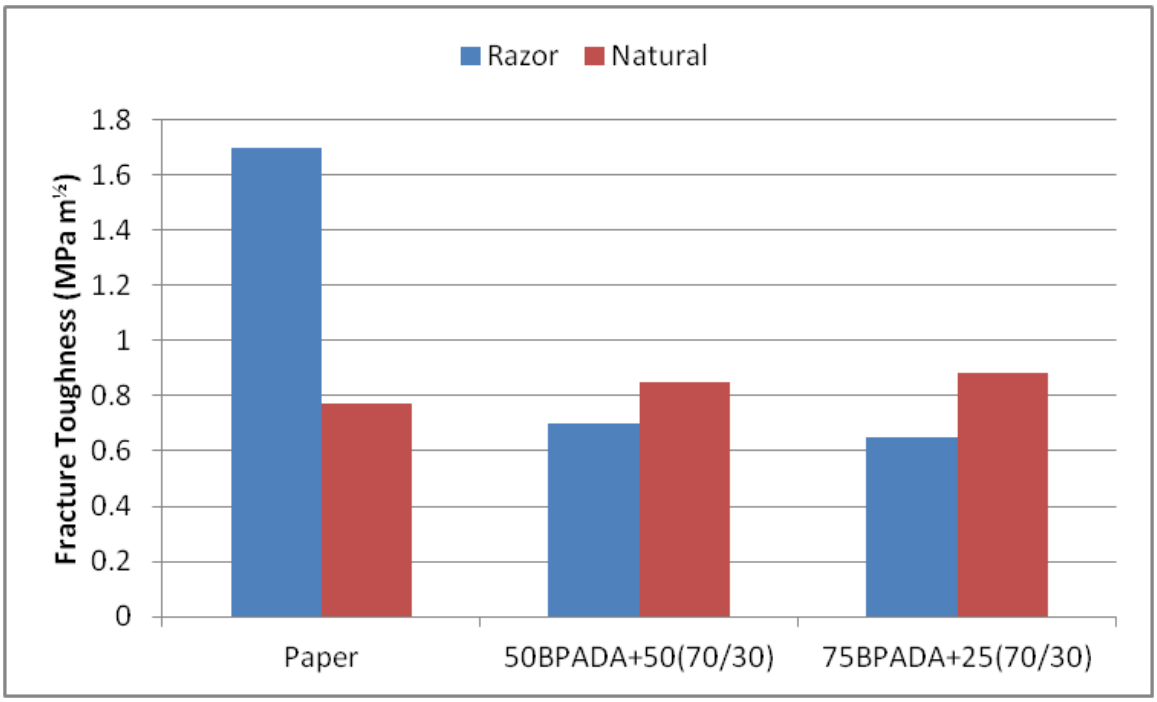

Figure 100: Literature razor and natural precrack influences on fracture toughness versus IPN system results

However, all of the samples were subjected to the same precrack procedure, and a few natural "pop-in" cracks developed during the procedure. As shown in Figure 100, the calculated fracture toughness for these samples was comparable to the razor precracked samples versus the 220% difference found in reference 4. Striations originating from the pre-crack tip have been noted by other researchers.[98] [99] Therefore, it appears that the higher fracture energy required is a real effect of the IPN formulation rather than a result of differences in the pre-crack condition.

5.7.4.1 Phase Interactions

The phase synergy prediction as defined by equation 22 seems to provide a reasonable fit for most of the composition families. The linear rule of mixtures relationship is modified by the interaction synergy parameter, , which is multiplied by the volume fractions of the two phases. The product of the two phases is proportional to the interface area between the two phases, so the synergy parameter may be viewed as may be viewed as a measure of the interaction between the two phases.

If the two networks were to have identical properties, a pure linear relationship with no enhancement or degradation at the network interfaces would be represented by an interaction synergy parameter of zero. Positive interaction was exhibited by the systems containing both (50-50)Epoxy and (70-30)Epoxy. Both of these systems contain diglycidyl ether of bisphenol A (DGEBA) which has a polymer backbone structure that is the same as the backbone used in the primary acrylate component, bisphenol A diacrylate (BPADA). These two monomers have less than a 5% difference in their solubility parameters. This close solubility parameter match may lead to synergistic atomic packing along the acrylate-epoxy network interface.

The surface of the initially cured acrylate network contains unreacted acrylate functional groups that might be able to interact with the epoxy phase. When BECA monomers are heated with BPADA up to 200 °C, the blend is still a liquid monomer mix when cooled down to room temperature. However, when DGEBA monomers are heated with BPADA up to 200 °C, the result is a copolymerized solid. Typical stress-strain curves for (50-50)Epoxy, (70-

30)Epoxy, BPADA and a 50% DGEBA + 50% BPADA thermally copolymerized blend are shown in Figure 101. The copolymerized material modulus is approximately equal to that of the (70-30)Epoxy. Therefore, it is reasonable to assume that some phase interaction will exist for the IPNs containing DGEBA.

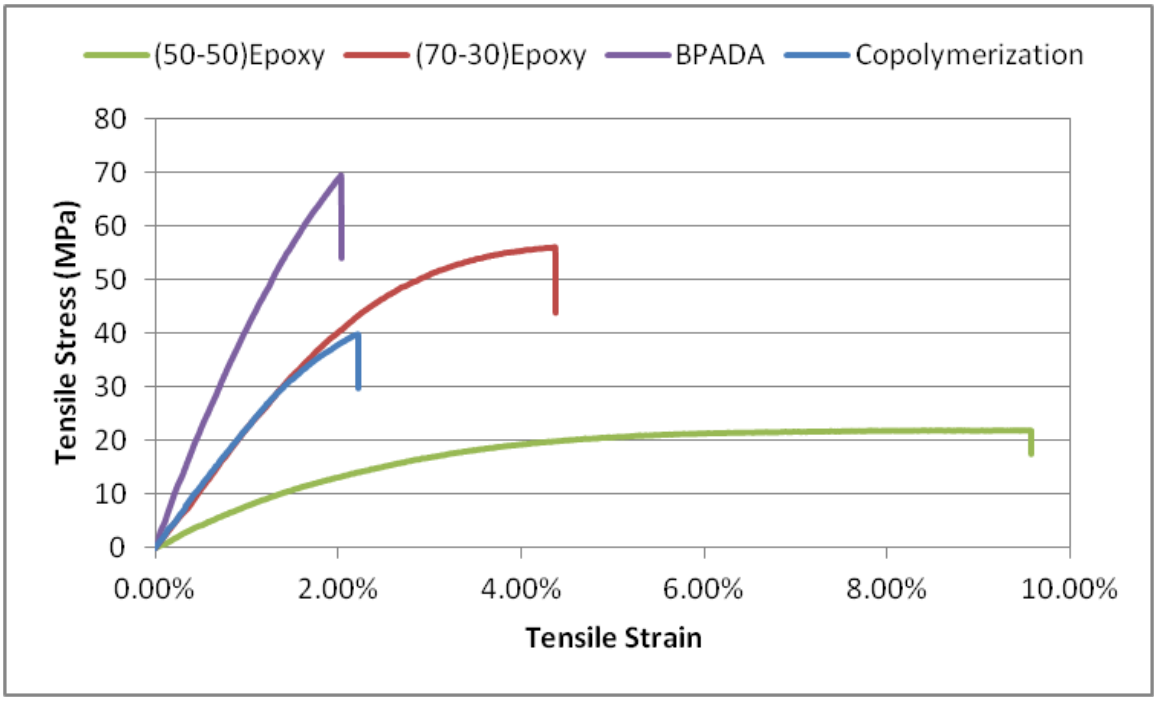

Figure 101: Typical stress-strain curve for a 50%DGEBA+50%BPADA copolymerization compared to (50-50)Epoxy, (70-30)Epoxy and BPADA curves

For the BPADA + BECA material system, the interaction synergy parameter was negative. This suggests an interface between the acrylate and epoxy networks that exhibits some degree of separation. Whereas DGEBA has is closely matched to the BPADA solubility parameter, the difference between BPADA and BECA is 38%. Molecular differences may lead to some steric hindrances to atomic packing along the interface.

Synergy between the two networks was modeled after the Kleiner modulus equation where the fracture toughness synergy of a 50% acrylate / 50% epoxy IPN was used to represent the synergy between the networks. This synergy value is multiplied by the product of the two network fractions. The product of the network fractions represents the amount of interface area present between the two networks.

The fracture toughness synergy parameter is plotted against the square of the solubility parameter difference between the acrylate and epoxy components, $(\Delta\delta)^2$, in Figure 102. From equation 8, this product is used to estimate the Flory interaction parameter between the acrylate and epoxy components. Lower values of $(\Delta\delta)^2$ indicate improved miscibility. The calculated correlation value is -0.980 which indicates a strong relationship between the synergy parameter and the miscibility of the acrylate and epoxy network monomers.

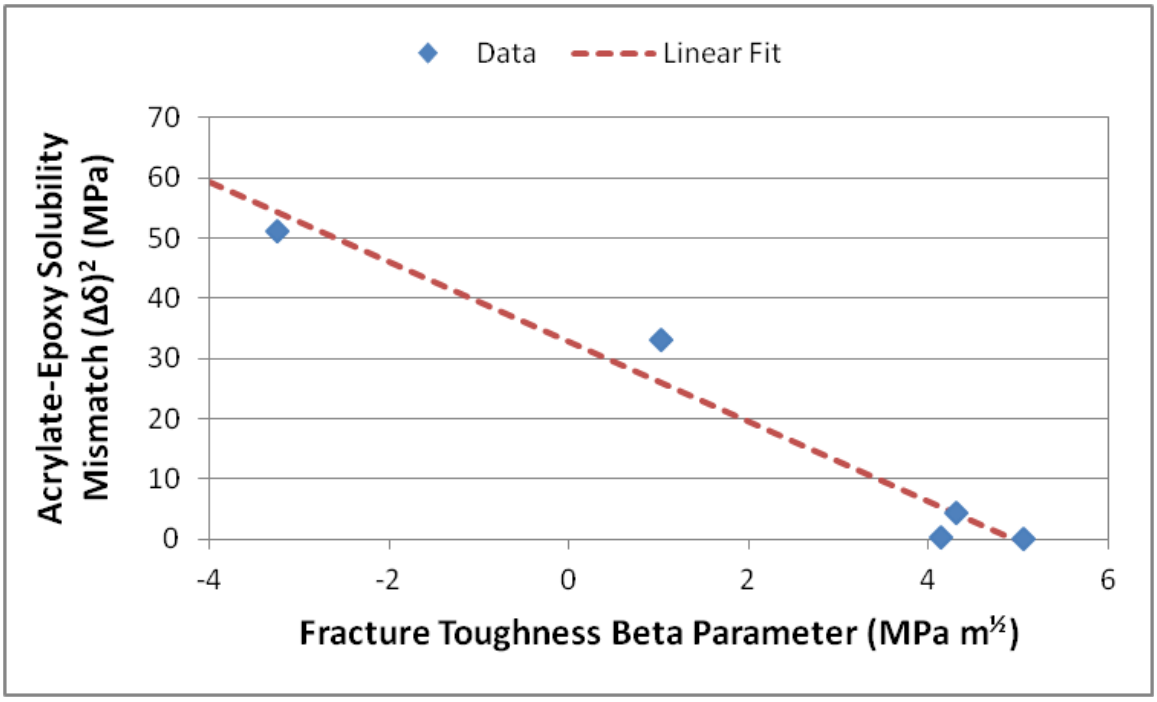

Figure 102: Fracture toughness synergy parameter versus square of the solubility mismatch

5.7.4.2 Shear Yielding

As noted in the literature review section, the primary toughening mechanism available in unfilled thermoset systems is shear yielding. Shear yielding reduces the stress concentration at the crack tip, resulting in a "blunting" of the crack tip. Shear yielding, in turn, is dependent on the polymer free volume. Previous IPN research has shown that an increase in free volume formed in midrange composition IPNs is associated with synergistic (better than a linear rule of mixtures) improvements in toughness while reductions in IPN free volume have been associated with toughness performance that is less than a linear rule of mixtures performance.[100] [101] Another property related to polymer free volume is glass transition temperature. With increased free volume, a decrease in glass transition temperature is expected. However, for the (80/20)acrylate + (50/50)epoxy composition family, the midrange IPN formulations exhibited a higher glass transition temperature than its pure acrylate or pure epoxy end points.

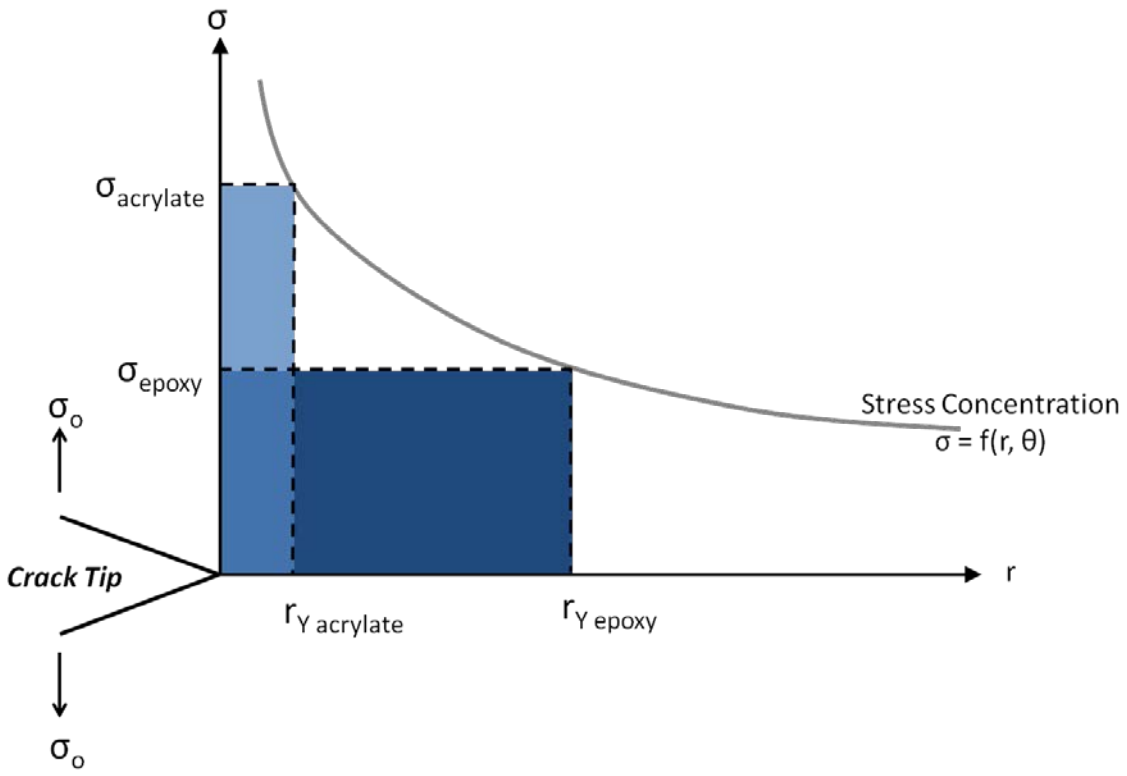

Figure 103: Tensile stress and radius of plastically yielded zone in materials with different yield stress (based on [102])

In single component or blended thermoset networks, the overall composition is homogeneous. Although heterogeneity has been noted at the microscopic level, no link has been proven between the heterogeneity and toughness. However, an IPN system has distinct material domains. Since the phase separation is at the nanoscopic level, the amount of interface area between the acrylate and epoxy systems is substantial, and the IPN properties may be dominated by the acrylate-epoxy interactions. As the crack tip moves from an acrylate domain and into an epoxy domain, the stress at the crack tip decreases since the epoxy has a lower modulus than the acrylate. The localized epoxy domain must undergo more deformation to strain it to failure. Since the epoxy modulus is lower than the bulk IPN modulus, this deformation results in a lower stress in the epoxy

domain than in the bulk IPN. If the failure strain for the epoxy is sufficiently lower than the bulk IPN strain to failure, the epoxy domain undergoes shear yielding, blunting the crack tip. A conceptual sketch of an SENB specimen is shown in Figure 104.

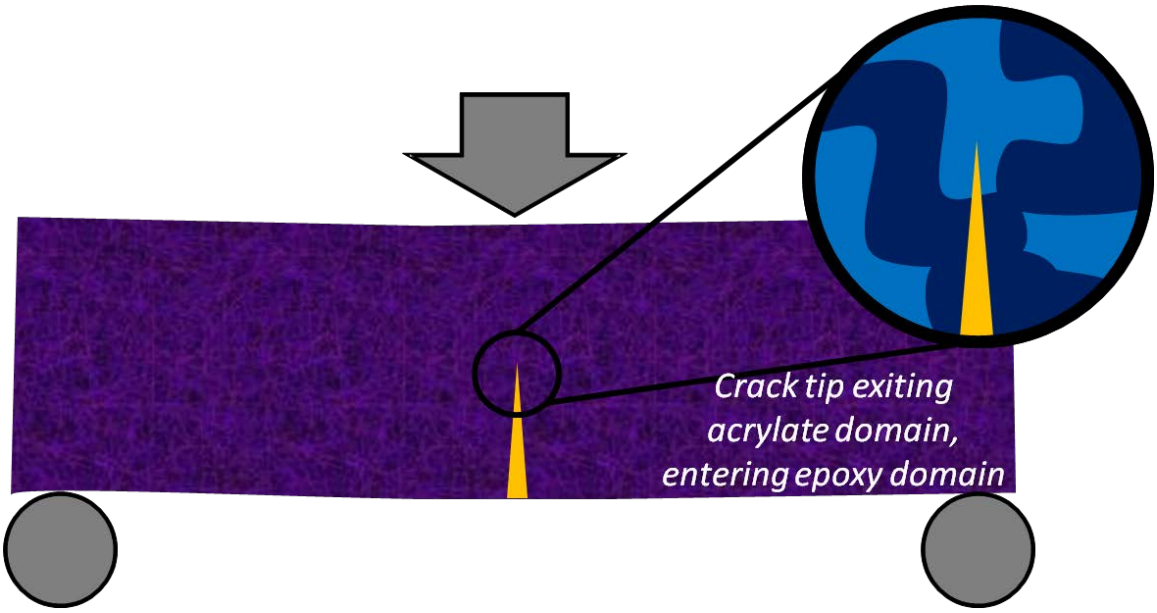

Figure 104: Conceptual SENB specimen showing crack growing from acrylate network into epoxy network

The modulus of resilience is the amount of energy that a material can absorb without experiencing plastic deformation. In the case of the acrylate polymers, the modulus of resilience is also the amount of energy the network can absorb prior to brittle fracture. From Table 8, it can be seen that the moduli of resilience for all of the pure epoxy compositions are higher than the moduli of resilience for the pure acrylate compositions. The fracture toughness synergy parameter has been correlated to the difference in resilience of the two individual networks in Figure 105. The amount of energy stored in the epoxy network when the acrylate network fractures as a percentage of the epoxy modulus

of resilience correlates well with the fracture toughness synergy parameter with a linear correlation value of 0.961.

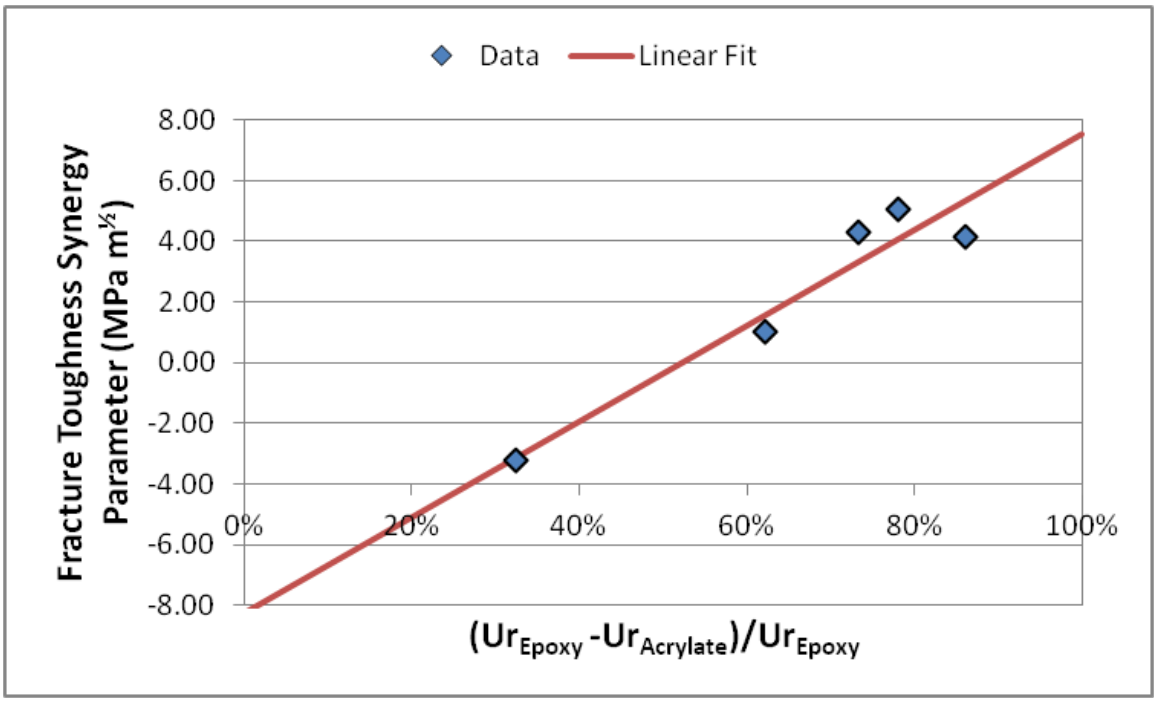

Figure 105: Fracture toughness synergy parameter versus percentage difference in network modulus of resilience

Stress-strain curves for the pure acrylate, pure epoxy and a 65% acrylate IPN in the (80-20)Acrylate + (50-50)Epoxy system are shown in Figure 106. These curves suggest an additional possibility for IPN toughening. In a heterogeneous network system, acrylate domains with the lowest cross sectional area in the direction of loading fail at a strain that is lower than the failure strain of the IPN. Since they are in intimate contact, the unfailed epoxy network surrounding the failed acrylate domain can transfer load back into the acrylate network via shear. In this case, the acrylate network behaves like a randomly oriented fiber in a discontinuously reinforced composite network with the epoxy network

functioning as a matrix adhesive. During crack extension, nanocracking of the acrylate network may enable larger deformation movement of the unfailed epoxy network.

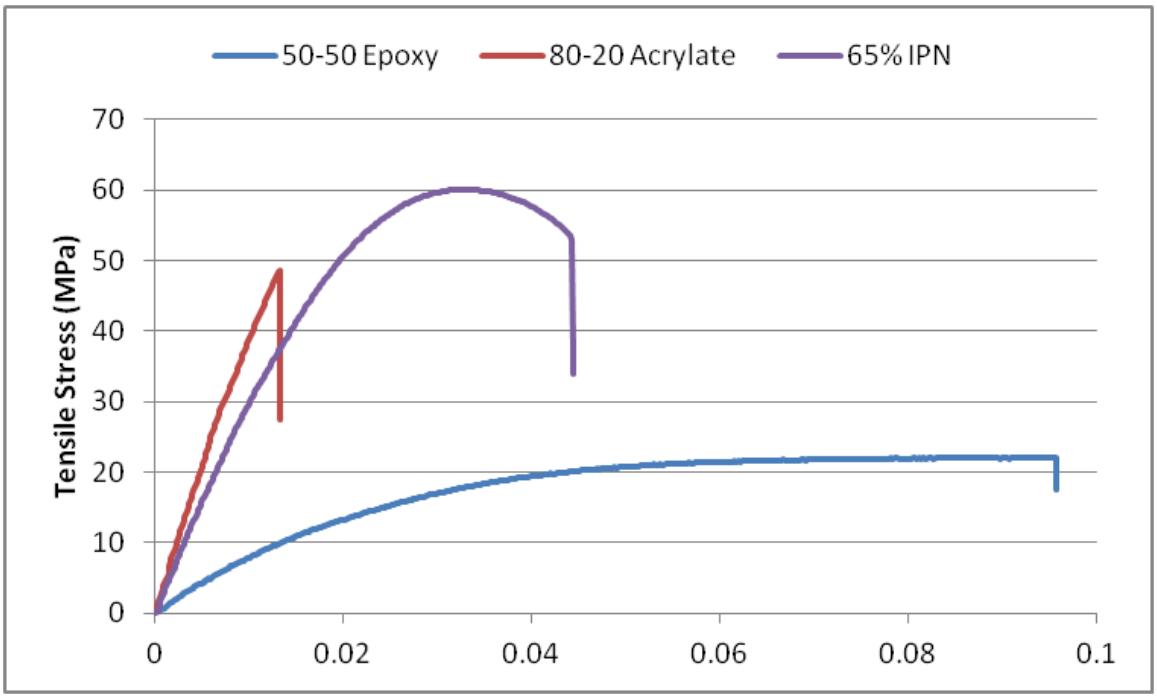

Figure 106: Typical stress-strain curves for an IPN system

The stress-strain curves for a rigid-rigid (e.g. stiff thermoplastic in a stiff thermoset) polymer system composed of poly(phenylene oxide) (PPO) in epoxy are shown in Figure 107. The toughened epoxy + PPO system was produced by dissolving PPO particles in hot epoxy monomer and then allowing the PPO to phase separate during cure. The composition tested had 500 parts DGEBA, 50 parts PPO, 12.5 parts styrene-maleic anhydride (to stabilize the PPO) and 29 parts piperidine as the curing agent. The uniaxial tension behavior of the modified epoxy was very similar to the unmodified epoxy (500 parts DGEBA, 29 parts piperidine). Fracture toughness, however, was increased by 20 percent. Crack tip

examinations revealed that the PPO particles were able to induce shear banding, resulting in crack branching and microcracking. [103]

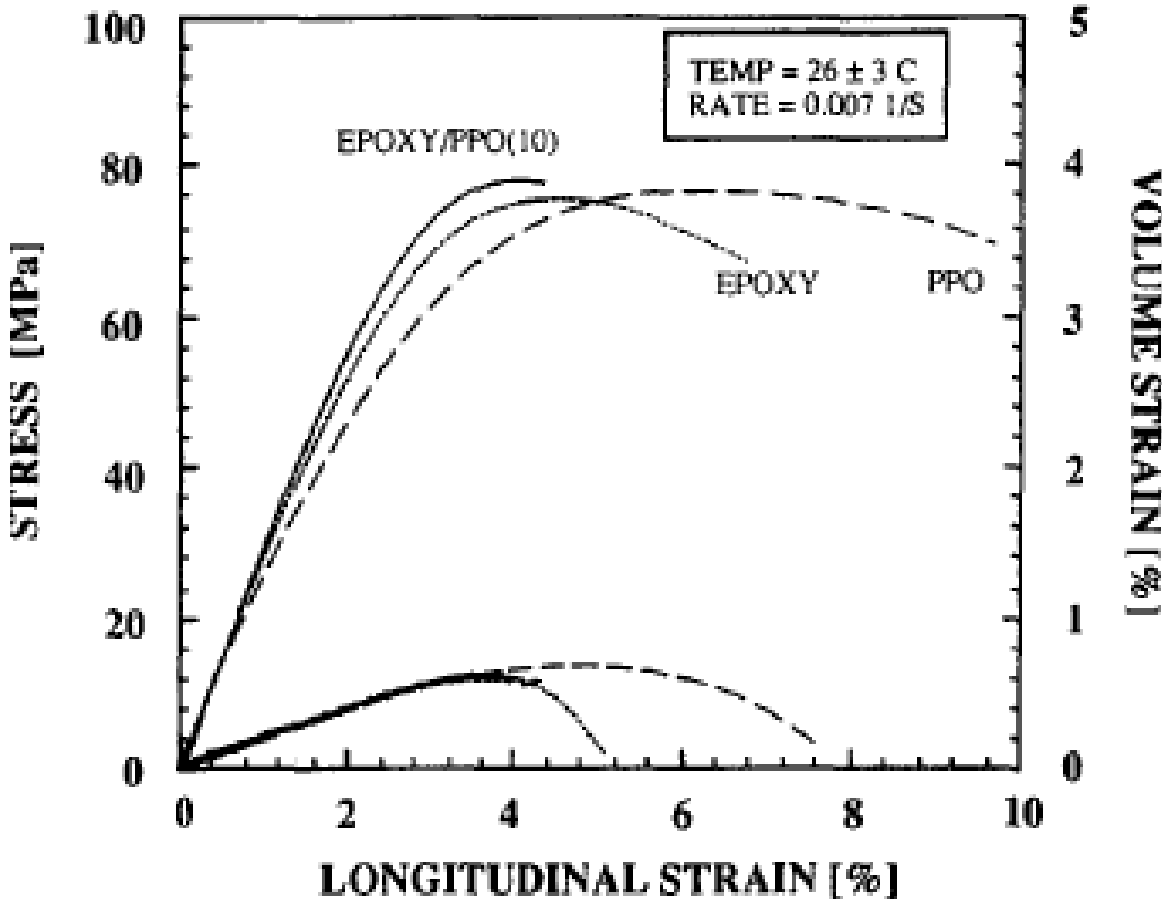

Figure 107: Rigid-rigid polymer toughening of epoxy by addition of poly(phenylene oxide) (taken from 103)

Research in the use of liquid crystal polymer units in which a portion of the polymer was based on polyethylene glycol 200 (designated as $LCEU_{200}$) also exhibits the fracture surface tearing as shown in Figure 108. The appearance of the fracture surface modified with $LCEU_{200}$ was attributed to phase separation which was indicative of a tough fracture. [104] The fracture appearance is similar to the tearing seen in Figure 90 and Figure 93. Impact

strength was increased from 4 kJ/m^2 for the unmodified resin to 14.5 kJ/m^2 for the LCEU$_{200}$ modified epoxy.

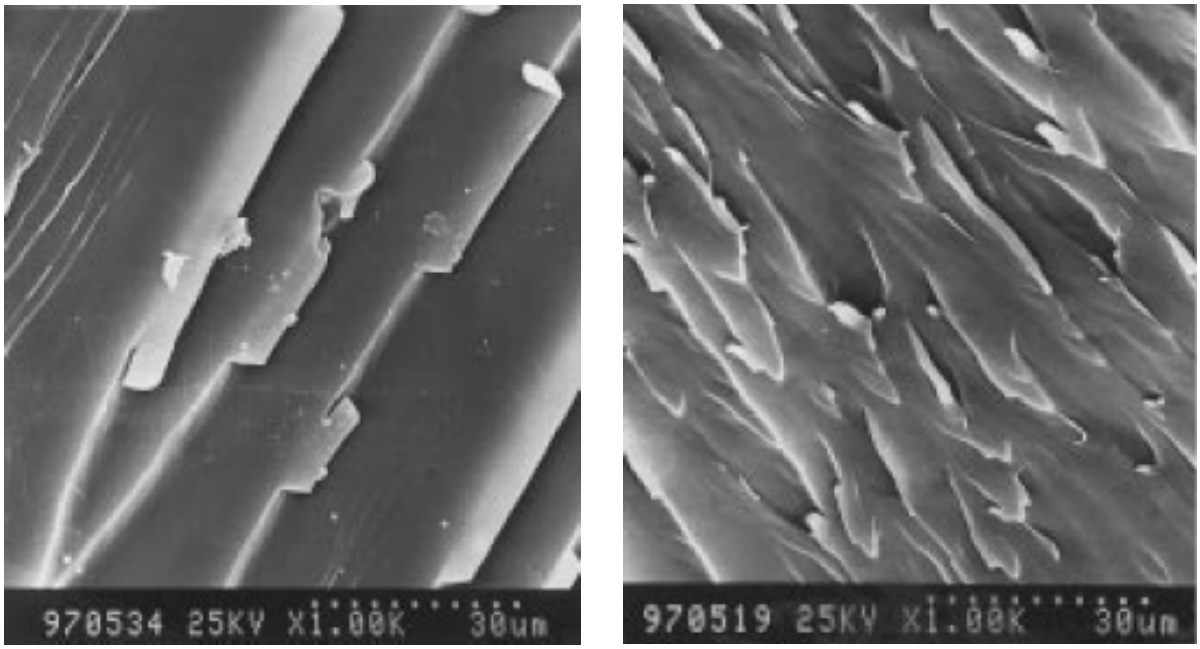

Figure 108: SEM images of impact fracture surfaces for DGEBA:DICY of ratio 100:6 (left) and DGEBA:DICY:LCEU$_{200}$ of ratio 100:6:10

The fracture surface of an epoxy toughened by dissolving poly(ether sulfone) (PES) into the epoxy monomer prior to curing is shown in Figure 109. The roughness of the fracture surface is attributed to plastic deformation out of the plane of crack propagation. This modification resulted in higher fracture toughness than the unmodified epoxy system. The primary toughening mechanisms for this material system were attributed to crack deflection and crack bifurcation. [105]

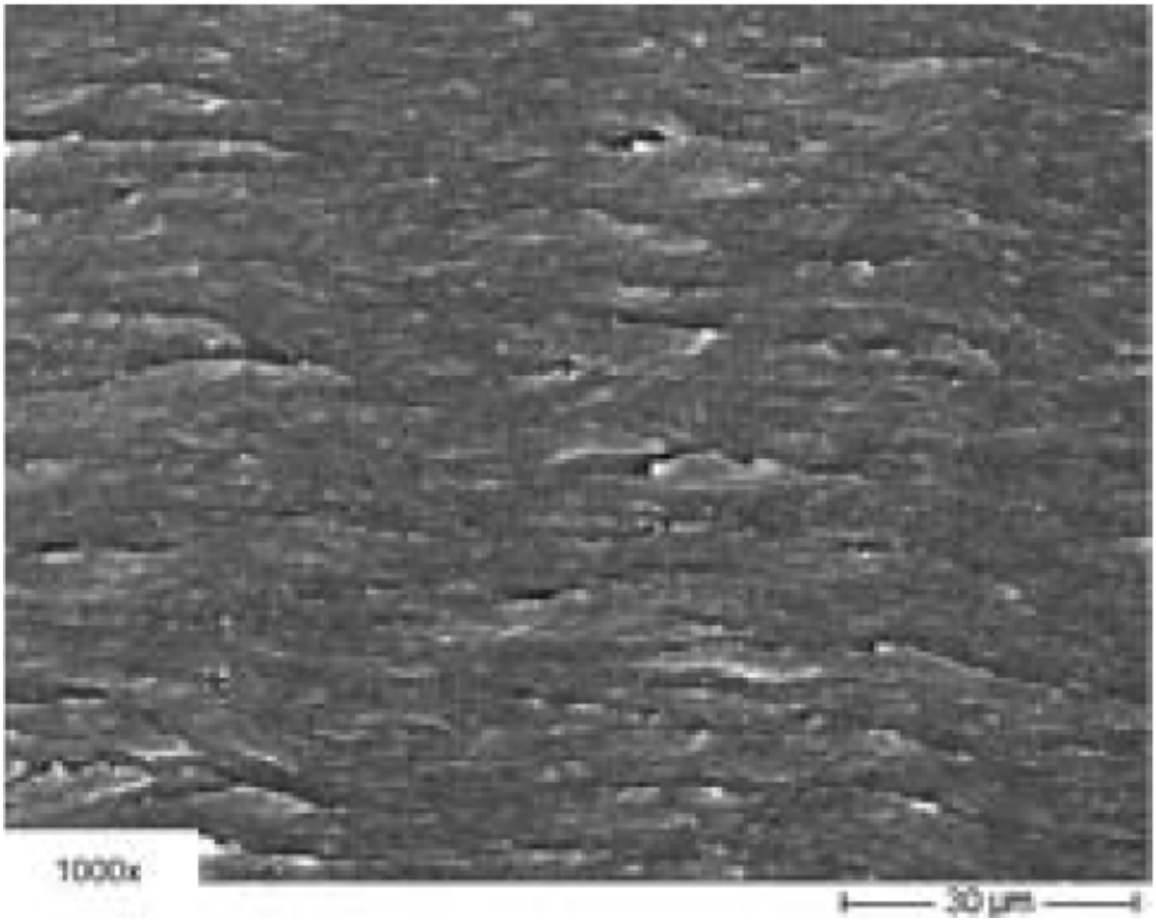

Figure 109: Fracture surface of electron beam cured epoxy resin with dissolved PES (from [105])

5.7.4.3 Monomer conversion

Finally, tensile test results show that strength peaks in the midrange IPN compositions. This may be due in part to a higher degree of acrylate monomer conversion. The presence of epoxy monomer in the electron beam curing IPN system slows down the reaction kinetics and avoids trapping unreacted acrylate sites inside of condensed microgels. FTIR investigation degree of conversion calculations show conversions as high as 92 percent conversion of acrylate in the midrange IPN compositions as opposed to only 62 percent

conversion in the pure acrylate compositions. The higher degree of conversion results in a higher concentration of density of covalent bonds, requiring more energy to fracture them.

5.8 Short Beam Shear

In addition to bonding applications, many thermoset adhesives are used as the matrix resin in fiber reinforced composite structure. The introduction of a fiber volume fraction of approximately 50 percent adds a third component to the IPN adhesive system. Differences in the fiber wetting characteristics of IPN adhesive component networks could potentially result in either positive or negative synergy.

To characterize the performance of the IPN as a matrix adhesive, it is necessary to select a test that is not dominated by the properties of the fiber reinforcement. Since fiber reinforcement is absent in the lamina interface, the performance of a laminate under interlaminar shear stress is governed by the properties of the matrix resin. Large interlaminar shear stresses may lead to delamination failures. The resistance to interlaminar shear crack initiation can be measured by conducting a short beam shear test. By loading a laminate beam specimen in three point bending with a short span length, then the specimen will fail at the point of maximum shear which is located at the midplane of the beam.

5.8.1 Short Beam Shear Sample Preparation

Post-cured laminate samples were cut with a diamond abrasive blade on a Do-All slicer with water lubrication. The target width to thickness ratio of 2.0 was selected per ASTM D2344.

Dimensions of the individual test specimens were measured after machining, and the average sample width and thickness values are shown in Table 10.

Table 10: Short beam shear specimen average width and thickness

	Acrylate	IPN	Epoxy	All
Average Width (mm)	12.01	11.97	11.95	11.98
Average Thickness (mm)	6.11	6.02	5.79	5.97

5.8.2 Short Beam Shear Testing

Short beam shear tests per ASTM D2344, Standard Test Method for Short-Beam Strength of Polymer Matrix Composite Materials and Their Laminates, were used to determine laminate interlaminar shear strength. Six specimens for each laminate type were tested using an Instron mechanical testing machine under laboratory conditions. A crosshead rate of 1mm/sec and a 10kN load cell were used during testing. The support span was set to 25.4mm according to the 4:1 length to thickness ratio of ASTM D2344.

5.8.3 Short Beam Shear Results

Short beam shear values were calculated using Equation 27 in accordance with ASTM D2344-00. Values are shown in Figure 110.

$$F_{SBS} = (0.75\ P_{max}) / (b\ h) \qquad \text{Equation 27}$$

Where F_{SBS} = *short beam shear strength*

P_{max} = *maximum load observed during the test*

b = *specimen width*

h = *specimen thickness*

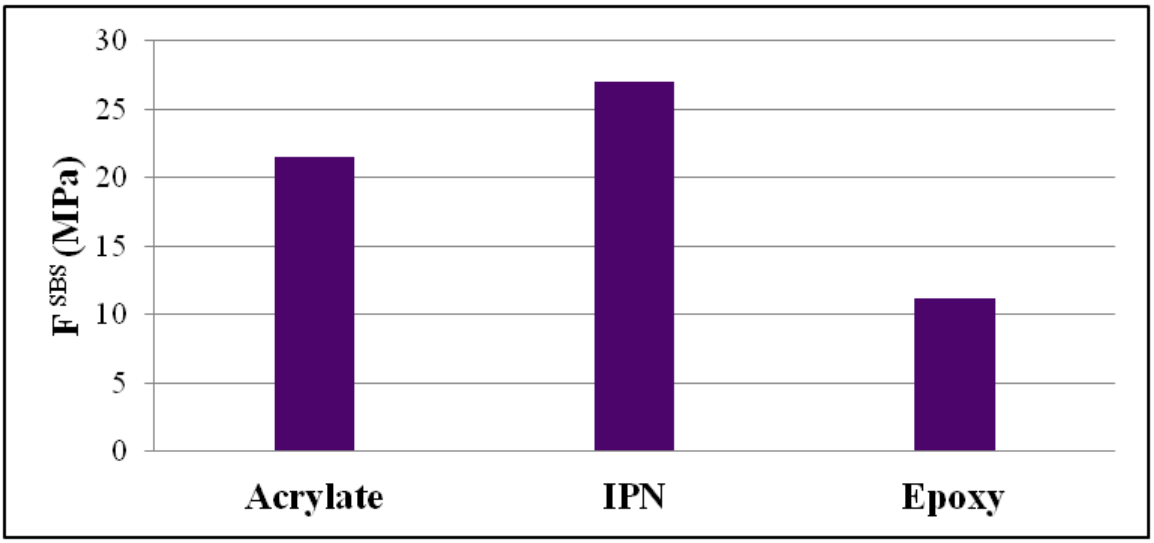

Figure 110: Short beam shear test results

Low variation was observed in the calculated short beam strength values. The standard deviations of samples ranged from 0.3 to 1.02 MPa. Comparing the average shear strength values, the IPN was 1.3 times stronger than the acrylate component and 2.4 times stronger than the epoxy component. All test samples failed due to interlaminar shear with a typical example shown in Figure 111.

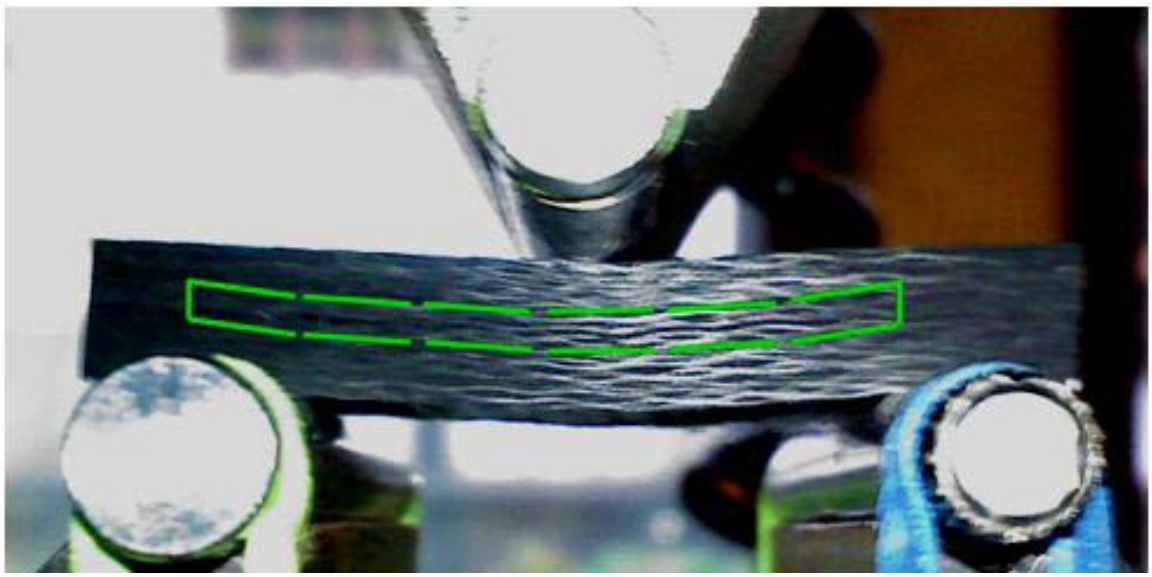

Figure 111: Failure mode of short beam shear sample with interlaminar crack outlined

Failed short beam shear specimens were trimmed using diamond abrasive saw blade to excise a section near the center of the specimen for examination of the failure surface. The sections were mounted onto aluminum SEM stubs and sputter coated with platinum. SEM images of the failed surfaces are shown in Figure 112.

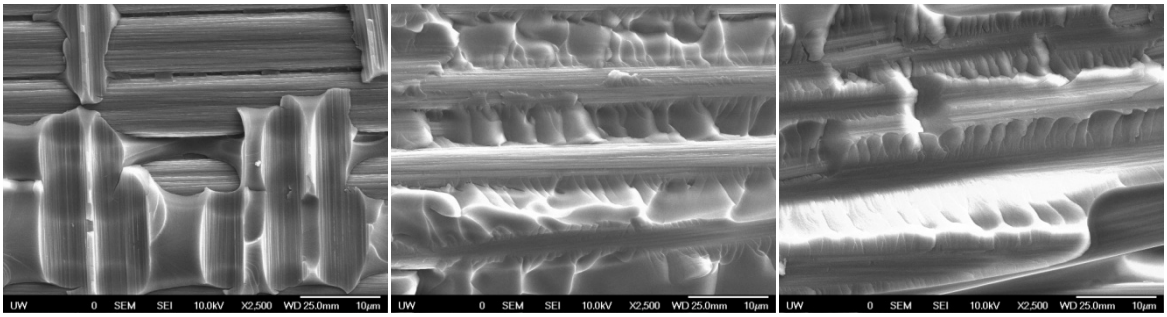

Figure 112: Failure surfaces for acrylate (left), epoxy (center) and IPN (right) short beam shear specimens

The acrylate matrix shows a brittle failure with an imprint of the carbon fibers left behind. Poor interaction between carbon fibers and the acrylate matrix adhesive has been noted by other researchers. [106] [107] [108] The carbon fiber/epoxy failure surface shows good adhesion between the fibers and the matrix with ductile fracture "river marks" clearly visible in the epoxy matrix. The carbon fiber/IPN failure surface is similar to the carbon fiber/epoxy failure surface. It also shows good adhesion with river marks in the IPN matrix.

5.8.4 Short Beam Shear Discussion

Fracture toughness of a fiber-matrix composite involves more complex mechanisms than the fracture toughness of bulk resins. It has been proposed that the presence of fibers restricts the crack-tip plastic zone size, reducing the degree of toughening that can be transferred from elastomer-toughened matrix polymers to composite laminates. [109] A first estimate can be based on replacing some of the bulk polymer plastic zone with rigid carbon

fibers. A more detrimental possibility is confining the plastic zone to the area defined by the inter-fiber spacing area ahead of the crack tip. This creates a restricted or "bound" plastic zone which is illustrated in Figure 113.

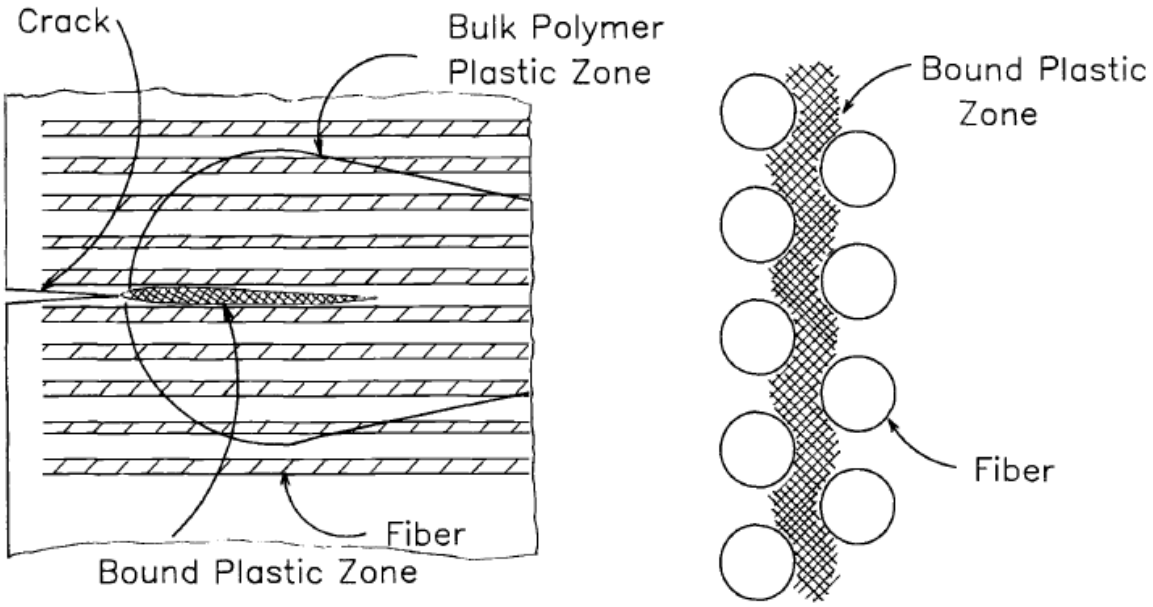

Figure 113: Bound matrix polymer plastic zone in fiber reinforced composite (modified from 110)

It has been observed that the ratio of $G_{IC\ (composite)}/G_{IC\ (resin)}$ decreases as the toughness of the resin increases, but it is not quite as severe as the limitations imposed by fiber spacing. Another explanation for the reduced translation in toughness from resin to composite is the state of hydrostatic stress imposed by adhesion to the carbon fibers. High hydrostatic tension in elastomer toughened epoxies tends to promote cavitation and voiding over shear yielding, resulting in the loss of toughness due to the inherent ductility of the primary matrix polymer. A third possible explanation for the reduced toughness is the size of the elastomeric particles relative to the fiber spacing. The effectiveness of elastomeric particles is reduced if they are the same magnitude as the fiber spacing. [110]

A review of the impact resistance of composite materials offered the following points:

- For improved impact resistance, the matrix material should have strength of at least 69 MPa and a strain to failure of at least 4%.
- The presence of fibers restricts the size of the plastic zone at the crack tip, so the positive effect of thermoplastic-toughened matrices is reduced. Compression after impact was found to correlate strongly with Mode II fracture toughness.
- Efforts to enhance the impact resistance of T300/MY-720 carbon fiber composites by coating the surfaces of the fibers with a thin layer of CTBN rubber significantly improved the threshold energy for damage initiation. [109] Based on a review of several polymer coatings applied to fibers, an effective rigid interlayer should be more ductile and compliant than the matrix material. [111]

Acrylate-epoxy IPNs may offer all of these advantages. The strength of the IPNs produced with (50-50)Epoxy fall about 6-15 MPa under the 69 MPa strength threshold while the IPNs produced with (70-30)Epoxy are at least 17 MPa higher. Failure strains ranged from 3.3% for the (80-20)Acrylate + (50-50)Epoxy IPNs to 4.3% for the BPADA + (70-30)Epoxy IPNs, but the both epoxy networks exhibited failure strains well in excess of 4%. These performance properties suggest that there is room to tailor the IPN DGEBA/PPGDE ratios to optimize performance. Additionally, since the epoxy is the highest energy monomer component, it should preferentially coat the carbon fibers, providing a thin, flexible/higher elongation interface that is more similar to the referenced CTBN coating than to that of a brittle

acrylate. Preferential wetting has been documented in matrices of epoxy-polyetherimde resins on glass fibers. [112]

6. General Discussion

The goal of this research was to develop IPN adhesive formulations, measure key performance properties, characterize the effect of composition variations and propose the origins of IPN toughening in a rigid-rigid acrylate-epoxy IPN system. The primary performance properties measured were strength and toughness, although the modulus density, glass transition temperature and degree of acrylate monomer conversion were also assessed in order to draw conclusions regarding IPN effects on the mechanical properties. These measured values were supplemented by microscopic techniques to reveal the IPN morphology.

Although the IPN formulations exhibited some non-linear elastic deformation, none of them demonstrated yielding behavior in tension. With elastic/brittle fracture behavior and the assumption that the defect size is comparable across all samples, strength is governed by fracture toughness.

The research conducted in this project has shown the following:

- The bulk samples produced were translucent rather than cloudy. Dynamic mechanical analysis of individual compositions revealed a single glass transition temperature, confirming that the samples represent IPNs rather than phase-separated blends.
- Preliminary morphology images are indicative of reaction-induced IPN phase separation on a nano scale rather than fully miscible blend.

- Synergy above that predicted by a linear rule of mixtures has been seen in several material properties – glass transition temperature, tensile strength, compression yield and fracture toughness.

Other researchers have been able to produce synergistic results with combinations of two or more polymers. To achieve good properties in polymer blends, some degree of miscibility between the components is beneficial. Miscibility can be enhanced by the use of compatibilizing agents such as block copolymers or with a third polymer that is highly compatible with the first two polymers. In a review paper of binary polymer-polymer blends that exhibit synergistic properties without the use of compatiblizers, the following conclusions were drawn:

1) Synergy can exist over a partial or full range of compositions, depending on the chemical structure of the polymers. Systems which undergo phase inversions can exhibit both positive and negative synergy across their composition ranges.
2) Synergy is present in amorphous, amorphous plus semi-crystalline or semi-crystalline plus semi-crystalline polymer blends.
3) Intermolecular interactions that enhance density above linear rule of mixtures additivity or exothermic enthalpy of mixing can lead to synergy in modulus, yield stress and tensile strength.
4) Miscibility between components of binary blends can be the result of interactions that also lead to better adhesion between phases. Interactions include hydrogen bonding, ester exchange reactions and physical entanglements.

5) Additional factors leading to synergistic properties include small domain sizes, good dispersion and some degree of intermolecular diffusion at domain boundaries.
6) Some similarity in chemical structure leads to synergism in mechanical behavior.
7) The presence of IPNs leads to load sharing and – in some compositions – to mechanical properties that are superior to those of either component polymer.
8) Synergist enhancement in toughness seems to be achieved only in phase separated blends with good interfacial adhesion. [113]

Synergy can exist in IPN properties such as hardness, impact strength, elongation to failure, glass transition temperature and mechanical damping. For polyurethane-poly(methyl methacrylate) IPNs, maximum property improvements were seen in the composition range of 60-70 percent of the strong, stiff poly(methyl methacrylate) component. [114] This synergy seems to be present in the acrylate-epoxy systems studied in this project.

The most widely studied thermoset toughening mechanisms are those associated with secondary phases: rigid filler particles, elastomeric particles or thermoplastic particles which phase separate during polymerization. However, the toughness behavior of rigid polymer – rigid polymer blends offers some insight into the toughness behavior of acrylate – epoxy IPNs. An example of the strength-toughness behavior of a polycarbonate-polymethylmethacrylate material system is shown in Figure 114. [113] The strength of this rigid polymer – rigid polymer blend exhibits the greatest departure from a linear rule of mixtures at the composition corresponding to the greatest synergy in toughness.

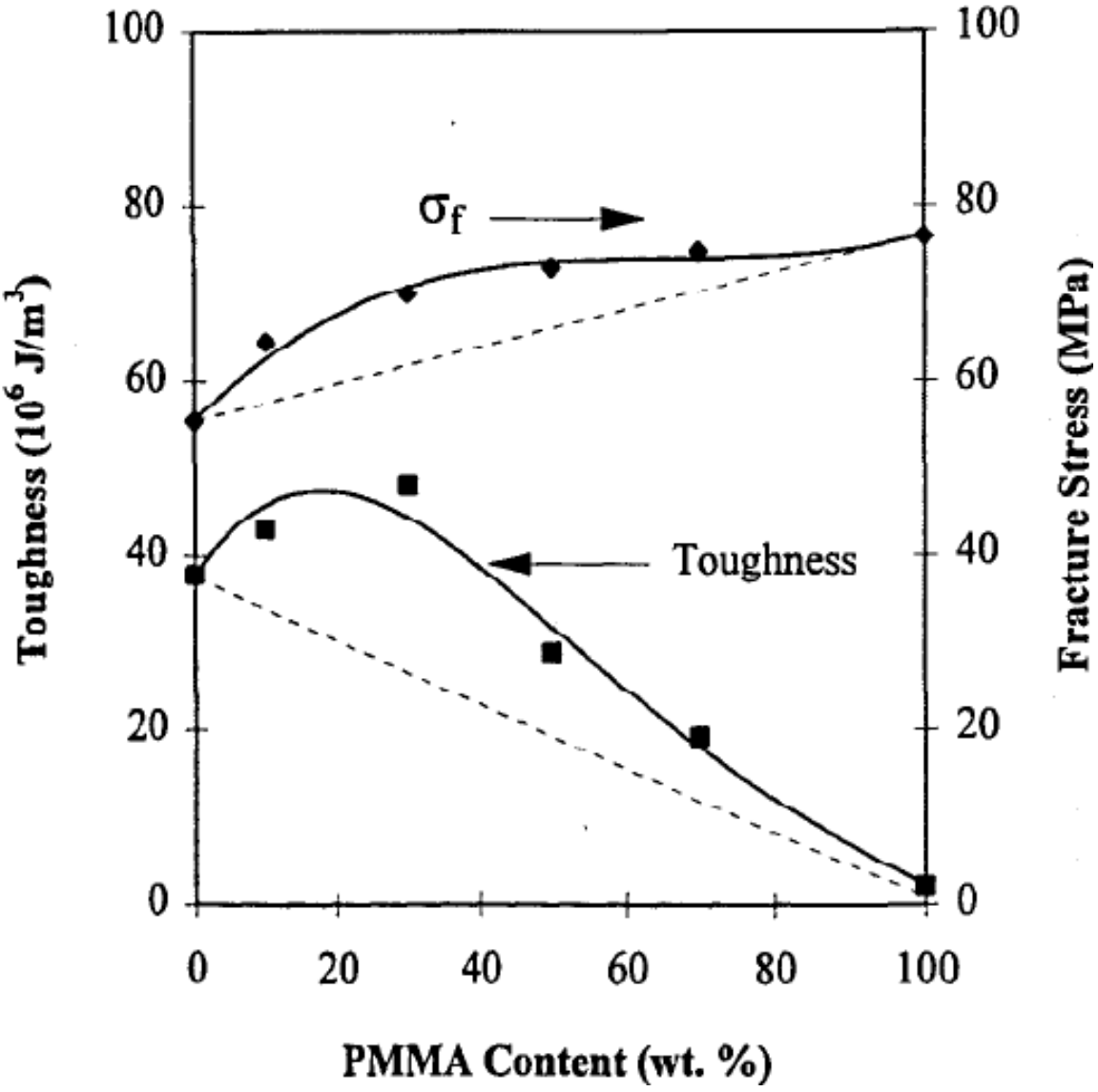

Figure 114: Strength-toughness relationship in a polycarbonate-polymethylmethacrylate (PMMA) material system blend (from [74])

In modeling the toughness performance of rigid polymer blends, it was found that localized yielding was enhanced due to stress concentrations if the modulus mismatch in plane stress conditions was at least 60 percent. [115] An increase in the interface area between two different polymer phases while maintaining the same volume fraction has also been shown

to increase toughness. [116] Since the phase separation in IPNs occurs at a small scale, they should have a large amount of interface area per unit volume.

The difference in strain to failure may also lead to development of another toughening mechanism – bridging. Within a bulk specimen loaded in plane strain, the acrylate networks will carry higher loads and will fail before the epoxy networks reach failure strain. As a result, there is a possibility that epoxy bridges may exist behind the crack. A possible epoxy bridge is show in the transmission electron microscope image in Figure 115. The osmium tetroxide (OsO_4) staining technique results in heavy osmium atoms being attached to unreacted acrylate double bonds. As a result, acrylate network domains show up as darker areas in the image.

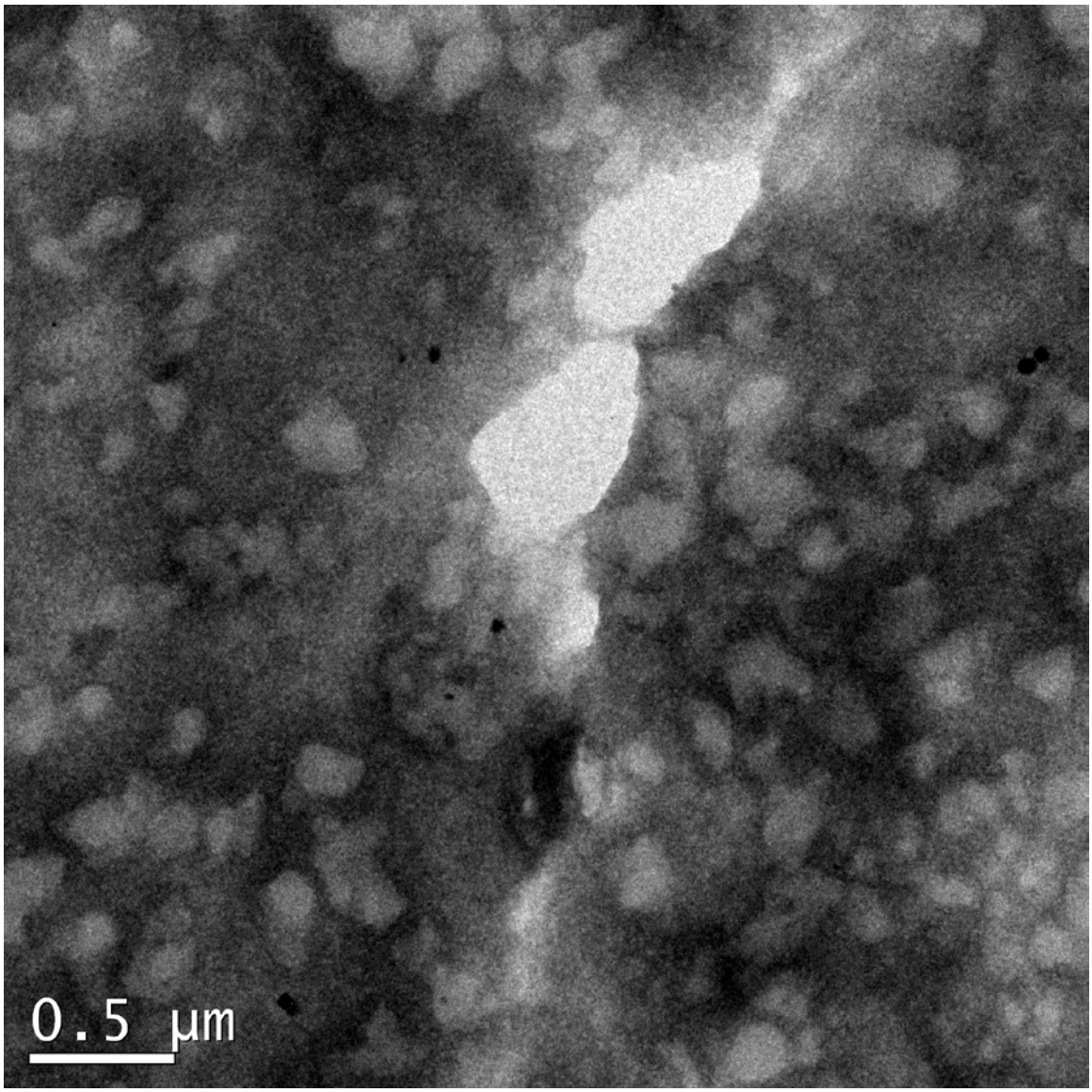

Figure 115: TEM image of 60% (80-20)Acrylate + 40% (50-50)Epoxy. Acrylate regions have been stained dark with OsO_4.

With a large amount of interface area per unit volume, interphase toughening is another possible toughening mechanism. Toughness is increased by crack deflection and crack-tip blunting with more compliant and thicker interphases. [117] Interactions between phases also lead to enhanced strength and fracture energy. [118] An example is provided in Figure 116 where the effect of surface preparation of silica fillers provides a clear increase in fracture

toughness for a photocured composite of 21 wt% bisphenol A diglycidyl methacrylate (bisGMA), 9 wt% triethylene glycol diisobutryrate (TEGDBA) and 70 wt% 17 µm diameter silica. [119] Thermal post-curing of the photocured composite resulted in an average toughness increase of 30 percent.

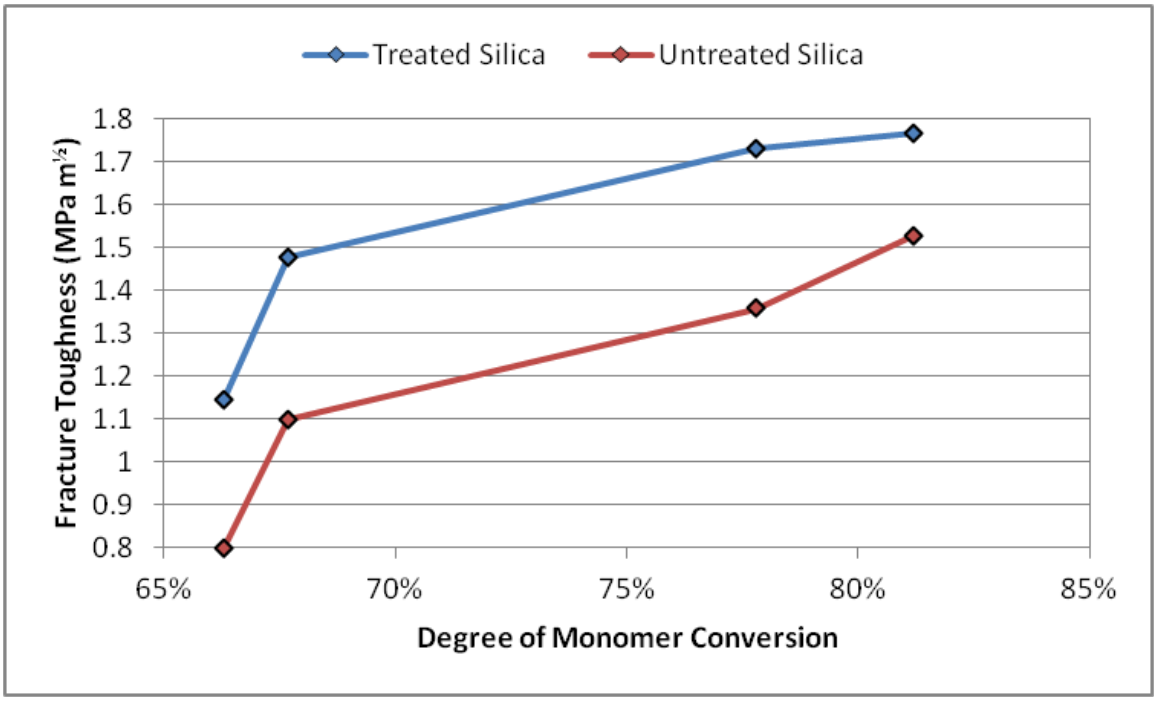

Figure 116: Effects of degree of monomer conversion and compatibilizing surface treatments on fracture toughness of bisGMA/TEGDMA resin filled with 70 wt% silica (adapted from 119)

Figure 116 suggests another source of IPN toughening. Beyond 68% degree of cure, fracture toughness is gained at a rate between 0.02-0.03 MPa per each additional percentage of monomer conversion. This seems reasonable since a higher degree of conversion translates to a higher number of covalent bonds per unit area that must be fractured in order for a crack to advance.

A related attribute comes from the role that chemical structure plays in the toughness of IPNs. In polymer blends, an increase in toughness is associated with improved packing efficiency, leading to a more dense material with a higher concentration of chemical bonds per unit volume. However, the Archimedes density measurements seem to rule out this particular mechanism.

Similarity in chemical structure also favors synergy in mechanical properties. [120] Both BPADA and DGEBA share the same bisphenol A backbone structure. Thermally activated co-polymerization of an epoxy and its acrylated has been shown to occur at 160 °C. [121] Simple confirmation tests were conducted with monomer mixes of 50% BPADA + 50% DGEBA and 50% BPADA + 50% BECA. Thermal curing agents were not added to either mixture, and both were heated up to 160 °C. The BPADA + DGEBA mixture did copolymerize, whereas the BPADA + BECA mixture remained a monomer mixture after thermal exposure. The similarity in the BPADA and DGEBA chemical structures could be expected, therefore, to produce covalent bonded cross-links in addition to physical entanglements at the interface between the two networks. Since no copolymerization occurs between BPADA and BECA monomers, the lack of interface chemical similarity may lead to the reduced properties of these IPNs.

A summary of toughening mechanisms versus IPN material system is provided in Table 5. No appreciable difference was found by varying the ratio of diacrylate to triacrylate, so the BPADA, (80-20)Acrylate and (60-40)Acrylate compositions are all grouped together.

Table 11: Potential IPN toughening mechanisms versus material system

Mechanism	Acrylate + (50-50) Epoxy	Acrylate + (70-30) Epoxy	Acrylate + BECA
Modulus Mismatch > 60%	Y	N	N
Increased interface area	Y	Y	Y
Thicker, compliant interphase	?	?	N
Chemical similarity	Y	Y	N

A graphical illustration of the potential toughening mechanisms available in acrylate-epoxy IPN systems is provided in Figure 117. These include:

A) Crack bifurcation: As the growing crack moves through a low modulus epoxy domain into a higher modulus the crack may continue to grow in the epoxy domain before finally propogating in the direction of maximum stress.

B) The epoxy has a higher strain to failure than the acrylate. In a plane strain fracture condition, the acrylate network will fail prior to failure of the epoxy network. Remaining epoxy network elements may bridge the crack and consume additional energy as they are deformed and finally fractured.

C) Due to the lower modulus in the epoxy network, the crack may be deflected around acrylate network domains leading to a longer crack path.

D) For the IPNs containing (50-50)Epoxy or (70-30)Epoxy, interactions are possible at the interface due to potential chemical cross linkages from DGEBA-BPADA copolymerizations or from increased entanglements due to the similarity in their chemical structures. This results in primary covalent bonds (due to

copolymerization) and/or enhanced secondary bonding (due to entanglements) at the interphase between the acrylate and epoxy networks.

E) As the crack tip advances from an acrylate network domain into an epoxy network domain, the modulus decreases. This may lead to crack tip blunting as the volume of material subjected to shear yielding increases.

F) If the modulus mismatch between the epoxy and acrylate domains is sufficient, stress concentrations will arise and lead to enhanced shear yielding.

G) Higher acrylate monomer conversion due to reduced reaction rates and enhanced monomer diffusion provided by the surrounding epoxy monomer may lead to a higher density of covalent bonds per unit volume.

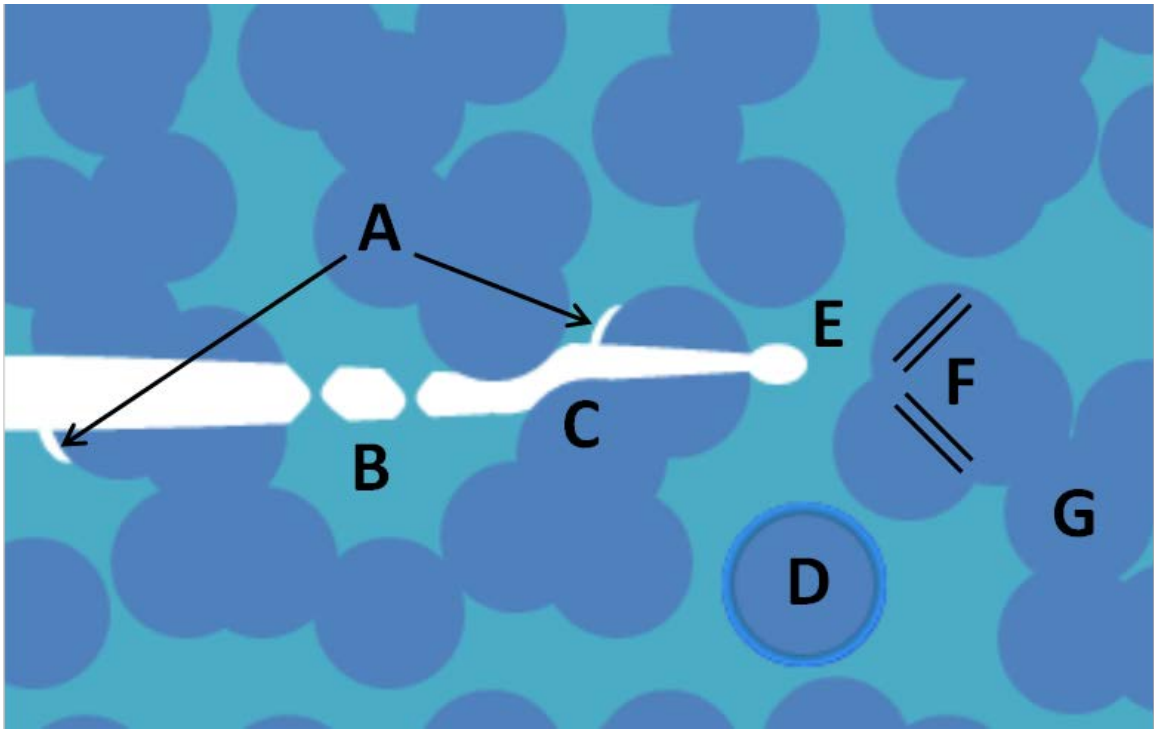

Figure 117: Potential IPN toughening mechanisms – A) Crack bifurcation, B) Crack bridging, C) Crack deflection, D) Network interactions, E) Crack tip blunting, F) Induced shear yielding, G) Degree of monomer conversion/enhanced packing density {dark blue = acrylate network}

Due to the advantages offered by electron beam curing, several researchers have tried to improve the toughness of electron beam cured acrylates. [122] [123] Some of these results are summarized in Table 12. Acrylated epoxies including the Ebecryl 600 BPADA used in this research represent the first three entries in the table. The fourth entry represents a cationically cured epoxy. None of these material systems have been toughened. The fifth and sixth entries provide comparisons to thermally cured epoxy adhesives. Cycom 977-2 is a conventional thermally cured, toughened epoxy matrix material whereas Hysol EA9394 is a room temperature cured, toughened epoxy paste adhesive. The final two entries involve secondary phase toughening of electron beam cured acrylates with the use of thermoplastic materials.

Table 12: Toughness of electron beam cured acrylates and epoxies

Resin	Toughness, K_{IC} (MPa $m^{½}$)
Epoxy-Acrylate	0.60 [122]
EB 600	0.80 [122]
EAR2	0.60 [122]
CR2	0.90 [122]
Cycom 977-2 (thermal)	1.12 [122]
Hysol EA9394 (paste)	2.13 [124]
EB 600 + 15 wt% BPaP20	1.15 [122]
Epoxy-Acrylate + Thermoplastic	2.00 [123]

The highest toughness achieved by these researchers was 2.00 MPa $m^{½}$. The compositions explored in this research project were produced to explore epoxy-acrylate IPN structure-property relationships. Optimization has not been attempted, but several of the acrylate-epoxy IPN compositions investigated in this research were able to achieve toughness values

in excess of 2.50 MPa $m^{½}$. It has been demonstrated through carbon fiber laminate short beam shear testing that these improvements in bulk adhesive properties may also translate to matrix adhesive applications. These promising results suggest that further development of acrylate-epoxy IPN adhesives is warranted.

7. Future Research

Several avenues remain to be explored with respect to IPN adhesives. Potential future research activities include the following:

- Addition of a third polymer phase such a elastomers or thermoplastics to the epoxy system – As referenced in the general discussion section, other researchers have developed secondary phase toughening agents – most notably thermoplastics – to toughen electron beam cured acrylates. This approach may or may not be synergistic with acrylate-epoxy IPNs.
- Incorporation of filler materials – The addition of solid particles may offer a pathway to further increasing the toughness of the acrylate-epoxy IPN systems. In an IPN system with flexible acrylates and stiff epoxies, it was noted that the addition of inorganic fillers resulted in a drop in fracture toughness since the higher surface energy epoxy preferentially coated the particles, depleting the epoxy composition in the bulk IPN. [125] With a strong acrylate, this effect may produce an opposite result in stiff acrylate/flexible epoxy IPN systems. Recent work with composite nanotubes has examined the use of polar curing agents such as imidazoles to improve dispersion. [126] Since imidazoles are used to cure the (50-50)Epoxy and (70-30)Epoxy networks, this may represent a synergistic approach.
- IPN strain deformation – Either the AFM or the confocal fluorescence techniques could be used to document the relative movements of the acrylate network relative to the epoxy network when an IPN sample is subjected to deformation. In-situ strain

fixtures could be developed to impose strains on an IPN sample while in either the AFM or confocal fluorescence microscope stages.

- Use as a matrix adhesive for carbon fiber composites – The short beam shear study identified a number of potential benefits from using acrylate-epoxy IPNs as matrix adhesives by adjusting the epoxy composition. These include improved impact resistance, enhanced compression after impact and increased threshold for fiber/matrix damage initiation.
- Damping and impact resistance of IPN matrix adhesives – Many thermoplastic IPNs have been developed for the automotive industry for use as sound damping materials. [127] The inherent damping of an IPN may offer enhanced resistance to impact damage including barely visible impact damage.
- Exploration of alternative acrylate-epoxy systems such as EB cured acrylate plus room temperature cured epoxy or use of a higher strength acrylate monomer.
- Exploration of "hot-wet cycle" impact on IPN adhesives or solvent/water vapor solubility in IPNs.

8. Conclusions

The motivation to conduct this research was to capture the advantages of room temperature curing via electron beam polymerization of acrylate monomers while providing toughening by incorporating a second network to produce an IPN.

- An IPN system composed of separate acrylate and epoxy networks has been produced. [128] [129]
- Synergy in mechanical properties has been demonstrated for glass transition temperature, tensile modulus, tensile strength, compression strength and fracture toughness. Properties of some IPNs are greater than the properties of both individual networks.
- The premise that the first network to cure can provide the strength of the system while the second network to cure can provide the toughness of the system has been validated with the (80-20)Acrylate + (50-50)Epoxy IPN system.
- Many additional opportunities exist for further investigation of electron beam cured plus thermally cured epoxy IPN adhesives.

9. Acknowledgements

This research has been funded by The Boeing Company. Cytec Engineered Products provided the Bisphenol A Diacrylate (Ebecryl 600) that was used in this research. Samples were electron beam cured at the Boeing Applied Physics Laboratory where technicians Jim Beymer and Jake Beedle were very accommodating for cure cycles that extended past normal business hours. I received periodic assistance and continuous support from members of the Flinn Research Group.

For their willingness to allow my free time plus a little more to be dedicated to research, I especially acknowledge my wife, MaryKay, and my children Katelyn, Aaron and Alyssa.

10. References

[1] L. B. Vogelesang, A. Vlot, Development of fibre metal laminates for advanced aerospace structures, Journal of Materials Processing Technology, Volume 103, Issue 1, 1 June 2000, p 1-5.

[2] D. W. Rhymer, W. S. Johnson, Fatigue damage mechanisms in advanced hybrid titanium composite laminates, International Journal of Fatigue, Volume 24, Issue 9, September 2002, p 995-1001

[3] Fawzia, S, R. Al-Mahaidi, X. Zhao, Experimental and finite element analysis of a double strap joint between steel plates and normal modulus CFRP, Composite Structures, 2006 (75), pp 156-162.

[4] Pocius, A. *Adhesion and Adhesives Technology, 2nd Edition*, Hanser, Munich, 2002.

[5] Loctite Aerospace, Hysol EA 9394 Epoxy Paste Adhesive Technical Data Sheet, 2002.

[6] H. Dodiuk, S. Kenig, Low temperature curing epoxies for structural repair, Progress in Polymer Science, Volume 19, Issue 3, 1994, p 439-467.

[7] V. Sauvant, J. L. Halary, Improvement of the performance of epoxy-amine thermosets by antiplasticizer-induced nano-scale phase separation during cure, Composites Science and Technology, Vol 62, No 4, 2002, p 481-486.

[8] Cognard, J, Some recent progress in adhesion technology and science, Comptes Rendus Chimie, Volume 9, Issue 1, Adhesion, January 2006, p 13-24.

[9] Kim, HK, DG Lee, Avoidance of Fabricational Thermal Residual Stresses in Co-Cured Bonded Metal-Composite Hybrid Structures, Journal of Adhesion Science Technology, 2006, p 959-979.

[10] da Silva, LFM, RD Adams, Adhesive joints at high and low temperatures using similar and dissimilar adherends and dual adhesives, International Journal of Adhesion and Adhesives, Vol 27, No 3, 2007, p 216-226.

[11] Lopata, VJ, CB Saunders, A Singh, CJ Janke, GE Wrenn, SJ Havens, Electron-beam-curable epoxy resins for the manufacture of high-performance composites, Radiation Physics and Chemistry, Vol 56, No 4, 1999, p 405-415.

[12] Burgess, J. Enhanced fracture properties beam cured epoxy materials, University of Washington Thesis, 2002.

[13] Fried, JR. *Polymer Science & Technology*, second edition, Prentice Hall, 2003.

[14] Decker, C, UV-Radiation Curing of Adhesives in *Handbook of Adhesives and Surface Preparation*, 2011, 221-243.

[15] Calorimetric Characterization of the Heterogeneities Produced by the Radiation-Induced Cross-Linking Polymerization of Aromatic Diacrylates

[16] Decker, C, UV-Radiation Curing of Adhesives in *Handbook of Adhesives and Surface Preparation*, 2011, 221-243.

[17] Hong, BT, KS Shin, DS Kim, Ultraviolet-Curing Behavior of an Epoxy Acrylate Resin System, Journal of Applied Polymer Science, Vol 98, No 3, p 1180-1185, 2005.

[18] Petrie, EM, *Epoxy Adhesive Formulations*, McGraw-Hill, p 36-41, 2006.

[19] Ooi SK, WD Cook, GP Simon, CH Such, DSC studies of the curing mechanisms and kinetics of DGEBA using imidazole curing agents, Polymer, Volume 41, Issue 10, May 2000, p 3639-3649.

[20] Heise, MS and GC Martin, Curing Mechanism and Thermal Properties of Epoxy-Imidazole Systems, Macromolecules, 22, 1989, p 99-104.

[21] Ham, YR, SH Kim, YJ Shin, DH Lee, M Yang, JH Min, JS Shin, A comparison of some imidazoles in the curing of epoxy resin, Journal of Industrial and Engineering Chemistry, Vol 16, p 556-559, 2010.

[22] Krezeminski, M, M Molinari, M Troyon, X Coqueret, Calorimetric Characterization of the Heterogeneities Produced by the Radiation-Induced Cross-Linking Polymerization of Aromatic Diacrylates, Macromolecules, Vol 43, 2010, p 3757-3763.

[23] Ponsaud, P, B Defoort, X Coqueret, A Microstructural Investigation of UV and EB-Cured Bisphenol-A Ethoxy Diacrylate by H NMR Relaxation Measurements, SAMPE

[24] Kulshreshtha, AK, C Vasile, Handbook of Polymer Blends and Composites, Volumes 1-4, Smithers Rapra Technology, 2002.

[25] Ruiz, CSB, LDB Machado, ES Pinto, MHO Sampa, Characterization of a clear coating cured by UV/EB radiation, Radiation Physics and Chemistry, Vol 63, 2002, p 481-483.

[26] Lipatov, YS, TT Alekseeva, Phase-Separated Interpenetrating Polymer Networks, Advances in Polymer Science, Vol 208, p 1-227, 2007.

[27] Gedde, UW, *Polymer Physics*, Chapman & Hill, 1995.

[28] Lipatov, Y. *Polymer reinforcement*, (electronic book) Knovel, 2001.

[29] Vazquez, A, AJ Rojas, HE Adabbo, J Borrajo, RJJ Williams, Rubber-modified thermosets: Prediction of the particle size distribution of dispersed domains, Polymer, Vol 28, p1156-1164, 1987.

[30] Lange, J, S Toll, JE Manson, A Hult, Residual stress build-up in thermoset films cured below their ultimate glass transition temperature, Polymer, Vol 38, No 4, 1997, p 809-815.

[31] Raghavan, J, Evolution of cure, mechanical properties, and residual stress during electron beam curing of a polymer composite, Composites: Part A, Vol 40, 2009, p300-308.

[32] Sangermano, M, W Carbonara, G Malucelli, A Priola, UV-Cured Interpenetrating Acrylic-Epoxy Polymer Networks: Preparation and Characterization, Macromolecular Materials and Engineer, Vol 293, No 6, p 515-520, 2008.

[33] Lange, J, S Toll, JE Manson, A Hult, Residual stress build-up in thermoset films cured below their ultimate glass transition temperature, Polymer, Vol 38, No 4, 1997, p 809-815.

[34] Svec, F, Preparation and HPLC applications of rigid macroporous organic polymer monoliths, Journal of Separation Science, Vol 27, No 10-11, 2004, p 747-766.

[35] Sayil, C, O Okay, Macroporous poly(N-isopropyl)acrylamide networks: formation conditions, Polymer, Vol 42, No 18, p7639-7652, 2001.

[36] Okay, O, Macroporous copolymer networks, Progress in Polymer Science, Vol 25, No 6, p 711-779, 2000.

[37] Sperling, LH, Interpenetrating Polymer Networks: An Overview, In Interpenetrating Polymer Networks; Klempner, D., et al., Advances in Chemistry, American Chemical Society, Washington, DC, 1994

[38] A comparison of the glass transition measured by DSC, TMA and DMA, Mettler-Toledo Application Note HB30, Accessed at www.mt.com/ta-handbooks on 5/31/2012.

[39] Sepe, MP, Dynamic Mechanical Analysis for Plastics Engineering, William Andrew Publishing/Plastics Design Library, (Knovel ebook accessed 4/15/2012), 1998.

[40] Menard, KP, Thermomechanical Analysis Basics: Part 1 It's All Free Volume, Perkin-Elmer application note, accessed at http://shop.perkinelmer.com/content/applicationnotes/app_thermalthermomechanalybasicspart1.pdf on 5/28/2012.

[41] Roulin-Moloney, AC, Fractography and Failure Mechanisms of Polymers and Composites, Elsevier Science, England, 1989.

[42] Plangsangmas, L, JJ Mecholsky, Jr., AB Brennan, Determination of Fracture Toughness of Epoxy Using Fractography, Journal of Applied Polymer Science, Vol. 72, No 2, p 257–268, 1999.

[43] Kinloch, AJ, Mechanics and Mechanisms of Fracture of Thermosetting Epoxy Polymers, in Advances in Polymer Science 72, Springer-Verlag, Berlin, p 45-67, 1985.

[44] Garg, AC, Y-W Mai, Failure Mechanics in Toughened Epoxy Resins – A Review, Composites Science and Technology, Vol 31, p 179-223, 1988.

[45] Kinloch, AJ, SJ Shaw, DA Tod, Deformation and fracture behavior of a rubber-toughened epoxy: 1. Microstructure and fracture studies, Polymer, Vol 24, p 1341-1354, 1983.

[46] Russell, B, R Chartoff, The influence of cure conditions on the morphology and phase distribution in a rubber-modified epoxy resin using scanning electron microscopy and atomic force microscopy, Polymer 46, p 785-798, 2005.

[47] Cho, JB, JW Hwang, K Cho, JH An, CE Park, Effects of morphology on toughening of tetrafunctional epoxy resins with poly(ether imide), Polymer, Vol 34 No 23, p 4832-4836, 1993.

[48] Teng, K-C, F-C Chang, Single-phase and multiple-phase thermoplastic/thermoset polyblends: 2. Morphologies and mechanical properties of phenoxy/epoxy blends, Polymer, Vol 37 No 12, p 2385-2394, 1996.

[49] Bucknall, CB, AH Gilbert, Toughening tetrafunctional epoxy resins using polyetherimide, Polymer, Vol 30, p213-217, 1989.

[50] Francis, B, VL Rao, S Jose, BK Catherine, R Ranaswamy, J Jose, S Thomas, Poly(ether ether ketone) with pendent methyl groups as a toughening agent for amine cured DGEBA epoxy resin, Journal of Materials Science, Vol 41, p 5467-5479, 2006.

[51] Ratna, D, Handbook of Thermoset Resins, Smithers Rapra Technology, 2009.

[52] Chen, C, RS Justice, DW Schaefer, JW Baur, Highly dispersed nanosilica-epoxy resins with enhanced mechanical properties, Polymer, Vol 49, No 17, p 3805-3815, 2008.

[53] Kim, J-K, Y-W Mai, High Strength, High Fracture Toughness Fibre Composites with Interface Control – A Review, Composites Science and Technology, Vol 41, p 333-378, 1991.

[54] Sperling, LH and V Mishra, The Current Status of Interpenetrating Polymer Networks, Polymers for Advanced Technologies, Vol 7, 1996, p 197-208.

[55] Technical Bulletin, "IPN Technology," Polymerics GmBH, Berlin, Germany, http://www.polymerics.de/technology/ipn_en.html, accessed 9/26/2009.

[56] Lipatov, Y. *Polymer reinforcement*, (electronic book) Knovel, 2001.

[57] Park, Y-J, D-H Lim, H-J Kim, D-S Park, I-K Sung, UV- and thermal-curing behaviors of dual-curable adhesives based on epoxy acrylate oligomers, International Journal of Adhesion and Adhesives, Vol 29, No 7, 2009, p 710-717.

[58] Chen, F, WD Cook, Curing kinetics and morphology of IPNs from a flexible dimethacrylate and a rigid epoxy via sequential photo and thermal polymerization, European Polymer Journal, Vol 44, No 6, 2008, p 1796-1813.

[59] Nowers, JR, JA Costanzo, B Narasimhan, Structure-property relationships in acrylate/epoxy interpenetrating polymer networks: Effects of the reaction sequence and composition, Journal of Applied Polymer Science, Vol 104, No 2, 2007, p 891-901

[60] Dean, KM, WD Cook, MY Lin, Small angle neutron scattering and dynamic mechanical thermal analysis of dimethacrylate/epoxy IPNs, European Polymer Journal, Vol 42, No 10, 2006, p 2872-2887.

[61] Nowers, JR, Narasimhan, B. The effect of interpenetrating polymer network formation on polymerization kinetics in an epoxy-acrylate system, Polymer 47, 2006, p 1108–1118.

[62] Dean, K, WD Cook, Effect of Curing Sequence on the Photopolymerization and Thermal Curing Kinetics of Dimethacrylate/Epoxy Interpenetrating Polymer Networks, Macromolecules, 25, 2002, p. 7942-7954.

[63] Dean, K, WD Cook, Azo initiator selection to control the curing order in dimethacrylate/epoxy interpenetrating polymer networks, Polymer International, Vol 53 No 9, 2004, p. 1305-1313

[64]Lin, Y, JW Stansbury, Kinetics Studies of Hybrid Structure Formation by Controlled Photopolymerization, Polymer, Vol 44, 2003, p 4781-4789.

[65] Dean, K, WD Cook, Effect of Curing Sequence on the Photopolymerization and Thermal Curing Kinetics of Dimethacrylate/Epoxy Interpenetrating Polymer Networks, Macromolecules, Vol 35 No 21, p 7942-7954, 2002.

[66]Sands, JM, SH McKnight, BK Fink, Interpenetrating Polymer Network (IPN) Adhesives for Electron Beam Cure, ARL-TR-2321, Army Research Laboratory, 2003.

[67] Dubuisson, A, D Ades, M Fontanille, Homogeneous Epoxy-Acrylic Interpenetrating Polymer Networks: Preparation and Thermal Properties, Polymer Bulletin, Vol 3, p 391-398, 1980.

[68] Litmanovich, AD, NA Plate, YV Kudryavtsev, Reactions in polymer blends: interchain effects and theoretical problems, Progress in Polymer Science, Vol 27, p 915-970, 2002.

[69] Cytec Material Data Sheet, Ebecryl 600 Bisphenol A Epoxy Diacrylate, accessed at Cytec.com on 8/19/2009.

[70] Elban, WL, JA Howarter, MC Richardson, PE Stutzman, AM Forster, AJ Nolte, GA Holmes, Influence of solvent washing on interlayer structure of alkylammonium montmorillonites, Applied Clay Science, Vol 61, p 29-36, 2012.

[71] Schneberger, GL, *Adhesives in manufacturing*, Marcel Dekker, 1983, p. 170.

[72] Sartomer Application Bulletin, Surface Tensions of Sartomer Monomers, Accessed at Sartomer.com 3/14/2010.

[73] Lange, J, J-A E Manson, A Hult, Build-up of structure and viscoelastic properties in epoxy and acrylate resins cured below their ultimate glass transition temperature, Polymer, Vol 37 No 26, p 5859-5868, 1996.

[74] Lange, J, Viscoelastic Properties and Transitions During Thermal and UV Cure of a Methacrylate Resin, Polymer Engineering and Science, Vol 39 No 9, p 1651-1660, 1999.

[75] Sawyer, LC, GT Grubb, GF Meyers, Polymer Microscopy, Third Edition, Springer, 2008.

[76] Pearce, PJ, CEM Morris, BC Ennis, Rubber toughening of practical tetraglycidyl methylenedianiline-piperidine adduct systems, Polymer, Vol 37 No 7, p 1137-1150, 1996.

[77] Verhoogt, H, J van Dam, A P de Boer, A Draaijer, PM Houpt, Confocal laser scanning microscopy: a new method for determination of the morphology of polymer blends, Polymer, Vol 34 No 6, p 1325-1329, 1993.

[78] Foldes-Papp, Z, U Demel, GP Tilz, Laser scanning confocal fluorescence microscopy: an overview, International Immunopharmacology, Vol 3 No 13-14, p 1715–1729, 2003.

[79] Hartman, A, P Boukamp, P Friedl, Confocal reflection imaging of 3D fibrin polymers, Blood Cells, Molecules, and Diseases, Vol 36 No 2, p 191–193, 2006.

[80] Wade Jr, LG, *Organic Chemistry*, Fifth Edition, Pearson Education, 2003.

[81] Menard, K, Dynamic Mechanical Analysis A Practical Introduction, CRC Press 1999.

[82] ASTM D7028, 2007, Standard Test Method for Glass Transition Temperature (DMA Tg) of Polymer Matrix Composites by Dynamic Mechanical Analysis (DMA), ASTM International, West Conshohocken, PA, 2006, DOI: 10.1520/D7028-07E01, www.astm.org

[83] Kalogeras, IM, W Brostow, Glass Transition Temperatures in Binary Polymer Blends, Journal of Polymer Science Part B: Polymer Physics, Vol 47, p 80-95, 2009.

[84] Pimbert, S, L Avignon-Poquillon, G Levesque, Relations between Glass Transition Temperatures in Miscible Polymer Blends and Composition: From Volume to Mass Fractions, Macromolecular Symposia, Vol 222, No 1, p 259-264, 2005.

[85] Frisch, KC, D Klempner, HL Frisch, Recent Advances in Polymer Alloys and IPN Technology, Materials & Design, Vol 4, No 4, p 821–827, 1983.

[86] Pavan, A, T Ricco, M Rink, High Performance Polymer Blends II: Density, Elastic Modulus Glass Transition Temperatures and Heat Deflection Temperature of Polyvinylchloride-(Acrylonitrile-Butadiene-Styrene) Blends, Materials Science and Engineering, Vol 48, p 9-15, 1981.

[87] Kleiner LW, FE Karasz, WJ MacKnight, Compatible glassy polyblends based upon poly(2,6-dimethyl-1,4-phenylene oxide): Tensile modulus studies, Polymer Engineering & Science, Volume 19, Number 7, p 519-524, 1979.

[88] Sartomer Technical Data Sheet, CN120 Epoxy Acrylate, accessed at sartomer.com 9/24/2009.

[89] Sartomer Technical Data Sheet, CN120C80 Epoxy Acrylate Blended with SR351, accessed at sartomer.com 9/24/2009.

[90] Sartomer Technical Data Sheet, CN120C60 Epoxy Acrylate Blended with SR351, accessed at sartomer.com 9/24/2009.

[91] Callister Jr, WD, Materials Science and Engineering An Introduction, Sixth Edition, John Wiley & Sons, 2003.

[92] Foreman, JP, S Behzadi, D Porter, PT Curtis, FR Jones, Hierarchical modeling of a polymer matrix composite, Journal of Materials Science, Vol 43, p 6642-6650, 2008.

[93] Ma, J, Q Qi, J Bayley, X-S Du, M-S Mo, L-Q Zhang, Development of SENB toughness measurement for thermoset resins, Polymer Testing, Volume 26, 2007, p 445-450.

[94] Cantwell, W.J., A.C. Roulin-Moloney, Fractography of unfilled and particulate-filled epoxy resins, Journal of Materials Science, Volume 23, 1988, p 1615-1631.

[95] Anderson, T.L., Fracture Mechanics Fundamentals and Applications, 3Rd Edition, Boca Raton, Taylor & Francis Group, 1985, p 360-361.

[96] Roulin-Moloney, A.C. editor, Fractography and Failure Mechanisms of Polymers and Composites, London, Elsevier Applied Science, 1989, p 234-240.

[97] Subramaniyan, A.K., C.T. Sun, Toughening polymeric composites using nanoclay: Crack tip scale effects on fracture toughness, Composites: Part A, Volume 38, 2007, p 34-43.

[98] Haris, A, T. Adachi, Y. Hayashi, W. Araki, Material characterization of blended epoxy resins related to fracture toughness, Journal of Materials Science, Volume 42, 2007, p 9859-9866.

[99] Ellis, B. Chemistry and Technology of Epoxy Resins, p 163-164.

[100] Lipatov, Y. Phase Separated IPNs

[101] Pater, R. Interpenetrating Polymer Network Approach to Tough and Microcracking Resistant High Temperatures Polymers. Part III. LaRC-RP71, Polymer Engineering & Science, Volume 31, 1991, p 28-33.

[102] Mayr, AE, WD Cook, GH Edward, Yielding behavior in model epoxy thermosets – I. Effect of strain rate and composition, Polymer, Vol 39, No. 16, 1998, p 3719-3724.

[103] Pearson, RA, AF Yee, Toughening mechanisms in thermoplastic-modified epoxies: 1. Modification using poly(phenylene oxide), Polymer, Vol 34, No 17, p 3658-3670, 1993.

[104] Zhang, B-L, G-L Tang, K-Y Shi, Y-C You, Z-J Du, J-F Yang, J Huang, A study on the properties of epoxy resin toughened by functionalized polymer containing rigid, rod-like moiety, European Polymer Journal, Vol 36, No 1, p 205-213, 2000.

[105] Wolff-Fabris, F, V Altstädt, U Arnold, M Döring, Electron Beam Curing of Composites, Hanser Publishers, p 63-67, 2011.

[106] Coqueret, X, M Krzeminski, P Pansaud, B Defoort, Recent advances in electron-beam curing of carbon fiber-reinforced composites, Radiation Physics and Chemistry, Vol 78 No 7-8, p 557-561, 2009.

[107] Vautard, F, P Fioux, L Vidal, J Schultz, M Nardin, B Defoort, Influence of the carbon fiber surface properties on interfacial adhesion in carbon fiber–acrylate composites cured by electron beam, Composites: Part A, Vol 42 No 7, p 859–867, 2011.

[108] Vautard, F, P Fioux, L Vidal, J Schultz, M Nardin, B Defoort, Influence of an oxidation of the carbon fiber surface on the adhesion strength in carbon fiber-acrylate composites cured by electron beam, International Journal of Adhesion & Adhesives, Vol 34, p93–106, 2012.

[109] Cantwell, WJ, J Morton, The impact resistance of composite materials – A review, Composites, Vol 22 No 5, p 347-362, 1991.

[110] Yee, AF, Modifying Matrix Materials for Tougher Composites, ASTM STP937, p 383- 396, 1978.

[111] Kim, J-K, Y-W Mai, High Strength, High Fracture Toughness Fibre Composites with Interface Control – A Review, Composites Science and Technology, Vol 41, p 333-378, 1991.

[112] Turmel, DJ-P, IK Partridge, Heterogeneous Phase Separation around Fibers in Epoxy/PEI Blends and its Effect on Composite Delamination Resistance, Composites Science and Technology, Vol 57, p 1001-1007, 1997.

[113] Hara, M, Sauer, JA, Synergism in Mechanical Properties of Polymer/Polymer Blends, Journal of macromolecular science. Reviews in macromolecular chemistry and physics, Vol 38, No 2, p 327-362, 1998.

[114] Akay, M, SN Rollins, Polyurethane-poly(methyl methacrylate) interpenetrating polymer networks, Polymer, Vol 34 No 9, p1865-1873, 1993.

[115] Sue, HJ, RA Pearson, AF Yee, Mechanical modeling of initiation of localized yielding under plane stress conditions in rigid-rigid polymer alloys, Polymer Engineering & Science, Vol 31, No 11, p 793-802, 1991.

[116] Liu, J, AJ Thompson, H-J Sue, FS Bates, MA Hilmyer, M Dettloff, G Jacob, N Verghese, H Pham, Toughening of Epoxies with Block Copolymer Micelles of Wormlike Morphology, Macromolecules, Vol 43, No 17, p 7238–7243, 2010.

[117] Wang, W, K Sadeghipour, G Baran, Finite element analysis of the effect of an interphase on toughening of a particle-reinforced polymer composite, Composites Part A, V39, No 6, p 956-964, 2008.

[118] Hara, M, Sauer, JA, Synergism in Mechanical Properties of Polymer/Polymer Blends, Journal of macromolecular science. Reviews in macromolecular chemistry and physics, Vol 38, No 2, p 327-362, 1998.

[119] Cook, WD, Fracture and Structure of Highly Crosslinked Polymer Composites, Journal of Applied Polymer Science, Vol 42 No 5, p 1259-1269, 1991.

[120] Wolff-Fabris, F, V Altstädt, U Arnold, M Döring, Electron Beam Curing of Composites, Hanser Publishers, p 63-67, 2011.

[121] Al-Sheikhly, M, McLaughlin, WL, Interpenetrating Polymer Network Formation by Electron-Beam Curing of Acrylated Epoxy Resin Blends in *Irradiation of Polymers*, ACS Symposium Series, Vol. 620, p 188-196, 1996.

[122] Defoort, B, E Chauray, P Ponsaud, X Coqueret, Improvement of Mechanical Properties of Acrylate Based EB Cured Composite Materials, SAMPE 2005.

[123] Coqueret, X, M Krzeminski, P Ponsaud, B Defoort, Recent advances in electron-beam curing of carbon fiber-reinforced composites, Radiation Physics and Chemistry, Vol 78 No 7-8, p 557–561, 2009.

[124] Guess, TR, ED Reedy, ME Stavig, Mechanical Properties of Hysol EA-9394 Structural Adhesive, Sandia National Laboratory Report SAND95-0229, 1995

[125] Karger-Kocsis, J, O Gryshchuk, J Frohlich, R Mulpaupt, Interpenetrating vinylester/epoxy resins modified with organophilic layered silicates, Composites Science and Technology, Vol 63 No 14, p 2045-2054, 2003.

[126] Throckmorton, J, SAMPE 2012 Student Presentation

[127] Sperling, LH, V Mishra, The Current Status of Interpenetrating Polymer Networks, Polymers for Advanced Technologies, Vol 7 No 4, p 197-209, 1996.

[128] United States Patent Application #20120052305, Composite Structures Using Interpenetrating Polymer Network Adhesives

[129] European Patent Application #11178793.3, Composite Structures Using Interpenetrating Polymer Network Adhesives